" ..... an iron, rectangular, abhorrent book,
one which no man would willingly read ..... "

'THE MINT'
by Lawrence of Arabia

"SPECTROSCOPIC STUDIES OF A HIGH TEMPERATURE PLASMA"

A Thesis submitted for the Degree of

DOCTOR OF PHILOSOPHY

in the

UNIVERSITY OF LONDON

by

JOHN ERNEST JENKINS

Department of Physics
Imperial College of Science & Technology
South Kensington
LONDON SW7

JULY 1970

ABSTRACT

In Part I of this thesis the Stark broadening parameters for a number of isolated HeI lines are calculated using the G.B.K.O. theory. The widths and shifts calculated from these parameters are compared with experiment assuming that the quasi-static approximation is valid for the ions. For the widths, these parameters are shown to be an improvement over those available previously; this improvement is attributed to the use of more accurate broadening functions. For the shifts the theory is less accurate and the results of the comparisons suggests that for electron densities $\lesssim 10^{16} cm^{-3}$ the motions of the ions must be taken into account whereas at higher electron densities the transition from the quadratic to the linear Stark effect appears to be important. Finally, Stark broadening parameters for 16 isolated lines are presented.

In Part II the possibility of using a Z-pinch discharge as a spectroscopic light source for the study of the Stark broadening of spectral lines at electron densities of $\sim 10^{16} cm^{-3}$ is investigated. This investigation is carried out by measuring, at various electron densities, the Stark broadening of three HeI lines (one of which contains a forbidden component) and one HeII line.

It is found that although such a device contains radial gradients, profiles which are in good agreement with theory can be obtained, in certain circumstances, without regard to spatial resolution. In general, however, spatial resolution is required if the device is to be operated over a wide range of conditions. During this investigation it was found that lines with forbidden components are particularly sensitive to the effects of radial gradients.

In the final Chapter of this thesis a method is given of extending the line-to-continuum ratio method of measuring the electron temperature of a helium plasma to helium plasmas with more than one ionization stage present.

ACKNOWLEDGEMENTS

I thank Professor W. R. S. Garton for his supervision, help and encouragement during the course of this work and for kindly allowing me to complete this thesis whilst a Research Assistant in his Group.

To Dr D. D. Burgess I gratefully acknowledge firstly his constructive criticism and encouragement of all aspects of this work, and secondly his friendship during my stay in the Spectroscopy Group.

To Dr D. E. Roberts I offer my thanks for making available a copy of his Stark broadening programme and for useful discussions.

Many people in the Spectroscopy Group have given me advice or assistance on various occasions. In particular I would like to thank Messrs J. Leveridge, S. Budd, C. Cairns, W. Lewis, J. Wheaton and Drs R. Learner, A. Edmunds and N. Fox. I would also like to acknowledge the occasional assistance of members of the Plasma Physics Group, notably Messrs A. Chapman, A. E. Dangor, S. Dolby, S. Fielding, C. B. Wheeler and L. Nyman and Dr Folkierski.

On many occasions I have to be grateful for the prompt attention and skill of the glassblower, Mr O. Hillbank.

For the care and attention which she has given to the typing of this manuscript I thank Joy Woodward.

I would like to give very special thanks to my wife Pam who by her help, patience and encouragement and her willingness to assume the major part of the responsibility concerned with the running of the home has contributed greatly to this work.

Finally I would like to thank the Science Research Council for financial support in the form of a Research Studentship. The experimental work in this thesis was performed as part of a contract supported by the U.K.A.E.A. Culham Laboratory.

TABLE OF CONTENTS

CHAPTER III (CONTINUED)

CHAPTER V (CONTINUED)

CHAPTER VI (CONTINUED)

PART II

CHAPTER X. (CONTINUED)

CHAPTER XI (CONTINUED)

CHAPTER I

AN OUTLINE OF THE MATERIAL TO BE PRESENTED IN THIS THESIS

Part I of this thesis, comprising Chapters II to VI inclusive, is concerned with a theoretical investigation of the Stark broadening of isolated helium lines in plasma.

In Chapter II broadening mechanisms in plasmas are discussed briefly. Following this general discussion Chapter III is concerned with Stark broadening only. Here the various Stark broadening mechanisms, and the quasi-static and impact theories of the broadening of spectral lines are discussed. Attention is then paid to the types of lines to which the modern Stark broadening theory has been applied and the methods of characterising their profiles are described.

Having thus prepared the background the experimental and theoretical aspects of the Stark broadening of helium lines are reviewed in Chapter IV and at the end of this Chapter the theoretical and experimental investigations which are to be undertaken in this thesis are described.

Chapter V contains a review of the G.B.K.O. theory of the Stark broadening of isolated lines and recent improvements to this theory are discussed.

In Chapter VI the author's calculations of the Stark broadening parameters of isolated HeI lines are described and the results of these calculations are compared with those of other workers and with experiment. The results and conclusions drawn from these investigations are discussed in detail. In the final part of the chapter tables are given of the Stark broadening parameters for 16 isolated HeI lines, calculated for various electron densities and temperatures.

Chapters VII-XIII inclusive comprise Part II of this thesis. The work that is described in this part is concerned with the possibility of using a Z-pinch discharge for the generation of high temperature low density helium plasma suitable for the investigation of the Stark broadening of HeI and HeII lines. The investigation is carried out by measuring the profiles of three HeI lines and one HeII line at various electron densities and temperatures and comparing the results with theory.

In the first part of Chapter VII the conventional methods of generating helium plasma suitable for Stark broadening measurements, are compared. Previous investigations of the Stark broadening of spectral lines which have been made using a Z-pinch discharge are then discussed. The remainder of the Chapter is devoted to a description of the Z-pinch discharge which is used in this investigation.

To help in the understanding of the diagnostic measurements which were carried out on the discharge the equilibrium of helium plasmas is discussed in Chapter VIII.

In Chapter IX the methods of measuring the electron temperature and density of the plasma are described, with particular attention being paid to the electron density measurements.

The method of measuring the line profiles is discussed in Chapter X and the results of these measurements are discussed in Chapter XI.

On the basis of the results given in Chapter XI the radial distributions of the electron density and total intensity of one of the HeI lines were measured. The measurement procedures and the results are presented in Chapter XII together with the results of calculations on the effects of radial gradients on the profile of one of the HeI lines.

Chapter XIII contains a summary of the results obtained in Part II and the conclusion which can be drawn from these results.

In the final chapter of the thesis a method is described of extending the 'line to continuum ratio' method of measuring electron temperatures in helium plasmas to helium plasmas which have more than one ionization stage present.

CHAPTER II

LINE BROADENING MECHANISMS IN PLASMAS

2.1. Introduction

The spectral lines emitted by atoms or ions immersed in a plasma may be broadened by a number of physical mechanisms. These mechanisms may be divided in to two classes:-

a) Mechanisms which broaden the spectral lines emitted by an atom, as observed in its rest frame.

b) Mechanisms which act on the emitted radiation.

In this chapter the broadening mechanisms which contribute to these two classes will be briefly summarised.

The following broadening mechanisms contribute to class A)

2.2. Natural Broadening

Because the life-times of atomic states are finite they must, from the uncertainty principle, have a finite width. For a line with upper state α and lower state β natural broadening results in an un-shifted Lorentzian (dispersion) profile with a half-width w given by:

$$w = \frac{\lambda^2}{2\pi c} \cdot \left(\sum_{\alpha'} A_{\alpha\alpha'} + \sum_{\beta'} A_{\beta\beta'} \right) \qquad (2.1)$$

where the A's are the spontaneous transition probabilities and the summation is over all spontaneous transitions originating from the upper and lower states of the line.

The natural line width, for lines in the visible, is typically $\sim 10^{-4}$ Å and is negligible in most laboratory plasmas. No shift is produced by this mechanism.

2.3. Pressure Broadening

Pressure broadening may be defined as the effects produced on the shapes, and positions, of spectral lines emitted by an atom or ion which is interacting with its surrounding particles. As the name suggests, the characteristic feature which distinguishes pressure broadening mechanisms from the other broadening mechanisms in class a) is their density dependence.

In line broadening theory the surrounding particles are usually called the perturbers and pressure broadening mechanisms can be classified according to the type of perturbers interacting with the radiating system. Since the temperatures required to produce an appreciable degree of ionisation in a plasma are usually also sufficiently high to dissociate any molecules which may be present, the perturber interactions which are of interest in plasmas are those between neutral atoms, ions, and electrons. The pressure broadening mechanisms in a plasma are:-

2.3.1. Van der Waals Broadening (perturbers :- neutral particles)

Van der Waals broadening is produced by the interaction of an emitting atom or ion with neutral perturbers. This broadening mechanism produces a Lorentzian profile with a

half width w , and shift d, given by Griem (1) to be:

$$w = \frac{\lambda^2}{c} \cdot \left(\frac{9\pi \hbar^5 R_a^2}{16 m^3 E_p^2} \right)^{2/5} \cdot v^{3/5} \cdot N \qquad (2.2)$$

$$d = -2/3 w$$

where λ is the wavelength of the line, N is the density of neutral perturbers, R_a^2 is the matrix element of the square of the co-ordinate vector of the radiating electron in state a, v is the velocity of the perturbers and E_p the excitation energy of the first excited state.

Because of the short range nature of the radiating system-neutral perturber interaction, broadening by this mechanism is only likely to be significant when the neutral particle densities are several orders of magnitude greater than those of the charged species, Wiese (2). Hence Van der Waals broadening is only likely to be important in weakly ionized plasmas.

2.3.2. Resonance Broadening (perturbers: same as radiating system)

When a neutral emitter interacts with other neutral atoms of the same kind, then lines which have one state in common with an allowed transition to the ground state will be resonance broadened. The profile produced by this mechanism

is an unshifted Lorentzian with a half-width w given by:

$$w = \frac{\lambda^2}{c} \cdot \left(\frac{g_1}{g_2} \right)^{\frac{1}{2}} \cdot \left(\frac{e^2 f}{2\,mc} \right) \cdot N \qquad (2.3)$$

where λ is the wavelength of a line with absorption oscillator strength f and whose upper and lower states have statistical weights of g_1 and g_2 respectively. N is the neutral particle density.

For the same reasons as those given in (2.3.1.) resonance broadening is only likely to be important in weakly ionized plasmas.

2.3.3. Stark Broadening (perturbers: charged particles)

Because of the long range nature of the Coulomb interaction, Stark broadening is usually the most important pressure broadening mechanism in laboratory plasmas (this is true even in plasmas of a low degree of ionization). As the work to be described in this thesis is mainly concerned with Stark broadening, this broadening mechanism will be considered in some detail in the following chapter.

2.4. Zeeman Broadening

If a plasma contains a magnetic field then the lines emitted by the plasma may be broadened by the Zeeman splitting of the atomic states. The half-width w produced by such a splitting is estimated to be (see (1)):

$$w \approx 10^{-9} \cdot \lambda^2 \cdot B \quad \text{angstroms}$$

where λ is the wavelength of the line in angstrom units and the magnetic field B is in kilogauss.

The broadening mechanisms in class b) are:

2.5. Doppler Broadening

The random motion of the emitting atoms or ions gives rise to Doppler broadening. If the atoms or ions have a Maxwellian velocity distribution then the emitted profile is Gaussian with a half width w given by:

$$w = 2 \left(\frac{2kT \ln 2}{Mc^2} \right)^{\frac{1}{2}} \cdot \lambda \qquad (2.4)$$

where M is the mass of the atom or ion and T is the atom or ion temperature. A shift of the profile will also result if the plasma is moving in the direction of the line sight. The magnitude of the shift d is given by:

$$d = \pm \frac{v_p}{c} \qquad (2.5)$$

where $\pm v_p$ is the plasma velocity

2.6. Radiative Transfer

Besides the broadening mechanisms discussed above a spectral line can also be broadened, or more correctly distorted, by the processes which occur as the line radiation passes through the plasma. The equation of radiative transfer for a medium which can absorb and emit radiation is:

$$dI_\nu(x) = \epsilon_\nu(x)dx - k_\nu(x)I_\nu(x)dx \qquad (2.6)$$

Here $I_\nu(x)$ is the intensity of radiation with frequency ν incident at a point x in the plasma. $dI_\nu(x)$ is the change in $I_\nu(x)$ over a distance dx measured along the direction of $I_\nu(x)$. $\epsilon_\nu(x)$ is the emission coefficient of the plasma and includes both spontaneous emission and scattering. $k_\nu(x)$ is the absorption coefficient, including stimulated emission (negative absorption). In a collision dominated plasma the scattering of radiation is usually negligible (except, possibly, for resonance lines) because electron collisions ensure that the absorption of a photon is unlikely to be followed by its re-emission. For a homogeneous plasma, assuming that scattering and continuous emission are negligible, the emission coefficient in the vicinity of a spectral line is given by:

$$\epsilon = \frac{h\nu}{4\pi} A_{21} N_2 L(\nu) \qquad (2.7)$$

where A_{21} is the transition probability for the line, N_2 is the population density of the upper state of the line, and $L(\nu)$ is the emission profile of the line. The absorption coefficient in the vicinity of a line, including stimulated emission is given by:

$$k_\nu = \frac{\pi e^2}{mc} f_{12} N_1 \left(1 - \frac{g_1}{g_2} \frac{N_2}{N_1} \right) L'(\nu) \qquad (2.8)$$

where it has again been assumed that the plasma is homogeneous. In (2.8) f_{12} is the absorption oscillator strength for the line, N_2, g_2 and N_1, g_1 are the population densities and statistical weights of the upper and lower states of the line respectively, and $L'(\nu)$ is the absorption profile of the line. In a collision dominated plasma the profiles $L'(\nu)$ and $L(\nu)$ are equal and are determined by one or more of the broadening mechanisms outlined in (2.2. - 2.5.).

It is the presence of the self absorption term in (2.6) which destroys the proportionality between the profile of a line emitted by an individual atom or ion in the plasma and the profile (of the same line) which emerges from the plasma.

To assess the importance of self absorption it is usual to calculate the optical depth at the line centre, τ_o. For a homogeneous plasma τ_o is given by:

$$\tau_o = k_{\nu_o} S \qquad (2.9)$$

$$\tau_o = \frac{\pi e^2}{mc} \cdot f_{12} \cdot N_1 \cdot \left(1 - \frac{g_1}{g_2} \cdot \frac{N_2}{N_1}\right) \cdot L(\nu_o) \cdot S \qquad (2.10)$$

where ν_o is the frequency of the line centre and S is the geometrical depth of the plasma. Absorption of the line will be negligible if τ_o satisfies:

$$\tau_o \ll 1$$

Alternatively, the absorption will be large if τ_o satisfies:

$$\tau_o \gg 1$$

For small, but non-negligible, optical depths the overall shape of the profile is not greatly affected, Burgess (3). However, because the absorption is largest near the peak of the line the height of the profile is reduced and the apparent half width increased. Roberts (22) shows that provided τ_o is less than 0.4 the half width of a Lorentzian profile is increased by less than 10%.

When τ_o is large the profile which emerges from the plasma besides being broadened by absorption may bear little

resemblance to that emitted by an atom or ion. Only on the line wings, where the absorption is small, will the shape be determined solely by the broadening mechanisms (2.2 - 2.5).

2.7. Instrumental Broadening

Although this chapter is concerned with broadening mechanisms which may occur within the plasma, it is fitting to consider at this point the broadening introduced by the instrument which is used to observe the line profile. For obvious reasons this broadening mechanism is referred to as instrumental broadening.

Instrumental broadening is caused by the finite resolution of the instrument used to make the profile observations. If $T(\lambda)$ is the true profile emitted by the plasma, $A(\lambda)$ is the instrument profile then the measured profile is related to these by the convolution integral:

$$M(\lambda) = \int_{-\infty}^{\infty} T(x)\, A(\lambda - x)\, dx \qquad (2.11)$$

2.8. Superposition of Broadening Mechanisms

When more than one broadening mechanism is responsible for the profile of a line, then providing the mechanisms are statistically independent, the resulting profile can be obtained by calculating the profiles corresponding to each mechanism.

separately and then using the convolution integral (2.11) to obtain the total profile. For a discussion of the case where the broadening mechanisms are not statistically independent see Griem (1) and the references therein. It should be noted that the broadening resulting from self absorption can only be calculated by solving the equation of radiative transfer (2.6) for the plasma.

CHAPTER III

THE THEORY OF THE STARK BROADENING OF SPECTRAL LINES IN A PLASMA

3.1. Introduction

This chapter contains a brief review of the basic principles underlying the various theoretical treatments of Stark broadening. For a more detailed discussion of the theory of Stark broadening the reader is referred to the work of Baranger (4), Griem (1) and Burgess (5).

3.2. Classification of Stark Broadening Mechanisms

The interaction V between a charged perturber and an emitter is usually well represented by the first term in the multipole expansion of the interaction (Baranger (4)) i.e. by:

$$V = -\underline{d} \cdot \underline{E} \qquad (3.1)$$

where $\underline{d}$ is the dipole moment of the emitter and $\underline{E}$ is the electric field produced by the perturber at the centre of the emitter. If the emitter is an ion the zeroth order term should also be included in (3.1). There are basically

two mechanisms by which the interaction (3.1) can broaden a spectral line. They are:

3.2.1. Direct Perturbation of the Energy Levels

When an atom is immersed in an electric field its energy levels are split into their Stark components (see Foster (6)). The positions of the Stark components depend on the electric field strength and the Stark coefficients for the levels which are calculated using time independent perturbation theory. In a plasma the electric field acting on an emitter depends on the positions of the perturbers. If the motions of the perturbers can be neglected the broadening results from averaging the positions of the Stark components over all values of the electric field produced by the different perturber configurations. Alternatively, if the positions of the perturbers, and hence the electric field, is changing rapidly then the shifts of the Stark components which occur during the time the system is radiating produce phase shifts in the emitted radiation. These phase shifts produce a broadening and shifts of the line (see 3.5.2).

The essential feature of this broadening mechanism is that the perturbations do not change the state of the radiating system. Perturbations which produce no change of state are said to be adiabatic.

3.2.2. Perturbation Induced Transitions

In some circumstances the perturbations of the radiating system by the charged particles may induce the radiating electron to undergo a transition to a neighbouring state and thereby terminate the radiation. Since the life time of the level is effectively reduced, by the uncertainty principle, the level will be broadened. In contrast to the mechanism discussed in (3.2.1.) this broadening mechanism cannot be described in terms of the Stark coefficients and the electric field. Here the rate of change of the electric field is the important factor.

Perturbations which produce a change of state are said to be non-adiabatic.

3.3. Conditions for Adiabaticity

The condition for adiabaticity can be derived as follows; if the radiating electron is perturbed by a collision for a time t_c, the duration of a collision (see 3.4), then the uncertainty in the energy of the radiating electron ΔE is given by $\hbar/t_c$. Now if ΔE is much less than the energy separation $E_{\alpha\alpha'}$ between the state α which the radiating electron occupies and the neighbouring state α' to which the electron may make an induced transition, then the perturbation will be

adiabatic since the probability of the electron changing its state will be small. Hence the condition for an adiabatic perturbation is given by:

$$t_c \gg \hbar/E_{\alpha\alpha'} \tag{3.2}$$

If the converse of this inequality holds, then during the perturbation it will not be possible to determine which of the states the electron occupies and the probability for a transition will be large. Hence the condition for a non-adiabatic perturbation is:

$$t_c \ll \hbar/E_{\alpha\alpha'} \tag{3.3}$$

Evaluation of the condition (3.3) for ion and electron perturbers (see (5)) shows that in general ions give rise to adiabatic perturbations, whereas electrons can, and often do, give rise to non-adiabatic perturbations. This is because of the large ratio of electron to ion velocities.

3.4. Characteristic Times in Line Broadening Phenomena

3.4.1. Emitter

A Fourier analysis of the profile of a line shows

that if $\Delta\omega$ is the frequency separation from the line centre then the time scales which are of interest in the formation of this part of the profile are of the order $1/\Delta\omega$.

3.4.2. Perturber

The characteristic time for a collision, the so-called 'collision time' t_c is defined by:

$$t_c = \rho/v \qquad (3.4)$$

where ρ is the impact parameter and v the velocity of the perturber. Because of the large differences in the velocities of the ions and electrons in a plasma the collision times for these particles satisfy $t_c(\text{ions}) \gg t_c(\text{electrons})$.

3.5. The Quasi-Static and Impact Regime

The large difference in the collision times of ions and electrons in a plasma allows the broadening to be divided into two mathematically separate regimes. They are:

3.5.1. Quasi-Static Regime ($t_c \gg 1/\Delta\omega$)

In the Quasi-Static regime the duration of the collision is much longer than the times of interest in the formation

of the line, i.e.

$$t_c \gg 1/\Delta\omega \qquad (3.5)$$

and therefore the perturber motions can be neglected during the radiation processes. Since the adiabatic condition (3.2) will also be valid, the broadening takes place through the mechanism described in (3.2.1). Because of their long collision times this approximation is usually valid for the treatment of the ion broadening. However, on the line wings ($\Delta\omega$ large) the quasistatic approximation should also be valid for the electrons. It should be noted that this approximation will break down near the line centre ($\Delta\omega \sim 0$).

An outline of the method of calculating the broadening in this approximation has already been given in sufficient detail in (3.2.1) and will not, therefore, be discussed further.

3.5.2. The Impact Regime ($t_c \ll 1/\Delta\omega$)

In the impact regime the collison time is short compared with the times of interest in the formation of the line, i.e.

$$t_c \ll 1/\Delta\omega \qquad (3.6)$$

This condition is the inverse of that required for the validity of the quasistatic approximation. Since (3.6) will be best satisfied when $\Delta\omega \sim 0$, the impact regime will be most appropriate for the treatment of those parts of the profile close to the line centre.

Lorentz (see (7)) was the first to consider the impact regime in the treatment of line broadening phenomena. In order to calculate the profile of a pressure broadened line, Lorentz made the following assumptions:

a) The emitters and perturbers could be represented by classical oscillators and hard spheres respectively.

b) The collision time t_c was much less than the time between collision $1/\omega_c$, where ω_c is the collision frequency.

c) Each collision interrupted the oscillator completely.

Lorentz Fourier analysed the radiation emitted by the randomly interrupted oscillators and obtained the following result for the line profile, $I(\Delta\omega)$:

$$I(\Delta\omega) = \frac{1}{1 + \left(\frac{\Delta\omega}{\omega_c}\right)^2} \qquad (3.7)$$

This profile has since become known as the Lorentz profile and arises whenever the broadening takes place in the impact

regime. It is to be noted that this theory does not predict a shift of the line. From (3.7) the $\frac{1}{2}$ - $\frac{1}{2}$ width of the profile is ω_c, the collision frequency.

The result obtained by Lorentz illustrates the following point. In deriving the profile it was assumed that $t_c \ll 1/\omega_c$ However, ω_c was found to be equal to the $\frac{1}{2}$ - $\frac{1}{2}$ width of the line, so that the condition that the duration of the collision be much less than mean time between collisions, i.e. the collisions are separated in time, corresponds to the condition (3.6) for the impact regime.

Although the Lorentz impact theory can in certain circumstances predict the correct form of the profile the theory has the following defects;

a) The interaction mechanism is not specified, nor for that matter is the perturbation.

b) The radiation emitted during a perturbation is neglected.

c) Contrary to experimental evidence, the theory does not predict a shift.

In the so-called 'phase shift model' of Stark broadening, Weisskopf (see (7)) it is assumed that the collisions are separated in time, and that these collisions cause

phase shifts in the emitted radiation rather than interrupt the radiation completely. Thus the perturbations are assumed to be adiabatic and therefore the broadening takes place through mechanism (3.2.1). The form of the interaction is specified and the perturber motions are characterized by their impact parameters and velocities. In calculating the phase shifts Weisskopf assumes that only collisions resulting in phase shifts greater than unity are effective in broadening the line. These collisions are caused by perturbers with impact parameters less than ρ_w the Weisskopf radius. This cut-off on the impact parameter is made necessary by the fact that Weisskopf's expresssion for the width diverges at large impact parameters. The resulting profile is an unshifted Lorentzian with a half-width w given by:

$$w = N \int v f(v) \pi \rho_w^2(v) dv \qquad (3.8)$$

where N is the perturber density, v is the perturber velocity and f(v) the velocity distribution function. The linear dependence on density arises from the assumption that the collisions are separated in time.

Lindholm (see (7)) in his 'adiabatic impact theory' also made the same initial assumptions as Weisskopf. However,

by using a procedure similar to the impact approximation in modern line broadening theory (see below), he is able to avoid the upper cut-off on the impact parameter. Hence all phase shifts were considered. The resulting profile is a shifted Lorentzian with a $\frac{1}{2}$ - $\frac{1}{2}$ width w and shift d given by:

$$w = N\int[1 - \cos\phi(\rho,v)]\,dv \qquad (3.9)$$

$$d = N\int[\sin\phi(\rho,v)]\,dv \qquad (3.10)$$

where N is the perturber density, $\phi(\rho,v)$ is the phase shift produced by a single perturber with impact parameter ρ and velocity v, and $\int dv$ is given by:

$$\int dv = \int vf(v)dv \int 2\pi\rho\, d\rho$$

Equations (3.9) and (3.10) show that the width arises mainly from collisions producing phase shifts of $\sim \pi$ and the shift from collisions which produce phase shifts of $\sim \pi/2$. The absence of a shift in the Weisskopf theory therefore results from the neglect of collisions which produce small phase shifts.

Lindholm also calculates the shift to width ratio and shows that it is a constant dependent only on the interaction between the emitter and perturber. For lines exhibiting the

quadratic Stark effect the shift to width has a value of $\sqrt{3}$.

Although an improvement on previous calculations, the adiabatic impact theory of Lindholm has two major limitations. Firstly, the model obviously does not take into account non-adiabatic effects due to electron collisions. Secondly, the model assumes that the collisions are separated in time. In a plasma this assumption is invalid because the long range nature of the Coulomb interaction results in many simultaneous perturbations of an emitter.

Both these difficulties are resolved by the formulation of the so-called 'Modern' line broadening theory by Baranger (8), and Kolb and Griem (9). The basis of this theory is the impact approximation.

3.5.3. The Impact Approximation

The impact approximation assumes that a time interval Δt (essentially an observation time) can be found such that the following conditions are satisfied:

a) The distribution of perturbers around the emitter at the beginning and end of the interval Δt are statistically independent.

b) Δt is so short that the wave functions of the emitter remain substantially unaltered.

For condition a) to be satisfied Δt must be longer than the electron correlation time, i.e.

$$\Delta t > 1/\omega_p \qquad (3.11)$$

where ω_p is the electron plasma frequency. Condition b) will be satisfied if the collisions are weak (i.e. collisions which have only a small effect on the emitter wave function) or alternatively, if Δt is much less than time between strong collisions (i.e. collisions which have a large effect on the emitter wave functions). If, at the worst, the line width results entirely from strong collisions, which terminate the emission completely, then the Lorentz impact theory (3.5.2) shows that the $\frac{1}{2}$-$\frac{1}{2}$ width w is equal to the collision frequency. Hence the interval between strong collisions is $\sim 1/w$ and condition b) will be satisfied provided:

$$\Delta t < 1/w \text{ (w is in angular frequency units)} \qquad (3.12)$$

From (3.11) and (3.12) the validity condition for the impact approximation is:

$$w \ll \omega_p \qquad (3.13)$$

The condition (3.13) can be identified with that for impact regime (3.6). Since $\omega_p \sim v_t / \rho_D$ where v_t is the thermal velocity of the perturbers and ρ_D is the Debye radius, (3.13) can be re-written as:

$$\frac{\rho_D}{v_t} \ll \frac{1}{w} \qquad (3.14)$$

But ρ_D is the largest impact parameter for a perturber (because of shielding for $\rho > \rho_D$ (see 3.6)) so that the left hand side (3.15) corresponds to the maximum duration for a collision. Consequently when the impact approximation is valid:

$$t_c \ll 1/w$$

It should be noted that (3.13) can be over-restricted since the perturbers which cause most of the broadening are not necessarily those with $\rho \sim \rho_D$.

As seen above, the weak collision assumption is of central importance in the impact approximation. A collision will be weak, in the sense discussed above, when:

$$Vt_c \ll \hbar \qquad (3.15)$$

where the interaction V is given by (3.1), t_c is the duration of a collision, and h is Plancks constant. The dipole moment in (3.1) can be estimated by $ea_o n^2$, where n is the principal quantum number of the upper state of the line, and the electric field due to a perturber by e/ρ^2, t_c is given by (3.4). Hence, the condition (3.15) for a weak collision becomes:

$$\rho v \gg \frac{e^2 a_o n^2}{\hbar} \sim 0.2\, n^2 \qquad (3.16)$$

Thus it is seen that the weak collision assumption is best satisfied for distant high velocity perturbers.

When the impact approximation is valid, i.e. the collisions are weak, the cumulative effects of many collisions are required to disturb the emitter appreciably. Because these collisions are weak their effect on the emitter can be calculated using a time dependent perturbation theory in which only the first non-vanishing term in the perturbation expansion need be retained. It is then found that the effects of many simultaneous perturbations are scalarly additive. Thus, the cumulative effect of N perturbers interacting with the emitter for time Δt can be found by calculating the average effect of a single perturber in time Δt and then multiplying by N. If, during the time Δt a strong collision

occurs then condition b) will not be satisfied. However, as seen above, when the impact approximation is valid, strong collisions are rare events. Thus when a strong collision occurs the weak collisions which are occurring at the same time can be ignored and only one perturber, the strong one, need be considered. Providing the weak collisions give the dominant contribution to the width then it is sufficient to estimate the strong collision contribution by assuming that these collisions completely interupt the emitter. The additional width can then be calculated from a Lorentz-Weisskopf type theory, i.e. Eqn (3.8).

It is found that when the perturbation calculation, for the effect on the emitter of the interaction with a single perturber, is evaluated the result can be expressed in terms of the so-called S matrix (see Baranger (loc. cit.)). This matrix contains all the information concerning the phase (adiabatic effects), and amplitude changes (non-adiabatic effects) of the wave functions produced by the weak collisions. In order to evaluate S a further approximation is usually made.

3.5.4. The Classical Path Approximation

Although the S-matrix can be evaluated using quantum mechanics, it is usual to make the 'classical path approximation'.

This approximation assumes that:

a) The perturbers can be treated as classical particles moving along well-defined trajectories.

b) The motion of a perturber remains undisturbed even when it interacts non-adiabatically with the emitter.

Condition a) will be valid if the perturber can be treated as a wave packet whose extent is negligible in comparison with its impact parameter, over the entire duration of the collision. Baranger (loc. cit.) shows that this is satisfied when the parameter satisfies:

$$\rho \gg \lambda \qquad (3.17)$$

where λ is the de Broglie wave length of the perturber. Essentially (3.17) says that the angular momentum of the perturber, about the emitter must be large. Condition b) will be valid when the energy ΔE transfered from the perturber to the emitter (an inelastic collision), or received by the perturber from the emitter (a super-elastic collision) is small compared with the incident energy E of the perturber. Thus the perturber can influence the emitter but the latter is assumed not to influence the perturber. This assumption

is usually referred to as the 'no back reaction' condition. If the energy E is identified with the mean thermal energy of the perturbers kT where T is the temperature of the plasma then the 'no back reaction' condition will be satisfied when:

$$kT \gg \Delta E \qquad (3.18)$$

Most non-adiabatic collisions lead to excitation, rather than de-excitation, of the radiating electron because cross-sections are usually much larger for the former process (Griem (1)). Hence ΔE corresponds to the energy separation between the state the radiating electron initially occupies and the next higher state.

It will be noted that when the condition (3.16), for a collision to be weak, is multiplied throughout by the mass of the perturber it is seen that the condition also corresponds to the angular momentum of the perturber being large. Consequently, when the impact approximation is valid the validity condition (3.17) for the classical path approximation will also be satisfied. Conversely, strong collisions arise from perturbers with small angular momenta for which the classical path approximation cannot be used. The effects produced by strong collisions must be calculated quantum mechanically.

These calculations would be extremely difficult because the Born approximation, which is applicable when the energy of the perturber is large in comparison with interaction energy, cannot be used. However, as stated previously, providing the weak collisions dominate the broadening a simple estimate of the strong collision contribution does not seriously affect the final result.

3.6. Debye Shielding and Ion-Ion Correlations

In the preceeding discussion it is assumed that the charged perturbers move independently of each other. However, because of the long range of the Coulomb interaction this assumption cannot be valid and interactions (or correlations) of the perturbers must be considered. The manner in which these interactions influence the ion and electron broadening are as follows:-

3.6.1. Ion Broadening

The interaction of an ion with its surrounding particles reduces the ion field strength and hence the amount of ion broadening. This reduction in field strength is caused by two effects. The first effect is Debye shielding whereby the cloud[1] of electrons, which on average surrounds and moves with an ion, screens the field of the ion. The second effect is

1) The term "cloud" is a statistical rather than physical concept since by charge neutrality the total number of electrons in the cloud can not exceed unity (in the case of a singly ionized plasma).

the repulsive interaction between the ions, usually referred to as 'ion-ion correlations', this effect corresponds to the screening of an ionic field by ions.

3.6.2. Electron Broadening

For the electron impact broadening the times of interest in the formation of the line (see 3.4.1) are usually so short that the ions are unable to move appreciably in these times. The ions, therefore, play no active part in the screening and simply act as a neutralizing background. The screening of a field due to an electron arises from the interactions with the surrounding electrons. In the study of line broadening phenomena it is usual to use the Debye approximation to calculate the electron shielding; however, see (5.3.5). The Debye approximation assumes, firstly, that the rapidly fluctuating potential, V(r) and charge density, in the vicinity of an electron, can be replaced by time averaged and smoothed values. Secondly, the electrostatic energies of the electrons are small compared with their thermal energies. In this approximation the potential V(r) due to an electron is given by:

$$V(r) = \frac{e}{r} \cdot \exp\left(\frac{-r}{\rho_D}\right) \qquad (3.19)$$

Assuming only electron shielding the Debye radius ρ_D is

given by:

$$\rho_D = \left[\frac{kT}{4\pi e^2 N_e}\right]^{\frac{1}{2}} \qquad (3.20)$$

Eqn (3.19) shows that for $r > \rho_D$, where r is the distance from the perturber, the potential, and hence the interaction, decreases rapidly. Thus when calculating the electron broadening of a spectral line, using a formalism which does not contain implicitly the effects of Debye shielding, care must be taken to exclude perturbers whose distance ρ from the emitter satisfies $\rho \gtrsim \rho_D$ otherwise the width and shift may be overestimated, or even diverge.

If $E_{\alpha\alpha'}$ is the energy separation between the levels α and α' then Debye shielding will be important when:

$$\omega_p \gtrsim \frac{E_{\alpha\alpha'}}{\hbar} \qquad (3.21)$$

where ω_p is the electron plasma frequency, and h Plancks constant. This result can be understood by considering the condition (3.3) for a perturbation induced transition, i.e. $\rho/v \lesssim \hbar/E_{\alpha\alpha'}$. Assuming that the important perturbers are those with the thermal velocity v_t then the maximum impact parameter a perturber can have and still induce a transition is given by:

$$\frac{\rho_{max}}{v_t} \sim \frac{\hbar}{E_{\alpha\alpha'}} \tag{3.22}$$

Now if $\rho_{max} \gtrsim \rho_D$ then according to the above discussion the perturbers with impact parameters satisfying $\rho_D \lesssim \rho \lesssim \rho_{max}$ are unlikely to produce transitions because the strength of their interaction is reduced by shielding. Hence, Debye shielding effects must be taken into account when $\rho_{max} \gtrsim \rho_D$, or from (3.22) when:

$$\frac{v_t \hbar}{E_{\alpha\alpha'}} \gtrsim \rho_D \tag{3.23}$$

Using $\frac{v_t}{\rho_D} \approx \omega_p$, (3.23) reduces to:

$$\omega_p \gtrsim \frac{\hbar}{E_{\alpha\alpha'}} = \omega_{\alpha\alpha'} \tag{3.24}$$

where $\omega_{\alpha\alpha'}$ is the frequency separation of the levels α and α'. Debye shielding will, therefore, be important when the plasma frequency is greater than the frequency separation between the levels α and α'. Conversely, Debye shielding will be negligible when the plasma frequency is much less than frequency separation between the levels α and α'.

3.7. The Classification of Lines and the Characterisation of their Profiles

In the line broadening literature the terms isolated lines, hydrogenic (or overlapping lines), and lines containing forbidden components often arise. These terms will now be defined and the factors which determine their profile will be briefly summarised. For simplicity it is assumed that only the upper level of the line is significantly broadened.

3.7.1. Isolated Lines

A line is described as isolated when its $\frac{1}{2}$-$\frac{1}{2}$ width w satisfies the condition:

$$w \ll \omega_{\alpha\alpha'} \qquad (3.25)$$

where $\omega_{\alpha\alpha'}$ is the unperturbed separation between the upper level of the line α and the nearest perturbing level α'. Assuming that the upper level of the line has an orbital angular momentum quantum number ℓ, the perturbing levels, for an isolated line, are determined by the parity selection rule $\Delta\ell = \pm 1$ and, for L-S coupling, $\Delta S = 0$.

If the line width in (3.25) is replaced by the splitting of the magnetic sublevels that would be produced by an electric field, then the condition for a line to be isolated is the same

as that for a line to be subject to the quadratic Stark effect. Hence, in a plasma, the splitting of the magnetic sub-levels of an isolated line, produced by the ion microfield, will be determined by the quadratic Stark effect. The broadening produced by this splitting is usually negligible in comparison with that produced by electron impacts. Since impact broadening produces a Lorentz profile (see 3.5.2.), the profile of an isolated line will be essentially Lorentzian with additional broadening, and some asymmetries, introduced by the overall shift of the magnetic sublevels in the ion microfield. In the absence of Debye shielding effects the width and shift of an isolated line are directly proportional to the electron density.

The Characterisation of the Profile of an Isolated Line

The Profile of an isolated line is characterised by the following Stark broadening parameters;

w = electron impact $\frac{1}{2}$-$\frac{1}{2}$ width (in wavelength units)

d = electron impact shift (" " ".)

α = ion broadening parameter

R = Debye Shielding parameter for the ion microfield

σ = a parameter which determines whether or not the ion broadening can be treated by the quasistatic approximation

These parameters are defined in Chapter V. If the quasistatic

approximation is valid for the ions ($\sigma > 1$) the profile of the line (in wavelength units) $I(\lambda)$ can be obtained from the so-called reduced profile $j_R(x, \alpha)$ using:

$$I(\lambda) = \frac{1}{w} j_R(x, \alpha) \qquad (3.26)$$

where

$$x = \frac{\lambda - \lambda_o - d}{w}$$

Here λ_o is the unperturbed wavelength of the line. If only half widths and shifts are required they can be calculated from:

$$w_T = [1 + 1.75\ \alpha\ (1 - 0.75.R)]w \qquad (3.27)$$

$$d_T = [d/w \pm 2.0\ \alpha\ (1 - 0.75.R)]\ w \qquad (3.28)$$

where w_T and d_T are the total $\frac{1}{2}$-$\frac{1}{2}$ width and shift respectively resulting from the electron and ion broadening. These equations are valid when $\alpha \leqslant 0.5$ and $R \leqslant 0.8$.

For the cases where the quasistatic approximation is not valid, i.e. when $\sigma < 1$ the reduced profiles $j(x, \alpha, \sigma)$, which are obtained using the adiabatic impact theory for the ions, should be used. Again, if only $\frac{1}{2}$-$\frac{1}{2}$ widths and shifts are required they can be obtained from:

$$w_T = (1 + 1.36\ \alpha^{8/9}\ \sigma^{-1/3})w \qquad (3.29)$$

$$d_T = (d/w \pm 2.36\ \alpha^{8/9}\ \sigma^{-1/3})w \qquad (3.30)$$

In this regime the line profile, resulting from the electron and ion broadening, is Lorentzian.

The reduced profiles $j_R(x, \alpha)$ and $j(x, \alpha, \sigma)$ are tabulated in (1) together with the line broadening parameters. However, more accurate values of the line broadening parameters than those given in (1) are tabulated in (6.10).

3.7.2. Hydrogenic (or Overlapping) Lines

If the upper level of a line is degenerate with respect to the orbital angular momentum quantum number the line is said to be hydrogenic. The Stark splitting of the magnetic sublevels of a hydrogenic line, produced by the ion microfield, are governed by the linear Stark effect. In contrast to isolated lines, the Stark splitting is the major factor in determining the overall shape of the profile. However, the detailed shape of the profile depends also on the electron impact broadening of the Stark components and since this broadening is of the same order as the Stark splitting the Stark components overlap (hence the name 'overlapping lines'). Another, and fundamental, difference between the broadening of an isolated and hydrogenic line is concerned with the perturbing levels. In the case of an isolated line the line radiation which arises from the perturbing levels falls in the region of the spectrum different to that of the line. For a hydrogenic line the perturbing levels and the levels which form the

upper state of the line are one and the same, i.e. the magnetic sublevels of the upper state split by the ion microfield. Consequently thelines originating from the perturbing levels also form the observed line. A perturbation induced transition, therefore, not only affects the radiation arising from the initial state but also that from the state into which the radiating electron is transfered. Hence the radiation from the two states will be correlated, and because of this, the electron impact broadening of a magnetic sublevel no longer produces a Lorentzian profile, but instead contains an asymmetry.

The half width of a hydrogenic line is proportional to $N_e^{\frac{2}{3}}$. This is because the Stark splitting of the line is proportional to the ion field strength, which is in turn proportional to $N_e^{\frac{2}{3}}$

The Characterisation of the Profile of a Hydrogenic Line

The profile of a hydrogenic line (in wavelength units) can be obtained from the so-called reduced profile $S(\alpha)$ by using:

$$I(\Delta\lambda) = S(\alpha)/F_o \qquad (3.31)$$

Here $\alpha = \Delta\lambda/F_o$ and is not to be confused with ion broadening parameters for an isolated line. $\Delta\lambda$ is the wavelength separation from the position of the unperturbed line, and F_o is the Holtzmark normal field strength. F_o is defined as the electric

field strength produced at the origin by an ion at a distance corresponding to the mean ion separation, i.e.,

$$F_o = [4\pi N_e/3]^{\frac{2}{3}} e \qquad (3.32)$$

Note that (3.32) is only valid for a singly ionized plasma.

Tabulations of the reduced profiles $S(\alpha)$ for a number of H and HeII lines are given in (1).

When only half widths are required they can be obtained from the relationship:

$$w = \left[N_e/C(N_e,T_e)\right]^{\frac{2}{3}} A^o \qquad (3.33)$$

where w is the half width of the line and $C(N_e,T_e)$ is coefficient that is only a weak function of the electron density and temperature These coefficients are also tabulated in (1).

3.7.3. Lines Containing Forbidden Components

Lines containing forbidden components arise when:

$$w \sim \omega_{\alpha\alpha'} \qquad (3.34)$$

where w and $\omega_{\alpha\alpha'}$ have already been defined in (3.7.1.). The

reasons for the appearance of the forbidden components may best be understood by considering the effect of increasing the electron density has on a line which may be considered to be isolated at low electron densities. When the electron density has increased to a value where the line width satisfies (3.34) the quadratic Stark effect, applicable to isolated lines, undergoes a transition to the linear effect. This transition is connected with the mixing of the wavefunctions of the levels α and α' by the ion field. A further result of the mixing is the breakdown of the parity selection $\Delta\ell = \pm 1$, and hence the appearance of forbidden components, corresponding to $\Delta\ell = 0$ or ± 2, at the expense of the intensity of the allowed component. The intensity of the forbidden component depends strongly on the degree of mixing, i.e. on the ion field strength which in turn depends on the electron density.

As the electron density is further increased the line, now comprising the allowed and forbidden components, will become hydrogenic.

The Characterisation of the Profiles of Lines with Forbidden Components

Because of the complex behaviour of lines containing forbidden components their profile must be calculated for each plasma condition, since scaling laws cannot be applied. Such calculations have only recently become available (see (11) and (12)).

CHAPTER IV

A REVIEW OF PREVIOUS INVESTIGATIONS OF THE STARK BROADENING OF HELIUM LINES

4.1. Introduction

Next to hydrogen lines, the lines emitted by neutral and ionized helium are the most suitable choice for experiments designed to test the predictions of the modern line broadening theory. This is because atomic matrix elements can be calculated with good accuracy (~5%) for helium and unperturbed energy levels are well known. The spectrum of neutral helium is also of considerable interest because it shows good examples of the types of line to which the modern line broadening theory has been applied, i.e. isolated lines, hydrogenic (or overlapping) lines, and lines which are neither isolated nor hydrogenic such as lines containing forbidden components.

Besides being a useful test of the modern line broadening theory the Stark broadening of helium lines has a practical application in the diagnosis of laboratory plasmas. Such lines are especially useful in the study of plasmas at temperatures where hydrogen would be fully ionized, or at high densities where hydrogen lines are so wide that they might interfere with other lines under investigation. An accurate knowledge of the

Stark profile of the HeI resonance line is required in the method of determining its oscillator strength from the saturated emission profile, (Lincke (21)). Recently, the Stark profiles of HeI lines which contain forbidden components, have become important in connection with the so called 'plasma satellites' (see Baranger and Mozer (40)) which may be excited on each side of a forbidden line when strong non-thermal oscillations exist in a plasma.

Outside the laboratory, the Stark broadening of helium lines is of astrophysical interest; notably in the study of the surface gravities of B-type stars.

4.2. Previous Investigations of the Stark Broadening of Helium Lines

The modern line broadening theory, developed independently by Baranger (8) and Kolb and Griem (9) was first applied to the Stark broadening of helium lines by Griem and Shen (13) who considered the lines of HeII with wavelengths 4686 A^{o} and 3203 A^{o}. As these lines are hydrogenic the method of calculating the profiles was a direct extension of that used for hydrogen lines such as H_{β} (14); except that the straight line paths of the perturbing electrons were replaced by hyperbolic lines to account for the Coulomb interaction between the ion and the individual perturbers. The accuracy of these calculations, which were made for a range of densities and temperatures, was expected to be $\sim 10\%$.

The preceding calculations were followed by those of Griem, Baranger, Kolb and Oertel (10) (usually referred to as the G.B.K.O. theory) who applied the theory to the Stark broadening of isolated neutral helium lines. Stark broadening parameters for 24 lines were calculated and the accuracy of the calculations was expected to be $\sim 20\%$.

G.B.K.O. compared their calculated half widths with the measurements of Wulff (15) which had been made a number of years before the introduction of the modern theory. Wulff used a pulsed arc and time integrated photographic recording

to obtain the profiles of a large number of neutral helium lines. The electron density in the arc was determined from the volume of the discharge, the initial pressure and the degree of ionization. Relative line intensities were used to determine the electron temperature. G.B.K.O. found that the electron densities, obtained from the measured half widths using their calculated parameters, only deviated by $\pm$ 10% from the mean value of $2.5 \times 10^{16} cm^{-3}$. This electron density is ~ 20% below that quoted by Wulff. The shifts were then calculated using the new electron density and were found to agree with the measured shifts to within the experimental accuracy. G.B.K.O. also analysed the measured half widths using the adiabatic theory of Lindholm (see(7)). The densities obtained using the adiabatic theory deviated by up to a factor of 1.5 from their mean value. Also the measured shift to width ratios were much less than the value of $\sqrt{3}$ predicted by the adiabatic theory.

Using the electron density above, G.B.K.O. also calculated the complete profiles of one isolated line (the HeI 4713 ^{o} line) and one line with a forbidden component (the HeI 3965A^{o} line). The resulting profiles were compared with those measured by Wulff and good agreement was found.

The first experimental attempts to verify the line broadening calculations for HeI and HeII lines were made by Berg et al (16) using a T-tube. Electron densities were measured from absolute continuous intensities and electron temperatures from line to continuum ratios, or from relative line intensities. Typical electron densities were $\sim 1.4 \times 10^{17} cm^{-3}$ and the temperatures were between 2×10^4 °K and 4.9×10^4 °K depending on the line under investigation. Shot-to-shot scanning was used to obtain the profiles. The measured and theoretical half widths, for both HeI and HeII lines, agreed to within 10%. However, the measured shifts were found to be systematically smaller than the calculated values. The poor agreement for the shifts was thought to be due either to inhomogeneities in the plasma, the neglect of electron correlations (Debye shielding) in the calculation of the shifts, or that for some of the lines the transition from the quadratic to the linear Stark effect occurs at lower ion field strengths than expected.

For one of the HeII lines measured by Berg et al, the HeII 4686A° line, a blue shift of ~ 1A° was found. At the time this shift was attributed to the so called 'plasma polarization shift'. However, a number of objections were raised to this interpretation, e.g. Burgess and Cooper (17), and

later measurements by Berg (18) failed to reproduce the earlier results. Instead, two SiIII lines were found on the blue wing of the line. Besides this result, Berg also measured the profile of the HeII 4686A° line for densities ranging from 10^{17} - 4 x 10^{17} cm^{-3}. Good agreement was found for the complete profile.

In the measurements of isolated lines discussed so far no attempt was made to cover a range of densities. Measurements of the half widths of isolated lines, over a range of densities were made by Botticher et al (19) using a stationary arc. Profiles were recorded photographically and electron densities and temperatures were obtained from absolute continuous measurements and relative line intensities respectively. Half widths and shifts were measured for densities ranging from 3 x 10^{15} - 3 x 10^{16} cm^{-3}. However, in a later publication (20) it is mentioned that for electron densities greater than 10^{16} cm^{-3} the measured half widths were systematically underestimated owing to an error in the photographic procedure. For densities less than 10^{16} cm^{-3} the measured half widths were generally in agreement with theory and also showed the expected linear dependence on density. The shifts are more interesting since they should not have been affected by the error in the photographic procedure. At low densities the

measured shifts were generally in good agreement with theory and most of the lines showed a linear increase with density. However, at higher densities significant departures from linearity occurred, the measured shifts being less than the theoretical values. These departures increased with density. Although no explanation was given by the original workers, this behaviour is consistent with the expected effects of Debye shielding (see 3.6).

An investigation of the asymptotic wing formula for isolated lines given by G.B.K.O. (see 5.2.1) and the asymmetries of these lines has been made by Roder and Stampa (20). Measurements were made at 3 different densities 3.8×10^{15}, 7.2×10^{15} and 1.7×10^{16} cm^{-3} using procedures similar to Botticher et al (19), except that the profiles were recorded photoelectrically. From these measurements two parameters were deduced. Firstly, from the measured slope of the wings the exponent n in the asymptotic wing formula, $I \propto \Delta\lambda^{-n}$ was obtained. Here I is the wing intensity and $\Delta\lambda$ the wavelength separation from the line centre. For the wing opposite that to which the line is shifted the value of n is 2 and for the other wing n gradually approaches the value 7/4. Secondly, the ion broadening parameter α can be obtained by measuring the asymmetry of the profiles. Measurements of n were made for a total of 11 lines

and α for 7 lines. The overall agreement was good except for a discrepancy of a factor of$\sim$2 in the value α for the HeI line at 4713A^{o}.

Lincke (21) re-evaluated the measurements of the half widths of isolated HeI lines made by Berg et al (loc. cit.), using the line broadening parameters calculated by Griem (1). He assumed that ion broadening could be treated by the quasi-static approximation. The results showed that the theoretical half widths were too large by typically $\sim$ 10%, but in some cases by as much as 16%. Measurements made by Lincke confirmed these results. Lincke thought that these discrepances probably resulted mainly from the neglect of the time dependence of the ion field which tends to over-estimate the width and possibly also from the neglect of Debye shielding in the calculations of the Stark broadening parameters.

Griem (1) also appliedthe G.B.K.O. theory to the Stark broadening of the isolated lines of singly charged ions. Measurements of the half widths of these lines (see Roberts (22)) revealed large discrepancies, up to a factor of 10, in the half widths. In an effort to explain these results, the G.B.K.O. theory was examined in some detail; notably by Oertel (23) and Roberts (22). Oertel's work led to a number of improvements of the theory as applied to the isolated lines of neutral

atoms. He found that the functions a(z) and b(z) (see (10)) used by G.B.K.O., to calculate the Stark broadening parameters, were numerically inaccurate. Oertel derives corrected functions and used them to calculate the Stark broadening parameters for the HeI 5876A° including Debye shielding. Later, Oertel (24) extended this work by including also the lower state broadening and the next higher term in the multipole exapnsion of the interaction, i.e. the quadrupole term. These calculations were performed for the four HeI lines at 5876A°, 3889A°, 4713A° and 5016A°. Although Oertel did not make a detailed comparison with the experimental widths available in the literature, he did note that the generally smaller widths predicted by his calculations were in better agreement with the experiments of Lincke than were those of Griem.

Profiles of lines with forbidden components have been measured by Wulff (15) and Sadjian et al (25). These measurements were made at a single density. Measurements of the half widths of such lines, over a range of densities, have been made by Botticher et al (loc.cit.), and Hermel and Seliger (26). However, theoretical profiles and half widths with which to compare the above measurements were not available. The only calculations, using the modern line broadening theory, of the complete profile of line with a forbidden components was reported in the G.B.K.O. paper and have already been commented on.

4.3. Proposed Theoretical and Experimental Investigations

The above review indicates the situation, with regard to the theoretical and experimental investigations of the Stark broadening of helium lines, at about the time the work to be described in this thesis was commenced. The following points were thought to be of especial interest and form the topics to be discussed in this thesis.

4.3.1. Theoretical Investigation

Stark broadening parameters for isolated HeI lines which have been calculated using the accurate a(z) and b(z) functions, and other modifications in the G.B.K.O. theory such as Debye shielding etc., were available for only four lines (24). Whether or not these parameters are an improvement over the original ones of G.B.K.O. (10) and Griem (1), is not yet known since a detailed comparison between theory and experiment does not appear to have been made. The following investigation was therefore undertaken by the present author:

a) Stark broadening parameters were calculated for a number of isolated HeI lines (mainly those for which experimental widths and shifts are available) and the results compared with the calculations of other workers.

b) The widths, shifts and ion broadening parameters obtained from the calculations were compared with experimental values.

c) The Stark broadening parameters for 16 isolated HeI lines were calculated.

The above work is described in Chapters V and VIand comprise the first part of this thesis.

4.3.2. Experimental Investigation

During the period that the theoretical investigation mentioned above was in progress the author was engaged in the design and construction of a Z-pinch pre-ionization discharge for a theta pinch. Measurements of the properties of the plasma generated in the Z-pinch, when operating in helium, suggested that the device might be suitable for use as a spectroscopic light source for the study of the Stark broadening of helium lines. With the purpose of investigating this possibility, whilst at the same time making a contribution to the knowledge of the Stark broadening of helium lines, the experiments to be outlined below were proposed.

As mentioned in the review a number of experimental investigations have been made of the Stark broadening of HeII lines and good agreement with theory was found. However, these measurements

have been made at electron densities greater than 10^{17} cm^{-3} and although there is no reason to believe that the theoretical profiles should not be just as accurate at lower electron densities it is important to confirm that this is indeed so.

It was also mentioned in the review that the measurements of the profiles of lines with a forbidden component have been made, at a fixed electron density, by a number of workers (see (15) and (25)). The variation with electron density of the half-width of such a profile has also been reported (see (26). But for astrophysical applications, such as the determination of the surface gravities of stars, it is the variation of the profile with electron density which is most important. As seen in the review no such investigation has been reported.

In view of the above discussion the following experimental investigations were undertaken:

a) The measurement of the Stark broadening of HeII lines at electron densities of $\lesssim 10^{16}$ cm^{-3}

b) The investigation of the variation with electron density of the profile of a line which contains a forbidden component.

These investigations comprising Chapters VII to XII form the second part of this thesis.

CHAPTER V

THE G.B.K.O. THEORY OF THE STARK BROADENING OF ISOLATED HeI LINES

In this chapter a review is given of the G.B.K.O. theory (1) of the Stark broadening of isolated HeI lines. Recent improvements to this theory will also be discussed.

The G.B.K.O. theory contains the following assumptions:

a) The impact approximation is valid, i.e. weak collisions dominate the broadening, and the motions of the perturbers can be treated by the classical path approximation.

b) The model of the atom is that of a single electron moving in a central potential. Fine structure is neglected. Thus the theory will predict the same widths for the lines of a multiplet.

c) Only the first term in the multipole expansion of interaction $V(t)$ between emitter and perturber is retained, i.e.

$$V(t) = - \underline{d} \cdot \underline{E}(t) \qquad (5.1)$$

where $\underline{d}$ is the dipole moment of the atom and $\underline{E}(t)$ is the total electric field of the perturbers at the centre of the atom.

5.1. Electron Impact Broadening of Isolated HeI Lines

As is usual with an impact theory, the profile of an isolated line broadened by electron impacts is Lorentzian. The profile, normalised to $\int I(\omega)\, d\omega = 1$, of a line arising from a transition from upper state α to lower state β is given by:

$$I_\alpha(\omega) = \frac{w}{\pi}\left[w^2 + (\omega - \omega_{\alpha\beta} - d)^2 \right]^{-1} \qquad (5.2)$$

where w and d are the electron impact $\frac{1}{2} - \frac{1}{2}$ width and shift of the line respectively, and $\omega_{\alpha\beta}$ is the unperturbed frequency of the line.

In the G.B.K.O. theory w and d, for the level α, are related to the corresponding diagonal matrix element of the operator Φ by:

$$w + id = \langle\alpha|\Phi|\alpha\rangle \qquad (5.3)$$

The operator Φ contains all the information concerning the effects of weak collisions on the emitter. Φ is related to the S matrix for a single electron collision by:

$$\langle\alpha|\Phi|\alpha\rangle = N_e \int v f(v)\, dv \int 2\pi\rho\, d\rho \left(1 - \langle\alpha|S|\alpha\rangle\right)_{AV} \qquad (5.4)$$

where $(\quad)_{AV}$ corresponds to an average over all orientations of a collision. The factor $(1 - \langle\alpha|S|\alpha\rangle)$ is evaluated by means of a perturbation expansion. The first order term vanishes (as do all the odd order terms for all multiples of the multipole expansion, Burgess (34)) when the angular average is performed. Of the even order terms only the second is retained. This so called second order dipole term is given by:

$$\frac{e^2}{\hbar} \sum \langle \alpha | r_\sigma | \alpha' \rangle \langle \alpha' | r_\nu | \alpha \rangle \int_{-\infty}^{\infty} dt_1 \int_{-\infty}^{t_1} dt_2 \cdot \exp\left[i\, \omega_{\alpha\alpha'} (t_1 - t_2)\right] \times E_{1\sigma}(t_1)\, E_{1\nu}(t_2) \tag{5.5}$$

when $\langle \alpha | r_\sigma | \alpha' \rangle$ etc. are components of the radial matrix elements connecting the upper state of the line α to a perturbing level α', $\omega_{\alpha\alpha'}$ is the angular frequency separation of the levels α and α'. The components $E_1(t_1)$ etc. of the electric field at times t_1 and t_2 due to a perturber as it moves from position $\underline{r}_1(t_1)$ to position $\underline{r}_1(t_2)$, are obtained from:

$$\underline{E}_1(t) = e\, \underline{r}_1(t)/r_1^3(t) \tag{5.6}$$

where the path of the perturber is given by:

$$\underline{r}_1(t) = \rho + \underline{v}t$$

After performing the integrations over time and the average over angles, (5.5) reduces to:

$$(1 - \langle\alpha|S|\alpha\rangle)_{AV} = \frac{2}{3}\left(\frac{\hbar}{m\rho v}\right)^2 \sum_{\alpha'} R^2_{\alpha\alpha'} \left[A(z_{\alpha\alpha'}) + iB(z_{\alpha\alpha'})\right] \tag{5.7}$$

where $z_{\alpha\alpha'} = \omega_{\alpha\alpha'}\rho/v$ and A(z) is expressed in terms of the K_o and K_1 Bessel functions:

$$A(z) = z^2\left[K_o^2(|z|) + K_1^2(|z|)\right] \tag{5.8}$$

The function B(z) is related to A(z) by a principle value integral:

$$B(z) = \frac{2zP}{\pi}\int_o^\infty \frac{A(z)}{z^2 - z'^2}\, dz'$$

The term $R^2_{\alpha\alpha'}$ in (5.7) stands for $|\langle\alpha|\underline{R}|\alpha'\rangle|^2$ where $\underline{R}$, the radius vectors of the atomic electron, is now in atomic units. It is worth noting at this point that term matrix element, used by G.B.K.O. for $\langle\alpha|\underline{R}|\alpha'\rangle$ is misleading since $\langle\alpha|\underline{R}|\alpha'\rangle$ is not symmetric in the initial and final state. $\langle\alpha|\underline{R}|\alpha'\rangle$ is in fact related to the standard radial integral for the

oscillator strength of the transition $\alpha \longrightarrow \alpha'$ (see ((6.3)).

After substituting (5.7) in (5.4), performing the integration over the impact parameter, and substituting the result in (5.3) the electron impact weak collision width and shift are found to be given by:

$$w + id = \frac{4\pi}{3}\left(\frac{\hbar}{m}\right)^2 N_e \int \frac{f(v)}{v}\, dv \sum_{\alpha'} |\langle \alpha | \underline{R} | \alpha' \rangle|^2 \left[a(z_{\alpha\alpha'}^{min}) + ib(z_{\alpha\alpha'}^{min})\right] \tag{5.9}$$

where

$$z_{\alpha\alpha'}^{min} = \frac{\omega_{\alpha\alpha'}\rho_{min}}{v} \tag{5.10}$$

and the function a(z) and b(z) which arise from the ρ integration are given by:

$$a(z) = \int_z^\infty \frac{A(z')}{z'}\, dz' \,, \quad b(z) = \int_z^\infty \frac{B(z')}{z'}\, dz'$$

Although the ρ integral in (5.4) is convergent at the upper limit ($\rho_{max} = \infty$) it diverges at the lower limit. The divergence occurs because at small ρ the collisions become strong and higher order terms in the expansion of the S matrix should be

included. Instead G.B.K.O. cut-off the ρ integration at an impact ρ_{min} defined by:

$$(1 - \langle\alpha|S|\alpha\rangle)_{AV} \sim 1 \tag{5.11}$$

and from (5.7)

$$\rho_{min}^2 \approx \tfrac{2}{3} \left(\frac{\hbar}{mv}\right)^2 \sum_{\alpha'} |\langle\alpha|\underline{R}|\alpha'\rangle|^2 \left[A(z_{\alpha\alpha'}^{min}) + iB(z_{\alpha\alpha'}^{min})\right] \tag{5.12}$$

The reason for this choice of cut-off can be seen by considering the expression for the S matrix given by Baranger (4), i.e.

$$\langle\alpha|S|\alpha\rangle = \exp(-\eta_\alpha - i\varphi_\alpha) \tag{5.13}$$

where η_α is a real positive number associated with inelastic collisions and φ_α is a real phase shift associated with elastic collisions. Now suppose the collisions are strong and mainly inelastic, so that η_α is large and $\varphi_\alpha \sim 0$, then from (5.13) $\langle\alpha|S|\alpha\rangle$ will be ~ 0. Alternatively, if the strong collisions are mainly elastic so that φ_α is large and $\eta_\alpha \sim 0$ then (5.13) will oscillate rapidly between ± 1 and the mean value be zero.

The above cases are obviously limiting. In general there is no true division between strong inelastic and strong elastic collisions. Consequently both types of collision will be contained in the strong collision term. However, it seems reasonable to take (5.11) as the condition for a strong collision.

Expression (5.9) therefore gives the $\frac{1}{2} - \frac{1}{2}$ width arising from weak inelastic collisions and the shift arising from weak elastic collisions. The weak elastic contribution to the width is contained in higher order terms which are not considered by G.B.K.O. These terms are usually, but not always, smaller than the weak inelastic contribution.

To account for strong collisions, G.B.K.O. assume that all collisions with $\rho < \rho_{min}$ interrupt the emitter completely. These collisions do not give rise to a shift because shifts are caused by small phase changes (see 3.5.2). The contribution to the $\frac{1}{2} - \frac{1}{2}$ width arising from strong collisions is therefore estimated by the Lorentz-Weiskopf theory (see 3.5.2), i.e.

$$w_s = N_e \int v f(v) dv \pi \rho_{min}^2 (v) \qquad (5.14)$$

As the strong collision cut-off procedure is somewhat arbitrary G.B.K.O. try to minimize the uncertainty by choosing ρ_{min}

such that the expressions for the width and shift reduce to two well defined limits; the so called high and low temperature limits.

5.1.1. High Temperature Limit

With increasing electron temperature, and hence increasing perturber velocity, the weak collision condition will be satisfied for increasingly smaller impact parameters. Consequently ρ_{min} will tend to zero with increasing temperature. Thus in the high temperature limit the strong collision term is negligible and the width and shift are given by:

$$w + id = \frac{4\pi}{3} \left(\frac{\hbar}{m}\right)^2 N_e \int \frac{f(v)dv}{v} \sum_{\alpha'} |\langle \alpha | \underline{R} | \alpha' \rangle|^2 \left[\ln(|z_{\alpha\alpha'}|)^{-1} \pm \frac{i\pi}{2} \right] \tag{5.15}$$

5.1.2. Low Temperature Limit

At low electron temperatures, and hence small perturber velocities, the adiabatic impact theory of Lindholm (see 3.5.2) is valid. This theory is only strictly valid for an S-state because in it the influence of the Stark effect on the magnetic sub-levels is neglected. Also the adiabatic assumption is not strictly valid because super elastic collisions can occur

even for small perturber velocities. However, both these effects should be small and G.B.K.O. give the following expression for the width and shift in the low temperature limit:

$$w + id = \left(\frac{\pi}{2}\right)^{5/3} \cdot \frac{\Gamma(\frac{1}{3})}{3^{2/3}} \cdot \left(\frac{\hbar}{m}\right)^{4/3} \cdot N_e \left[\sum_{\alpha'} \frac{|\langle \alpha | \underline{R} | \alpha' \rangle|}{\omega_{\alpha\alpha'}}\right]^{2/3} \cdot \langle v^{\frac{1}{3}} \rangle_{AV} \cdot (1 \pm i\sqrt{3}) \tag{5.16}$$

G.B.K.O. obtain agreement with these two limits by choosing different cut-offs for the width and shift. The final expression for the electron impact width and shift of an isolated HeI line is:

$$w + id = N_e \int f(v)dv \left\{ \pi v \rho_{min}^2(v) + \frac{4\pi}{3v} \left(\frac{\hbar}{m}\right)^2 \sum_{\alpha'} |\langle \alpha | \underline{R} | \alpha' \rangle|^2 \left[a(z_{\alpha\alpha'}^{min}) + ib\left(\tfrac{3}{4} z_{\alpha\alpha'}^{min}\right)\right]\right\} \tag{5.17}$$

where ρ_{min} is defined by:

$$\rho_{min}^2 = \tfrac{2}{3} \left(\tfrac{3}{4}\right)^{-3/2} \left(\frac{\hbar}{mv}\right)^2 \left| \sum_{\alpha'} |\langle \alpha | \underline{R} | \alpha' \rangle| \left[A(z_{\alpha\alpha'}^{min}) + iB(z_{\alpha\alpha'}^{min})\right] \right| \tag{5.18}$$

The functions $a^{(z)}$, $b^{(z)}$, $A^{(z)}$ and $B^{(z)}$, as calculated by G.B.K.O., are given in (1); however, see (5.3.1). It should be noted that in obtaining (5.17) the integration over ρ is extended to infinity, thus Debye shielding is neglected. Equations (5.17) and (5.18) are used by G.B.K.O. to calculate the electron impact $\frac{1}{2}$ - $\frac{1}{2}$ width and shift to width ratio for 24 isolated HeI lines.

The matrix elements are calculated by taking an average of hydrogenic values, and values obtained using hydrogen-like wave functions in which either the charge, or the principal quantum number (i.e. the Coulomb approximation (see (1)) are adjusted to give measured bound state energies.

Broadening and shift of both the upper and lower states are taken into account by adding the widths and subtracting the shifts of upper and lower states.

In the calculations of HeI line broadening parameters, made by Griem (1), the matrix elements are calculated using the Coulomb approximation. Debye shielding and lower state broadening and shift are neglected.

5.2. Ion Broadening of Isolated HeI Lines

In the G.B.K.O. theory the ion broadening is treated by two approximations:

a) The Quasi-Static approximation (valid for small ion velocities).

b) The Adiabatic impact approximation (valid for large ion velocities).

To assess which of these approximations is applicable in a given situation G.B.K.O. introduced a parameter σ which they defined as the ratio of the characteristic time for an ion perturber t_c to that of line radiation t_r i.e. $\sigma = t_c/t_r$

From (3.5) and (3.4.1)

$$\sigma = \frac{\rho_i}{v_i} \Delta\omega$$

G.B.K.O. assume that ρ_i is given by the mean ion separation, v_i by the mean ion velocity $\bar{v}_i$, and $\Delta\omega$ by the electron impact $\frac{1}{2}$-$\frac{1}{2}$ width w (expressed in angular frequency units). Hence:

$$\sigma = \frac{w}{v_i} \left[\frac{4\pi N_e}{3}\right]^{-\frac{1}{3}} \qquad (5.19)$$

Here it is assumed that the plasma is single ionized. From (3.5.1) the quasi-static approximation is valid where $t_c >> t_r$ or in terms of the above parameter, when $\sigma > 1$. Conversely, the adiabatic impact approximation is valid when $\sigma < 1$.

However, by comparing the line profiles obtained using the quasi-static approximation for the ions with those obtained by taking into account the time dependence of the ion field (see 5.2.2) for $\sigma \sim 1$, Griem (1) has demonstrated that the quasi-static approximation gives an adequate representation of the profile even when $\sigma = 1$. Hence the quasi-static approximation is valid when $\sigma \geqslant 1$.

5.2.1. Quasistatic Approximation ($\sigma \geq 1$)

In the absence of ion broadening, the electron impact profile of a line arising from a transition from an upper state α to a lower state β is given by (5.2). To calculate the ion broadening G.B.K.O. assume that the broadening produced by the Stark splitting of the magnetic sub-levels is negligible compared with electron impact broadening. Thus the ion broadening is assumed to result entirely from the over all Stark shift of the magnetic sub-levels. Since an isolated line is subject to the quadratic Stark effect (see (3.7.1)), the shift $\Delta\omega_\alpha$ of the level α, produced by an ion field of strength F, is given by:

$$\Delta\omega_\alpha = C_\alpha F^2 \qquad (5.20)$$

where the shift is measured from the unperturbed position of the line $\omega_{\alpha\beta}$, and C_α is the quadratic Stark coefficient of the level α, averaged over the magnetic sub-levels of the level α. C_α is given by:

$$C_\alpha = \frac{1}{3}\left(\frac{\hbar}{me}\right)^2 \sum_{\alpha'} \frac{|\langle\alpha|\underline{R}|\alpha'\rangle|^2}{\omega_{\alpha\alpha'}} \qquad (5.21)$$

Taking the unperturbed position of the line as the origin of the frequency ω, the equation of the line (5.2) in the presence

of an ion field F becomes:

$$I_\alpha(\omega) = \frac{w}{\pi}\cdot\left[w^2 + (\omega - C_\alpha F^2 - d)^2 \right]^{-1} \qquad (5.22)$$

The complete profile is then obtained by averaging the profile (5.22) over the distribution W(F) of the ion field, i.e.

$$I_\alpha(\omega) = \frac{w}{\pi}\cdot\int \frac{W(F)dF}{w^2 + (\omega - C_\alpha F^2 - d)^2} \qquad (5.23)$$

Equation (5.23) is simplified by introducing the following parameters:

$$\beta = F/F_o$$

where F_o is the Holtzmark normal field strength (see (3.7.2)), the ion broadening parameter which is defined by:

$$C_\alpha F_o^2 = w\alpha^{4/3}$$

or using (5.21), (5.29):

$$\alpha = \frac{4\pi N_e}{3}\cdot\left[\frac{1}{3w}\cdot\left(\frac{\hbar}{m}\right)^2\cdot\sum_{\alpha'}\frac{|\langle\alpha|\underline{R}|\alpha'\rangle|^2}{\omega_{\alpha\alpha'}} \right]^{\frac{3}{4}} \qquad (5.24)$$

and:

$$x = (\omega - d)/w$$

The so-called reduced profile is then obtained, i.e.

$$j(x,\alpha) = \frac{1}{\pi} \int \frac{W(\beta)\,d\beta}{1 + (x - \alpha^{4/3}\beta^2)^2} \qquad (5.25)$$

G.B.K.O. evaluated $j(x,\alpha)$ using for W(F) the Holtzmark distribution function (which neglects the effects of Debye shielding of the ion field and ion-ion correlations) for various values of α and for $-2 \leqslant x \leqslant 5$. For values of x greater than those given above G.B.K.O. derive the following asymptotic wing formula::

$$j(x,\alpha) = \frac{1}{\pi x^2} + \frac{3d}{4x^{7/4}} \quad \text{for } x/\alpha > 0 \qquad (5.26)$$

$$j(x,\alpha) = \frac{1}{\pi x^2} \quad \text{for } x/\alpha < 0 \qquad (5.27)$$

These formulae show that as a consequence of the ion broadening the profiles will be asymmetric, the asymmetry being on the wing towards which the line is shifted. This asymmetry arises because there is a finite probability of an ion coming extremely

close to the emitter and thereby creating a huge electric field. Such fields can shift the line a considerable distance from its unperturbed position.

Griem (27) later obtained improved reduced profiles by using ion field strength distribution functions calculated by Baranger and Moser (28). These functions, which include the effects of Debye shielding and ion-ion correlations, depend on a parameter R, the ratio of the mean ion separation and the Debye radius, i.e.

$$R = \frac{\rho_m}{\rho_D} = \left(\frac{4\pi}{3} N_e\right)^{-\frac{1}{3}} \left(\frac{kT_e}{4\pi e^2 N_e}\right)^{\frac{1}{2}} \qquad (5.28)$$

$$= e(4\pi)^{1/6} 3^{1/3} N_e^{1/6} (kT_e)^{-\frac{1}{2}}$$

The reduced profiles are represented by $j_R(x,\alpha)$ and can be found in (1). For values of x greater than those given in the tables in (1) the asymptotic wing formula can still be used since the wings of the line are formed by single perturbers coming extremely close to the emitter. For such perturbers shielding and correlation effects are obviously negligible.

By inspection of the reduced profiles $j_R(x,\alpha)$ Griem obtained approximate expressions for the $\frac{1}{2}$ - $\frac{1}{2}$ width and shift of an isolated line broadened by both ions and electrons. These expressions are given in (3.7.1)

5.2.2. Adiabatic Impact Theory ($\sigma \ll 1$)

At low densities and high temperatures the quasistatic approximation may no longer be valid for the ions. G.B.K.O. treat this regime ($\sigma \ll 1$) by assuming firstly, that the perturbations produced by the ions do not overlap in time, so that their interactions are scalarly additive. Secondly, at the line centre, the perturbations are adiabatic, so that the broadening and shift are due to phase shifts in the emitted radiation. They also neglect the splitting of the magnetic sublevels by the ion field. For the case $\sigma \ll 1$ G.B.K.O. obtain the following results for the total $\frac{1}{2}$ - $\frac{1}{2}$ width W_T and shift d_T resulting from electron and ion broadening:

$$w_T = (1 + 1.36\, \alpha^{8/9}\, \sigma^{-1/3})w$$

$$d_T = (\frac{d}{w} \pm 2.36\, \alpha^{8/9}\, \sigma^{-1/3})w$$

where w and d are the electron impact $\frac{1}{2}$ - $\frac{1}{2}$ width and shift respectively, and α is the ion broadening parameter. In this limit the line profile is Lorentzian. For the case $\sigma \leq 1$ reduced profiles $j(x, \alpha, \sigma)$ are calculated for various values of α and σ. These profiles can be found in (1). If x is larger than the values given in the tables, the asymptotic wing formula (5.26) and (5.27), can be used.

5.3. Improvements to the G.B.K.O. Theory

A number of improvements have been made to the G.B.K.O. theory; notably by Oertel (23,24) and Cooper and Oertel (29). In essence, most of the improvements correspond to the inclusion of higher order effects in the calculation of the electron impact broadening. The overall structure of the theory remains unaltered. The improvements are as follows:

5.3.1. a(z) and b(z) Functions

Oertel (23) found numerical inaccuracies in the a(z) and b(z) functions used to calculate the Stark broadening parameters for isolated HeI lines by G.B.K.O., and later by Griem (1). For both functions the errors are positive, and amount to $\sim 5\%$ at a(0.1) increasing to $\sim 40\%$ at a(2.0). Similarly for b(z) the errors are $\sim 2\%$ at b(0.1) and $\sim 20\%$ at b(2.0). Thus the errors will be most significant when z is large, i.e. low electron temperatures or large $\omega_{\alpha\alpha'}$

Whereas G.B.K.O. obtained a(z) numerically Oertel was able to derive the following analytic expression:

$$a(z) = |z| \; K_0(|z|) \; K_1(|z|) \qquad (5.29)$$

where the K_n are modified Bessel functions.

5.3.2. Multipole Expansion

Oertel (24) and Coopper and Oertel (loc. cit), included the quadrupole term in the multipole expansion of the interaction V(t) i.e. the quadrupole term. The expression for the interaction including this term is:

$$V(t) = \frac{e^2}{\underline{r}} \left[\frac{\underline{R}.\underline{r}}{\underline{r}^2} + 3 \frac{(\underline{R}.\underline{r})^2 - \underline{r}^2\underline{R}^2}{2\,\underline{r}^4} \right] \qquad (5.30)$$

where $\underline{R}$ is the radius vector of the atomic electron in atomic units, and $\underline{r}$ the radius vector of the perturber, with the emitter as the origin. With this additional term the S matrix for a single collision (5.7) becomes:

$$(1 - \langle\langle \alpha|S|\alpha\rangle\rangle)_{AV} = \tfrac{2}{3}\left(\frac{\hbar}{m\rho v}\right)^2 \sum_{\alpha'} R^2_{\alpha\alpha'} \left[A(z_{\alpha\alpha'}) + iB(z_{\alpha\alpha'})\right] + \frac{1}{10}\left(\frac{a_o}{\rho}\right)^2 \sum_{\alpha''} R^4_{\alpha\alpha''} \left[A_4(z_{\alpha\alpha''}) + iB_4(z_{\alpha\alpha''})\right] \qquad (5.31)$$

where $R^2_{\alpha\alpha'} = \langle\alpha|\underline{R}|\alpha'\rangle^2$, and $R^4_{\alpha\alpha''} = \langle\alpha|\underline{R}^2|\alpha''\rangle^2$, $A_4(z)$ and $B_4(z)$ are functions which arise from the quadrupole term in (5.30) and are analogous to the dipole functions $A(z)$ and $B(z)$, the perturbing levels α'' being determined by the quadrupole selection rules $\Delta\ell = 0, \pm 2$. The expression for the width and shift becomes:

$$w + id = N_e \int vf(v)dv \left\{ \frac{4\pi}{3} \left(\frac{h}{mv}\right)^2 \sum_{\alpha'} R^2_{\alpha\alpha'} \left[a(z^{min}_{\alpha\alpha'}) + ib(z^{min}_{\alpha\alpha'})\right] + \frac{\pi}{5} a_o^2 \left(\frac{h}{mv}\right)^2 \frac{1}{v^2} \sum_{\alpha''} \omega_{\alpha\alpha''} R^4_{\alpha\alpha''} \left[a_4(z^{min}_{\alpha\alpha''}) + ib_4(z^{min}_{\alpha\alpha''})\right]\right\} \quad (5.32)$$

where $a_4(z)$ and $b_4(z)$ are analogous functions to $a(z)$ and $b(z)$ and z^{min} is identical with that given in (5.1) but with ρ_{min} defined by putting $(1 - \langle\alpha|S|\alpha\rangle)_{AV} = 1$ in (5.31). The inclusion of the second order quadrupole term therefore, gives additional contributions to the weak inelastic width and weak elastic shift. With regard to the latter there exists some confusion in the literature. Sahal-Brechot (30) states that the quadrupole term is zero for the shift. This would of course conflict with the above result. However, an examination of the equations in (30) shows that the latter author is refering to the first order quadrupole which does indeed vanish in the impact regime (see 5.1). The second order quadrupole was not considered in her calculation of the shifts.

5.3.3. Inclusion of the Lower State Broadening and Shift

When the broadening and shift of both the upper and lower state are considered G.B.K.O. show that the result (5.4), for the upper state only, should be replaced by:

$$w + id = N_e \int v f(v) dv \int 2\pi \rho d\rho \; (1 - \langle \alpha | S | \alpha \rangle \langle \beta | S^* | \beta \rangle)_{AV} \quad (5.33)$$

where S* is the complex conjugate of S, and β refers to the lower state. However, to include the lower state broadening and shift in their tabulated Stark broadening parameters. G.B.K.O. did not use (5.33) but instead, calculated the width and shift of the upper and lower states of the line separately using (5.17). To obtain the total broadening and shift the widths are added and the shifts subtracted. This procedure overestimates the strong collision contribution to the width because ρ_{min} should be defined by:

$$(1 - \langle \alpha | S | \alpha \rangle \langle \beta | S^* | \beta \rangle)_{AV} \sim 1 \quad (3.34)$$

rather than by the application of (5.11) separately to the upper and lower state. If ρ_{min} is calculated from (5.34), and only the dipole term is included in the interaction then it is correct to add the widths and subtract shifts of the upper and lower states.

However, if the quadrupole term is present Cooper and Oertel (loc. cit.) show that an interference term is present in the expression for the width. This so called quadrupole interference term arises from elastic collisions and is negative

It therefore reduces the width. The appearance, and the nature, of the interference term can be understood by considering the expression (5.13) for the S matrix. The S matrix for the upper state α is :

$$\langle \alpha | S | \alpha \rangle = e^{-\eta_\alpha \quad -i\phi_\alpha} \tag{3.35}$$

but for weak collisions η_α and ϕ_α are small so that (5.35) can be written as:

$$\langle \alpha | S | \alpha \rangle \quad = 1 - \eta_\alpha \quad - i\phi_\alpha$$

Similarly for the lower state

$$\langle \beta | S^* | \beta \rangle \quad = 1 - \eta_\beta \quad \mp i\,\phi_\beta$$

Hence:

$$1 - \langle \alpha | S | \alpha \rangle \langle \beta | S^* | \beta \rangle \quad = \eta_\alpha + \eta_\beta \quad \mp i(\phi_\alpha \quad - \phi_\beta) \tag{5.36}$$

$$- \eta_\alpha \eta_\beta \quad - \phi_\alpha \phi_\beta$$

When (5.36) is averaged over angles the inelastic interference term $\eta_\alpha \eta_\beta$ vanishes because the inelastic broadening of the

upper and lower states are statistically independent. However, the elastic interference term $\phi_\alpha \phi_\beta$ will not vanish because, during a collision, the same polarizing field will act on the upper and lower states. Hence the width and shift will be given by:

$$w \sim \eta_\alpha + \eta_\beta - \phi_\alpha \phi_\beta \qquad (5.36)$$

$$d \sim \phi_\alpha - \phi_\beta \qquad (5.37)$$

Incidentally, (5.36) and (5.37) show that, in the absence of the interference term, the widths of the upper and lower states can be added and the shifts subtracted.

5.3.4. Back Reaction

For low temperatures or large perturbing level separations, the no 'back reaction' condition (3.19), in the classical path approximation, will not be satisfied. An analogous situation occurs in the Coulomb excitation of nuclei by the impacts of charged particles. Alder et al (37) who made a theoretical study of Coulomb excitation, found that the effects of the 'back reaction' could be approximately taken into account by substituting for the perturber velocity v, occurring in the expressions for the classical cross-sections, some mean value of the initial

and final velocity v_i and v_f. The cross- sections thus obtained were found to be in good agreement with those obtained using a full quantum mechanical treatment, even for impact energies close to threshold. This procedure, referred to as 'symmetrization' has been applied to the G.B.K.O. theory by Oertel (loc. cit.) and Cooper and Oertel (loc. cit.) with a view to obtaining improved widths for HeI lines at temperatures where $kT_e \sim \hbar\omega_{\alpha\alpha'}$

The method is to 'symmetrize' the inelastic functions A(z) and a(z) by replacing $z_{\alpha\alpha'}$ with a 'symmetrized' version $\tilde{z}_{\alpha\alpha'}$ which is defined as follows. The expression for $z_{\alpha\alpha'}$ is re-written in the form:

$$\tilde{z}_{\alpha\alpha'} = \frac{\rho v\, \omega_{\alpha\alpha'}}{v^2} \qquad (5.38)$$

It is then argued that when the classical path approximation is valid the angular momentum of a perturber about the emitter must be large (see 3.54), and since the change in ℓ , $\Delta\ell$, in a single inelastic collision can only be $\Delta\ell = \pm 1$, it can be assumed that ℓ and hence ρv are constant for the collision. Following the symmetrization procedure given by Seaton (32) the term v^2 in (5.38) is replaced by $(v_i^2 + v_f^2)/2$, i.e.

$$\tilde{z}_{\alpha\alpha'} = \frac{\rho v_i \omega_{\alpha\alpha'}}{(v_i^2 + v_f^2)/2}$$

Conservation of energy requires that:

$$\frac{m}{2}\ (v_i^2 - v_f^2) = \hbar\omega_{\alpha\alpha'}$$

so that finally:

$$\tilde{z}_{\alpha\alpha'} = \frac{\rho v_i \omega_{\alpha\alpha'}}{(v_i^2 - \frac{\hbar\omega_{\alpha\alpha'}}{m})} \qquad (5.39)$$

The integration over perturber velocities, for terms containing $a(\tilde{z}_{\alpha\alpha'})$ is started at velocities satisfying $v_i^2 > 2\hbar\omega_{\alpha\alpha'}/m$, and also $A(\tilde{z}_{\alpha\alpha'}) = 0$ if $v_i^2 < \frac{2\hbar\omega_{\alpha\alpha'}}{m}$. For superelastic collisions the integration is started at $v_i = 0$. As the functions $b(z)$ and $B(z)$ correspond to elastic terms they are not symmetrized and the velocity integration is started at $v_i = 0$.

However, the $b(z)$ and $B(z)$ functions are indirectly affected by the symmetrization procedure through the dependence of z^{min} on ρ_{min} which in turn depends on $A(z)$ (see 5.12).

The major objection to this procedure is that when $kT_e \sim \hbar\omega_{\alpha\alpha'}$ only strong collisions can give inelastic effects and since these perturbers come close to the emitter their angular momentum will be small. For low temperatures, i.e. $z_{\alpha\alpha'}$ large Baranger ([4]) gives for ρ_{min} the following expression:

$$\rho_{min}^3 \sim \lambda\!\!\!^{-3}\, n^4 \,(2\epsilon/\hbar\omega_{\alpha\alpha'}) \qquad (5.40)$$

where $\lambda\!\!\!^{-}$ is the Broglie wavelength, n is the principal quantum number of the level α, and ϵ is the energy of the perturber. For n = 3 and $\epsilon \sim \hbar\omega_{\alpha\alpha'}$ (5.40) gives $\rho_{min} \sim 6\lambda\!\!\!^{-}$ or $\ell = 6$. Thus the angular momentum is certainly not large. However, Seaton (32) shows that even when $\ell = 5$ the symmetrized calculations (in his case cross-sections) are in good agreement with the full quantum mechanical calculations. Hence, even for small ℓ the symmetrized procedure should lead to improved widths for $kT_e \sim \hbar\omega_{\alpha\alpha'}$

5.3.5. Debye Shielding

In the expression (5.9), for the weak collision width and shift of an isolated line, the integration over the impact parameter ρ is extended from ρ_{min} to infinity. However, because of Debye shielding (see 3.6), the integration should be cut-off at an upper impact parameter ρ_D corresponding to the radius of the Debye sphere centred at the emitter. For isolated lines, the neglect of the Debye shielding can often be justified because the integration over ρ is convergent for $\rho < \rho_D$. But when $\omega_{\alpha\alpha'} \sim \omega_p$ (see 3.6), the neglect of Debye shielding will result in the width, and especially the shift, being over-estimated.

To include the effects of Debye shielding G.B.K.O. suggested, from empirical arguments, that the electric field of a perturber should be shielded. However, in order to avoid counting Debye shielding effects twice only one of the fields, in the expression (5.5) for the second order term of the single perturber S matrix, should be shielded. The shielded field $E_{1S}(t)$ is given in terms of the unshielded field (5.6) by:

$$E_{1S}(t) = E_1(t) \cdot \left[1 + \frac{\underline{r}_1(t)}{\rho_D}\right] \cdot \exp\left[\frac{-\underline{r}_1(t)}{\rho_D}\right] \qquad (5.41)$$

Rather than evaluate (5.5) with the shielded field (5.41) included, two unshielded fields are used by G.B.K.O. but a cut-off ρ_{max} the so called 'equivalent cut-off' is introduced, which is so defined, that an identical result is obtained. It is shown that ρ_{max} is given by:

$$\rho_{max} = 1.123\ \rho_D \qquad (5.42)$$

and is applicable to both the width and shift. In deriving this result G.B.K.O. make the following assumptions:

a) The splitting $\omega_{\alpha\alpha'}$ is small or v large so that the exponential in (5.5) can be neglected (this condition is equivalent to $z_{\alpha\alpha'}$ satisfying $z_{\alpha\alpha'} < 1$

b) The maximum and minimum impact parameters satisfy

$$\rho_{max} >> \rho_{min} \tag{5.43}$$

When Debye shielding is included the expression (5.9) for the weak collision width and shift becomes:

$$w + id = \frac{4\pi}{3}\left(\frac{\hbar}{m}\right)^2 N_e \int \frac{f(v)}{v}\, dv \sum |\langle \alpha | \underline{R} | \alpha' \rangle|^2 \left[a(z_{\alpha\alpha'}^{min}) - a(z_{\alpha\alpha'}^{max}) + ib(z_{\alpha\alpha'}^{min}) - ib(z_{\alpha\alpha'}^{max})\right] \tag{5.44}$$

where $z_{\alpha\alpha'}^{max}$ is defined by:

$$z_{\alpha\alpha'}^{max} = \frac{\omega_{\alpha\alpha'}}{v} \cdot \rho_{max} = 1.123 \cdot \frac{\omega_{\alpha\alpha'}}{v} \beta_D \tag{5.45}$$

Recalling that:

$$z_{\alpha\alpha'}^{min} = \frac{\omega_{\alpha\alpha'}}{v} \cdot \rho_{min}$$

then $z_{\alpha\alpha'}^{max}$ can be expressed in the form:

$$z_{\alpha\alpha'}^{max} = \frac{\rho_{max}}{\rho_{min}} \; z_{\alpha\alpha'}^{min}$$

The total width is obtained by adding the strong collision

width (5.14). For some collisions, notably those with small v condition b) above will not be satisfied and collisions with $\rho_{min} > \rho_{max}$ may occur in the theory. In order to prevent these unphysical collisions contributing to the width and shift, Oertel (loc. cit.) and Cooper and Oertel (loc. cit.) in their calculations require that ρ_{max} and ρ_{min} satisfy:

$$\rho_{max} = \max (\rho_{min}, \rho_{max})$$

and (5.46)

$$\rho_{min} = \min (\rho_{min}, \rho_{max})$$

Although giving a method of including Debye shielding, G.B.K.O. neglect such effects in the calculation of the Stark broadening parameters; as also did Griem (1) when he recalculated these parameters. The first, and to date the only, published line broadening parameters for isolated lines which include Debye shielding, using the above prescription are those of Oertel for the HeI lines at 3889, 5016, 5876 and 4713 A^{o}.

However, since the above calculations were published Chappel et al (33) have reconsidered the method of including Debye shielding. Using results taken from plasma kinetic theory they conclude that in the limit where the static Debye potential is valid (i.e. low velocities) both electric fields in (5.5) should be shielded. The equivalent cut-off then occurs at:

$$\rho_{max} = 0.682\ \rho_D \qquad (5.48)$$

Using quantum field theory Burgess (64) has recently resolved these conflicting results. Burgess's work shows firstly, that only one of the fields in (5.5) should be shielded. Secondly, that in line broadening problems it is never correct to use the static Debye potential. However, when Burgess reduces his expression for the width, which contains only one shielded field and the correct frequency dependent Debye potential, to the static limit the result is identical with that obtained using two shielded fields and a static Debye potential. He, therefore, concludes that although the conclusions of Chappel et al, regarding the shielding of both fields in the interaction, is incorrect their expression for the equivalent cut-off, is correct in the static limit. Burgess also shows that for the shift the G.B.K.O. value of the equivalent cut-off should be used.

5.3.6. Number of Perturbing Levels

The Stark broadening parameters calculated by G.B.K.O. take into account a maximum of five perturbing levels. Roberts (22), in a theoretical study of several ArII lines, shows that up to ~ 13 perturbing levels are required to ensure adequate convergence of the width and shift. In some instances

the direction of the shift can be particularly sensitive to the number of perturbing levels included in the calculations. This is because the shift, unlike the width, depends not only on the separations between the perturbing levels and the upper state of the line, but also on their relative positions. For example if the two nearest perturbing lie above and below the upper state of the line, and are separated equally from it, then the shifts produced by the perturbing levels will be equal and opposite and hence cancel. If another perturbing level is now included in the calculation then the shift produced will depend on whether this perturbing level lies above or below the upper state of the line. Consequently, if only a limited number of perturbing levels are included then the magnitude and direction of the calculated shift could possibly depend on the manner in which these levels are chosen.

5.4. Ion Broadening

The ion broadening parameter α defined by G.B.K.O. (see Eqn (5.24)) takes into account the broadening and shift of the upper state of the line only. The general expression for α , which takes into account both the broadening and shift of the upper and lower states of the line is:

$$\alpha = \frac{4\pi N_e}{3}\left\{\frac{1}{3w}\cdot\left(\frac{\hbar}{m}\right)^2\left[\sum_{\alpha'}\frac{|\langle\alpha|\underline{R}|\alpha'\rangle|^2}{\omega_{\alpha\alpha'}} - \sum_{\beta'}\frac{|\langle\alpha|\underline{R}|\alpha'\rangle|^2}{\omega_{\beta\beta'}}\right]\right\}^{\frac{1}{2}} \qquad (5.49)$$

where α and β are the upper and lower states of the line respectively. It can be seen from (5.49) that depending on the signs of the summations, α and hence the ion broadening can either be increased or reduced by the addition of the lower state. Which of these occurs depends on the level structure of the atom, i.e. on whether the important perturbing levels lie above or below the state

The ion broadening parameters calculated by Cooper and Oertel (24) are based on (5.49).

CHAPTER VI

THE CALCULATION AND COMPARISON WITH EXPERIMENT OF THE STARK BROADENING PARAMETERS OF ISOLATED HeI LINES

6.1. Introduction

This chapter is concerned with the author's calculations of the Stark broadening parameters of isolated HeI lines and the conclusions that can be drawn from a comparison of the results with previous calculations and experiments. In the final part of this chapter the Stark broadening parameters for 16 isolated lines, which have been calculated by the author, are given.

At the time these calculations were carried out the improvements to the G.B.K.O. theory, discussed in the preceding chapter, had been applied to only four isolated HeI lines, Oertel (24). The electron impact width and shift to width ratios (the ion broadening parameters were not calculated) of the four lines were calculated for a range of electron densities and temperatures. No attempt was made to compare the results with experiment. Since the publication of Oertel's calculations the method of including one of the improvements (Debye shielding) has been modified.

Recently Cooper and Oertel (29) have published the Stark broadening parameters (excluding shift to width ratios) of

eleven isolated HeI lines. With the exception of the 5016 A^{o} line the parameters were calculated for a single electron density ($N_e = 10^{16} cm^{-3}$) only. These calculations include all the improvements given in (5.3); indeed the details of the discussion in (5.3)is based mainly on a pre-print of this paper. However, although the authors were aware of the recent modifications to the method of including Debye Shielding, the procedure used in their calculations is the same as that used by Oertel. Consequently, the parameters calculated by Cooper and Oertel should be identical with those of Oertel. A comparison of the respective parameters confirms this conclusion. Cooper and Oertel did not compare their calculations with experiment.

6.2. Improvements Included in the Calculations

A computer programme, written by Roberts, (22) for the calculation of the Stark broadening parameters of isolated ArII lines, was used as the basis for the present calculations. Essentially, this programme evaluates the expression (5.17) given by G.B.K.O. for the width and shift of an isolated line, but neglects all of the improvements given in (5.3) except the last. With regards to the additional improvements, it was decided to include in the calculations only those improvements which are likely to be important for neutral helium lines; and in particular for those lines for which experimental data exists. The considerations leading to the choice of improvements will now be given.

Improvement 1) $a(z)$ and $b(z)$ functions; included.

The improved $a(z)$ and $b(z)$ functions are included in the calculations. Computational difficulties are also eased by this step since $a(z)$ can now be expressed analytically see (5.3.1)

Improvement 2) Multipole Expansion; Not included

The work of G.B.K.O. shows that most of the broadening of neutral helium lines is caused by distant perturbers. It follows therefore that since the dipole interaction varies as r^{-2} and the quadrupole interaction as r^{-3} the former will give

the major contribution. At low temperatures, or large $\omega_{\alpha\alpha'}$ close collisions are important and the quadrupole interaction may become significant. However, these collisions must be included in the strong collision term: the uncertainty in which (a factor of ~ 2) would outweigh any error resulting from the neglect of the quadrupole term. There is no strong collision term for the shift and here the neglect of the quadrupole interaction may be serious. In spite of the possible importance of the quadrupole contribution to the shift for the conditions mentioned above, this term was neglected in the calculations.

Improvement 3) Lower State Broadening and Shift; Not included

To a first approximation the ratio of the widths of the upper and lower states of a line is given by (see 5.1).

$$\frac{w_\alpha}{w_\beta} \sim \frac{|\langle \alpha |\underline{R}| \alpha' \rangle|^2}{|\langle \beta |\underline{R}| \beta' \rangle|^2} \cdot \frac{a(z^{min}_{\alpha\alpha'})}{a(z^{max}_{\beta\beta'})} \qquad (6.1)$$

where only the nearest perturbing level is considered and the integration over the velocity distribution has been neglected, as also has the strong collision terms which usually only contributes $\sim$ 20% to the broadening. As usual, the upper level of the line is denoted by α , and the nearest perturbing level by α', β and β' are the corresponding quantities for the lower

state and the z's are given by:

$$z^{min}_{\alpha\alpha'} = \frac{\omega_{\alpha\alpha'}}{v} \rho^2_{min}(\alpha) \ , \ z^{min}_{\beta\beta'} = \frac{\omega_{\beta\beta'}}{v} \rho^2_{min}(\beta)$$

It should be noted that if the broadening of the upper and lower state are treated correctly only one value of ρ_{min} results (see 5.3.3). However, to the approximation considered here it is sufficient to treat them separately.

The values of ρ_{min} are given approximately by (see 5.1)

$$\rho^2_{min}(\alpha) \sim \frac{|\langle\alpha|\underline{R}|\alpha'\rangle|^2}{v} \left| A(z^{min}_{\alpha\alpha'}) + iB(z^{min}_{\alpha\alpha'}) \right| \quad (6.2)$$

The expression for the lower state is similar. Usually A(z) and B(z) can be estimated by ~ 1 and 0 respectively. If n_α is the principal quantum number of the level α, $|\langle\alpha|\underline{R}|\alpha'\rangle|^2$ is of the order n^4_α and therefore (6.2) is given approximately by:

$$\rho^2_{min}(\alpha) \sim \frac{n^4_\alpha}{v}$$

and similarly for the lower level . Finally, the ratio of the width of the upper and lower level is:

$$\frac{w_\alpha}{w_\beta} \sim \frac{n^4_\alpha}{n^4_\beta} \frac{a(z^{min}_{\alpha\alpha'})}{a(z^{min}_{\alpha\alpha'})} \quad (6.3)$$

where z's are now given by:

$$z^{min}_{\alpha\alpha'} \sim \frac{\omega_{\alpha\alpha'}}{v^2} \cdot n^4_\alpha \, , \; z_{\beta\beta'} \sim \frac{\omega_{\beta\beta'}}{v^2} \; n^4_\beta \qquad (6.4)$$

For lines in the visible the neglect of the lower state broadening will be most serious for those lines originating from the n = 3 levels since the upper state broadening will be relatively small compared with the lines originating from levels with $n > 3$. Typical values of $\omega_{\alpha\alpha'}$ and $\omega_{\beta\beta'}$ for an n = 3 to n = 2 transition are ~ 500 cm^{-1} and $\sim 10^4$ cm^{-1} respectively and hence:

$$z_{\alpha\alpha'} \sim 0.1 \; z_{\beta\beta'}$$

When inelastic collisions are important $z_{\alpha\alpha'} < 1.0$, say $\sim .1$ then from the values of a(z):

$$a(z_{\alpha\alpha'}) \sim 8 \; a \; (z_{\beta\beta'})$$

If $z_{\alpha\alpha'}$ where larger then $a(z_{\beta\beta'})$ would be even smaller. Hence the ratio (6.3) is estimated to be:

$$\frac{w_\alpha}{w_\beta} \sim 40$$

The neglect of the lower state broadening should, therefore, produce errors of $\lesssim 3\%$ for lines originating from the $n = 3$ levels and considerably less for those from higher levels. But for the shift, the neglect of the lower level, may lead to larger errors. The ratio of the upper to the lower state shift is given by:

$$\frac{d_\alpha}{d_\beta} \sim \frac{|\langle \alpha | \underline{R} | \alpha' \rangle|^2}{|\langle \beta | \underline{R} | \beta' \rangle|^2} \frac{b(z_{\alpha\alpha'}^{min})}{b(z_{\beta\beta'}^{min})} \qquad (6.5)$$

In contrast with $a(z)$, $b(z)$ falls off slowly with increasing z. For $n = 3$ to $n = 2$ transitions:

$$\frac{d_\alpha}{d_\beta} \sim 10$$

and, errors of $\sim 10\%$ may be expected. But for lines originating from levels with $n > 3$ the error will be $\lesssim 2\%$.

Hence, except for possibly the shifts of lines originating from levels with $n = 3$, the neglect of the lower state broadening and shift should lead to errors of $\lesssim 3\%$.

Improvement 4) Back Reaction; Not included

The effects of the back reaction on the perturber motion can be neglected when (see 5.3.4).

$$kT_e >> \hbar \omega_{\alpha\alpha'}$$

Since all the experimental studies of isolated HeI lines have been made using plasmas with electron temperatures in excess of 10^4 °K see (Ch.IV), and the typical splittings for lines in the visible are $\lesssim 500$ cm^{-1} the ratio of kT_e to $\omega_{\alpha\alpha'}$ will be at least ~ 15. Thus the symmetrization procedure can be neglected for the nearest perturbing level, and since $\sim$ 80% of the line width is contributed by inelastic collisions to the nearest perturbing level, the procedure can be neglected for all the perturbing levels when $T_e \gtrsim 10^4$ °K

Improvement 5) Debye Shielding; Included

Debye shielding is important when (see 3.6)

$$\omega_{\alpha\alpha'} \lesssim \omega_p$$

Previous calculations of HeI Stark broadening parameters, which include Debye shielding Oertel (24), used the equivalent cut-off (see 5.3.5) $\rho_{max} = 1.12\, \rho_D$ for both the width and shift. The same cut-off procedure is also used in the recent calculations of Cooper and Oertel (29). Recent theoretical work by Burgess (see 5.3.5.) has shown that although the above value is correct for the shift, the cut-off for the width should be that equivalent

to shielding both electric fields in the expression for the width. Chappel et al (33) show that in this case the correct cut-off is $\rho_{max} = 0.682\,\rho_D$. It will be recalled that Burgess also concludes that the use of the static Debye potential, on which the above cut-offs are based, is never valid for electron impact broadening. Clearly, more work is required on the frequency dependence of the shielding, but from Burgess's and Chappel et al's papers it appears that the best approximation is to include Debye shielding using the second of the above cut-offs.

Improvement 6) Number of Perturbing Levels; Included

As the shifts can be particularly sensitive to the number of perturbing levels included in the calculation (see (5.3.6.)) this improvement is included in the calculations.

6.3. Modifications to the Stark Broadening Programme

Since the original version of the Stark broadening programme has been described in detail by Roberts (22) only the modifications made to this programme by the present author will be described. The modifications were made in order to include the improvements mentioned above.

The functions A(z) and a(z) are generated within the

programme using expressions (5.8) and (5.29) respectively. Expansions for the modified Bessel functions $K_o(|z|)$ and $K_1(|z|)$ in the range $0 \leq z \leq \infty$, are taken from (62). Previously these functions had been obtained by a linear interpolation of the values given by Griem (1).

Originally, the values of the functions B(z) and b(z) and also the expressions for their asymptotic expansions were taken from the paper by Oertel (23). This procedure was unsatisfactory because for the range $z \leq 5.0$ the functions were only presented in a graphical form, from which it was difficult to obtain accurate values. Later, the numerical values of these functions given by Cooper and Oertel (29), were used. However, this modification produced a negligible change in the calculated parameters. Values of B(z) and b(z), intermediate to those given by Cooper and Oertel, were obtained by graphical interpolation, and the number of points entered into the programme was such that values of the functions could be obtained with sufficient accuracy by a linear interpolation.

As the programme was already capable of handling a large number of perturbing levels, improvement 6) was included without the need to modify the programme.

Neglecting the quadrupole interaction, lower state broadening and shift, and the correction for the back reaction

but including Debye shielding, the electron impact width and shift of an isolated line originating from a level α is given by:

$$w + id = N_e \int f(v)dv \left\{ \pi v \ \rho^2_{min}(v) + \frac{4\pi}{3} \left(\frac{\hbar}{m}\right)^2 \right.$$
$$\sum_{\alpha'} |\langle \alpha | \underline{R} | \alpha' \rangle|^2 \left[a(z^{min}_{\alpha\alpha'}) - a(z^{min}_{\alpha\alpha'}) \right.$$
$$\left. \left. + ib(\tfrac{3}{4} z^{min}_{\alpha\alpha'}) - ib(\tfrac{3}{4} z^{max}_{\alpha\alpha'}) \right] \right\}$$

where:

$$z^{min}_{\alpha\alpha'} = \frac{\omega_{\alpha\alpha'} \rho_{min}}{v} \quad , \text{ and } z^{max}_{\alpha\alpha'} = \frac{\omega_{\alpha\alpha'} \rho_{max}}{v}$$

with ρ_{min} and ρ_{max} given by:

$$\rho^2_{min}(v) = \tfrac{2}{3}(\tfrac{3}{4})^{-3/2} \left(\frac{\hbar}{mv}\right)^2 \left| \sum_{\alpha'} |\langle \alpha | \underline{R} | \alpha' \rangle|^2 \right. \tag{6.7}$$
$$\left. \left[A(z^{min}_{\alpha\alpha'}) + iB(z^{min}_{\alpha\alpha'}) \right] \right|$$

$$\rho_{max} = 0.682 \ \rho_D \quad \text{for the width}$$

$$= 1.12 \ \rho_D \quad \text{for the shift}$$

where all the quantities appearing in the expressions have been defined in (5.1). With the above choice for ρ_{min} designated 'cut-off 1' the expressions for the width and shift reduce correctly to the high and low temperature limits (see 5.1.1 & 5.1.2). Provision was also made in the programme to include another minimum impact parameter cut-off designated 'cut-off 2' defined by:

$$2\rho_{min}^2(v) = \frac{2}{3}\left(\frac{\hbar}{mv}\right)^2 \left| \sum_{\alpha'} |\langle\alpha|\underline{R}|\alpha'\rangle|^2 \left[A(z_{\alpha\alpha'}^{min}) + iB(z_{\alpha\alpha'}^{min})\right] \right| \qquad (6.8)$$

and the factor $\frac{3}{4}$ appearing in the b(z) functions in (6.6) are omitted. Only the high temperature limit is obtained using this procedure. Cut-off 2 and $\rho_{max} = 1.12\rho_D$ for both the width and shift were used by Oertel when calculating the line broadening parameters given in (24).

The velocity integration was also modified. For terms corresponding to inelastic transitions, i.e. terms containing A(z) and a(z), the integration was started at the threshold velocity $v_{\alpha'}$ corresponding to each perturbing level, i.e.

$$v_{\alpha'} = \left[\frac{2\hbar\omega_{\alpha\alpha'}}{m}\right]^{\frac{1}{2}}$$

These functions were put equal to zero for electron velocities below threshold. For super elastic collisions the velocity integration was started at zero velocity. This modification had a negligible effect on the calculated parameters.

The matrix elements occurring in (6.6), (6.7) and (6.8) are calculated from the expressions:

$$|\langle\alpha|\underline{R}|\alpha'\rangle|^2 = (\ell + 1)(2\ell + 3)\sigma^2 \quad \text{for} \quad \ell + 1$$
$$= (2\ell - 1)\sigma^2 \quad \text{for} \quad \ell - 1$$

where ℓ is the orbital angular momentum quantum number and σ is the radial factor (in atomic units), which is defined by:

$$\sigma^2 = \frac{1}{4\ell_>^2 - 1}\left[\int R_{n\ell}(r) \cdot R_{n',\ell'}(r) r dr\right]^2$$

where $\ell_>$ is the larger of ℓ and ℓ' and the $R_{n\ell}(r)$ are the normalised radial wavefunctions of the jumping electron multiplied by r. σ is calculated within the programme using the Coulomb approximation (see (1)). Energy levels were taken from Martin (35).

Finally the ion broadening parameter α and the Debye Shielding parameter $\underline{R}$ for the ion field were calculated from (5.24) and (5.28) respectively, and the parameter σ was calculated from (5.19) using for v_i the mean relative ion velocity (assuming $T_i = T_e$).

6.4. Verification of the Accuracy of the Calculated Stark Broadening Parameters

In order to verify that the neglect of the lower state broadening and shift, quadrupole interaction, and the back reaction on the perturber does not lead to serious errors the programme was used to re-calculate the Stark broadening parameters of the four HeI lines that had previously been calculated by Oertel (24). Oertel's calculations included all the modifications given in (5.3). However, he also used for ρ_{min} cut-off 2, and $\rho_{max} = 1.12\ D$ for both the width and shift. The cut-offs ρ_{min} and ρ_{max} in the present programme were, therefore, made temporarily the same as those used by Oertel.

Table (6.1) lists the $\frac{1}{2}$-$\frac{1}{2}$ widths and shift to width ratios obtained using the programme. Oertel's results are shown in brackets. Values of α cannot be compared as they do not appear to have been calculated by Oertel. It can be seen that the widths are in excellent agreement over the entire range of densities and temperatures. The largest discrepancy is $\sim 4\%$ for the 4713 A^{o} line, whereas typical discrepancies are $\lesssim 2\%$, and appear to be random in nature. At the highest temperature quoted in Table (6.1), the shifts are also in agreement to better than 10% but for the lines at 3889 A^{o} and 5016 A^{o} the agreement becomes poorer as the electron temperature decreases.

TABLE (6.1) COMPARISON OF OERTELS PARAMETERS AND THOSE CALCULATED USING THE PROGRAMME DESCRIBED IN SECTION (6.3) OERTELS VALUES ARE SHOWN IN BRACKETS

TRANSITION	$\lambda(A^o)$	T (^oK)	10^{15}		10^{16}		10^{17}		10^{18}	
			w(A^o)	d/w	w(A^o)	d/w	w(A^o)	d/w	w(A^o)	d/w
$2^3S - 3^3P$	3889	10,000	1.08-2	.56	1.08-1	.54	1.08	.48	10.2	.31
			(1.06-2	.77)	(1.06-1	.73)	(1.06	.66)	(10.0	.45)
		20,000	1.14-2	.43	1.14-1	.41	1.14	.37	10.9	.25
			(1.14-2	.52)	(1.14-1	.51)	(1.14	.45)	(10.9	.32)
		40,000	1.14-2	.33	1.14-1	.33	1.14	.30	11.1	.21
			(1.16-2	.36)	(1.16-1	.35)	(1.16	.32)	(11.3	.23)
$2^1S - 3^1P$	5016	10,000	3.53-2	-.50	3.51-1	-.45	3.24	-.32	23.7	-.19
			(3.55-2	.45)	(3.54-1	-.38)	(3.26	-.26)	(23.9	-.12)
		20,000	3.27-2	-.40	3.26-1	-.36	3.06	-.26	24.5	-.15
			(3.30-2	-.39)	(3.29-1	-.33)	(3.09	-.24)	(24.9	-.13)
		40,000	2.96-2	-.31	2.95-1	-.28	2.82	-.20	23.9	-.11
			(3.03-2	-.33)	(3.02-1	-.28)	(2.88	-.20)	(24.5	-.12)
$2^3P - 3^3P$	5876	10,000	1.65-2	-.35	1.65-1	-.34	1.65	-.29	15.7	-.13
			(1.67-2	-.35)	(1.67-1	-.33)	(1.67	-.28)	(15.7	-.13)
		20,000	1.70-2	-.17	1.70-1	-.16	1.70	-.13	16.4	-.02
			(1.71-2	-.18)	(1.71-1	-.16)	(1.70	-.13)	(16.4	-.02)
		40,000	1.70-2	-.04	1.70-1	-.04	1.70	-.01	16.6	+.07
			(1.72-2	-.06)	(1.72-1	-.05)	(1.71	-.02)	(16.7	+.06)
$2^3P - 4^3S$	4713	10,000	3.51-2	1.11	3.51-1	1.07	3.51	.97	33.7	.63
			(3.39-2	1.3)	(3.39-1	1.3)	(3.38	1.2)	(32.6	.74)
		20,000	4.12-2	.90	4.12-1	.88	4.12	.82	40.2	.61
			(4.07-2	.96)	(4.07-1	.96)	(4.06	.90)	(39.7	.67)
		40,000	4.45-2	.73	4.45-1	.71	4.45	.67	48.8	.54
			(4.47-2	.76)	(4.47-1	.74)	(4.49	.70)	-	-

For $T_e = 10^4$ °K the discrepancies are $\sim 30\%$ and 15% for the 3889 A° and 5016 A° lines respectively. The present calculations predict a smaller shift for the 3889 A° line but a larger one for the 5016 A° line.

Numerical errors cannot account for the discrepancies in the shifts in view of the excellent agreement for the widths, and hence the discrepancies must arise from one or more of the additional improvements to the G.B.K.O. theory that are included in Oertel's calculations. It is worthwhile considering which of these is the most important.

The symmetrization procedure, used by Oertel to correct for the back reaction on the perturber, would have a negligible effect on the shift for the following reasons. Firstly, for the reasons given in (5.3.4), the functions (B(z) and b(z) are not symmetrized. Secondly, the procedure can only affect the shift through its effect on ρ_{min} and hence z^{min}. But as both B(z) and b(z) are slowly varying functions this effect will be negligible. Finally, the condition $kT_e > \hbar\omega_{\alpha\alpha'}$ for the neglect of the back reaction is well fulfilled for both lines. The discrepancies in the shifts must, therefore, result from the neglect in the present calculations of either the lower state interaction, or the quadrupole interaction, or both.

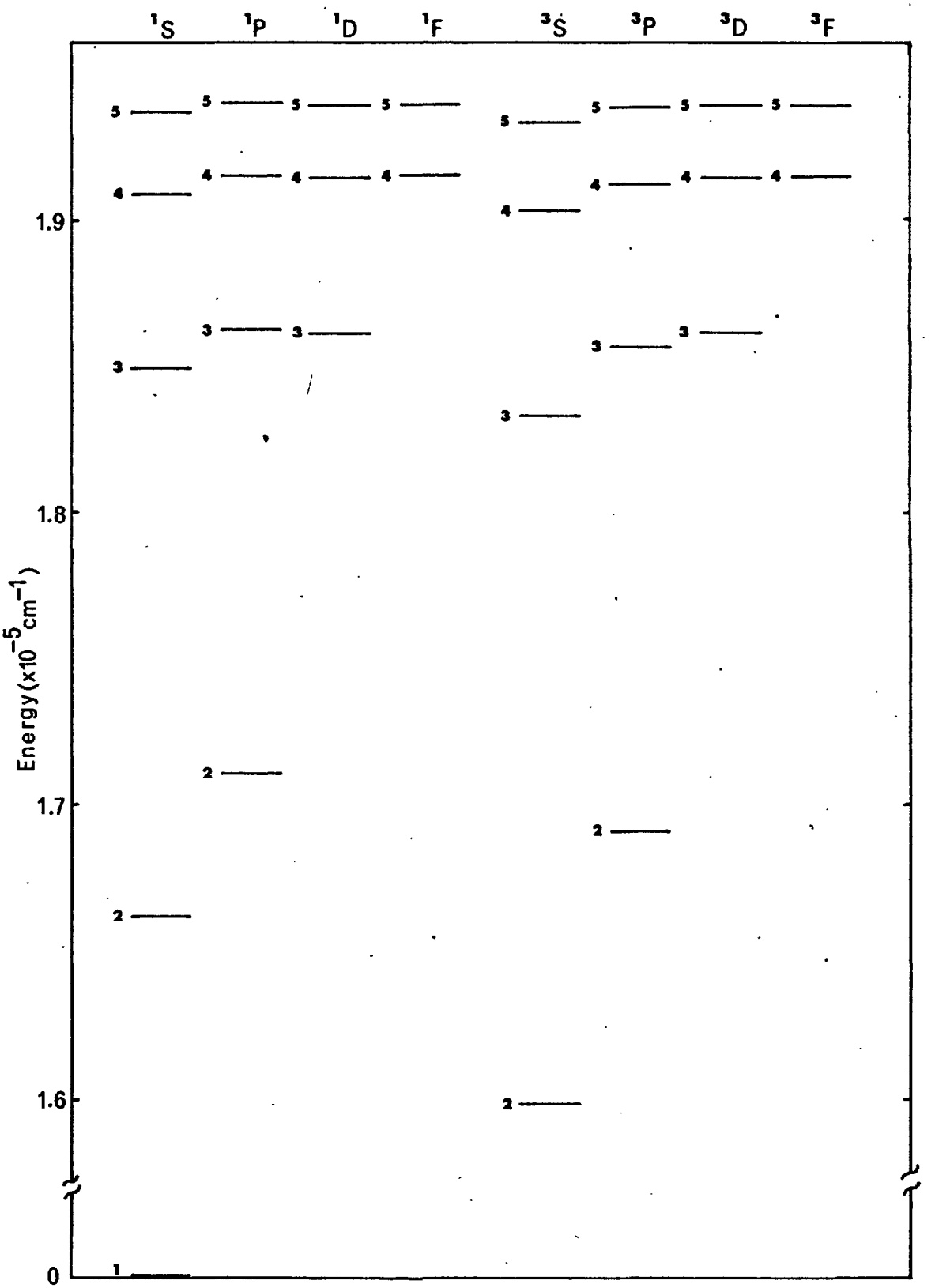

Fig.(6.1) Energy Levels of HeI

An examination of the results for the 3889 A^{o} ($2s\,^{3}S$ - $2p\,^{3}P$) and 5016 A^{o} ($2s\,^{1}S$ - $1p\,^{1}P$) and the HeI energy level diagram, Fig. 6.1 shows that the inclusion of the lower state interaction would also not explain the discrepancies. This follows from the fact that if the lower state shift were to be included, the total shift of 3889 A^{o} line will be less than that predicted by the single state calculation and that of the 5016 A^{o} line increased. In both cases the reverse of this behaviour is observed (see Table (6.1)).

Consideration of the quadrupole interaction shows that the shift of the upper state of both lines arises mainly from the interaction with levels with $n \geqslant 4$; there is no interaction with the $n = 3$ levels and only a weak interaction with $n = 2$, $\ell = 1$ level. In the case of 3889 A^{o} line this shift will reinforce the red shift produced by the dipole interaction with $3d\,^{3}D$ level. But for the 5016 A^{o} line, the quadrupole shift will reduce the dipole shift, since the latter is to the blue. Hence, Oertel's calculations which include both the dipole and quadrupole interactions, when compared with calculations which include only the dipole interaction, would be expected to predict a larger shift to the red for the 3889 A^{o} line and a smaller shift to the blue for the 5016 A^{o} line. This is in agreement with the observed discrepancies. It would appear that the neglect in the present calculations, of the quadrupole term in

the multipole expansion of the interaction is the cause of the discrepancies in the shifts predicted by the two sets of calculations.

Further support for the above explanation is obtained from the temperature dependence of the discrepancies, since the argument in (6.2) shows that the quadrupole contribution to the shift may become increasingly important with decreasing electron temperature. It is interesting to note that possible importance of the quadrupole contribution to the electron impact shift of certain isolated lines has not been previously emphasised.

Oertel did not publish the ion broadening parameters for the lines shown in Table (6.1) but they have been calculated recently by Cooper and Oertel (29), for $N_e = 10^{16} cm^{-3}$, taking into account both the upper and lower states. These values together with those obtained from the present calculations are given in Table (6.2) and the agreement is seen to be excellent.

Conclusion

It has been shown that, for the widths, the approximations made in the author's calculations result in negligible errors for the widths and ion broadening; at least for electron temperatures satisfying $10^4\ ^oK \leq T_e \leq 4 \times 10^4\ ^oK$. But for the electron impact shifts the neglect of the quadrupole interaction can, for certain lines, i.e. the 3889 A^o and 5016 A^o, give rise

to errors as large as $\sim 30\%$ at $T_e = 10^4$ °K. However, since most of the experimental observations of isolated HeI lines have been made at $T_e \gtrsim 2 \times 10^4$ °K, Table (6.1) shows that the error for the 5016 A° line should be $\sim 10\%$ and that for the 3889 A° line $\sim 20\%$.

TABLE (6.2)

Comparison of the calculated ion broadening parameters for $N_e = 10^{16} cm^{-3}$

$\lambda(A^o)$	$T_e(^oK)$		
	10^4	2×10^4	4×10^4
3889	0.072 (0.073)*	0.069 (0.069)	0.069 (0.067)
5016	0.163 (0.161)	0.172 (0.169)	0.293 (0.309)
5876	0.062 (0.063)	0.061 (0.062)	0.061 (0.062)
4713	0.112 (0.116)	0.099 (0.101)	0.094 (0.094)

* Cooper and Oertel's values are shown in brackets.

6.5. The Effect on the Width of Shielding both Fields in the Interaction

In the calculations discussed so far Debye shielding is included by shielding only one field in the interaction (5.5). More recent treatments of this effect (see (5.3.5)) have shown that, to a first approximation both fields in the interaction should

be shielded (this statement is not strictly accurate; see 5.3.5 for further discussion) when calculating the width but only one field when calculating the shift. As stated previously (see 6.3) this modification was included in the programme by putting $\rho_{max} = 0.682\,\rho_D$ and $\rho_{max} = 1.123\,\rho_D$ when calculating the width and shift respectively.

The effect of this modification on the widths of the lines given in Table (6.1) can be seen by examining Table (6.3) where the widths corresponding to the one and two shielded field cases have been tabulated for electron densities of 10^{16}, 10^{17} and 10^{18} cm^{-3} and an electron temperature of 2×10^4 °K.

TABLE (6.3)

Effect on Electron Impact $\frac{1}{2}$-$\frac{1}{2}$ Width of Shielding both Fields in the Interaction, for $N_e = 10^{16}$, 10^{17}, and 10^{18} cm^{-3} and $T_e = 2 \times 10^4$ °K

λ(A°)	$N_e = 10^{16}$ cm^{-3}		$N_e = 10^{17}$ cm^{-3}		$N_e = 10^{18}$ cm^{-3}	
	w_1	w_2	w_1	w_2	w_1	w_2
3889	0.114	0.114	1.14	1.14	10.9	10.1
5016	0.326	0.322	3.06	2.85	24.5	20.9
5876	0.170	0.170	1.70	1.69	16.4	15.2
4713	0.412	0.412	4.12	4.12	40.2	37.1

Key: w_1 Electron impact $\frac{1}{2}$-$\frac{1}{2}$ width in angstroms for one field shielded in the interaction

w_2 " " " " for both fields

As expected, the effect of shielding both fields in the interaction is to reduce the width below that predicted by the single shielded field calculations. Because the nearest neighbour splitting $\omega_{\alpha\alpha'}$ for the lines shown in Table (6.3) is smallest for the 5016 A^{o} line, this line shows the largest reduction in width, i.e. ~7% and ~15% at $N_e = 10^{17}$ and $10^{18} cm^{-3}$ respectively. Debye shielding is relatively less important for the remaining lines and consequently the reduction in the widths is negligible at $N_e = 10^{17} cm^{-3}$ and ~ 10% at $N_e = 10^{18} cm^{-3}$.

Table (6.3) also shows that if Debye shielding had been neglected, then the electron impact width of the 5016 A^{o} line, for $N_e = 10^{17}$ and $10^{18} cm^{-3}$, would have been overestimated by ~13% and 36% respectively; the latter result is not really meaningful because at $N_e \sim 10^{18} cm^{-3}$ the $\frac{1}{2}$-$\frac{1}{2}$ width of the 5016 A^{o} line is comparable with the splitting between the upper state of the line and the nearest perturbing level and consequently the isolated line approximation will no longer be valid (see also (6.10)). In the case of the remaining lines the neglect of Debye shielding would have a negligible effect on the width for $N_e = 10^{17} cm^{-3}$ but would cause an overestimate of the width by ~ 10% for $N_e = 10^{18} cm^{-3}$.

It is important to note that the reductions in the widths resulting from Debye shielding, mentioned above, refer

to the electron impact widths only. Since the total line width results not only from the electron impact broadening but also from the ion broadening, for which Debye shielding effects have already been taken into account by means of the ion field strength distribution function, the reduction in the total width will be less than the above values.

6.6. Comparison of the Calculated Stark Broadening Parameters for some Isolated HeI lines

Collected in Table (6.4) are the line broadening parameters for the HeI 3889, 5016 5876 and 4713 A^{o} lines calculated for $N_e = 10^{16} cm^{-3}$ and $T_e = 2 \times 10^4$ ^{o}K by Cooper and Oertel (24), Griem (1), G.B.K.O. (10) and the author. Table (6.5) illustrates the important differences amongst the various sets of calculations.

The parameters given in column (b) of Table (6.4) are taken from two separate sets of calculations. The widths and ion-broadening parameters are taken from the recent paper by Cooper and Oertel (29) and the shifts from the shift to widths ratios calculated by Oertel (24).

In the discussion which follows special attention will be given to the calculations of Griem since these are the most commonly used in the interpretation of experimentally determined widths.

TABLE (6.4)

Comparison of the Calculated Stark Broadening Parameters for Four Isolated HeI lines for N_e^{16} cm^{-3} and $T_e = 2 \times 10^4$ °K

λ(A°)		(a) THIS WORK	(b) C.O.	(c) GRIEM	(d) G.B.K.O.
3889	w	0.114	0.115	0.128	0.123
	d	0.047	0.059	0.049	0.042
	α	0.069	0.069	0.063	0.063
5016	w	0.322	0.331	0.370	0.352
	d	-0.12	-0.11	-0.10	-0.17
	α	-0.17	-0.17	-0.16	-0.16
5876	w	0.170	0.169	0.186	0.181
	d	-0.027	-0.028	-0.023	-0.024
	α	-0.061	-0.062	-0.058	-0.057
4713	w	0.412	0.406	0.518	0.490
	d	0.36	0.39	0.43	0.50
	α	0.10	0.10	0.084	0.095

Key: a) This work

b) Widths and ion broadening parameters taken from Cooper and Oertel (29) and shifts from Oertel (24)

c) Griem (1)

d) G.B.K.O. (10)

TABLE (6.5)

Comparison of the Differences Amongst the Various Calculations

ITEM	THIS WORK	OERTEL (24)	COOPER and OERTEL (29)	GRIEM (1)	G.B.K.O. (10)
a) Numerically accurate a(z) and b(z) functions	+	+	+	-	-
b) Quadrupole term in multipole expansion of the interaction	-	+	+	-	-
c) Lower state broadening and shift	-	+	+	-	+*
d) Debye shielding	+	+	+	-	-
e) ρ_{min} cut-off used (see 6.3)	2	2	2	1	1
f) Number of perturbing levels	>5	>5	>5	≤5	≤5
g) Matrix elements	C.A.**	C.A.	C.A.	C.A.	***

Key:
- \+ = Item included
- \- = Item not included
- * = Included only by calculating widths and shifts of upper and lower state separately
- ** C.A. = Coulomb Approximation
- *** = An average of the matrix elements obtained using Coulomb Effective charge and Hartree-Fock approximations

6.6.1. Widths

At $N_e = 10^{16} cm^{-3}$ Debye shielding has a negligible effect on the widths of the lines given in Table (6.4) (the largest effect, a 3% reduction in width, occurs for the 5016 A^o line as calculated in column (a)), and since Debye shielding is neglected entirely in the calculations of Griem and G.B.K.O. the differences in the widths must arise from factors other than Debye shielding effects.

Table (6.4) shows that there is excellent agreement between this work (column (a)) and that of Cooper and Oertel (column (b)). When Debye shielding can be neglected this result is to be expected since the previous comparison of the widths calculated by the author (see (6.4)) (which differ from the widths given in column (a) in that only one field, rather than both fields, in the interaction is shielded) with those calculated by Oertel showed excellent agreement.

Comparison of the widths calculated by Griem column (c) and G.B.K.O., column (d) with those given in columns (a) and (b) shows that the former widths are consistently larger. More specifically, Griem's widths for the 3889, 5106, 5876 and 4713 A^o lines are larger by 12, 15, 9 and 26% respectively than the widths given in column (a). The widths calculated by G.B.K.O. are in somewhat better agreement with this work (the corresponding

differences for the lines are 8, 9, 6 and 19% respectively) but are systematically smaller than those calculated by Griem.

The differences between widths calculated by Griem and those calculated in this work probably arise from one, or more, of the improvements included in the later calculations. These improvements correspond to the use of the accurate a(z) and b(z) functions, the introduction of Debye shielding, and the use of more perturbing levels. It is of interest to determine which of these improvements is responsible for the differences in the widths. Debye shielding need not be considered because this effect is negligible for the conditions at which the widths in Table (6.4) were calculated (see above). The use of more perturbing levels can also be eliminated because this modification tends to increase the width and, consequently, if Griem had used more perturbing levels in his calculations, the widths, and hence the differences in the widths predicted by the two sets of calculations, would have been even larger. Another factor which must be considered is that for the ρ_{min} cut-off Griem (and G.B.K.O.) used 'cut-off' 1 whereas the author used 'cut-off' 2. The latter yields widths which are smaller by typically 3% only (see (6.7.1)) and consequently this difference is too small to account for the discrepancies. It must be concluded that the differences in the widths arise from Griem's use of the numerically inaccurate a(z) function; the b(z) function only affects the

shift. Support for this conclusion was obtained by recalculating the width of the 3889 A^{o} line using the values of a(z) that had been used by Griem and G.B.K.O.. The resulting widths, which are shown in Table (6.6), are seen to be in excellent agreement. The table shows that the above explanation can also account for the differences between the widths calculated in this work and those of G.B.K.O. Table (6.6).

TABLE (6.6)

Comparison of the $\frac{1}{2}$-$\frac{1}{2}$ Widths of the 3889 A^{o} Line Calculated using the same Values of the Function a(z)

$N_e = 10^{16} cm^{-3}$;; $T_e = 2 \times 10^{4}\ ^{o}K$

CALCULATION	w(A^{o})
This work	0.124
Griem	0.128
G.B.K.O.	0.123

The conclusion, concerning the cause of the differences in the widths, appears to be at variance with work of Oertel (24). Oertel claims that the use of the numerically inaccurate a(z) functions only changes the widths by typically 1% to 5%. This conclusion is surprising because a comparison of Oertel's

results with those of Griem show differences that range from 12% to 26%.

The comparisons of the calculated widths which have been made here and in (6.4) have been restricted to values of T_e satisfying $10^4 \leq T_e(^\circ K) \leq 4 \times 10^4$. By comparing the Stark broadening parameters calculated in this work, for values of T_e outside this range with those calculated by Cooper and Oertel it was found that the electron impact width of 3889 A° line calculated here is larger by 11% for T_e = 2500 $^\circ K$ and smaller by 12% for T_e = 80,000 $^\circ K$ than the corresponding values calculated by Cooper and Oertel. For the 5876 A° line the corresponding values are 10% and 2% respectively. It was found that the discrepancies at $T_e = 2500^\circ K$ result mainly from the neglect in this work of the correction for the back reaction on the perturber (see (6.2)) whereas those at $T_e = 80{,}000^\circ K$ result from the neglect of the lower state broadening.

6.6.2. Shifts

Whereas Debye shielding has a negligible effect on the widths of the lines shown in Table (6.4.), at $N_e = 10^{16}$ cm^{-3}, the effect on the shift can be significant. For example Debye shielding reduces the shift of the 5016 A° line by $\sim$ 10%. Debye shielding effects have been included when calculating the

shifts given in columns (a) and (b) but not for those given in columns (c) and (d). For convenience, shifts rather than shift to width ratios are given in Table (6.4).

Since the shifts given in Columns (a) and (b) are identical to the respective calculations given in Table (6.1) for $N_e = 10^{16} cm^{-3}$, the reader is referred to (6.4) for the explanation of the discrepancies which exist between the shifts given in these columns.

The shifts given in columns (a), (c) and (d) are all calculated neglecting the quadrupole term in the multipole expansion of the interaction; consequently any discrepancies amongst these shifts must be caused by other factors. The calculations of Griem and G.B.K.O. also neglect Debye shielding effects and if it is assumed that other differences in the methods of calculation (see Table (6.5)) have a negligible effect on the shifts, then these shifts should be larger than those given in column (a) which are calculated taking into account Debye shielding effects. No such systematic trend is observed. The shifts calculated by Griem, when compared with those in column (a) are found to be larger by 5% and 20% in the case of 3889 A^o and 7413 A^o lines respectively. The shifts calculated by G.B.K.O. are in even poorer agreement with the shifts given in column (a) (and with those given in column (c)) the 5016 A^o and 4713 A^o are larger by 50% and 40%

respectively, and the 3889 A^{o} lines being smaller by 10%. The calculations of Griem and G.B.K.O. contain a number of factors which could be responsible for these discrepancies; in particular, the neglect of Debye shielding effects, the use of the numerically inaccurate b(z) function and the use of a limited number of perturbing levels.

6.6.3. Ion Broadening Parameters

Of the ion broadening parameters given in Table (6.4) only those in column (b) have been calculated taking into account the influence of the lower state.

As expected from the previous comparison of ion broadening parameters (see 6.4), and in circumstances where Debye shielding effects have a negligible effect on the electron impact widths, the ion broadening parameters given in columns (a) and (b) of Table (6.4) are in excellent agreement.

The ion broadening parameters calculated by Griem (see column (c)) are systematically smaller than those given in columns (a) and (b). G.B.K.O.'s results (see column (d)) although in slightly better agreement are also systematically smaller. The most likely explanation of these discrepancies is that an insufficient number of perturbing levels are used in the calculations of Griem and G.B.K.O.

6.7. Comparison of the Theoretical Widths, Shifts and Ion Broadening Parameters with Experiment

A comparison was made between the available experimental widths, shifts and ion broadening parameters for HeI lines and the theoretical values based on the present calculations, and those of Griem (1). The experimental data was taken from the works of Berg et al (16), Lincke (21), Wulff (15), Botticher et al (19) and Roda and Stampa (20). The results of the comparison are as follows:

6.7.1. Widths

Table (6.7) shows the experimental half widths (the data of Wulff will be considered separately for reasons to be mentioned later) together with the theoretical values. The latter are calculated from the line broadening parameters using the relationship (3.2.7.) which assumes that the quasistatic approximation is valid for the ions. To assess whether or not the use of this approximation is justified, the parameter σ has also been tabulated. In an attempt to decide which of the two ρ_{min} cut-offs, given in (6.3), is the most suitable both values are used in the comparison. Ratios of the experimental to calculated widths are also given and the mean value of this ratio and standard deviation, for each of the calculations, is given in Table (6.8).

TABLE(6.7) COMPARISON OF MEASURED AND CALCULATED LINE WIDTHS
(DATA WITH INDEPENDENT ELECTRON DENSITY MEASUREMENTS)

TRANSITION	$\lambda(A^o)$	N_e ($10^{16} cm^{-3}$)	T_e ($10^3 {}^oK$)	$w_m(A^o)$	$w_c(1)$ $w_c(2)$ $w_c(3)$ (ANGSTROMS)			R(1)	R(2)	R(3)	σ	$\omega_{\alpha\alpha'}/\omega_p$
$2^3P - 3^3P$	5876	16.0	49.0	5.5(a)	6.4	6.2	6.7	.86	.89	.82	.7	4.5
		13.0	43.0	4.9(a)	5.0	4.9	5.4	.98	1.0	.91	.7	5.0
$2^1S - 3^1P$	5016	17.0	24.0	13.0(a)	13.2	13.0	16.4	.99	1.0	.79	2.2	.84
		9.3	22.8	7.2(b)	7.5	7.4	9.0	.96	.97	.80	1.8	1.14
$2^3P - 4^3S$	4713	13.0	20.0	14.0(a)	13.3	13.2	16.0	1.05	1.06	.88	3.8	8.5
		9.3	22.8	9.1(b)	10.0	9.5	11.5	.91	.96	.79	2.9	10.0
$2^3S - 3^3P$	3889	15.0	26.0	4.5(a)	4.1	4.0	4.4	1.1	1.12	1.02	1.5	4.6
$2^3S - 4^3P$	3188	15.0	29.0	13.4(a)	12.6	12.4	14.3	1.06	1.08	.94	6.1	2.0

KEY

w_m = MEASURED HALF WIDTHS
- a) Berg et al (16)
- b) Lincke (21)

w_c = CALCULATED HALF WIDTHS

$w_c(1)$ = Half widths based on present calculations (cut-off 1)

$w_c(2)$ = Half widths based on present calculations (cut-off 2)

$w_c(3)$ = Half widths as calculated by Lincke (21) using line broadening parameters calculated by Griem (1)

R(1) = $w_m/w_c(1)$ etc.

TABLE (6.8)

Mean value of $\bar{R}$ of the ratio of experimental to theoretical half widths

(Data with independent electron density measurements)

CALCULATION	$\bar{R}$
1	0.99 ± 0.07
2	1.01 ± 0.07
3	0.88 ± 0.07

Key: 1 - Present calculations (cut-off 1)
2 - Present calculations (cut-off 2)
3 - Calculation of Griem (1)

TABLE (6.10)

Mean value of $\bar{R}$ of the ratio of experimental to theoretical half widths

(Data without independent electron density measurements)

CUT-OFF	$N_e(10^{16}cm^{-3})$	$\bar{R}$
1	2.55	$1.01 \pm .06$
2	2.65	$0.99 \pm .07$

Key: N_e = Electron density for which the best agreement with the experimental widths is obtained using cut-offs 1 and 2

The following conclusions can be drawn from the comparison. They are:

a) The present calculations are in better agreement with experiment than those of Griem. In the case of the present calculations the ratio of experiment to theory (see Table(6.7)) is within 1% of unity whereas Griem's calculation gives widths which are on average too large by $\sim$12%. The latter value is in good agreement with the -10% empirical correction to widths calculated from Griem's line broadening parameters suggested by Lincke (see 4.2).

b) The choice of the ρ_{min} cut-off does not appear to be critical, since the calculations based on cut-offs 1 and 2 give equally good agreement. This result is a consequence of the fact that in helium the broadening is dominated by distant weak inelastic collisions.

c) As Debye shielding is important only for the line at 5016 A° (see the ratio $\omega_{\alpha\alpha'}/\omega_p$ in Table(6.7)) it appears that the improved agreement between theory and experiment stems from the use of the corrected line broadening functions. The increase in the number of perturbing levels over that used by Griem would not explain the improvement because if Griem had also included this modification the calculated

widths would have been larger and thus in even worse agreement with experiment.

d) It was assumed, in calculating the half widths given (Table (6.7)) that the ions broadening can be treated by the quasistatic approximation. Griem demonstrated theoretically (see 5.2) that the quasistatic approximation can be used when $\alpha > 1$. Examination of the values of given in Table (6.7) shows that typically $\alpha \sim 1$. Consequently, the good agreement between theory and experiment confirms Griem's conclusion concerning the condition for the validity of the quasistatic approximation, however see (6.7.2)

It will be recalled (see 4.2) that Lincke's explanation of the discrepancies between the measured half widths of isolated HeI lines and the calculations of Griem, was that these calculations neglect the time dependence of the ion field, i.e. the quasistatic approximation is assumed, and also Debye shielding effects. In the light of the above results it appears that the discrepancies arise from neither of these approximations but rather from Griem's use of the numerically inaccurate function.

Wulff's data was treated in a different manner to that used above. The reason for this departure is that a previous study of this data(see(4.2)) showed that the measured electron density

appeared to be too high by $\sim 20\%$. However, as this data was obtained under identical conditions the electron density can be used as a parameter which may be varied until the best agreement between the experimental and theoretical half widths is obtained. Hence, this method tests the internal consistency of the theory for a number of lines. Wulff's value of the electron temperature, 3×10^4 ^oK, was used throughout the calculations, which were made using both ρ_{min} cut-offs. The results are shown in Table (6.9).

Table (6.10) gives the electron density corresponding to the best agreement between theory and experiment, and the mean value of the ratio of experiment to theory, for the two ρ_{min} cut-offs.

Again the agreement between the theory and experiment is excellent (better than 1%). However, the density at which the best agreement is obtained differs by $\sim 4\%$ for the two different ρ_{min} cut-offs, cut-off 1 predicting a smaller density as expected since the increase in ρ_{min}, which results from the use of this cut-off is only partially offset by a decrease in the weak collision term. Without an independent density estimate it is impossible to decide which cut-off is the most appropriate. The results suggest that in an experiment designed to choose between the two cut-offs the accuracy of the electron

TABLE (6.9) COMPARISON OF MEASURED AND CALCULATED LINE WIDTHS
(DATA WITHOUT INDEPENDENT ELECTRON DENSITY MEASUREMENTS)

TRANSITION	$\lambda(A^o)$	$w_m(A^o)$ a)	CUT-OFF 1		CUT-OFF 2		σ	$\omega_{\alpha\alpha'}/\omega_p$
			$N_e(1) = 2.55 \times 10^{16} cm^{-3}$		$N_e(2) = 2.65 \times 10^{16} cm^{-3}$			
			$w_c(1)(A^o)$	R(1)	$w_c(2)(A^o)$	R(2)		
$2^1P - 4^1S$	5048	2.3	2.37	.97	2.38	.97	1.8	11.5
$2^1S - 3^1P$	5016	0.95	1.01	.94	1.04	.91	0.7	2.4
$2^3P - 4^3S$	4713	1.45	1.35	1.07	1.35	1.07	1.2	18.4
$2^3P - 5^3S$	4121	3.1	3.24	.96	3.25	.95	3.5	9.7
$2^3S - 3^3P$	3889	0.37	0.34	1.09	.34	1.07	0.5	10.7

KEY

w_m = MEASURED HALF WIDTHS

a) WULFF (15)

w_c = CALCULATED HALF WIDTHS

$w_c(1)$ = Half width based on present calculations (cut-off 1)

$w_c(2)$ = Half width based on present calculations (cut-off 2)

$R(1) = w_m/w_c(1)$ etc.

$N_e(1)$ = Electron density for which the best agreement with the experimental widths is obtained using cut-off 1 etc.

density measured must be better 4%. However, in view of the small difference in the derived electron density, such an experiment would appear to be futile.

Finally, the results also confirm the conclusions concerning the significance of the parameter σ

6.7.2. Shifts

A comparision between the experimental and calculated shifts is complicated by two factors. Firstly, shifts are more difficult to measure accurately than widths (this is especially true for pulsed light sources). Secondly, the theoretical shifts are usually less accurate than the widths because they are much more sensitive to shielding effects than widths, and they are also subject to cancellation effects (see 5.3.6). In regard to the present calculations the shifts of n = 3 levels will be uncertain to some extent because of the neglect of lower state shift, and the electron impact quadrupole shift. In spite of these limitations it was thought to be of interest to make a comparison with experiment.

The data for the comparison was taken from the works of Berg et al (16), Lincke (21), Wulff (15) and Botticher et al (19). Table(6.11) shows the data taken from the first two references together with the ratio of experiment to theory. Mean values

TABLE (6.11)COMPARISON OF MEASURED AND CALCULATED LINE SHIFTS
(DATA WITH INDEPENDENT ELECTRON DENSITY MEASUREMENTS)

TRANSITION	$\lambda(A^o)$	N_e	T_e	$d_m(A^o)$	$d_c(1)$	$d_c(2)$	$d_c(3)$	R(1)	R(2)	R(3)	σ	$\omega_{\alpha\alpha'}/\omega_p$
		$(10^{16} cm^{-3})$	$(10^3\ ^oK)$		(ANGSTROMS)							
$2^3P - 5^3P$	5876	16.0	49.0	+0.7(a)	-0.38	-0.45	-0.3	-	-	-	.7	4.5
		13.0	43.0	0.0(a)	-0.31	-0.38	-0.3	-	-	-	.7	5.0
$2^1S - 3^1P$	5016	17.0	24.0	-4.8(a)	-3.3	-3.5	-6.0	1.45	1.37	0.80	2.2	0.84
		9.3	22.8	-1.7(b)	-1.84	-1.9	-2.1	.93	0.90	0.81	1.8	1.14
$2^3P - 4^3S$	4713	13.0	20.0	+6.0(a)	+5.6	+5.7	+7.0	1.07	1.05	0.86	3.8	8.5
		9.3	22.8	+4.3(b)	+4.1	+4.0	+4.9	1.02	1.08	0.88	2.9	10.0
$2^3S - 3^3P$	3889	15.0	26.0	+1.2(a)	+0.87	+0.89	+1.0	1.4	1.3	1.2	1.5	4.6
$2^3S - 4^3P$	3188	15.0	29.0	+4.1(a)	+2.65	+2.8	+3.4	1.5	1.5	1.2	6.1	2.0

KEY

d_m = MEASURED SHIFTS
- a) Berg et al (16)
- b) Lincke (21)

d_c = CALCULATED SHIFTS

$d_c(1)$ = Shift based on present calculations (cut-off 1)

$d_c(2)$ = Shift based on present calculations (cut-off 2)

$d_c(3)$ = Shift as calculated by Wiese (2) using line broadening parameters calculated by Griem (1)

R(1) = $d_m/d_c(1)$ etc.

TABLE (6.12)

Mean value $\overline{R}$ of experimental to theoretical shifts

(Data with independent electron density measurements)

CALCULATION	$\overline{R}$
1	$1.23 \pm .23$
2	$1.20 \pm .23$
3	$0.96 \pm .17$

Key: 1 - Present calculations (cut-off 1)
2 - Present calculations (cut-off 2)
3 - Calculations of Griem (1)

TABLE (6.14)

Mean value of $\overline{R}$ of the ratio of experimental to theoretical shifts

(Data without independent electron density measurements)

CUT-OFF	$N_e (10^{16} cm^{-3})$	$\overline{R}$
1	2.55	$1.37 \pm .37$
2	2.65	$1.32 \pm .36$

Key: N_e = Electron density for which best agreement with experimental widths is obtained using cut-offs 1 and 2

of this ratio, and the standard deviation, are shown in Table (6.12). In cases where the predicted shift is in the wrong direction to that measured it is meaningless to give the ratio of experiment to theory. Consequently the data was rejected. Such a situation occurs for the measurement of the 5876 A^{o} line made by Berg et al. Here, the measured shift is to the red whereas the present calculation and those of Griem predict a shift to the blue. Although the magnitude of measured shift may be possibly in error it is unlikely that the direction of the shift has been measured incorrectly and therefore the calculated shift must be suspect. Because of the excellent agreement between the present calculations and those of Oertel for the 5876 A^{o} line (see Table 6.1), the errors in the electron impact shift, arising from the neglect of the quadrupole interaction and the lower state, can be assumed to be negligible. The calculations also show that at the temperature at which the 5856 A^{o} line was measured, the shift of the line results almost entirely from the ion broadening (this can be seen from the line broadening parameters for the 5876 A^{o} line given in (6.11)). Hence, assuming that the direction of the shift had been measured correctly, the discrepancy in the calculated shift must arise from the treatment of the ion broadening.

To return to Table (6.11) the good agreement shown for the shifts calculated from Griem's parameters would appear to be

fortuitous for two reasons. Firstly, the b(z) functions used by Griem in the calculation of the shifts were numerically inaccurate (see 4.2). Secondly, Debye shielding was neglected.

For both values of ρ_{min} the present calculations give shifts which are too small by ~ 20%. The addition of the electron impact quadrupole shift would in some cases improve the agreement. This can be seen by examining the calculations of Oertel, Table (6.1). For the 4713 A^{o} and 3889 A^{o} lines Oertel's calculations yield electron impact shifts which are larger, at $T = 2 \times 10^{4}$ ^{o}K (which approximates to the temperature at which the measurements were made), by ~ 10% and ~20% respectively than the present calculations. It should be noted that these percentages refer to the increase in the electron impact shift, and since the total shift is the algebraic sum of the electron impact shift and the shift due to the ion field, the actual increase in shift will be less than these values. For the 5016 A^{o} line Oertel's calculations give an electron impact shift which is smaller by ~ 8% which would bring Lincke's measurement into better agreement but worsen that of Berg et als.

Table (6.13) shows the shifts measured by Wulff together with the calculated shifts, using both ρ_{min} cut-offs, and the the ratios of experiment to theory. Table (6.14) gives the mean value of the ratio of experiment to theory together with the

TABLE(6.13) COMPARISON OF MEASURED AND CALCULATED LINE SHIFTS
(DATA WITHOUT INDEPENDENT ELECTRON DENSITY MEASUREMENTS)

TRANSITION	$\lambda(A^o)$	$d_m(A^o)$ a)	CUT-OFF 1 $N_e(1) = 2.55 \times 10^{16} cm^{-3}$		CUT-OFF 2 $N_e(2) = 2.65 \times 10^{16} cm^{-3}$		σ	$\omega_{d\alpha'}/\omega_p$
			$d_c(1)(A^o)$	R(1)	$d_c(2)(A^o)$	R(2)		
$2^1P - 4^1S$	5048	+ 2.0	+ 1.74	1.15	+ 1.80	1.11	1.8	11.5
$2^1S - 3^1P$	5016	- 0.55	- 0.45	1.16	- 0.52	1.07	0.7	2.1
$2^3P - 4^3S$	4713	1.4	+ 1.09	1.28	+ 1.11	1.26	1.2	18.4
$2^3P - 5^3S$	4121	2.8	+ 2.40	1.17	+ 2.48	1.13	3.5	9.7
$2^3S - 3^3P$	3889	+ 0.3	+ 0.14	2.10	+ 0.15	2.03	0.45	10.7

KEY

d_m = MEASURED SHIFTS

a) WULFF (15)

d_c = CALCULATED SHIFTS

$d_c(1)$ = Present calculations (cut-off 1)

$d_c(2)$ = Present calculations (cut-off 2)

$R(1) = d_c(1)/d_m$, etc.

$N_e(1)$ = Value of the electron density for which the best agreement with the experimental widths is obtained using cut-off 1 etc.

standard deviation. The electron density used in these calculations is in each case that which gave the best agreement for the widths. The results show that the calculated shifts are systematically low by $\sim$ 30%. For the 3889 A° line the discrepancy is surprisingly large (a factor of 2) and in part this may result from experimental error because of the small shift involved. Again, Oertel's results would tend to improve the agreement for the 3889 A° and 4713 A° lines but will worsen that for the 5016 line.

Botticher et al (19) measured the shifts of a number of isolated HeI lines for electron densities ranging from $\sim 3 \times 10^{15}$ to $3 \times 10^{16} cm^{-3}$. Electron temperatures ranged from $\sim 14000^{\circ}K$ at the lowest density to $\sim 18000^{\circ}K$ at the highest. The results are shown in Fig.(6.2)and(6.3) Fig.(6.2)corresponds to transitions from P state and Fig.(6.3)those from S states. The curves giving the theoretical values of the shifts were calculated from the Stark broadening parameters using (3.20) which assumes that the ions can be treated by the quasi-static approximation. These parameters were taken from Griem (1) and the present calculations using cut-off 1; the curves corresponding to Griems parameters were in fact calculated by the authors of (19) and these values have been used in the figures. The triangles shown in the figures correspond to the calculations of Oertel. Graphical interpolation was used to

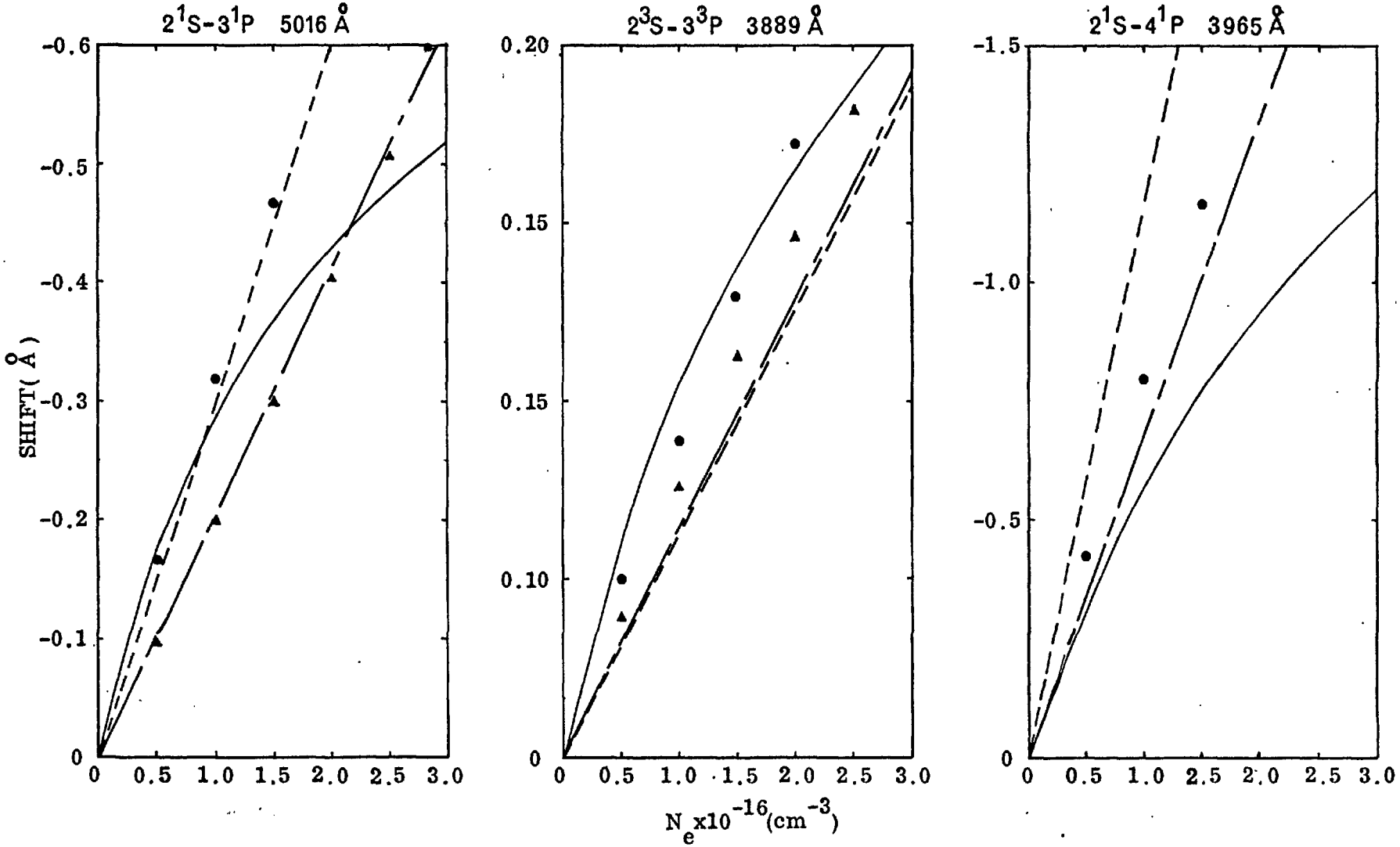

Key; ——Measured Shifts(Botticher et al). – – – – Calculated Shifts(Griem).
▲ " " (Oertel). Quasi-static Approx. for Ions
——— " " (This Work).
● " " (This Work). Adiabtic Impact Approx. for Ions

Fig.(6.2) Comparison of Measured and Calculated Shifts of HeI Lines.

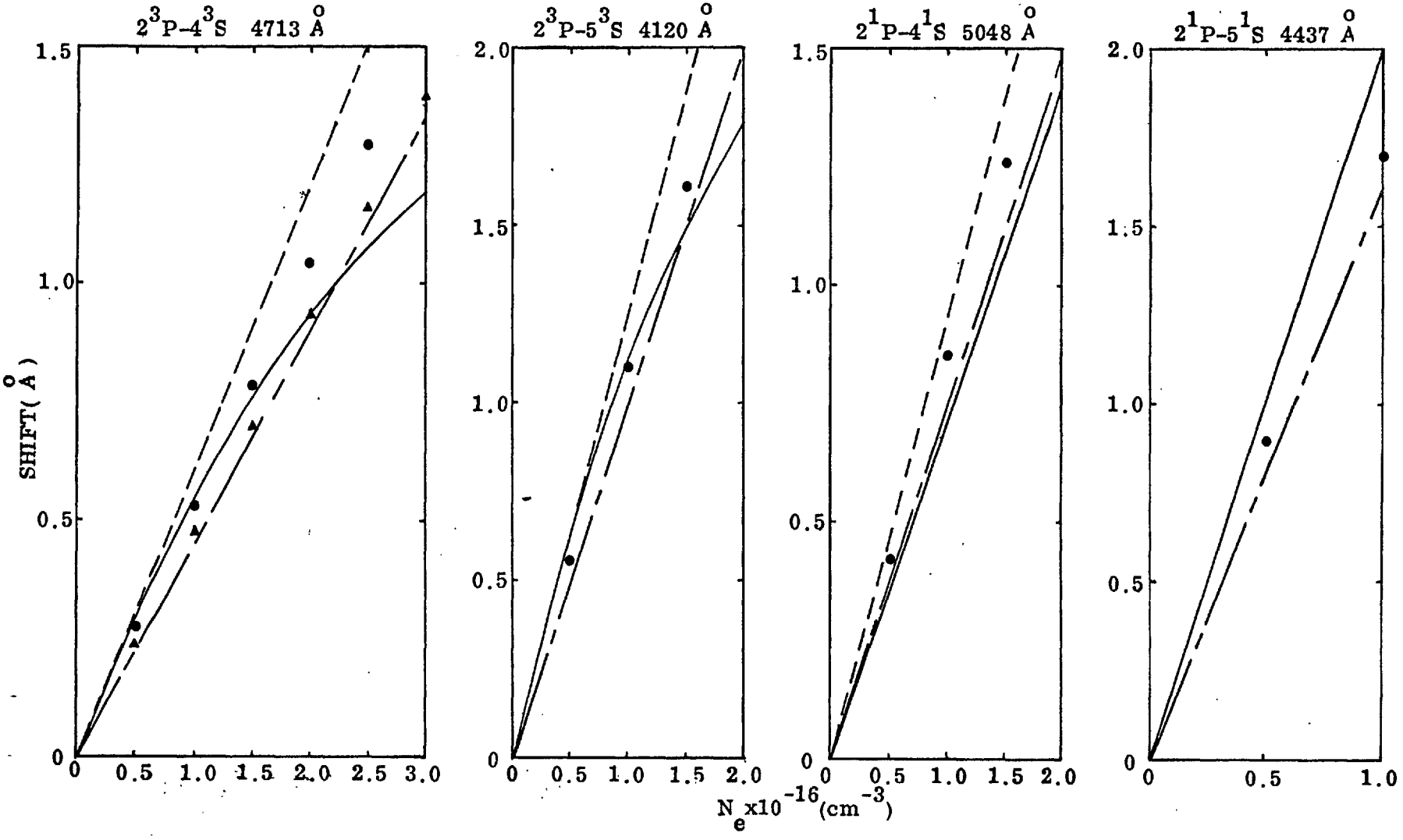

Key; ——Measured Shifts(Botticher et al). – – – – Calculated Shifts(Griem).
▲ " " (Oertel). Quasi-static Approx. for Ions
——— " " (This Work).
● " " (This Work). Adiabtic Impact Approx. for Ions

Fig.(6.3) Comparison of Measured and Calculated Shifts of HeI Lines

obtain values of Oertel's parameters, see Table (6.1) which corresponded to the experimental conditions. Since Oertel's parameters do not include α it was necessary to take the values of α from the present calculations and scale them to Oertel's electron impact widths using (5.24). The errors arising from this procedure should be negligible (see(6.4)

An examination of Figs(6.2)and(6.3)shows that in general the agreement between theory and experiment is poor and with exception of the 3889 A^{o} line Oertel's calculations do not lead to any significant improvement. In many cases the calculations not only fail to predict the correct magnitude of the shift (discrepancies $>$ 50% occur) but also the density dependence. For five out of the seven lines studied a pronounced curvature of the shift versus electron density curve is observed, whereas all the calculations predict a linear density dependence. The explanation of this linear dependence is that as the electron density increases the ion contribution to the shift, which varies as $N_e^{4/3}$, tends to compensate for the reduction in the electron impact shift produced by the increase in Debye shielding and the electron temperature.

Another, and surprising result, is that for lines arising from S states the density dependence of the shift appears to depend on the multiplicity of the upper state (see Fig.(6.3)).

Lines from ^3S levels show a non-linear behaviour whereas for the analogous lines from ^1S levels the behaviour is linear.

The fact that Oertel's calculations, which include all the higher order effects that might be expected to contribute significantly to the electron impact shift (see 5.3), do not result in significant improvements suggests that the reason for the discrepancies might be found in the treatment of the ion contribution to the shift. A similar conclusion to this has already been reached in connection with the discrepancies in the shift of the 5876 A° line observed by Berg et al (16).

Berg et al (16) attempted to explain some of the discrepancies, which they had observed, between the measured and calculated shifts of isolated HeI lines, by suggesting that the calculated shifts are too large because of the transition to the linear Stark effect at high ion field strengths, i.e. high electron densities. For the 3965 A° line, which shows the largest discrepancies, there is experimental evidence to support this conclusion. Wulff's measurements of the profile of the 3965A° line (15), made at an electron density of $\sim 2.5 \times 10^{16} cm^{-3}$ (see 6.7.1), shows the presence of a forbidden component resulting from the transition $2^1S - 4^1D$. For the reasons discussed in (3.7.3.) the appearance of this

forbidden component indicates that a transition from the quadratic to the linear Stark effect is taking place. Furthermore, the splitting between the upper state of the 3965 A^{o} line and the nearest perturbing level is relatively small ($\sim 46\ cm^{-1}$) in comparison with that for the other lines, and hence, the transition from the quadratic to the linear Stark effect would be expected to take place at much lower densities than that for the other lines. Consequently, at the densities encountered in Botticher et al's experiment the use of the quadratic Stark effect will overestimate the shift of 3965 A^{o} line. Since the transition from the quadratic to the linear Stark effect will become increasingly important as the electron density is increased the experimentally determined shift will fall increasingly below the calculated value, as observed. The transition from the quadratic to the linear Stark effect would also explain the high density behaviour observed of the other lines. The low density behaviour cannot be explained by such an effect, the reason being that at low electron densities the quadratic Stark effect should certainly be operative. Consequently the calculations should predict the correct slope, at the origin, of the shift versus density curve. With exception of 3965 A^{o} line, the agreement, between the measured and calculated slopes is not observed (the calculations of Griem show good agreement for three of the lines, but for the

reasons previously discussed, this must be regarded as fortuitous). The results obtained at low electron densities suggest that there is an additional contribution to the shift.

In the G.B.K.O. treatment of the quasistatic ion broadening and shift of isolated HeI lines, only the second order dipole term in the interaction is retained (the first order dipole term vanishes because there is no permanent dipole moment). However, the first order contribution of the next higher term in the multipole expansion of the interaction may contribute significantly to the broadening and shift; especially in cases where the induced dipole moment is small. The quadrupole and induced dipole interactions differ in two respects. Firstly, whereas the induced dipole moment interacts with the electric field, the quadrupole moment interacts with the gradient of the electric field. Secondly, the shifts of the magnetic sub-levels produced by the induced dipole interaction are all in the same direction whereas those produced by the quadrupole interaction depend on the value of m, the magnetic quantum number (see Unsold (36)). Muller (37) has investigated theoretically the first order quadrupole contributuon to the quasistatic ion broadening and shift of isolated HeI lines. To assess the conditions for which the quadrupole contribution to the broadening and shift of line will be important, Muller

compared the quadratic Stark shift d_4 with the quadrupole shift d_3 of a level with principle quantum n. The electric field and the gradient of the field were assumed to be produced by an ion situated at the mean ion seperation ρ_i. The quadratic Stark shift is given by:

$$d_4 = \frac{hc|C_4|}{\rho_i^4} \tag{6.8}$$

where C_4 is the quadratic Stark coefficient. For a P level the quadrupole shift is given by:

$$d_3 = \frac{4}{15} \cdot \langle n | r^2 | n \rangle \cdot \frac{e^2}{\rho_i^3} \tag{6.9}$$

Assuming the level n is close to being hydrogenic the matrix element $\langle n | r^2 | n \rangle$ can be estimated by:

$$\langle n | r^2 | n \rangle = \frac{a_o^2 n^2}{2} \left[5n^2 + 1 - 3\ell(\ell+1) \right]$$

where ℓ is the orbital quantum number of the level and a_o is the Bohr radius. In deriving Eqns (6.8) and (6.9) an average over the shifts of the various magnetic sub-levels has been taken. From (6.8) and (6.9) the ratio of the shifts is given by:

$$\frac{d_4}{d_3} = \frac{15}{4} \frac{hc}{e^2} \frac{C_4}{\langle n | r^2 | n \rangle} \cdot \frac{1}{\rho_i} \tag{6.10}$$

The above result shows that the quadrupole contribution to the shift will result mainly from distant ions, and since the fields produced by these ions will be small they will mainly influence the region of the profile close to the core of the line. Near the line centre the quasistatic approximation is no longer valid see (3.5.1) and the adiabatic impact theory must be used for the ions. However, in the impact regime the first order quadrupole contribution to the width and shift vanishes when the average over collision angles is performed see (5.1). Except possibly in cases where C_4 is small, the quadratic Stark effect will be responsible for the formation of the line wings since these are formed by close ions.

Assuming that the plasma is singly ionized then ρ_i is given by (3.32) and (6.10) becomes:

$$\frac{d_4}{d_3} = \frac{hc}{e^2} \frac{C_4}{\langle n | r^2 | n \rangle} \cdot \left(\frac{4\pi N_e}{3}\right)^{\frac{1}{2}} \qquad (6.11)$$

Thus, with decreasing electron density, the quadrupole contribution to the shift of the Stark components will become increasingly important. By setting the ratio of the shifts equal to unity Muller derived a critical electron density $(N_e)_c$. For $N_e \gg (N_e)_c$ the quadrupole contribution will be negligible. In Table (6.15)Mullers values of $(N_e)_c$ are given, for 3889 A°, 3965 A° and 5016 A° lines, together with the

value of $(N_e)_c$ corresponding to a value of N_e which d_3 is 20% of d_4. Lines arising from s states do not appear in the table because such states are spherically symmetric and therefore do not possess a quadrupole moment.

Table (6.15)

Critical Electron Densities for a Number of HeI Lines

TRANSITION	$\lambda(A^o)$	$(N_e)_c$	
		$d_3 = d_4$	$d_3 = 0.2 \cdot d_4$
$2^3S - 3^3P$	3889	1.3×10^{16}	1.6×10^{18}
$2^1S - 4^1P$	3965	6.2×10^{13}	7.7×10^{15}
$2^1S - 3^1P$	5016	5.3×10^{13}	6.6×10^{15}

The results given in Table (6.15) show that at the densities encountered in the experiments of Botticher et al the quadrupole contribution to the quasistatic ion broadening and shift could be significant. Difficulties arise, however, when the directions of the shifts are considered. Using the 'nearest neighbour' approximation to calculate the gradient of the ion field, Muller shows that the quadrupole interaction increases the energy of a P-level. Consequently, for the

5016 A^{o} line, the quadrupole shift will reinforce that due to the quadratic Stark effect, see Fig. (6.1) and as observed, an additional blue shift will result. For the 3889 A^{o} line the quadrupole and quadratic Stark shifts are in opposite directions. The observed shift should, therefore, be less than calculated shift which is contrary to observed behaviour. Further difficulties are encountered when the discrepancies for the 4713 A^{o} and 4120 A^{o} lines are considered. Since the upper states of these lines are S states the quadrupole interaction can influence only the lower states, and since the lines have the same lower state, the discrepancies should be the same for both lines. The observed discrepancies in fact differ by a factor ~ 2. It must, therefore, be concluded that the neglect of the first order quadrupole interaction, in the treatment of the quasistatic ion broadening, cannot explain the observed discrepancies. In view of the results given in Table (6.15) this conclusion is surprising. A possible explanation is that Muller's analysis neglects the fact that the first order quadrupole contribution will only be realised in practise if the quasistatic approximation is still valid when $N_e \lesssim (N_e)_c$. In most cases this will be unlikely because the quasistatic approximation becomes less applicable as the electron density decreases. If the quasistatic approximation is invalid then, as discussed above, the adiabatic impact

theory must be used instead, with the result that the first order quadrupole contribution to the broadening and shift vanishes. Hence, a more rigorous analysis of this contribution to the width and shifts of a line should also consider the magnitude of the parameter σ. For example, for the lines shown in Table (6.15), and assuming the electron densities are those for which $d_3 = d_4$, the values of σ are 0.3, 0.02 and 0.1 for the 3889 A^o, 5016 A^o and 3965 A^o lines, respectively. These values of σ indicate that the quasistatic approximation is likely to be only marginally valid for 3889 A^o line and invalid for the 5016 A^o and 3965 A^o lines. Consequently, Muller's estimate of the first order quadrupole contribution to the broadening and shift of these lines will be much too large.

A more likely explanation of the discrepancies in the shifts, observed at low electron densities, is the breakdown of the quasistatic approximation. In (6.7.1) it was seen that for the calculation of the widths the quasistatic approximation can still be used when $\sigma \sim 1$. This is not necessarily true for the shifts because here the ion contribution is usually much larger and discrepancies resulting from the breakdown of the quasistatic approximation might be much more noticeable. To investigate this possibility the ratio of the experimental to theoretical shifts for $N_e = 10^{16}$ cm^{-3} are

plotted against σ , see Fig.(6.4). The results show that the discrepancies do tend to increase as σ becomes smaller, i.e. as the quasistatic approximation becomes less reliable. It might be expected, therefore, that improved agreement would result if the ion contribution is calculated using the adiabatic impact theory, see (5.2.2) rather than the quasi-static approximation. Using (3.30), which gives the total shift of an isolated line resulting from electron and ion impacts, the shifts were recalculated. The results are shown in Figs (6.2) and (6.3).

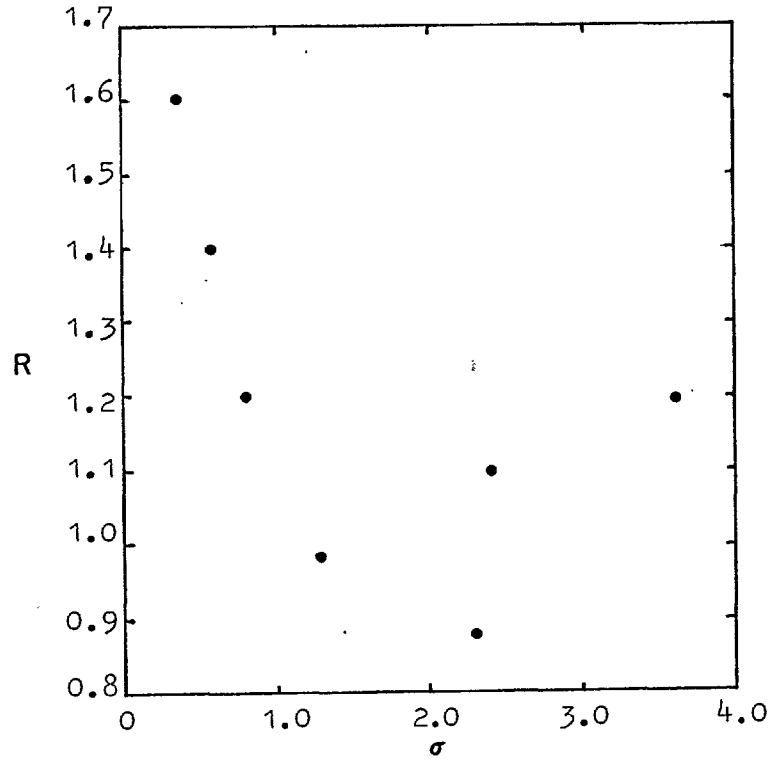

Fig. (6.4) Ratio of Experimental to Theoretical Shift for $N_e = 10^{16} cm^{-3}$ versus σ .

With the exception of the 5048 and 3965 A^{o} lines Figs (6.2) and (6.3) show that there is improved agreement between the calculated and observed shifts as the electron density tends to zero. This result is consistent with the above explanation of the discrepancies, because as the electron density decreases the time dependence of the ion field becomes increasingly important for the treatment of the ion broadening (see 5.2).

If the above interpretation of the discrepancies in the shifts is correct then the results given here would constitute the first realization of the dynamic effects of ions in line broadening studies.

From the comparison between the shifts measured by Botticher et al and the values calculated by the author and others, a rather complex behaviour of the variation with electron density of the ion contribution to the shift of an isolated line emerges. It appears that at low electron densities ($\lesssim 10^{16} cm^{-3}$), the time dependence of the ion field must be taken into account when calculating the shift. At high electron densities the quasi-static approximation is valid but it appears that the linear rather than the quadratic Stark effect predominates.

6.7.3. Ion Broadening Parameters

As described in (4.2) the ion broadening parameters for a number of isolated HeI lines have been measured by Roder and Stampa (20). The results are shown in Table (6.16) together with the ion broadening parameters calculated by the author, and those of Griem (1). Mean values, and standard deviations, of the ratio of the measured to calculated ion broadening parameters are given in Table (6.17).

TABLE (6.17)

Ratio $\overline{R}$ of Experimental and Theoretical Ion Broadening Parameters

Calculation	$\overline{R}$
1	1.01 ± 0.4
2	1.07 ± 0.4

Key: Calculation 1 = This work

" 2 = Griem (1)

Although the results given in Table (6.17) show that the author's calculations tend to be in slightly better agreement with the experimental values this improvement can not be regarded as significant because of the large standard deviation

Table (6.16) Comparison of Measured and Calculated Ion Broadening Parameters.

		$N_e = 3.8 \times 10^{15} cm^{-3}$					$N_e = 7.2 \times 10^{15} cm^{-3}$					$N_e = 1.7 \times 10^{16} cm^{-3}$				
TRANSITION	(A^o)	α_m	$\alpha_c(1)$	$\alpha_c(2)$	R(1)	R(2)	α_m	$\alpha_c(1)$	$\alpha_c(2)$	R(1)	R(2)	α_m	$\alpha_c(1)$	$\alpha_c(2)$	R(1)	R(2)
2^3P-3^3D	5876	0.0	0.045	0.048	-	-	0.05	0.053	0.056	0.94	0.89	0.05	0.065	0.07	0.77	0.71
2^1S-3^1P	5016	0.14	0.13	0.13	1.08	1.08	0.14	0.16	0.15	0.88	0.93	0.17	0.18	0.20	0.94	0.85
2^3S-3^3P	3889	0.0	0.05	0.05	-	-	0.04	0.06	0.065	0.67	0.62	0.05	0.07	0.08	0.71	0.63
2^1S-4^1P	3965	-	0.23	0.24	-	-	0.25	0.27	0.29	0.93	0.86	0.25	0.33	0.38	0.76	0.66
2^1P-4^1S	5048	-	-	-	-	-	0.19	0.11	0.11	1.70	1.67	0.12	0.13	0.14	0.92	0.86
2^3P-4^3S	4713	0.04	0.08	0.083	0.5	0.48	0.14	0.09	0.096	1.56	1.46	0.20	0.11	0.12	1.82	1.67
2^3P-5^3S	4120	-	0.11	0.12	-	-	0.18	0.13	0.14	1.38	1.29	-	0.17	0.17	-	-

Key;

α_m = Measured Ion Broadening Parameter(Roder and Stampa).

$\alpha_c(1)$ = Calculated Ion Broadening Parameter(Griem)

$\alpha_c(2)$ = " " " " (This Work).

$R(1) = \alpha_m/\alpha_c(1)$.

$R(2) = \alpha_m/\alpha_c(2)$.

of the results. Table (6.16) shows that in general the agreement between experiment and theory becomes poorer with increasing electron density. For lines originating from P or D levels discrepancies as large as ~ 30% occur but typical discrepancies are ~ 20%; the experimental values being in general smaller than the theoretical ones. In the case of lines originating from S levels discrepancies as large as ~ 70% occur, and show large variations with electron density. For example, the ratio of the experimental to theoretical ion broadening parameter for the 4713 A^{o} ($2^{3}P - 4^{3}S$) line is ~ 50% less than unity for $N_e = 3.8 \times 10^{15} cm^{-3}$ and ~ 70% greater than unity for $N_e = 1.7 \times 10^{16} cm^{-3}$.

These discrepancies may to some extent result from experimental difficulties such as poor signal to noise ratios and the determination of the background intensity, which are encountered when making measurements on the wings of a profile. It is interesting to note, however, than an investigation made by Wiese and Murphy (38) of the intensity distribution on the far wings of an isolated OI line showed that the asymptotic wing formula predicted the correct slope of the wings but not the intensities; Roder and Stampa's method of determining α_{wing} depends on the validity of the asymptotic formula.

Until further experimental studies of the accuracy of of the asymptotic wing formula have been made the significance of the discrepancies in the ion parameters can not be assessed.

Errors in the asymptotic wing formula could arise possibly from the neglect of the electron contribution to the quasi-static wing broadening or by the transition from the quadratic to the linear Stark effect. Such a transition might be expected to take place at the high electric fields which are responsible for the wings of a line.

6.8. Recent Measurements of the Stark Broadening of Isolated HeI Lines

Greig et al (39) have recently made a detailed study of the Stark Broadening of the HeI lines at 3889 A^{o} (width only) and 5016 A^{o} (width and shift) in T-tube generated plasma. Electron densities, determined from the broadening of the hydrogen line H_{β}, varied from 10^{16} to $6 \times 10^{17} cm^{-3}$. Electron temperatures were in the range 2×10^{4} ^{o}K to 3×10^{4} ^{o}K. The measurements were compared with the calculations of Griem (1) and Oertel (24).

For the 3889 A^{o} line the final results of the comparison were expressed in terms of the mean value of the ratio of the electron density obtained from the half width of this line, using first Oertel's then Griem's Stark broadening parameters, to that obtained from the broadening of H_{β}. However, if the uncertainty ($\sim$ 4%) in the electron density determined from the broadening of H_{β} is neglected, then each ratio is equal to

the ratio of the experimental to theoretical half widths. The ratios obtained using Oertel's and Griem's Stark broadening parameters are respectively 1.01 ± 0.07 and 0.91 ± 0.06, for measurements made over the entire density range. In the case of the 5016 A° line the experimental and theoretical widths were compared directly. For $N_e \lesssim 10^{17} cm^{-3}$ the ratios are 0.98 ± 0.04 and 0.88 ± 0.05 for Oertel's and Griem's Stark broadening parameters respectively. The above results are in excellent agreement with those given in (6.7.1). However, for $N_e > 10^{17} cm^{-3}$ the experimental width of the 5016 A° line deviates considerably from the calculated values. At $N_e \sim 3 \times 10^{17} cm^{-3}$ the experimental width is ~ 25% less than the theoretical width. A tentative explanation of this behaviour, given by the authors, was that the estimates of Debye shielding effects available at the time were too low. However, they though that a more detailed evaluation of such effects would be unlikely to account for all of the observed discrepancy.

The conclusions of these authors are essentially correct since it is now known (see 5.3.5) that for the width, both electric fields in the interaction (5.5.) should be shielded, to a first approximation. However, when the present calculations, which include Debye shielding effects in this manner, are compared with the calculations of Oertel the reduction in

the width is only ~ 10% which does not entirely account for the discrepancies.

The most likely explanation of this behaviour is in terms of the transition from the quadratic to the linear Stark effect. It will be recalled that this effect has already been considered in connection with the shift measurements of Botticher et al (see 6.7.2). The calculated $\frac{1}{2}$-$\frac{1}{2}$ width of the 5016 A^{o} line for N_e $3 \times 10^{17} cm^{-3}$ is within a factor of ~ 2.5 of the splitting between the upper state of the line and the nearest perturbing level. Consequently, the condition (3.22) for the validity of the isolated line approximation is not satisfied. When the isolated line approximation begines to break down the behaviour of a line will be governed by the transition from the quadratic to the linear Stark effect (see 3.7.3.) In the former regime the width of a line scales as N_e whereas in the latter regime it scales as $N_e^{\frac{2}{3}}$. Thus, when this transition takes place the width will increase more slowly with N_e as observed.

The shift of the 5016 A^{o} line shows large discrepancies for practically the entire electron density range, even when the measurements are compared with Oertel's calculations. At $N_e \sim 10^{16} cm^{-3}$ the calculated shift is too small by the ~ 20%. whereas at $N_e \sim 3 \times 10^{17} cm^{-3}$ it is too large by the ~ 30%.

No explanation of the low density behaviour was given by the authors but that at high densities was again though to result possibly from an underestimate of Debye shielding effects. However, the behaviour of the shift of 5016 A^{o} line observed by Grieg et al, as the electron density is varied is similar to that observed by Botticher et al. This is illustrated in Fig. (6.5) where the ratios of the experimental to calculated shifts corresponding to the measurements of Botticher et al and the author s calculations, and the measurements of Grieg et al and the calculations of Oertel, are plotted. Because of the similarity between the two sets of measurements the interpretation of the results obtained by Greig et al can be considered to be the same as that used for the results obtained by Botticher et al. The reader is therefore referred to (6.7.2) for further discussion.

6.9. Summary of Results and Conclusions

The results obtained in Part I and the conclusion that can be drawn from them are summarised briefly below.

When calculating the widths and ion broadening parameters of isolated HeI lines which fall in the visible region of the spectrum the errors that arise from neglecting higher order effects such as lower state broadening, the quadrupole term in the multipole expansion and the back reaction of the atom on the perturber

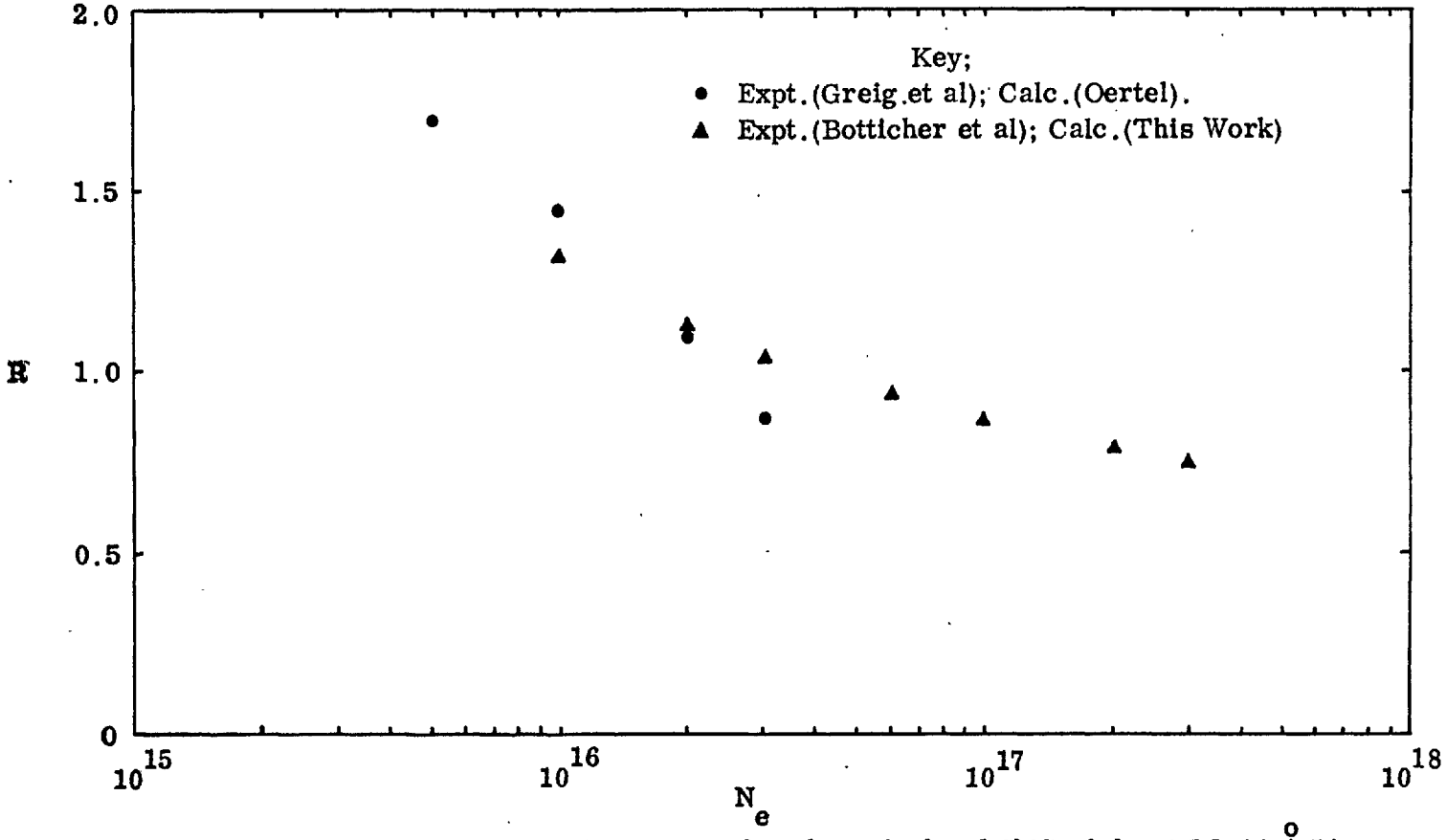

Fig.(6.5) The Ratio R of the Measured to the Calculated Shift of the HeI 5016 Å Line.

are negligible for T_e satisfying $10^4 \leq T_e(^\circ K) \leq 4 \times 10^4$ and even for T_e satisfying $2.5 \times 10^3 \leq T_e(^\circ K) \leq 8 \times 10^4$ the errors in the widths are expected to be $\sim$ 10%.

At low electron temperatures the neglect of the quadrupole term in the interaction can for certain lines lead to discrepancies when calculating the electron shift. For example at $T_e = 10^4$ °K the discrepancies are $\sim$ 30% and $\sim$15% for the 3889 and 5016 A° lines respectively, but at $T_e = 4 \times 10^4$ °K the discrepancies are negligible.

The comparisons between theory and experiment have shown that the line widths calculated from the Stark broadening parameters given in this work, using the quasi-static theory for the ions are in better agreement with experiment than those obtained from the Stark broadening parameters calculated by Griem (1). For example, using the author's calculations the average ratio of experimental to theoretical widths is ≈ 1.0 compared with ≈ 0.9 when Griem's calculations are used. This improvement stems mainly from the more accurate values of the functions a(z) used in this work. These results confirm the -10% correction to the widths calculated from Griem's parameters which has been suggested on empirical grounds by Lincke (21).

The comparisons between the theoretical and experimental widths also show that the ion broadening can be treated by the

quasi-static approximation even when the characteristic frequency of the ion field is of the same order as the electron impact $\frac{1}{2}$-$\frac{1}{2}$ width (i.e. $\sigma \sim 1$). A similar conclusion has been reached theoretically by Griem (1).

In contrast to the good agreement between theory and experiment found for the widths, the shifts calculated from the Stark broadening parameters given in this work, again, using the quasi-static theory for the ions, are in general systematically smaller than the measured shifts for $N_e \gtrsim 10^{16} cm^{-3}$, whereas for $N_e \lesssim 10^{16} cm^{-3}$ the reverse is true; similar results are obtained when the Stark broadening parameters of other workers are used. The explanation of the results for $N_e \lesssim 10^{16} cm^{-3}$ appears to be that although σ is ~ 1 the quasi-static approximation is not valid for the ions (i.e. the ion motions can not be neglected). This result conflicts with that obtained for the widths (see above). However, the two can be reconciled because the ions have a larger effect on the shift of an isolated line that they do on the width (see (3.2.7), and (3.2.8)) and hence the effects produced by the breakdown of the quasi-static approximation would be expected to be much more noticeable for the shifts. The discrepancies observed at $N_e \gtrsim 10^{16}$ cm^{-3} appear to be attributable to the transition from the quadratic to the linear Stark effect.

A comparison of the calculated and experimental ion broadening parameters shows that for some lines discrepancies as large as a factor of 2 are observed. It is suggested that these discrepancies might arise from the asymptotic wing formula which were used in the experimental determination of the ion broadening parameters (see (4.2)).

6.10 Tables of Stark Broadening Parameters for 16 Isolated HeI Lines

The Stark broadening parameters for 16 isolated HeI lines were calculated using the procedure outlined in (6.1). For the ρ_{min} cut-off 'cut-off 2' was used. To select the lines the work of Martin (35) was used. From this comprehensive wavelength list lines were chosen such that:

a) The wavelength of the line, with the exception of $1^1S - 2^1P$ 584 A^o line satisfies $2{,}000 < \lambda < 8{,}000$ A^o

b) The intensity of the line is $\gtrsim 100$ on the intensity scale used by Martin

This method of selection gave a total of 16 lines and they are listed in Table (6.18) together with splitting $\omega_{\alpha\alpha'}$ of the nearest perturbing level.

A number of factors can determine the range of validity and

accuracy of the calculated Stark broadening parameters. These factors are considered below.

At sufficiently high electron densities the isolated line approximation (see 3.7.1) will break down for any line. An estimate of the electron density range over which a line may be considered to be isolated can be obtained by comparing the splitting $\omega_{\alpha\alpha'}$ between the upper state of the line and the nearest perturbing level, with quasi-static $\frac{1}{2}$-$\frac{1}{2}$ width w_H of a hydrogenic line, whose upper state has the same principal quantum number n as the upper state of the line w_H is given by (see (13)),

$$w_H \approx 5n^2 \frac{h}{m} N_e^{\frac{2}{3}}$$

$$= 1.2\, n^2 N_e^{\frac{2}{3}} \text{ cm}^{-1}$$

where N_e is in units of 10^{16}cm^{-3}. Because w_H will overestimate the width of line whose upper state is non-degenerate in ℓ, the orbital quantum number, an estimate of the electron density below which a line can be considered to be isolated is given by:

$$N_e < (N_e)_c$$

where

$$(N_e)_c = \left[\frac{\omega_{\alpha\alpha'}}{1.2n^2}\right]^{3/2} \qquad (6,9)$$

TABLE (6.18)

Transitions, Wavelengths, The Separations of the Nearest Perturbing Level and the Critical Density for the Validity of the Isolated Line Approximations for the Lines which Stark Broadening Parameters have been Calculated

TRANSITIONS	$\lambda(A^o)$	$\omega_{\alpha\alpha'}(cm^{-1})$	$(N_e)_c \times 10^{16} cm^{-3}$
$2^1P - 3^1S$	7281.4	-1344. *	1.4×10^3
$2^3P - 3^3S$	7065.2	-2328.	3.2×10^3
$2^1P - 3^1D$	6678.2	- 104.4	30.0
$2^1P - 4^1D$	4921.9	- 5.52	0.15
$2^3P - 4^3D$	4471.5	- 7.21	0.23
$2^3P - 3^3D$	5876.6	537.0	3.5×10^2
$2^1P - 4^1S$	5047.7	- 552.5	1.5×10^2
$2^1S - 3^1P$	5015.7	104.4	30.0
$2^3P - 4^3S$	4713.4	- 918.9	3.3×10^2
$2^1P - 5^1S$	4437.6	- 278.9	28.0
$2^3P - 5^3S$	4120.8	- 453.7	59.0
$2^1S - 4^1P$	3964.7	46.26	3.7
$2^3S - 3^3P$	3888.7	- 537.0	3.5×10^2
$2^3S - 4^3P$	3187.8	- 227.4	41.0
$2^3S - 5^3P$	2945.1	- 116.5	7.6
$1^1S - 2^1P$	584.3	4857.4	3.2×10^5

* Negative sign indicates that nearest perturbing level is situated above upper level of line and vice versa

In (6.9) $\omega_{\alpha\alpha'}$ is cm^{-1} and $(N_e)_c$ is in units of $10^{16} cm^{-3}$. The value of $(N_e)_c$ for each of the lines selected is also given in Table (6.18). More specifically by comparing the value of $(N_e)_c$ given in Table (6.18) for 5016 A^o line with the results obtained for this line by Greig et al (see 6.8) the following condition for a line to be considered as isolated is suggested.

$$N_e \leqslant 0.2\ (N_e)_c \tag{6.10}$$

When calculating the Stark broadening parameters the critical density $(N_e)_c$ was used only as a guide to the range of N_e used in the calculations. In general, the calculations were terminated at values of $N_e > (N_e)_c$; this must be borne in mind when using the tables.

For the equivalent cut-off procedure to be valid the condition $\rho_{max} / \rho_{min} \gg 1$ must be satisfied (see 5.3.5). The upper impact parameter can be estimated by:

$$\rho_{max} \sim \rho_D = 6.9 \times 10^{-8} \left(\frac{T_e}{N_e}\right)^{\frac{1}{2}} \text{ cm} \tag{6.11}$$

where T_e is in ^oK and N_e is in units of $10^{16} cm^{-3}$. Baranger (4) gives two estimates for ρ_{min}, one valid for $z_{\alpha\alpha'}$ (see 5.1) small, the other for $z_{\alpha\alpha'}$ large. The two expressions for ρ_{min} are respectively:

$$\rho_{min} \approx \lambda\!\!\!^{-} n^2 \tag{6.12}$$

$$\rho_{min} \approx \lambda\!\!\!^{-} n^{4/3} (2E/\hbar\, \omega_{\alpha\alpha'}) \tag{6.13}$$

where λ is the De Broglie wavelength, n is the principal quantum number of the upper state of the line α, E is the perturber energy, and $\omega_{\alpha\alpha'}$ has the usual meaning. If in (6.12) and (6.13) ρ_{min} is evaluated using the mean electron velocity $(8kT_e/\pi m)^{\frac{1}{2}}$ and E is assumed to be equal to kT_e, then from (6.12), (6.13) and (6.11) the ratio of ρ_{max}/ρ_{min} becomes:

$$\rho_{max}/\rho_{min} \approx 4 \times 10^6 \frac{T_e}{N_e^{\frac{1}{2}}} \cdot \frac{1}{n^2} \text{ (for } z_{\alpha\alpha'} \text{ small)} \quad (6.14)$$

$$\rho_{max}/\rho_{min} \approx 3 \times 10^6 \frac{T_e^{\frac{2}{3}}}{N_e^{\frac{1}{2}}} \omega_{\alpha\alpha'}^{\frac{1}{3}} \frac{1}{n^{4/3}} \text{ (for } z_{\alpha\alpha'} \text{ large)} \quad (6.15)$$

where T_e is in ^oK, N_e is in units of $10^{16} cm^{-3}$ and $\omega_{\alpha\alpha'}$ is in cm^{-1}. When using the tables of Stark broadening parameters (6.14) or (6.15) should be used to ensure that errors do not arise from the breakdown of the equivalent cut-off procedure.

As discussed in (6.6.1) the errors in the widths produced by neglecting the correction for the back reaction of the atom on the perturber, and the lower state broadening are less than 10% provided T_e satisfies $2500 < T_e(^oK) < 80{,}000$ and are negligible if T_e satisfies $10^4 \leq T(^oK) \leq 4 \times 10^4$. Since the temperature range used in these calculations is $5000 \leq T_e(^oK) \leq 60{,}000$ the errors resulting from the neglect of these effects will be $\sim 5\%$ at the limits of T_e, for lines arising from levels with n=3,

and negligible of intermediate values of T_e. For lines arising from levels with $n \geqslant 4$ the errors should be negligible for the entire range of T_e. Since the ion broadening parameter is proportional to $(1/w)^{\frac{3}{4}}$, where w is the electron impact $\frac{1}{2}$-$\frac{1}{2}$ width the errors produced by making the approximations mentioned should be even smaller than those for the widths.

The errors in the electron impact shifts produced by neglecting the quadrupole term in the interaction can be important for certain lines at low electron temperatures (see (6.4)) and errors will also arise from the neglect of the lower state shift. However, the results in (6.7.2.) suggest that the major uncertainties in the shifts arise from factors other than the above approximations; notably from the ion contribution to the shift. In spite of the uncertainties, it was though worthwhile to calculate the electron impact shifts because the only other calculations which are available and which include Debye shielding effects and the use of the numerically accurate b(z) functions, are those made by Oertel for 4 HeI lines (see (6.4)). It is hoped that the shifts given in the following tables will at least assist in the interpretation of experimentally determined shifts and that, possibly, they might also stimulate a systematic investigation of the shifts of isolated HeI lines.

The Stark broadening parameters for the 16 lines listed in Table (6.18) are presented in the following Table (6.19).

A separate page is devoted to each spectral line and the wavelength of the line is given at the top of the page. For each electron density the Stark broadening parameters are calculated for the range of electron temperatures mentioned above and the results are presented in five columns. Column one corresponds to T_e in ^oK, column two to the electron impact $\frac{1}{2}$-$\frac{1}{2}$ width in Angstrom units, column three to the shift to width ratio (with the convention that a shift to the red is positive) and the final column contains the parameter σ which is calculated from:

$$\sigma = 5.30 \times 10^9 \frac{w}{\lambda^2} \cdot \frac{1}{T_e^{\frac{1}{2}}} \cdot \frac{1}{N_e^{\frac{1}{3}}}$$

where w is the electron impact $\frac{1}{2}$-$\frac{1}{2}$ width in A^o, λ is the wavelength of the line in A^o, T_e is in ^oK and N_e is units of $10^{16} cm^{-3}$. This relationship was calculated from (5.19) using for v_i the mean relative ion velocity ($= \sqrt{2}$ x the mean ion velocity).

The Debye shielding parameter for the ion field (see 5.2.1.) is not given in the tables since it does not depend on the electron impact width or shift. This parameter can be calculated from:

$$R = 41.7 N_e^{1/6} T_e^{-1/2}$$

where N_e is in units of $10^{16} cm^{-3}$ and T_e is in ^oK.

TABLE (6.19)

Stark Broadening Parameters for 16 isolated HeI lines

WAVELENGTH OF LINE = 7281.35 ANGSTROMS

CUT-OFF USED = 2

ELECTRON DENSITY = 1.00E 14

T(K)	W(A)	S/W	ALPHA	SIGMA
5000.	2.65E-03	1.32E 00	2.93E-02	1.74E-02
10000.	3.29E-03	1.10E 00	2.49E-02	1.52E-02
20000.	3.80E-03	8.99E-01	2.24E-02	1.24E-02
40000.	4.02E-03	7.35E-01	2.14E-02	9.32E-03
60000.	4.02E-03	6.55E-01	2.15E-02	7.59E-03

ELECTRON DENSITY = 1.00E 15

T(K)	W(A)	S/W	ALPHA	SIGMA
5000.	2.65E-02	1.31E 00	5.22E-02	8.06E-02
10000.	3.29E-02	1.09E 00	4.44E-02	7.08E-02
20000.	3.80E-02	8.95E-01	3.99E-02	5.77E-02
40000.	4.02E-02	7.33E-01	3.81E-02	4.33E-02
60000.	4.02E-02	6.53E-01	3.82E-02	3.53E-02

ELECTRON DENSITY = 1.00E 16

T(K)	W(A)	S/W	ALPHA	SIGMA
5000.	2.65E-01	1.27E 00	9.28E-02	3.75E-01
10000.	3.29E-01	1.07E 00	7.89E-02	3.29E-01
20000.	3.80E-01	8.82E-01	7.09E-02	2.68E-01
40000.	4.02E-01	7.24E-01	6.78E-02	2.01E-01
60000.	4.02E-01	6.46E-01	6.79E-02	1.64E-01

ELECTRON DENSITY = 1.00E 17

T(K)	W(A)	S/W	ALPHA	SIGMA
5000.	2.65E 00	1.16E 00	1.65E-01	1.74E 00
10000.	3.29E 00	1.00E 00	1.40E-01	1.53E 00
20000.	3.79E 00	8.42E-01	1.26E-01	1.25E 00
40000.	4.02E 00	6.98E-01	1.21E-01	9.34E-01
60000.	4.02E 00	6.24E-01	1.21E-01	7.61E-01

ELECTRON DENSITY = 1.00E 18

T(K)	W(A)	S/W	ALPHA	SIGMA
5000.	2.39E 01	8.54E-01	3.17E-01	7.29E 00
10000.	3.12E 01	8.26E-01	2.59E-01	6.73E 00
20000.	3.68E 01	7.30E-01	2.30E-01	5.60E 00
40000.	3.94E 01	6.21E-01	2.18E-01	4.25E 00
60000.	3.95E 01	5.60E-01	2.18E-01	3.47E 00

WAVELENGTH OF LINE = 7065.19 ANGSTROMS

CUT-OFF USED = 2

ELECTRON DENSITY = 1.00E 14

T(K)	W(A)	S/W	ALPHA	SIGMA
5000.	1.39E-03	1.46E 00	2.59E-02	9.65E-03
10000.	1.78E-03	1.23E 00	2.15E-02	8.74E-03
20000.	2.16E-03	1.01E 00	1.86E-02	7.50E-03
40000.	2.42E-03	8.23E-01	1.71E-02	5.94E-03
60000.	2.48E-03	7.28E-01	1.67E-02	4.99E-03

ELECTRON DENSITY = 1.00E 15

T(K)	W(A)	S/W	ALPHA	SIGMA
5000.	1.39E-02	1.45E 00	4.60E-02	4.48E-02
10000.	1.78E-02	1.23E 00	3.83E-02	4.06E-02
20000.	2.16E-02	1.01E 00	3.31E-02	3.49E-02
40000.	2.42E-02	8.21E-01	3.04E-02	2.76E-02
60000.	2.48E-02	7.27E-01	2.98E-02	2.32E-02

ELECTRON DENSITY = 1.00E 16

T(K)	W(A)	S/W	ALPHA	SIGMA
5000.	1.39E-01	1.42E 00	8.19E-02	2.08E-01
10000.	1.78E-01	1.21E 00	6.80E-02	1.89E-01
20000.	2.16E-01	1.00E 00	5.88E-02	1.62E-01
40000.	2.42E-01	8.15E-01	5.40E-02	1.28E-01
60000.	2.48E-01	7.22E-01	5.29E-02	1.08E-01

ELECTRON DENSITY = 1.00E 17

T(K)	W(A)	S/W	ALPHA	SIGMA
5000.	1.39E 00	1.33E 00	1.46E-01	9.67E-01
10000.	1.78E 00	1.16E 00	1.21E-01	8.76E-01
20000.	2.16E 00	9.69E-01	1.05E-01	7.52E-01
40000.	2.42E 00	7.95E-01	9.60E-02	5.96E-01
60000.	2.48E 00	7.06E-01	9.41E-02	5.00E-01

ELECTRON DENSITY = 1.00E 18

T(K)	W(A)	S/W	ALPHA	SIGMA
5000.	1.36E 01	1.03E 00	2.62E-01	4.42E 00
10000.	1.76E 01	9.94E-01	2.17E-01	4.03E 00
20000.	2.15E 01	8.73E-01	1.87E-01	3.48E 00
40000.	2.41E 01	7.34E-01	1.71E-01	2.76E 00
60000.	2.48E 01	6.58E-01	1.68E-01	2.32E 00

WAVELENGTH OF LINE = 6678.15 ANGSTROMS

CUT-OFF USED = 2

ELECTRON DENSITY = 1.00E 14

T(K)	W(A)	S/W	ALPHA	SIGMA
5000.	4.16E-03	6.28E-01	4.65E-02	3.24E-02
10000.	3.78E-03	5.79E-01	4.99E-02	2.08E-02
20000.	3.40E-03	5.40E-01	5.41E-02	1.33E-02
40000.	3.06E-03	5.00E-01	5.86E-02	8.42E-03
60000.	2.87E-03	4.72E-01	6.15E-02	6.45E-03

ELECTRON DENSITY = 1.00E 15

T(K)	W(A)	S/W	ALPHA	SIGMA
5000.	4.16E-02	6.06E-01	8.27E-02	1.50E-01
10000.	3.78E-02	5.62E-01	8.88E-02	9.68E-02
20000.	3.40E-02	5.28E-01	9.61E-02	6.15E-02
40000.	3.06E-02	4.89E-01	1.04E-01	3.91E-02
60000.	2.87E-02	4.63E-01	1.09E-01	2.99E-02

ELECTRON DENSITY = 1.00E 16

T(K)	W(A)	S/W	ALPHA	SIGMA
5000.	4.05E-01	5.47E-01	1.50E-01	6.80E-01
10000.	3.71E-01	5.16E-01	1.60E-01	4.40E-01
20000.	3.35E-01	4.91E-01	1.73E-01	2.81E-01
40000.	3.02E-01	4.60E-01	1.87E-01	1.79E-01
60000.	2.84E-01	4.37E-01	1.96E-01	1.38E-01

ELECTRON DENSITY = 1.00E 17

T(K)	W(A)	S/W	ALPHA	SIGMA
5000.	3.25E 00	4.39E-01	3.14E-01	2.54E 00
10000.	3.15E 00	4.31E-01	3.22E-01	1.74E 00
20000.	2.95E 00	4.24E-01	3.38E-01	1.15E 00
40000.	2.74E 00	4.06E-01	3.58E-01	7.56E-01
60000.	2.61E 00	3.89E-01	3.71E-01	5.88E-01

ELECTRON DENSITY = 1.00E 18

T(K)	W(A)	S/W	ALPHA	SIGMA
5000.	1.61E 01	3.69E-01	9.47E-01	5.84E 00
10000.	2.02E 01	3.68E-01	8.00E-01	5.18E 00
20000.	2.17E 01	3.77E-01	7.58E-01	3.93E 00
40000.	2.19E 01	3.68E-01	7.53E-01	2.80E 00
60000.	2.16E 01	3.54E-01	7.61E-01	2.26E 00

WAVELENGTH OF LINE = 5876.62 ANGSTROMS

CUT-OFF USED = 2

ELECTRON DENSITY = 1.00E 14

T(K)	W(A)	S/W	ALPHA	SIGMA
5000.	1.53E-03	-5.78E-01	-2.08E-02	1.54E-02
10000.	1.65E-03	-3.56E-01	-1.97E-02	1.17E-02
20000.	1.70E-03	-1.74E-01	-1.92E-02	8.56E-03
40000.	1.70E-03	-4.60E-02	-1.92E-02	6.06E-03
60000.	1.68E-03	2.88E-03	-1.94E-02	4.87E-03

ELECTRON DENSITY = 1.00E 15

T(K)	W(A)	S/W	ALPHA	SIGMA
5000.	1.53E-02	-5.70E-01	-3.70E-02	7.14E-02
10000.	1.65E-02	-3.51E-01	-3.50E-02	5.44E-02
20000.	1.70E-02	-1.70E-01	-3.41E-02	3.98E-02
40000.	1.70E-02	-4.37E-02	-3.41E-02	2.81E-02
60000.	1.68E-02	4.77E-03	-3.45E-02	2.26E-02

ELECTRON DENSITY = 1.00E 16

T(K)	W(A)	S/W	ALPHA	SIGMA
5000.	1.53E-01	-5.47E-01	-6.59E-02	3.31E-01
10000.	1.65E-01	-3.36E-01	-6.23E-02	2.53E-01
20000.	1.70E-01	-1.60E-01	-6.07E-02	1.85E-01
40000.	1.70E-01	-3.64E-02	-6.07E-02	1.31E-01
60000.	1.68E-01	1.08E-02	-6.14E-02	1.05E-01

ELECTRON DENSITY = 1.00E 17

T(K)	W(A)	S/W	ALPHA	SIGMA
5000.	1.51E 00	-4.76E-01	-1.18E-01	1.52E 00
10000.	1.63E 00	-2.88E-01	-1.11E-01	1.16E 00
20000.	1.69E 00	-1.26E-01	-1.08E-01	8.53E-01
40000.	1.70E 00	-1.23E-02	-1.08E-01	6.05E-01
60000.	1.67E 00	3.10E-02	-1.09E-01	4.87E-01

ELECTRON DENSITY = 1.00E 18

T(K)	W(A)	S/W	ALPHA	SIGMA
5000.	1.17E 01	-2.93E-01	-2.55E-01	5.46E 00
10000.	1.39E 01	-1.46E-01	-2.23E-01	4.61E 00
20000.	1.52E 01	-1.68E-02	-2.09E-01	3.57E 00
40000.	1.58E 01	7.09E-02	-2.03E-01	2.61E 00
60000.	1.58E 01	1.02E-01	-2.04E-01	2.13E 00

WAVELENGTH OF LINE = 5047.74 ANGSTROMS

CUT-OFF USED = 2

ELECTRON DENSITY = 1.00E 14

T(K)	W(A)	S/W	ALPHA	SIGMA
5000.	5.40E-03	1.21E 00	4.75E-02	7.36E-02
10000.	6.52E-03	9.99E-01	4.12E-02	6.29E-02
20000.	7.26E-03	8.14E-01	3.81E-02	4.95E-02
40000.	7.44E-03	6.64E-01	3.74E-02	3.59E-02
60000.	7.30E-03	5.91E-01	3.79E-02	2.87E-02

ELECTRON DENSITY = 1.00E 15

T(K)	W(A)	S/W	ALPHA	SIGMA
5000.	5.40E-02	1.19E 00	8.45E-02	3.42E-01
10000.	6.52E-02	9.86E-01	7.33E-02	2.92E-01
20000.	7.26E-02	8.06E-01	6.77E-02	2.30E-01
40000.	7.44E-02	6.59E-01	6.64E-02	1.67E-01
60000.	7.30E-02	5.86E-01	6.74E-02	1.33E-01

ELECTRON DENSITY = 1.00E 16

T(K)	W(A)	S/W	ALPHA	SIGMA
5000.	5.40E-01	1.12E 00	1.50E-01	1.59E 00
10000.	6.52E-01	9.46E-01	1.30E-01	1.36E 00
20000.	7.26E-01	7.81E-01	1.20E-01	1.07E 00
40000.	7.44E-01	6.41E-01	1.18E-01	7.74E-01
60000.	7.30E-01	5.72E-01	1.20E-01	6.20E-01

ELECTRON DENSITY = 1.00E 17

T(K)	W(A)	S/W	ALPHA	SIGMA
5000.	5.25E 00	9.21E-01	2.73E-01	7.17E 00
10000.	6.41E 00	8.27E-01	2.35E-01	6.19E 00
20000.	7.18E 00	7.04E-01	2.16E-01	4.91E 00
40000.	7.39E 00	5.87E-01	2.11E-01	3.57E 00
60000.	7.26E 00	5.26E-01	2.14E-01	2.86E 00

ELECTRON DENSITY = 1.00E 18

T(K)	W(A)	S/W	ALPHA	SIGMA
5000.	5.56E 00	3.44E 00	2.61E 00	3.53E 00
10000.	3.61E 01	7.17E-01	6.42E-01	1.62E 01
20000.	5.70E 01	5.39E-01	4.56E-01	1.81E 01
40000.	6.35E 01	4.62E-01	4.21E-01	1.42E 01
60000.	6.41E 01	4.18E-01	4.18E-01	1.17E 01

WAVELENGTH OF LINE = 5015.68 ANGSTROMS

CUT-OFF USED = 2

ELECTRON DENSITY = 1.00E 14

T(K)	W(A)	S/W	ALPHA	SIGMA
5000.	3.70E-03	-6.28E-01	-4.88E-02	5.11E-02
10000.	3.53E-03	-5.20E-01	-5.06E-02	3.44E-02
20000.	3.27E-03	-4.17E-01	-5.36E-02	2.26E-02
40000.	2.96E-03	-3.23E-01	-5.77E-02	1.45E-02
60000.	2.77E-03	-2.76E-01	-6.07E-02	1.10E-02

ELECTRON DENSITY = 1.00E 15

T(K)	W(A)	S/W	ALPHA	SIGMA
5000.	3.70E-02	-6.05E-01	-8.68E-02	2.37E-01
10000.	3.53E-02	-5.04E-01	-9.01E-02	1.60E-01
20000.	3.27E-02	-4.04E-01	-9.54E-02	1.05E-01
40000.	2.96E-02	-3.13E-01	-1.03E-01	6.71E-02
60000.	2.77E-02	-2.68E-01	-1.08E-01	5.12E-02

ELECTRON DENSITY = 1.00E 16

T(K)	W(A)	S/W	ALPHA	SIGMA
5000.	3.60E-01	-5.42E-01	-1.58E-01	1.07E 00
10000.	3.45E-01	-4.55E-01	-1.63E-01	7.28E-01
20000.	3.22E-01	-3.66E-01	-1.72E-01	4.79E-01
40000.	2.93E-01	-2.82E-01	-1.84E-01	3.08E-01
60000.	2.74E-01	-2.40E-01	-1.94E-01	2.35E-01

ELECTRON DENSITY = 1.00E 17

T(K)	W(A)	S/W	ALPHA	SIGMA
5000.	2.86E 00	-4.22E-01	-3.34E-01	3.95E 00
10000.	2.93E 00	-3.56E-01	-3.27E-01	2.86E 00
20000.	2.85E 00	-2.83E-01	-3.35E-01	1.97E 00
40000.	2.66E 00	-2.11E-01	-3.52E-01	1.30E 00
60000.	2.52E 00	-1.75E-01	-3.66E-01	1.01E 00

ELECTRON DENSITY = 1.00E 18

T(K)	W(A)	S/W	ALPHA	SIGMA
5000.	1.26E 01	-3.19E-01	-1.09E 00	8.11E 00
10000.	1.84E 01	-2.44E-01	-8.27E-01	8.34E 00
20000.	2.09E 01	-1.81E-01	-7.51E-01	6.71E 00
40000.	2.13E 01	-1.23E-01	-7.40E-01	4.84E 00
60000.	2.09E 01	-9.39E-02	-7.50E-01	3.87E 00

WAVELENGTH OF LINE = 4921.93 ANGSTROMS

CUT-OFF USED = 2

ELECTRON DENSITY = 1.00E 14

T(K)	W(A)	S/W	ALPHA	SIGMA
5000.	2.23E-02	3.78E-01	2.21E-01	3.19E-01
10000.	1.90E-02	3.39E-01	2.48E-01	1.93E-01
20000.	1.51E-02	3.15E-01	2.95E-01	1.08E-01
40000.	9.90E-03	3.06E-01	4.06E-01	5.02E-02
60000.	6.93E-03	3.05E-01	5.30E-01	2.87E-02

ELECTRON DENSITY = 1.00E 15

T(K)	W(A)	S/W	ALPHA	SIGMA
5000.	1.96E-01	3.15E-01	4.33E-01	1.30E 00
10000.	1.71E-01	2.85E-01	4.78E-01	8.06E-01
20000.	1.39E-01	2.66E-01	5.61E-01	4.61E-01
40000.	9.22E-02	2.61E-01	7.61E-01	2.17E-01
60000.	6.50E-02	2.62E-01	9.89E-01	1.25E-01

ELECTRON DENSITY = 1.00E 16

T(K)	W(A)	S/W	ALPHA	SIGMA
5000.	1.47E 00	2.42E-01	9.53E-01	4.55E 00
10000.	1.37E 00	2.22E-01	1.00E 00	3.00E 00
20000.	1.16E 00	2.11E-01	1.14E 00	1.79E 00
40000.	7.95E-01	2.11E-01	1.51E 00	8.69E-01
60000.	5.70E-01	2.14E-01	1.94E 00	5.09E-01

WAVELENGTH OF LINE = 4713.38 ANGSTROMS

CUT-OFF USED = 2

ELECTRON DENSITY = 1.00E 14

T(K)	W(A)	S/W	ALPHA	SIGMA
5000.	2.79E-03	1.35E 00	4.22E-02	4.36E-02
10000.	3.51E-03	1.12E 00	3.55E-02	3.88E-02
20000.	4.12E-03	9.07E-01	3.15E-02	3.22E-02
40000.	4.45E-03	7.31E-01	2.97E-02	2.46E-02
60000.	4.49E-03	6.44E-01	2.96E-02	2.02E-02

ELECTRON DENSITY = 1.00E 15

T(K)	W(A)	S/W	ALPHA	SIGMA
5000.	2.79E-02	1.33E 00	7.51E-02	2.02E-01
10000.	3.51E-02	1.11E 00	6.32E-02	1.80E-01
20000.	4.12E-02	9.01E-01	5.60E-02	1.50E-01
40000.	4.45E-02	7.27E-01	5.29E-02	1.14E-01
60000.	4.49E-02	6.41E-01	5.26E-02	9.40E-02

ELECTRON DENSITY = 1.00E 16

T(K)	W(A)	S/W	ALPHA	SIGMA
5000.	2.79E-01	1.27E 00	1.33E-01	9.40E-01
10000.	3.51E-01	1.07E 00	1.12E-01	8.37E-01
20000.	4.12E-01	8.81E-01	9.96E-02	6.95E-01
40000.	4.45E-01	7.14E-01	9.49E-02	5.31E-01
60000.	4.49E-01	6.31E-01	9.34E-02	4.37E-01

ELECTRON DENSITY = 1.00E 17

T(K)	W(A)	S/W	ALPHA	SIGMA
5000.	2.78E 00	1.09E 00	2.38E-01	4.35E 00
10000.	3.50E 00	9.71E-01	2.00E-01	3.88E 00
20000.	4.12E 00	8.19E-01	1.77E-01	3.22E 00
40000.	4.45E 00	6.73E-01	1.67E-01	2.46E 00
60000.	4.48E 00	5.97E-01	1.66E-01	2.03E 00

ELECTRON DENSITY = 1.00E 18

T(K)	W(A)	S/W	ALPHA	SIGMA
5000.	8.05E 00	1.86E 00	1.07E 00	5.86E 00
10000.	2.90E 01	7.33E-01	4.10E-01	1.49E 01
20000.	3.71E 01	6.65E-01	3.41E-01	1.35E 01
40000.	4.16E 01	5.66E-01	3.13E-01	1.07E 01
60000.	4.25E 01	5.08E-01	3.08E-01	8.93E 00

WAVELENGTH OF LINE = 4471.48 ANGSTROMS

CUT-OFF USED = 2

ELECTRON DENSITY = 1.00E 14

T(K)	W(A)	S/W	ALPHA	SIGMA
5000.	1.41E-02	3.66E-02	1.95E-01	2.45E-01
10000.	1.24E-02	1.28E-02	2.14E-01	1.53E-01
20000.	1.05E-02	1.12E-02	2.43E-01	9.15E-02
40000.	7.68E-03	2.00E-02	3.08E-01	4.72E-02
60000.	5.71E-03	2.60E-02	3.84E-01	2.86E-02

ELECTRON DENSITY = 1.00E 15

T(K)	W(A)	S/W	ALPHA	SIGMA
5000.	1.23E-01	-6.91E-02	3.85E-01	9.91E-01
10000.	1.11E-01	-7.25E-02	4.14E-01	6.36E-01
20000.	9.64E-02	-5.78E-02	4.62E-01	3.89E-01
40000.	7.15E-02	-3.85E-02	5.78E-01	2.04E-01
60000.	5.37E-02	-2.76E-02	7.16E-01	1.25E-01

ELECTRON DENSITY = 1.00E 16

T(K)	W(A)	S/W	ALPHA	SIGMA
5000.	9.39E-01	-1.84E-01	8.37E-01	3.52E 00
10000.	9.10E-01	-1.57E-01	8.57E-01	2.41E 00
20000.	8.22E-01	-1.22E-01	9.25E-01	1.54E 00
40000.	6.26E-01	-9.33E-02	1.13E 00	8.30E-01
60000.	4.75E-01	-8.15E-02	1.40E 00	5.14E-01

WAVELENGTH OF LINE = 4437.55 ANGSTROMS

CUT-OFF USED = 2

ELECTRON DENSITY = 1.00E 14

T(K)	W(A)	S/W	ALPHA	SIGMA
5000.	1.25E-02	1.13E 00	6.90E-02	2.21E-01
10000.	1.47E-02	9.24E-01	6.10E-02	1.84E-01
20000.	1.60E-02	7.51E-01	5.75E-02	1.41E-01
40000.	1.60E-02	6.11E-01	5.75E-02	9.96E-02
60000.	1.55E-02	5.43E-01	5.88E-02	7.89E-02

ELECTRON DENSITY = 1.00E 15

T(K)	W(A)	S/W	ALPHA	SIGMA
5000.	1.25E-01	1.09E 00	1.23E-01	1.03E 00
10000.	1.47E-01	9.03E-01	1.09E-01	8.54E-01
20000.	1.60E-01	7.37E-01	1.02E-01	6.54E-01
40000.	1.60E-01	6.01E-01	1.02E-01	4.63E-01
60000.	1.55E-01	5.35E-01	1.05E-01	3.67E-01

ELECTRON DENSITY = 1.00E 16

T(K)	W(A)	S/W	ALPHA	SIGMA
5000.	1.25E 00	9.81E-01	2.19E-01	4.75E 00
10000.	1.47E 00	8.36E-01	1.93E-01	3.96E 00
20000.	1.60E 00	6.93E-01	1.82E-01	3.04E 00
40000.	1.60E 00	5.70E-01	1.82E-01	2.15E 00
60000.	1.55E 00	5.09E-01	1.86E-01	1.70E 00

ELECTRON DENSITY = 1.00E 17

T(K)	W(A)	S/W	ALPHA	SIGMA
5000.	9.96E 00	7.36E-01	4.61E-01	1.76E 01
10000.	1.31E 01	6.73E-01	3.75E-01	1.64E 01
20000.	1.48E 01	5.80E-01	3.42E-01	1.31E 01
40000.	1.52E 01	4.85E-01	3.36E-01	9.47E 00
60000.	1.48E 01	4.35E-01	3.42E-01	7.56E 00

ELECTRON DENSITY = 1.00E 18

T(K)	W(A)	S/W	ALPHA	SIGMA
5000.	1.51E-01	2.15E 01	1.07E 02	1.24E-01
10000.	2.12E 01	1.16E 00	2.62E 00	1.23E 01
20000.	7.43E 01	4.31E-01	1.02E 00	3.05E 01
40000.	1.05E 02	3.21E-01	7.89E-01	3.04E 01
60000.	1.11E 02	2.88E-01	7.57E-01	2.62E 01

WAVELENGTH OF LINE = 4120.82 ANGSTROMS

CUT-OFF USED = 2

ELECTRON DENSITY = 1.00E 14

T(K)	W(A)	S/W	ALPHA	SIGMA
5000.	6.66E-03	1.25E 00	6.12E-02	1.36E-01
10000.	8.22E-03	1.03E 00	5.23E-02	1.19E-01
20000.	9.40E-03	8.28E-01	4.73E-02	9.61E-02
40000.	9.89E-03	6.62E-01	4.55E-02	7.15E-02
60000.	9.83E-03	5.83E-01	4.57E-02	5.80E-02

ELECTRON DENSITY = 1.00E 15

T(K)	W(A)	S/W	ALPHA	SIGMA
5000.	6.66E-02	1.22E 00	1.09E-01	6.32E-01
10000.	8.22E-02	1.01E 00	9.30E-02	5.52E-01
20000.	9.40E-02	8.17E-01	8.41E-02	4.46E-01
40000.	9.89E-02	6.55E-01	8.09E-02	3.32E-01
60000.	9.83E-02	5.77E-01	8.13E-02	2.70E-01

ELECTRON DENSITY = 1.00E 16

T(K)	W(A)	S/W	ALPHA	SIGMA
5000.	6.65E-01	1.13E 00	1.94E-01	2.94E 00
10000.	8.22E-01	9.56E-01	1.65E-01	2.56E 00
20000.	9.40E-01	7.83E-01	1.49E-01	2.07E 00
40000.	9.89E-01	6.32E-01	1.44E-01	1.54E 00
60000.	9.83E-01	5.58E-01	1.45E-01	1.25E 00

ELECTRON DENSITY = 1.00E 17

T(K)	W(A)	S/W	ALPHA	SIGMA
5000.	6.19E 00	8.62E-01	3.64E-01	1.27E 01
10000.	7.90E 00	8.01E-01	3.03E-01	1.14E 01
20000.	9.17E 00	6.84E-01	2.71E-01	9.40E 00
40000.	9.73E 00	5.64E-01	2.59E-01	7.05E 00
60000.	9.70E 00	5.01E-01	2.60E-01	5.74E 00

ELECTRON DENSITY = 1.00E 18

T(K)	W(A)	S/W	ALPHA	SIGMA
5000.	1.68E-01	4.37E 01	5.45E 01	1.60E-01
10000.	1.88E 01	1.33E 00	1.58E 00	1.26E 01
20000.	5.99E 01	5.09E-01	6.63E-01	2.85E 01
40000.	7.71E 01	4.14E-01	5.49E-01	2.59E 01
60000.	8.05E 01	3.70E-01	5.31E-01	2.21E 01

WAVELENGTH OF LINE = 3964.73 ANGSTROMS

CUT-OFF USED = 2

ELECTRON DENSITY = 1.00E 14

T(K)	W(A)	S/W	ALPHA	SIGMA
5000.	1.02E-02	-6.02E-01	-8.77E-02	2.26E-01
10000.	9.59E-03	-5.06E-01	-9.20E-02	1.50E-01
20000.	8.72E-03	-4.18E-01	-9.88E-02	9.63E-02
40000.	7.72E-03	-3.40E-01	-1.08E-01	6.03E-02
60000.	7.11E-03	-3.01E-01	-1.15E-01	4.53E-02

ELECTRON DENSITY = 1.00E 15

T(K)	W(A)	S/W	ALPHA	SIGMA
5000.	1.01E-01	-5.56E-01	-1.57E-01	1.04E 00
10000.	9.52E-02	-4.70E-01	-1.64E-01	6.91E-01
20000.	8.67E-02	-3.90E-01	-1.76E-01	4.45E-01
40000.	7.68E-02	-3.17E-01	-1.93E-01	2.79E-01
60000.	7.08E-02	-2.80E-01	-2.06E-01	2.10E-01

ELECTRON DENSITY = 1.00E 16

T(K)	W(A)	S/W	ALPHA	SIGMA
5000.	8.79E-01	-4.54E-01	-3.11E-01	4.19E 00
10000.	8.58E-01	-3.87E-01	-3.16E-01	2.89E 00
20000.	8.01E-01	-3.20E-01	-3.33E-01	1.91E 00
40000.	7.21E-01	-2.58E-01	-3.60E-01	1.22E 00
60000.	6.69E-01	-2.26E-01	-3.81E-01	9.21E-01

ELECTRON DENSITY = 1.00E 17

T(K)	W(A)	S/W	ALPHA	SIGMA
5000.	5.09E 00	-3.31E-01	-8.32E-01	1.13E 01
10000.	6.07E 00	-2.74E-01	-7.29E-01	9.50E 00
20000.	6.24E 00	-2.22E-01	-7.14E-01	6.91E 00
40000.	5.97E 00	-1.72E-01	-7.39E-01	4.67E 00
60000.	5.67E 00	-1.47E-01	-7.67E-01	3.63E 00

WAVELENGTH OF LINE = 3888.65 ANGSTROMS

CUT-OFF USED = 2

ELECTRON DENSITY = 1.00E 14

T(K)	W(A)	S/W	ALPHA	SIGMA
5000.	9.68E-04	7.59E-01	2.49E-02	2.22E-02
10000.	1.08E-03	5.67E-01	2.28E-02	1.76E-02
20000.	1.14E-03	4.30E-01	2.20E-02	1.31E-02
40000.	1.14E-03	3.37E-01	2.20E-02	9.26E-03
60000.	1.11E-03	2.97E-01	2.24E-02	7.39E-03

ELECTRON DENSITY = 1.00E 15

T(K)	W(A)	S/W	ALPHA	SIGMA
5000.	9.68E-03	7.50E-01	4.42E-02	1.03E-01
10000.	1.08E-02	5.61E-01	4.06E-02	8.18E-02
20000.	1.14E-02	4.26E-01	3.90E-02	6.09E-02
40000.	1.14E-02	3.34E-01	3.91E-02	4.30E-02
60000.	1.11E-02	2.95E-01	3.98E-02	3.43E-02

ELECTRON DENSITY = 1.00E 16

T(K)	W(A)	S/W	ALPHA	SIGMA
5000.	9.68E-02	7.20E-01	7.86E-02	4.80E-01
10000.	1.08E-01	5.43E-01	7.22E-02	3.80E-01
20000.	1.14E-01	4.13E-01	6.94E-02	2.83E-01
40000.	1.14E-01	3.25E-01	6.95E-02	2.00E-01
60000.	1.11E-01	2.88E-01	7.07E-02	1.59E-01

ELECTRON DENSITY = 1.00E 17

T(K)	W(A)	S/W	ALPHA	SIGMA
5000.	9.54E-01	6.33E-01	1.41E-01	2.20E 00
10000.	1.07E 00	4.87E-01	1.29E-01	1.75E 00
20000.	1.14E 00	3.75E-01	1.24E-01	1.31E 00
40000.	1.14E 00	2.98E-01	1.24E-01	9.25E-01
60000.	1.11E 00	2.65E-01	1.26E-01	7.38E-01

ELECTRON DENSITY = 1.00E 18

T(K)	W(A)	S/W	ALPHA	SIGMA
5000.	6.91E 00	4.42E-01	3.20E-01	7.39E 00
10000.	8.98E 00	3.46E-01	2.63E-01	6.79E 00
20000.	1.01E 01	2.73E-01	2.41E-01	5.40E 00
40000.	1.05E 01	2.22E-01	2.34E-01	3.96E 00
60000.	1.04E 01	2.00E-01	2.36E-01	3.21E 00

WAVELENGTH OF LINE = 3187.75 ANGSTROMS

CUT-OFF USED = 2

ELECTRON DENSITY = 1.00E 14

T(K)	W(A)	S/W	ALPHA	SIG A
5000.	3.01E-03	6.99E-01	4.38E-02	1.03E-01
10000.	3.30E-03	5.21E-01	4.09E-02	7.98E-02
20000.	3.39E-03	3.94E-01	4.01E-02	5.79E-02
40000.	3.28E-03	3.07E-01	4.10E-02	3.97E-02
60000.	3.15E-03	2.70E-01	4.23E-02	3.11E-02

ELECTRON DENSITY = 1.00E 15

T(K)	W(A)	S/W	ALPHA	SIGMA
5000.	3.01E-02	6.79E-01	7.78E-02	4.79E-01
10000.	3.30E-02	5.08E-01	7.27E-02	3.71E-01
20000.	3.39E-02	3.85E-01	7.13E-02	2.69E-01
40000.	3.28E-02	3.01E-01	7.30E-02	1.84E-01
60000.	3.15E-02	2.65E-01	7.53E-02	1.44E-01

ELECTRON DENSITY = 1.00E 16

T(K)	W(A)	S/W	ALPHA	SIGMA
5000.	3.00E-01	6.18E-01	1.39E-01	2.21E 00
10000.	3.29E-01	4.69E-01	1.29E-01	1.72E 00
20000.	3.38E-01	3.57E-01	1.27E-01	1.25E 00
40000.	3.28E-01	2.81E-01	1.30E-01	8.55E-01
60000.	3.15E-01	2.48E-01	1.34E-01	6.70E-01

ELECTRON DENSITY = 1.00E 17

T(K)	W(A)	S/W	ALPHA	SIGMA
5000.	2.58E 00	4.66E-01	2.77E-01	8.84E 00
10000.	3.00E 00	3.61E-01	2.47E-01	7.26E 00
20000.	3.17E 00	2.78E-01	2.37E-01	5.43E 00
40000.	3.13E 00	2.20E-01	2.39E-01	3.79E 00
60000.	3.03E 00	1.95E-01	2.45E-01	2.99E 00

ELECTRON DENSITY = 1.00E 18

T(K)	W(A)	S/W	ALPHA	SIGMA
5000.	3.76E 00	6.24E-01	2.09E 00	5.98E 00
10000.	1.49E 01	1.88E-01	7.42E-01	1.68E 01
20000.	2.20E 01	1.31E-01	5.55E-01	1.75E 01
40000.	2.45E 01	1.10E-01	5.11E-01	1.38E 01
60000.	2.47E 01	1.00E-01	5.08E-01	1.13E 01

WAVELENGTH OF LINE = 2945.11 ANGSTROMS

CUT-OFF USED = 2

ELECTRON DENSITY = 1.00E 14

T(K)	W(A)	S/W	ALPHA	SIGMA
5000.	7.83E-03	6.35E-01	6.61E-02	3.14E-01
10000.	8.41E-03	4.72E-01	6.27E-02	2.38E-01
20000.	8.46E-03	3.57E-01	6.24E-02	1.69E-01
40000.	8.04E-03	2.79E-01	6.49E-02	1.14E-01
60000.	7.63E-03	2.45E-01	6.74E-02	8.82E-02

ELECTRON DENSITY = 1.00E 15

T(K)	W(A)	S/W	ALPHA	SIGMA
5000.	7.83E-02	6.02E-01	1.18E-01	1.46E 00
10000.	8.41E-02	4.50E-01	1.11E-01	1.11E 00
20000.	8.46E-02	3.42E-01	1.11E-01	7.86E-01
40000.	8.04E-02	2.67E-01	1.15E-01	5.28E-01
60000.	7.63E-02	2.35E-01	1.20E-01	4.09E-01

ELECTRON DENSITY = 1.00E 16

T(K)	W(A)	S/W	ALPHA	SIGMA
5000.	7.52E-01	5.05E-01	2.16E-01	6.50E 00
10000.	8.19E-01	3.83E-01	2.02E-01	5.00E 00
20000.	8.30E-01	2.93E-01	2.00E-01	3.59E 00
40000.	7.93E-01	2.30E-01	2.07E-01	2.42E 00
60000.	7.54E-01	2.03E-01	2.15E-01	1.88E 00

ELECTRON DENSITY = 1.00E 17

T(K)	W(A)	S/W	ALPHA	SIGMA
5000.	4.47E 00	3.15E-01	5.67E-01	1.79E 01
10000.	6.22E 00	2.27E-01	4.42E-01	1.77E 01
20000.	6.91E 00	1.75E-01	4.08E-01	1.39E 01
40000.	6.95E 00	1.39E-01	4.07E-01	9.85E 00
60000.	6.74E 00	1.22E-01	4.16E-01	7.80E 00

WAVELENGTH OF LINE = 584.33 ANGSTROMS

CUT-OFF USED = 2

ELECTRON DENSITY = 1.00E 14

T(K)	W(A)	S/W	ALPHA	SIGMA
5000.	1.05E-06	-3.35E-01	-3.81E-03	1.06E-03
10000.	1.43E-06	-1.01E-01	-3.01E-03	1.03E-03
20000.	1.86E-06	6.14E-02	-2.47E-03	9.45E-04
40000.	2.24E-06	1.57E-01	-2.15E-03	8.06E-04
60000.	2.41E-06	1.88E-01	-2.04E-03	7.06E-04

ELECTRON DENSITY = 1.00E 15

T(K)	W(A)	S/W	ALPHA	SIGMA
5000.	1.05E-05	-3.34E-01	-6.77E-03	4.94E-03
10000.	1.43E-05	-1.01E-01	-5.35E-03	4.78E-03
20000.	1.86E-05	6.16E-02	-4.40E-03	4.39E-03
40000.	2.24E-05	1.58E-01	-3.82E-03	3.74E-03
60000.	2.41E-05	1.88E-01	-3.62E-03	3.28E-03

ELECTRON DENSITY = 1.00E 16

T(K)	W(A)	S/W	ALPHA	SIGMA
5000.	1.05E-04	-3.31E-01	-1.20E-02	2.30E-02
10000.	1.43E-04	-9.98E-02	-9.51E-03	2.22E-02
20000.	1.86E-04	6.22E-02	-7.82E-03	2.04E-02
40000.	2.24E-04	1.58E-01	-6.80E-03	1.74E-02
60000.	2.41E-04	1.88E-01	-6.44E-03	1.52E-02
80000.	2.49E-04	2.01E-01	-6.28E-03	1.37E-02

ELECTRON DENSITY = 1.00E 17

T(K)	W(A)	S/W	ALPHA	SIGMA
5000.	1.05E-03	-3.24E-01	-2.14E-02	1.07E-01
10000.	1.43E-03	-9.59E-02	-1.69E-02	1.03E-01
20000.	1.86E-03	6.43E-02	-1.39E-02	9.47E-02
40000.	2.24E-03	1.59E-01	-1.21E-02	8.07E-02
60000.	2.41E-03	1.89E-01	-1.15E-02	7.08E-02

ELECTRON DENSITY = 1.00E 18

T(K)	W(A)	S/W	ALPHA	SIGMA
5000.	1.05E-02	-2.99E-01	-3.81E-02	4.95E-01
10000.	1.43E-02	-8.34E-02	-3.01E-02	4.79E-01
20000.	1.86E-02	7.11E-02	-2.47E-02	4.40E-01
40000.	2.24E-02	1.63E-01	-2.15E-02	3.75E-01
60000.	2.41E-02	1.92E-01	-2.04E-02	3.29E-01

CHAPTER VII

CONSTRUCTION OF THE Z-PINCH DISCHARGE

7.1 Introduction

In (4.3.2) experiments are proposed concerning the measurements of the Stark broadening of helium lines in a plasma generated by a Z-pinch discharge. Since the use of such a device is a departure from the usual sources that have been used to date in the study of the Stark broadening of helium lines in plasmas, the first part of this chapter will be devoted to a brief survey of the more conventional sources. The remaining part of the chapter will be devoted to the details of the construction and operation of the Z-pinch discharge.

7.2 Methods of Generating Helium Plasmas

The requirements of the ideal source for the study of the Stark broadening of spectral lines are as follows;

a) The plasma should be easily, and reproducibly produced and the degree of ionization should be such that Stark broadening is the dominant mechanism.

b) The plasma should be homogeneous

c) It should be possible to measure electron densities and temperatures in as direct a manner as is possible

and with the minimum number of theoretical assumptions about the state of the plasma.

d) Electron densities and temperatures should be capable of being varied.

The following is a brief survey of the methods that have been used to generate helium plasma for the study of Stark broadening. For a more comprehensive survey see Griem (1).

7.2.1. Pulsed Arcs

Because of the relatively high temperature $\sim 2 \times 10^4$ °K required to obtain an appreciable degree of ionization in helium D.C. arcs cannot be used. Instead recourse must be made to pulsed arcs. Typical of such arcs are those used by Wulff (15) and Botticher et al (19). Current pulses of ~ 1 m sec duration are used and the diameter of the plasma is usually < 10 mm and typically~5 mm. Densities and temperatures are usually measured using L.T.E. relations. The main disadvantage of these sources is their limited density and temperature range, typically $N_e \lesssim 10^{16} cm^{-3}$ and $T_e \lesssim 3 \times 10^4$ °K. Also precautions must be taken to avoid errors arising from radial gradients.

7.2.2. Conventional Shock Tubes

As a result of the high sound speed of helium, conventional shock tubes, i.e. the diaphragm type, cannot be used efficiently

to produce helium plasmas suitable for Stark broadening measurements (Kolb and Griem (41)). Explosively driven shock tubes have been used with some success (Seay (42)). But besides being unsuitable for laboratory use these devices have the major disadvantage that a large part of the apparatus must be rebuilt after each shot.

7.2.3. Electromagnetic Shock Tubes

To date most of the important work on the experimental verification of the Stark broadening of helium lines has been performed using electromagnetically driven shock tubes of the 'T-tube' type; see for example Berg et al (16) and Lincke (21). These devices have a high repetition rate so that shot-to-shot scanning can be employed. With these devices electron densities and temperatures can be varied between $\sim 10^{16}\,cm^{-3}$ to $\sim 10^{19}\,cm^{-3}$ and $2 \times 10^4\,^oK$ to $10^5\,^oK$ respectively, but they are operated typically at $N_e \sim 10^{17}\,cm^{-3}$ and $T_e \sim 3 \times 10^4\,^oK$. However, to obtain a reasonable operating range with a single device it is necessary to use mixtures of gases and to operate with and without shock reflectors. Densities and temperatures are usually determined from L.T.E. relations or Stark broadening measurements using hydrogen lines. The major disadvantage of the T-tube is that the reproducibility is generally poor and it is necessary, when scanning a profile, for example, to monitor continuously the

electron density in order to eliminate spurious shots. Grieg et al (39) have found that to obtain good reproducibility the position of the shock reflector (when used) is critical, and that the manner in which the gas is delivered can be important. Even after both these factors have been optimised Grieg et al find that if a $\pm$ 5% consistency in the plasma conditions is required approximately 20% of the shots must be rejected. At the expense of greater complexity, the reproducibility of a 'T-tube' can be improved by carefully shaping the discharge chamber and by the use of pre-ionization, Berg et al (43).

7.3. Z-Pinch Discharges

Although Z-pinches have been studied for many years, and copious literature exists (see Glasstone and Loveberg (44)) these devices have not been extensively used as spectroscopic light sources. In fact, to the best of the authors knowledge only two references exist which describe the use of this type of discharge for the measurement of Stark broadening parameters. The first is that of Burgess (3) who used a Z-pinch operating in argon to investigate the shift to width ratio for a number of ArII lines. The second is that of Roberts (22) who measured the Stark broadening parameters of a number of ArII lines using a stabilized Z-pinch. The work of Roberts is important in that it lays the foundations of the diagnostic methods which can be used on such a device; notably the exploitation of laser interferometry.

Electron densities and temperatures attained in the discharges mentioned above were ~ $10^{17}cm^{-3}$ and~3 x 10^{4} ^{o}K respectively, but Z-pinches have been used to obtain electron densities of ~$10^{19}cm^{-3}$ see(56) , and the work to be described in (9.4) suggests that densities as low as $10^{15}cm^{-3}$ can be attained at peak compression and if lower densities are required observations can be made in the afterglow. Thus the conditions attainable in a Z-pinch are comparable to, or even better than, those of a T-tube.

The Z-pinch would appear to have three important advantages over the T-tube. Firstly, the electron density can be measured easily and independently of either the existence of L.T.E. in the plasma , or the assumptions of Stark broadening theory, or a knowledge of the electron temperature, using laser interferometry (see 9.4). Secondly, the Z-pinch is extremely reproducible on both a long and short term basis (Roberts (loc.cit) see also (11.5.2)) so that continuous monitoring of the discharge is generally not required. Thirdly, the electron density can be varied easily by altering the filling pressure (9.4.4)

The major disadvantage of the Z-pinch is that by virtue of the method of generation it must contain radial gradients. Of course, the T-tube will also have radial gradients associated with the boundary layer between the plasma and the wall. But it might be expected that these gradients are less severe than those which exist between the plasma, the confining magnetic field, and the walls of a Z-pinch discharge. However, the work

of Burgess (loc. cit.) and Roberts (loc. cit.) suggests that the effects of radial gradients are small. Burgess measured the profile of an isolated ArII line by observing the plasma in the radial direction; the Abel inversion procedure was not used. Theory predicts that the profile of such a line should be Lorentzian and this was confirmed by the measurements. This result would only be expected if the effects of radial gradients are small. Roberts, using the same procedure as Burgess to observe the plasma, measured the profiles of a number of ArII lines. If the Stark broadening parameters derived from these measurements are compared with those obtained by Jalufka, Oertel and Ofelt, (45) using a T-tube, the results are found to be in good agreement. Again, this result would only be expected if the effects of radial gradients in the Z-pinch are small.

7.4. Construction of the Z-Pinch Apparatus

The Z-pinch apparatus, to be described here, was built by the author for the pre-ionization of a theta pinch discharge. Plate (7.1) shows the Z-pinch pre-ionization assembly in position on the theta pinch; for clarity, the nearest return conductor has been removed. The quartz discharge tube has an internal diameter of 45 mm and the distance between the electrodes is 75 cm. A vacuum seal was maintained between the electrodes and the discharge tube by means of a 'Wilson seal' arrangement. Fig. (7.1) shows a cross section of Z-pinch electrode assemblies.

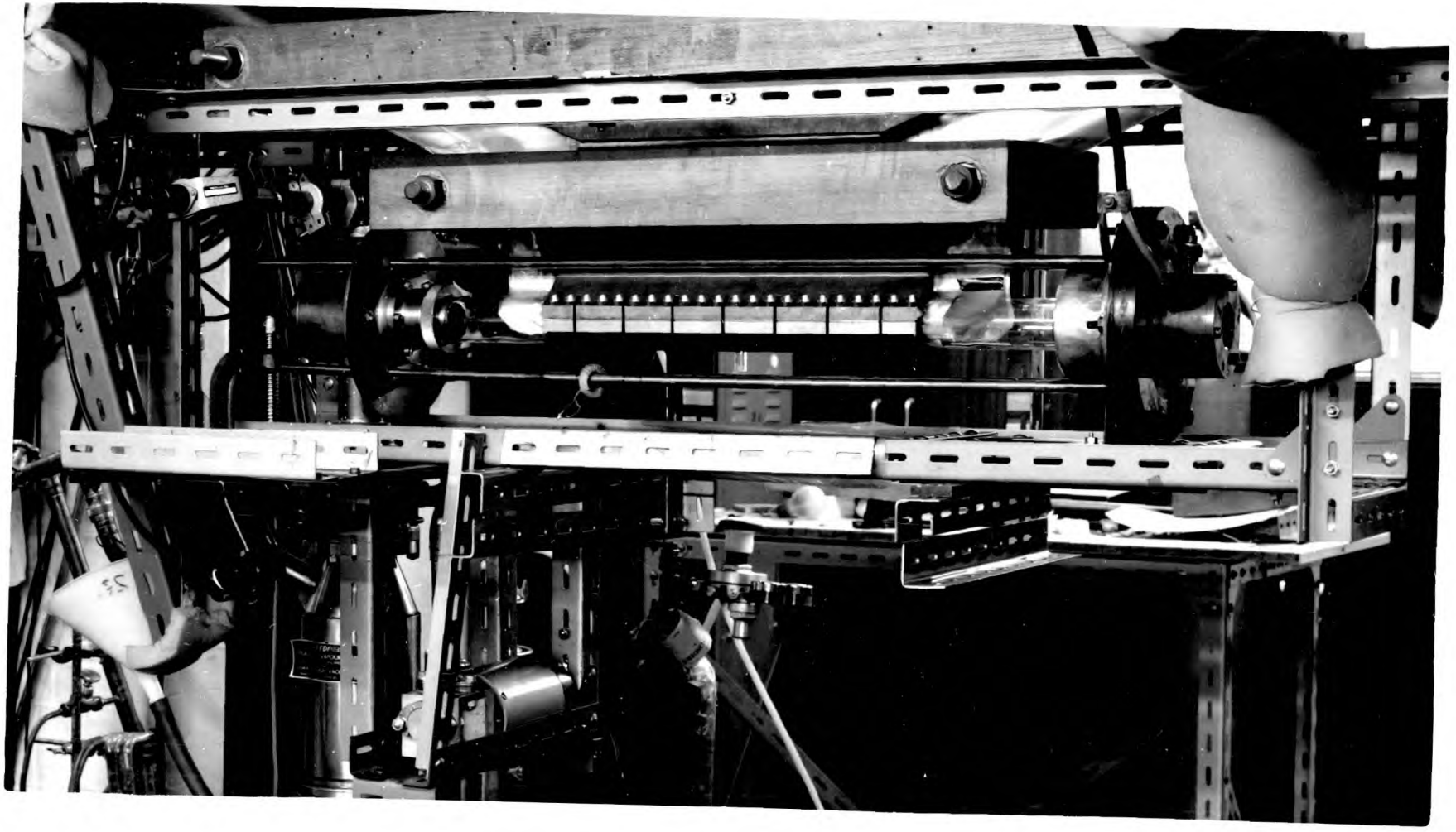

Plate (7.1) Z-Pinch Apparatus.

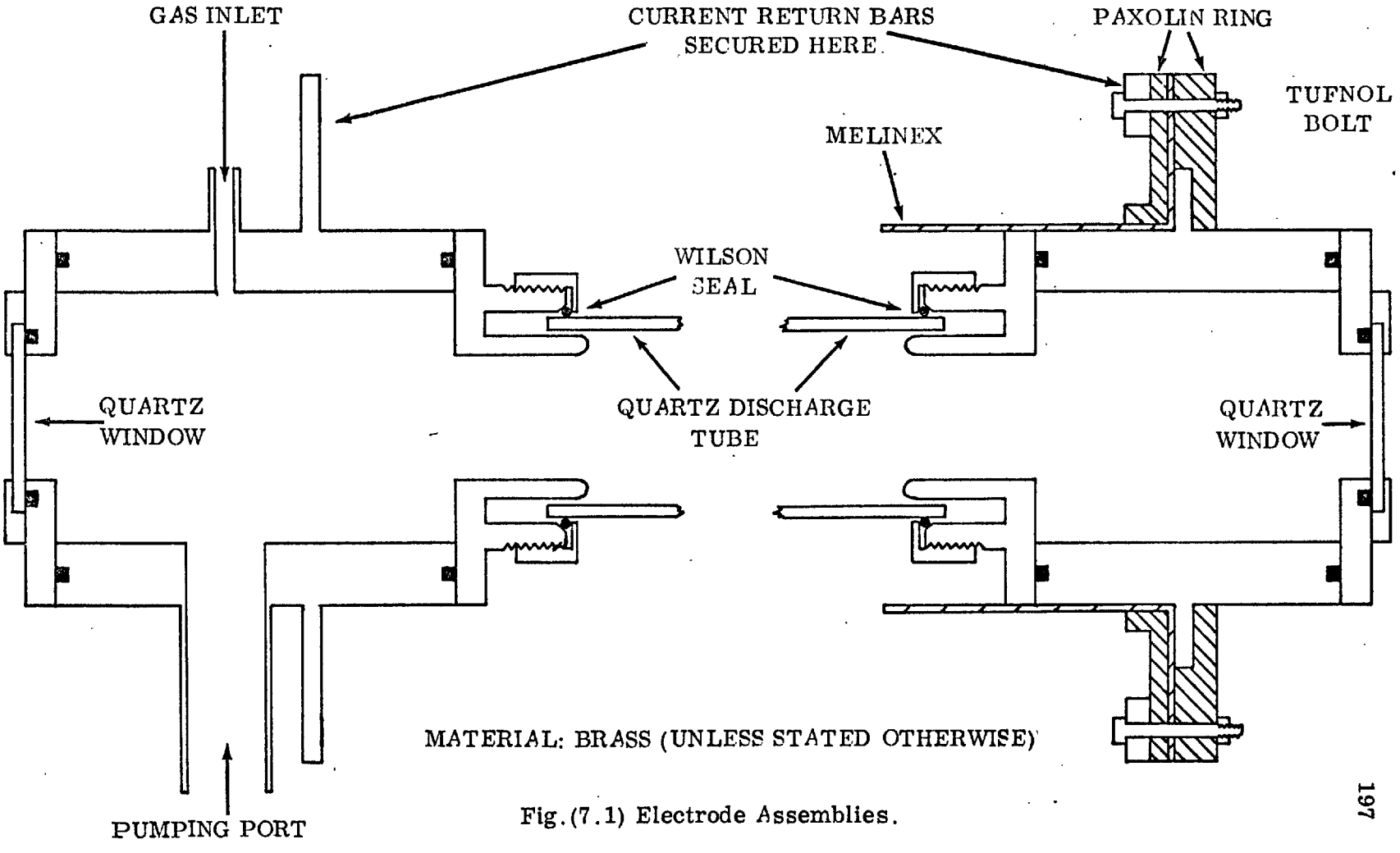

Fig.(7.1) Electrode Assemblies.

7.4.1. Electrode Assemblies

Both electrode assemblies were supported on a rigid frame suspended beneath the theta pinch coil (see Plate (7.1)). The earth electrode (the electrode to the left of the theta pinch coil in Plate (7.1)), which contained the pumping ports and gas supply inlets, was rigidly fixed to the frame, with a diffusion pump suspended beneath it.

Details of the construction of the high voltage electrode are shown in Fig. (7.1). The Paxolin ring, shown in Fig. (7.1), served two purposes, it insulated the high voltage electrode from the annular ring into which the return conductors were fixed, and also rigidly fixed this ring to the central electrode to make the complete assembly. The additonal insulation shown in the figure was a 'top hat' arrangement constructed out of layers of Melinex and bonded with Melinex cement. This provided insulation between the central electrode and the return bars. To prevent flash over from the theta pinch coil, P.V.C. tubing was threaded over the return conductors. To allow free access to the coil assembly, the high voltage electrode and return conductors could be removed as a complete assembly without disturbing the earth electrode.

Both electrode assemblies contained windows through which the plasma could be observed in the axial direction.

The annular electrodes, which protruded into the discharge tube to form the electrode surface, were made demountable from the main electrode assemblies so that if necessary another set of annular electrodes could be made for different sized tubes without the need to replace the main electrode assemblies. The mean diameter of the annular electrode surface was 3.7 cm and the internal diameter was 3.3 cm.

7.4.2. Vacuum System

As shown in Fig. (7.2) the vacuum system comprised a two inch mercury diffusion pump fitted with a liquid nitrogen cold trap and an electrically operated baffle valve. This pump was backed by an Edwards 1SC 450A rotary pump. The roughing line for the discharge tube (see Fig. (7.2)) contained a liquid nitrogen cold trap to prevent oil from back streaming into the discharge tube and was controlled by a solenoid valve.

The pumping of the discharge tube was controlled from the theta pinch control desk by means of the electrically operated valves.

The pressure in the discharge was monitored from the control desk using a Leybold-Elliot combitron gauge system, which could be used over a pressure range of 1.0 to 10^{-5} torr. The base pressure of the system was typically $\sim$ 2 x 10^{-5} torr.

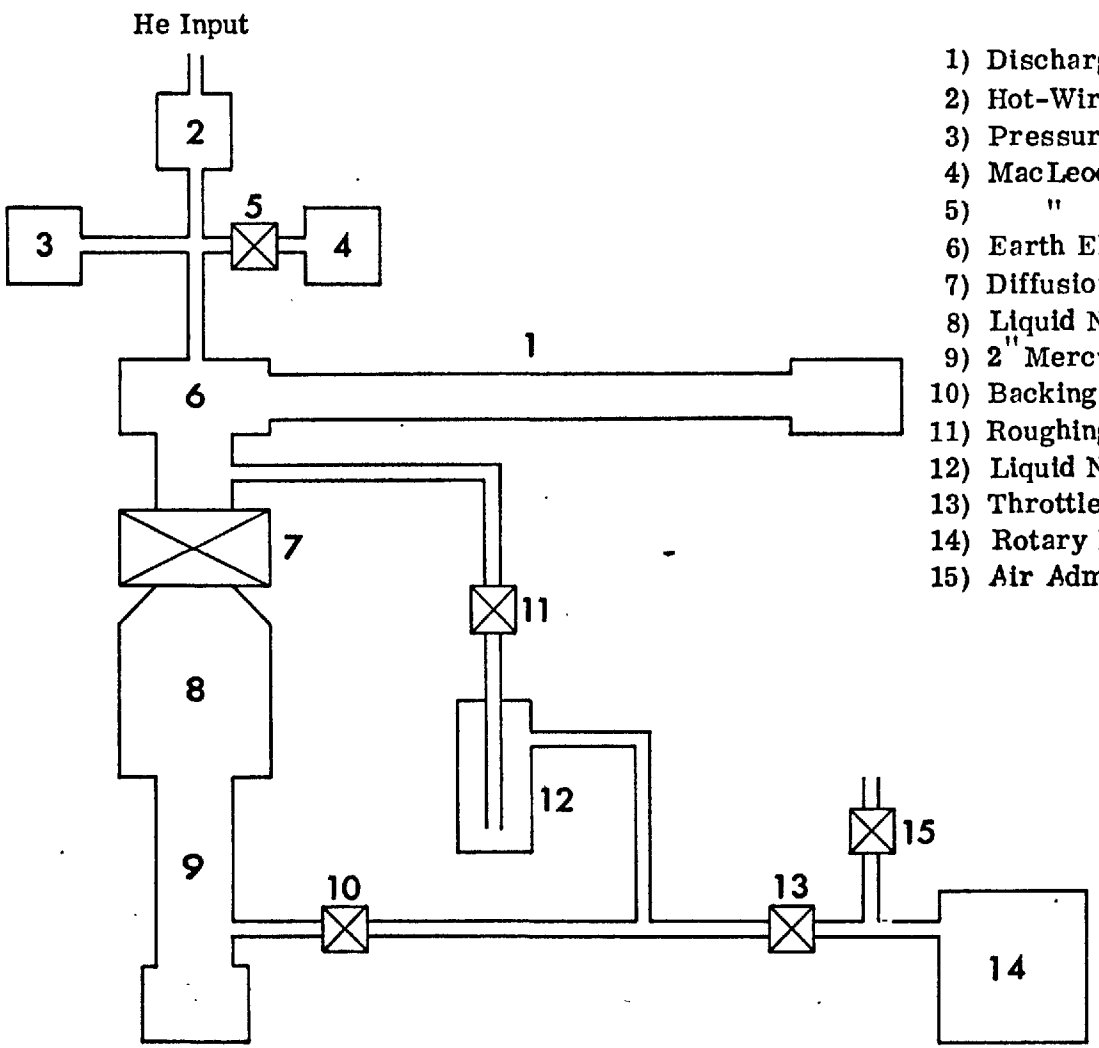

1) Discharge Tube.
2) Hot-Wire Leak Valve.
3) Pressure Gauges (Thermotron and Ionization).
4) MacLeod Vacstat Gauge.
5) " " Isolation Valve.
6) Earth Electrode.
7) Diffusion Pump Isolation Valve (Electrically Operated).
8) Liquid Nitrogen Cold Trap.
9) 2" Mercury Diffusion Pump.
10) Backing Line Valve.
11) Roughing Line Valve (Electrically Operated).
12) Liquid Nitrogen Cold Trap.
13) Throttle Valve.
14) Rotary Pump.
15) Air Admitance Valve.

Fig.(7.2) Vacuum System of the Z-Pinch Apparatus.

Since the above gauge system was not calibrated an Edwards Vacuustat McLeod gauge was used to measure the filling pressure during an experiment.

7.4.3. Gas Supply System

During an experiment helium was pumped continuously through the discharge tube and removed via the roughing line, with the diffusion pump shut off. This method of operation was more convenient than filling the discharge tube for each discharge.

The gas was leaked into the discharge by means of a 'hot wire' leak valve. This consisted essentially of a brass tube connected to the gas inlet port of the earth electrode. The end of the tube, nearest the discharge tube, was hemispherical and at its centre a fine hole had been drilled. Helium was supplied to the tube at a pressure of typically 10 p.s.i.. The rate at which gas leaked from the end of the tube was controlled by means of a P.T.F.E. pad held against the orifice by a wire under tension. A heating current passed through the wire alters its tension and hence the leak rate. Currents varying from 0 - 1 amp were supplied to the wire.

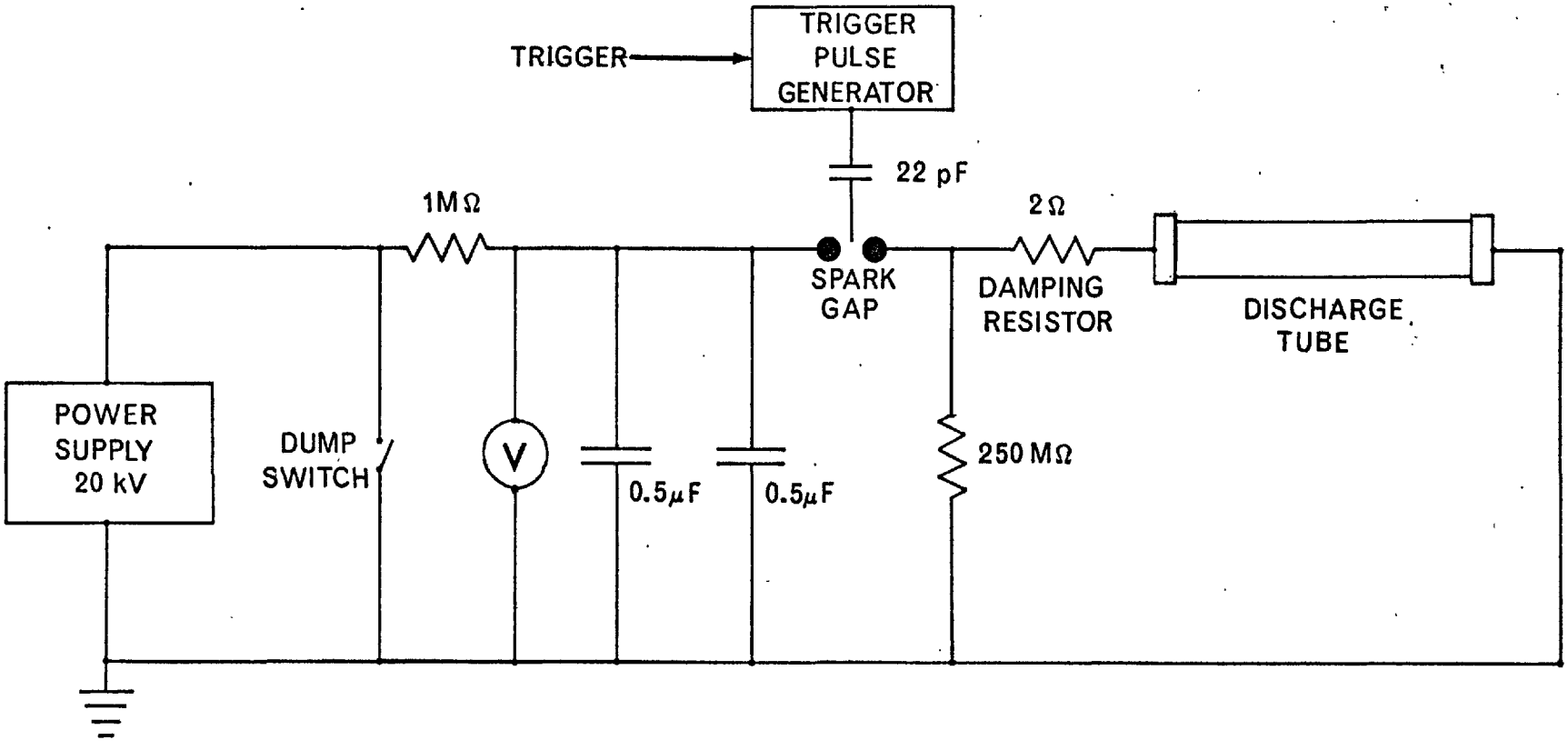

Fig.(7.3) Circuit Diagram of the Z-Pinch Apparatus.

7.4.4. Condenser Bank

A schematic diagram of the condenser bank circuit is shown in Fig. (7.3). The bank consists of 2 low inductance 0.5 μF capacitors connected in parallel to the electrodes of the discharge tube via a spark gap and a 2 Ω damping resistor. In operation the condensers were charged automatically to 20 KV and then discharged through the tube by means of a -25 KV voltage pulse supplied to the trigger pin of the spark gap. The discharge current reached a peak of $\sim$ 5 KA in 2 μs, independent of the filling pressure, and current zero occurred $\sim$ 8 μs after initiation. A Rogowski coil, connected to a passive integrator was used to monitor the current.

CHAPTER VIII

EQUILIBRIUM IN HELIUM PLASMAS

8.1. Introduction

Before discussing the measurements of electron temperature and density of the helium plasma formed in the Z-pinch discharge it will be useful to consider the type of equilibrium that might prevail in the plasma. Preliminary measurements showed that electron densities and temperatures were typically $\sim 10^{16} cm^{-3}$ and $\sim 4 \times 10^{4} {}^{o}K$, respectively at the time of peak compression.

8.2. L.T.E. in a Homogeneous Plasma in the Steady State

When the state of a system can be described by the same laws which govern a system in thermodynamic equilibrium, with the exception of Planck's radiation law, then the system is said to be in local thermodynamic equilibrium (L.T.E.).

In a spatially homogeneous plasma in the steady state L.T.E. will prevail if (see McWhirter (46)):-

a) The velocity distribution of the free electrons is Maxwellian.

b) The population densities of the bound states of the atoms and ions are controlled exclusively by electron collisions.

According to Wilson (47) condition a) is valid if:

$$t_{ee} << t_{rad}, t_{en}, t_{p} \tag{8.1}$$

where t_{ee} is the electron-electron relaxation time, and is given by (47):

$$t_{ee} \sim \frac{0.3\, T_e^{3/2}}{N_e \ln \Lambda} \quad \text{sec} \tag{8.2}$$

where T_e is in ^{o}K and $\ln \Lambda$ is a slowly varying function of N_e and T which is tabulated by Spitzer (48).

t_{rad} is the energy decay time for radiative energy losses from the plasma. From the work of Griem (1) the following estimates of the energy decay times for line and continuum radiation were obtained.

$$t_{rad}(\text{contd}) = \frac{1.4 \times 10^{11}\, T_e^{\frac{1}{2}}}{\sum_{Z} Z^2 N^Z + \sum_{n,Z} \frac{Z^4 N^Z}{n^3}} \text{ sec.} \tag{8.3}$$

where the first and second terms in the denominator arise from the free-free and free-bound transitions in the Coulomb fields of Z times charged ions respectively, N^Z is the number density of the ions, n is the principal quantum number of the levels into which recombination takes place, T_e is in ^{o}K, and free-free and

free bound Gaunt factors have been neglected.

$$t_{rad}(\text{line}) = \frac{0.5\ T_e^{3/2}}{\sum_Z N^{Z-1} \exp\left(-\frac{E_2^{Z-1}}{kT_e}\right)} \quad \text{sec.} \qquad (8.4)$$

where N^{Z-1} is the number density of atoms or ions with charge Z-1 (Z = 1 for HeI, etc) E_2^{Z-1} is the energy of the first excited state, and T_e is in ^oK. Because this expression neglects the self absorption of the resonance line, which is usually important, the energy decay time obtained from (8.4) will be a lower limit.

The other quantities in (8.1) are the energy heating time t_{en} and the particle containment time t_p. These depend on the method used to generate and contain the plasma.

From (8.2), using $N_e \sim 10^{16} cm^{-3}$ and $T_e \sim 4 \times 10^4\ ^oK$, t_{ee} is found to be $\sim 4 \times 10^{-11}$ sec. A lower limit on t_{rad}(contd) can be obtained by assuming that $N^Z = N_e$ and Z = 2. It is also sufficient, for the purpose of the present estimate, to take the first term in the sum over n only. The value of t_{rad} (contd) is then $\sim 1.4 \times 10^{-4}$ sec. For $T_e \sim 4 \times 10^4\ ^oK$ the plasma should be close to being fully ionized and therefore t_{rad} (line) can be evaluated assuming $N^{Z-1} = N_e$. t_{rad}(line) is then $\sim 2.5 \times 10^{-5}$ sec (a lower limit). The heating and particle containment times should be of the order of the time to peak current say $\sim 10^{-6}$ sec. Hence, the inequalities (8.1)

are well satisfied and therefore the free electrons in the Z-pinch plasma can be expected to have a Maxwellian velocity distribution.

Many investigations have been made of the minimum electron density required for the validity of condition b); see for example Griem (1), McWhirter (46) and Wilson (47). The basic criterion is that the electron density must be large enough to ensure that the collisional depopulation rate of a bound state is an order of magnitude larger than the corresponding radiative rate. This may be expressed by:

$$N_e X_n \geqslant 10 A_n \qquad (8.5)$$

where X_n is a coefficient representing the total collisional de-population rate of the level n and A_n, the total radiative de-population rate. A slight modification of this condition is necessary if the state considered is the ground state. It is then required that the electron collision <u>population</u> rate be an order of magnitude greater than the corresponding radiative rate.

McWhirter (46) has evaluated (8.5) for a two level atom assuming hydrogenic oscillator strengths and excitation functions and found that:

$$N_e \geqslant 1.6 \times 10^{12} T_e^{\frac{1}{2}} E_{mn}^3 \quad cm^{-3} \qquad (8.6)$$

where E_{mn} is the energy separation of the levels m and n in eV, and Te is in ^{o}K. If N_e satisfies (8.6) then the levels m and n will be in L.T.E. to better than 10%.

8.3. Critical Densities for HeI and HeII to be in L.T.E. in an Optically Thin Plasma

The inequality (8.6) is most difficult to satisfy for the largest energy gap in the term scheme. In the case of HeI this corresponds to $1s^1S - 2p^1P$ (21 eV) and for HeII to $1s^2S - 2p^2P$ (40 eV). Using $T_e = 4 \times 10^4\ ^{o}K$ the critical densities for L.T.E. are:

$$N_e(\text{HeI}) \geqslant 2.4 \times 10^{18} cm^{-3}$$

$$N_e(\text{HeII}) \geqslant 2.0 \times 10^{19} cm^{-3}$$

The energy gaps of the states above the first excited state are much less than that between the ground state and first excited state and at the above densities, these states will also be in L.T.E. with ground state and the free electrons.

The critical density, as estimated above, should be accurate for HeII since (8.6) was derived for a hydrogenic system. However, the lower states of HeI are far from hydrogenic and also the presence of the singlet and triplet systems should be taken into account. Consequently, the critical density derived

above might deviate considerably from the correct HeI value. Drawin (49) calculated the population densities of the lower states of HeI, in an optically thin plasma, for various electron densities by solving the rate equations which describe the populations of the levels. Account was taken of the singlet and triplet systems and the coupling of these systems by electron collisions. From Table (1b) of this reference, for $T_e = 4 \times 10^4$ °K and $N_e = 10^{19} cm^{-3}$, the population density of the ground state is still a factor 4 greater than the L.T.E. value. Hence, for HeI the value of the critical density estimated from (8.6) is probably an order of magnitude too low.

8.4 Critical Densities for HeI and HeII to be in L.T.E. in an Optically thick Plasma

A reduction in the value of the critical densities is expected if the resonance radiation is substantially self absorbed. This arises because the absorption effectively reduces the radiative population rate of the ground state, and therefore also the electron density necessary to satisfy the inequality (8.6).

Assuming total absorption of the HeI resonance line Deutsch (50) finds that for L.T.E. at $T_e = 2 \times 10^4$ °K the electron density must satisfy:

$$N_e \text{ (HeI)} > 1.4 \times 10^{18} cm^{-3}$$

For the higher temperature considered here, this value would have to be slightly increased. Absorption of the HeII resonance line has been considered by Drawin (51). For the largest density he quotes, i.e. $N_e = 10^{18} cm^{-3}$, and $T_e = 4 \times {}^4 {}^{o}K$, the ground state density of HeII is still ~ 50% above the L.T.E. value even for total absorption of the resonance line. Hence, for HeII to be in L.T.E. when the resonance radiation is totally absorbed the electron density must satisfy:

$$N_e \text{ (HeII)} \gtrsim 5 \times 10^{18} \text{ cm}^{-3}$$

Conclusions

The above considerations show that even in the most favourable circumstances the electron density in the discharge is at least two orders of magnitude too low for HeI and HeII to be in L.T.E.

8.5. Partial L.T.E. for a Homogenous Plasma in the Steady State

For L.T.E. the population densities of all the states of an atom or ion must be determined exclusively by collision processes. If the population densities of only some of the states are determined by these processes the plasma is said to be in 'partial L.T.E.'. The degree of ionization of such a plasma may deviate considerably from the L.T.E. value.

The condition (8.5), for a level to be in L.T.E. is most easily satisfied for excited states. This is because the collisional excitation rate from one level to another of higher energy is inversely proportional to the energy separation of the two levels. Since the separation decreases with increasing principal quantum number n, this rate will increase with n. At the same time the spontaneous radiative decay rate decreases with increasing n. Hence, there will always be some value of n for which condition (8.5) is valid, provided n lies below the reduced ionization limit.

Griem (1) has shown that for a given value of N_e the population density of a level with principal quantum number n will be within 10% of the L.T.E. value if n satisfies the condition:

$$n^{17/2} \geqslant 7 \times 10^{18} \frac{Z^7}{N_e} \left(\frac{kT_e}{Z^2 E_H}\right)^{\frac{1}{2}} \qquad (8.7)$$

where Z is the charge on the core of the atom or ion (Z = 1 for neutrals, etc.) and E_H is the ionization potential of hydrogen. It is to be noted that with increasing N_e the value n satisfying (8.7) will decrease until the ground state is reached. This shows how partial L.T.E. goes over to complete L.T.E. with increasing N_e, as expected.

For $N_e \sim 10^{16} cm^{-3}$ and $T_e \sim 4 \times {}^4 {}^{\circ}K$ evaluation of (8.7) shows that levels with $n \geqslant 3$ for HeI and $n \geqslant 4$ for HeII will be in L.T.E

At a given electron density, the level corresponding to the smallest value of n which satisfies (8.7) is sometimes called the 'thermal limit' (47). The population densities of levels above and including the thermal limit will be in L.T.E. with respect to each other and since they extend to the reduced ionization limit, they will also be in L.T.E. with the ground state of the next ionization stage and the free electrons. The relative population densities of these levels, will therefore, be given by the ratio of their Boltzmann factors, i.e.

$$\frac{N_n^{Z-1}}{N_m^{Z-1}} = \frac{g_n^{Z-1}}{g_n^{Z-1}} \exp\left(\frac{E_m^{Z-1} - E_n^{Z-1}}{kT_e}\right) \qquad (8.8)$$

where Z-1 is the charge on the atom or ion (Z = 1 for neutrals, etc.), $N_{n,m}^{Z-1}$ are the population densities of the states n and m, with statistical weights $g_{n,m}^{Z-1}$ and energies $E_{n,m}^{Z-1}$. The population density N_n^{Z-1} of a state n will be related to the ground state population density N_1^Z of the next higher ionization stage, and the density N_e of the free electrons by a Saha equation of the form (see Griem (1)).

$$N_n^{Z-1} = \left(\frac{2\pi\hbar^2}{mkT_e}\right)^{3/2} \frac{g_n^{Z-1}}{2g_1^Z} N_e N_1^Z \exp\left(\frac{E_\infty^{Z-1} - E_n^{Z-1}}{kT_e}\right) \qquad (8.9)$$

where g_1^Z is the statistical weight of the ground state of the next higher ionization stage and E^{Z-1} the ionization potential

of the atom or ion with charge (z-1). The other quantities are the same as those occurring in (8.8). The population densities of levels below the thermal limit may deviate considerably from their L.T.E. values.

8.6. The Coronal Model

In (8.4) it is shown that the plasma produced in the Z-pinch discharge will not be in L.T.E.. The opposite extreme of the L.T.E. model is the coronal model in which collisions control the excitation and ionization processes and radiative processed control the de-excitation processes.

According to the coronal model the population density N_n of a level with principal quantum number n relative to the ground state population density N_1 is given by:

$$\frac{N_n}{N_1} = \frac{N_e X_{1n}}{A_n} \qquad (8.10)$$

Also the state of ionization of the plasma is found to be independent of N_e and is given by:

$$\frac{N^z}{N^{z-1}} = S/\alpha \qquad (8.11)$$

where N^z and N^{z-1} are the population densities of the ions with charge z and z-1 respectively, S is the collisional ionization

coefficient and α the radiative recombination coefficient.

Wilson (47) derives the following condition for the validity of the coronal model.

$$N_e \leq 1.5 \times 10^{10} E_\infty^{-\frac{1}{2}} (kT_e)^4 \text{ cm}^{-3} \qquad (8.12)$$

where E_∞ is the ionization potential of atom or ion and kT_e is the electron temperature (both in eV). For $T_e \sim 4 \times 10^4$ °K the critical densities for HeI and HeII are $\sim 10^{12}$ and 5×10^{11} cm^{-3} respectively. Since the electron density in the discharge is typically a factor of 10^4 larger than these critical densities, the state of the plasma cannot be described by the coronal model.

3.7. Time Dependent Homogeneous Helium Plasmas

For a time dependent helium plasma it is necessary to verify that the relaxation times for ionization and recombination are sufficiently short compared with such times as the life time of the plasma and times over which N_e and T_e are changing. If the relaxation times are short compared with the times of interest then the population densities of the atomic states will pass through a series of quasi-stationary states which are determined by the instantaneous values of N_e and T_e. If the relaxation times are longer than the times of interest the population densities of the atomic states will depend not only on the instantaneous values of N_e and T_e but also on the past history of the plasma.

The relaxation time $\tau_{z-1,j}$ for establishing a steady state population in a state j of an atom, after a sudden change of N_e or T_e with charge z-1, is given by (see Drawin(51)).

$$\frac{1}{\tau_{z-1,j}} \approx N_e S_j + \frac{N_z N_e}{N_{z-1,j}} (1 - \Lambda_j) R_j + \sum_{i<j}^{j-1} (N_e F_{ji} + A_{ji}) + \sum_{k>j}^{P} \left[N_e C_{jk} + \frac{N_{z-1,k}}{N_{z-1,j}} (1 - \Lambda_{jk}) A_{kj} \right] \qquad (8.13)$$

together with the condition for the steady states:

$$\frac{dN_{z-1,j}}{dt} = 0, \text{ with } j = 1, 2, \ldots.$$

In (8.13) $N_{z-1,j}$ and N_z are the number densities of particles in successive ionization stages, the A's are spontaneous transition probabilities, S and R are the ionization and radiative recombination rate coefficients respectively, C and F are the excitation and de-excitation rate coefficients respectively, and the Λ's are reduction factors which account for radiative absorption of free-bound and free-free radiation ($\Lambda = 1$ for the optically thin case and 0 for the optically thick case).

The treatment of radiative absorption in (8.13) is schematic only. Ideally, the relaxationtimes for the various

states should be obtained by solving simultaneously the coupled rate equations and the equation of radiative transfer.

When considering the relaxation time of the ground state (j=1) (8.13) is valid only if the plasma is undergoing ionization. This is because collisional de-excitation from excited states and three body recombination, which can be important when the plasma is close to the steady state, have been neglected.

Drawin ([49]) has calculated the relaxation time for HeI assuming an optically thin plasma and for HeII (51) with varying degrees of self absorption. These values of τ_j are tabluated in Tables (8.1) and (8.2) for $N_e = 10^{16} cm^{-3}$ and for various values of the electron temperature. The optically thick HeII case corresponds to 90% self absorption for each of the lines of the resonance series and 90% photoionization from the ground state (these values have only been included to give some indication of the effects of self absorption on the relaxation times and do not necessarily correspond to the amount of absorption expected in the system under investigation).

The tables illustrate the following points:

a) The relaxation time for the ground state is considerably longer than that for the excited states. This arises because spontaneous emission sets an upper limit of $\sim 10^{-8}$ sec for the relaxation times of excited states, which is further reduced

TABLE (8.1) HeI $N_e = 10^{16} cm^{-2}$

$T_e \times 10^{-3}(^oK)$	τ_j (sec)		
	1^1S	2^1S	2^3S
20	5.2,-4	1.6,-10	3.9,-9
30	1.3,-5	1.3,-10	1.7,-9
60	3.9,-7	1.0,-10	6.1,-9
120	3.7,-8	9.5,-11	3.4,-10

TABLE (8.2) HeII $N_e = 10^{16} cm^{-3}$

$T_e \times 10^{-3}(^oK)$	τ_j (sec)			
	OPT. THIN		OPT. THICK	
	n=1	n=2	n=1	n=2
24	3.8	1.7,-10	-	1.7,-10
32	3.2,-2	1.7,-10	3.2,-3	1.7,-10
64	2.4,-5	1.7,-10	2.4,-6	1.7,-10
128	6.6,-7	1.7,-10	6.6,-8	1.7,-10

by collisional excitation and de-excitation. Even the metastable levels of HeI (see Table (8.1)), whose radiative relaxation times are long in comparison with non-metastable levels, have short relaxation times because of the large collisional rates to nearby levels. In contrast, for an optically thin plasma, the ground state population density can only decay by collisional ionization and collisional excitation into states above the thermal limit (see 8.5) which is then followed rapidly by ionization (see Griem (1)). Consequently, the ground state relaxation times given in Tables (8.1) and (8.2) are effectively the ionization relaxation times for the complete ionization of HeI and HeII, respectively.

b) The relaxation times for the HeII ground state is longer than that for HeI. This is a consequence of the smaller collisional rates out of the ground state of HeII compared with those for HeI.

c) The ground state relaxation times show a strong temperature dependence. This results from a similar dependence of the ground state ionization and excitation rate coefficients.

d) Absorption of resonance radiation and photoionization reduces the relaxation time of the ground state. This will only be true for a plasma in which ionization is the dominant process.

If recombination dominates the reverse will be true since reabsorption of the resonance radiation will tend to inhibit the recombination process. The relaxation times of excited states are unaffected by self absorption.

Since it is intended to observe the discharge at the time of peak compression the relaxation time of interest will be that for ionization. The ionization relaxation times given in Tables (8.1) and (8.2), i.e. the ground state relaxation times, are the times for complete ionization of HeI and HeII respectively. In order to obtain relaxation times for partial ionization these times must be multiplied by the corresponding degree of ionization of HeI and HeII respectively.

Drawin (52) has calculated the degree of ionization of HeI and HeII in a non-thermal steady-state optically thin plasma by solving the rate equations describing the population densities of the various states. The results are shown in Fig.(8.2).

By multiplying the relaxation times for the ground states given in Tables (8.1) and (8.2) by the corresponding degrees of ionization obtained from Fig. (8.1) estimates of the ionization relaxation times τ_i for HeI and HeII in an optically thin plasma with $N_e = 10^{16} cm^{-3}$, were obtained. The results are shown in Tables (8.3) and (8.4). Because the formation of HeII ions requires first the ionization of HeI, the total

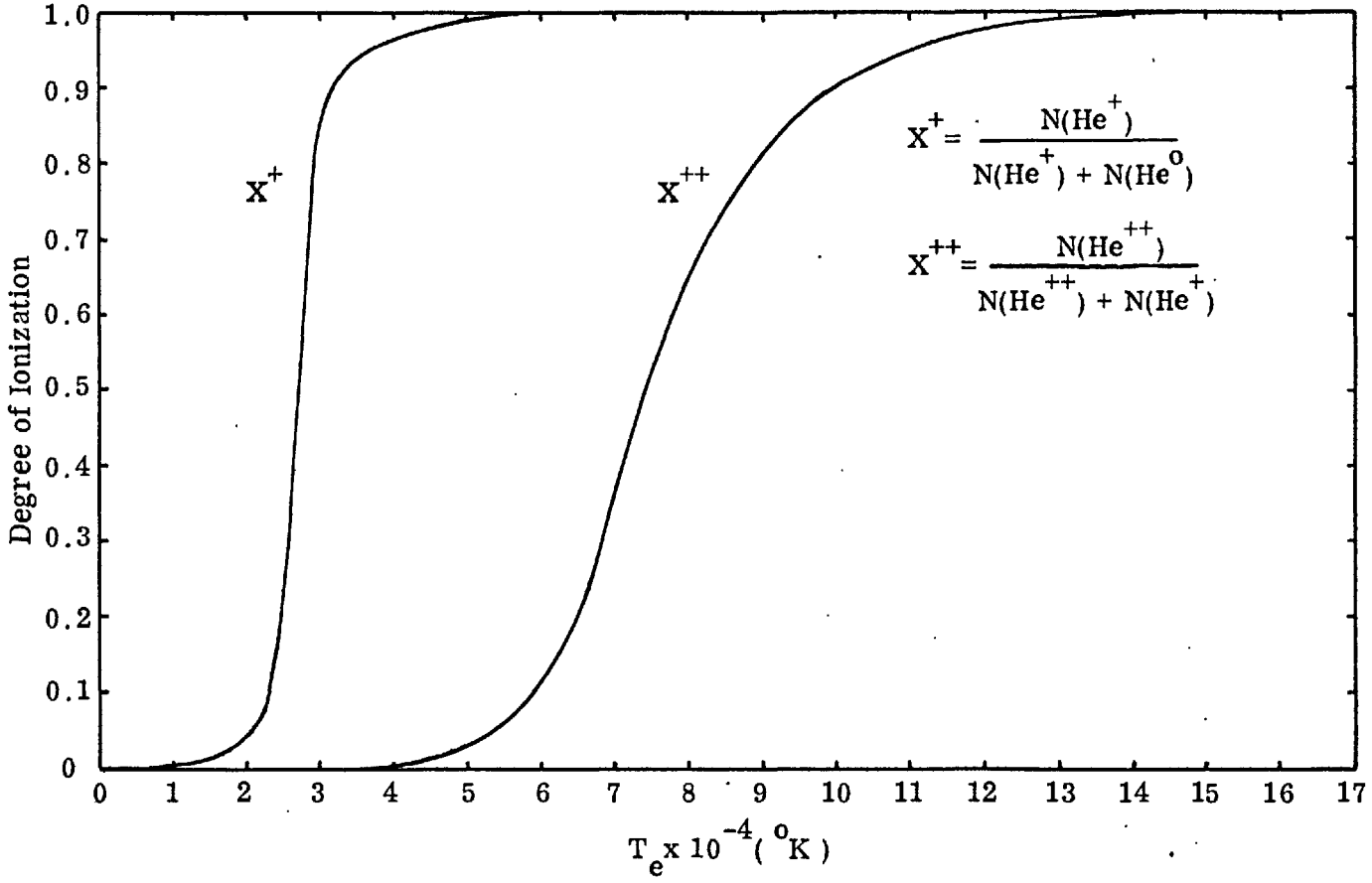

Fig.(8.2) Degree of Ionization of HeI and HeII as a Function of T_e for a Non-Thermal Plasma in the Steady State with $N_e = 10^{16}$ cm.$^{-3}$

TABLE (8.3)

Ionization Relaxation Time for HeI ($N_e = 10^{16} cm^{-2}$)

$T_e \times 10^{-3}$ °K	τ_i (μsec)
20	100.
30	11.
40	2.0
60	0.4

TABLE (8.4)

Ionization Relaxation Times for HeII ($N_e = 10^{16} cm^{-3}$)

$T_e \times$ $^{-3}$ °K	τ_i (μsec)	τ_{iT} (μsec)
32	-	-
40	0.3	2.0
64	5.0	7.0
128	0.7	0.7

Key: $_{iT}$ = Total relaxation time for HeII

relaxation time for the ionization of HeII ions is given by the sum of the individual relaxation times for HeI and HeII. These results are given in the third column of Table (8.4).

Recalling that heating and containment are $\sim 1\mu$sec. it is seen that the ionization relaxation times are such that ionization equilibrium is unlikely to be attained in the times of interest. Even if self-absorption of the resonance radiation reduced the ionization relaxation times by as much as an order of magnitude they would still be such that the attainment of ionization equilibrium would be only marginal. In contrast, the relaxation times for excited states of HeI and HeII are so short, when compared with times of interest, that they may be considered to be instantaneous. Thus partial L.T.E. will be established instantaneously.

CHAPTER IX

ELECTRON TEMPERATURE AND DENSITY MEASUREMENTS

9.1. Introduction

The following diagnostics were carried out to obtain qualitative and quantitative information about the behaviour of the Z-pinch discharge when operating in helium.

a) Time integrated survey spectra of the discharge were recorded.

b) The electron temperature of the plasma was measured spectroscopically.

c) A laser illuminated interferometer system was used to measure the electron number density on the axis of the discharge.

Framing camera observations were made of the collapse and subsequent expansion of the luminous part of the discharge, but these observations will only be considered when they have a direct bearing on the subject under discussion.

9.2. Time Integrated Survey Spectra

The main aims of this investigation were to examine the behaviour of the spectra as a function of filling pressure and

to detect impurity lines which might interfere with the measurements of line profiles and intensities.

The plasma was observed in the axial direction using a Hilger medium quartz spectrograph. Spectra were recorded on HPS plates at filling pressures of 0.1, 0.2, 0.3 and 0.4 torr, each exposure usually comprising 50 discharges. For identification purposes an iron arc or helium lamp reference spectrum was recorded on the same plate alongside each plasma spectrum. The wavelength of the strongest lines emitted by the plasma were determined with the aid of reference lines in the usual manner.

9.2.1. Results

Plate (9.1) shows the variation of the helium spectrum with filling pressure (the reference spectra were omitted for this experiment). At the highest filling pressure, 0.4 torr, the HeI spectrum only was observed. , The HeII 4686 A^{o} and 3203 A^{o} lines began to appear at 0.3 torr and 0.2 torr, and 0.1 torr were comparable in intensity to the HeI lines. From the steady increase in the HeII line intensity with respect to that of HeI with decreasing filling pressure it was concluded that the electron temperature increased as the filling pressure was lowered.

The main impurity lines in the spectrum were found to be those of silicon and, to a lesser extent oxygen, from the

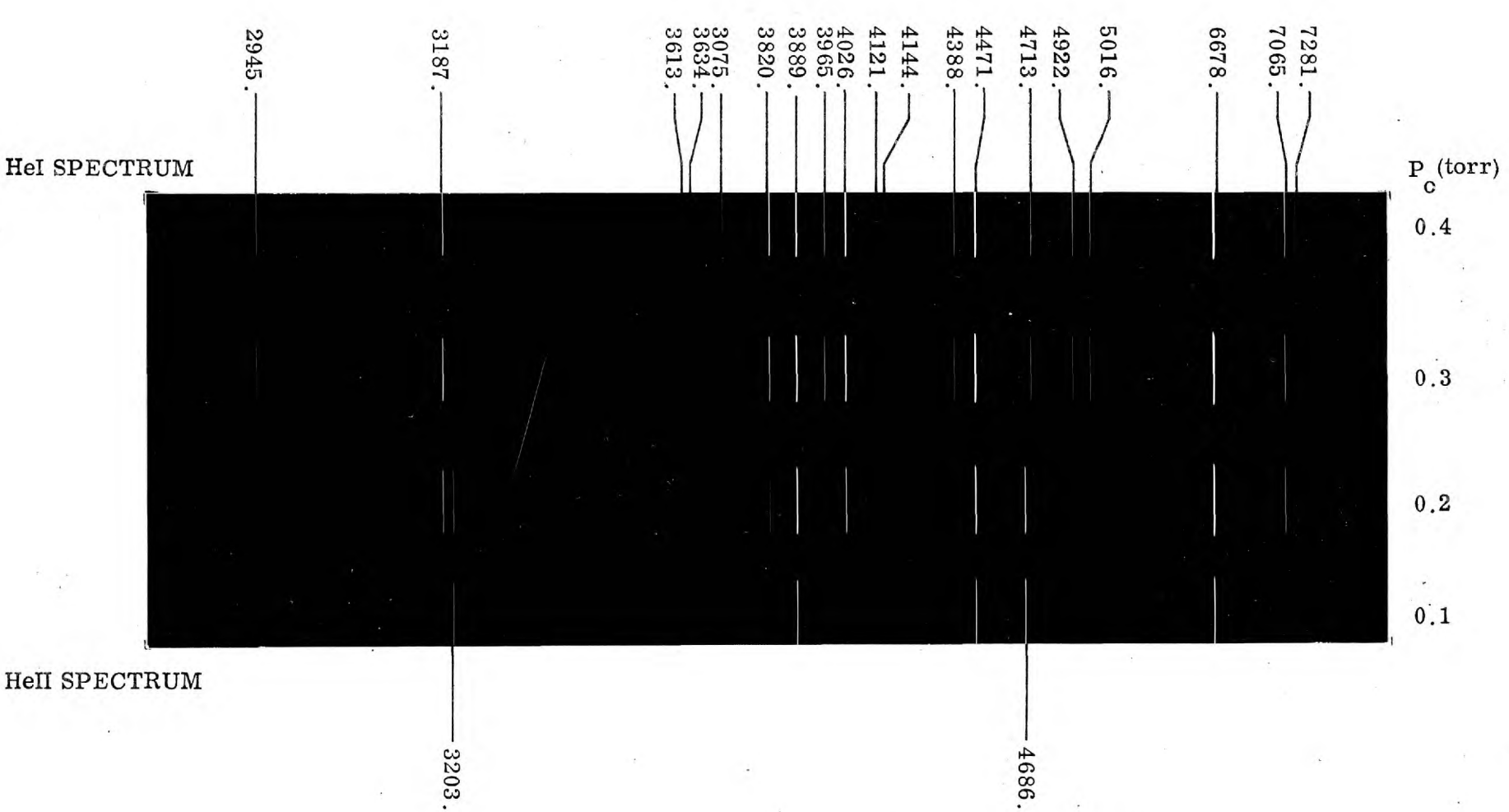

Plate (9.1) Time-Integrated Spectra of the Discharge

Recorded at Various Filling Pressures

discharge tube walls, and of hydrogen present as a contaminant of the helium. In the case of silicon, lines of SiI, SiII and SiIII were observed. However, as Plate (9.1) shows, the spectra are remarkable free of impurity lines.

9.3. Temperature Measurements

An adaptation of a method due to Griem (1) was used to measure the electron temperature. Briefly, this method assumes that the ratio of the total intensities of the HeII 4686 A^{o} and HeI 5876 A^{o} lines can be interpreted in terms of a model which relates the population density of the upper state of each line to the ground state of the next higher ionization stage and to free electron density using the Saha equation (see (8.5)). The intensity ratio then becomes:

$$\frac{I'}{I} = \frac{f'g'\,\lambda^3}{fg\,\lambda'^3} \cdot \exp\left(\frac{E'_{\infty} - E' - E_{\infty} + E}{kT_e}\right) \cdot \frac{N^{++}}{N^{+}} \qquad (9.1)$$

where the dashed quantities refer to the HeII line. The quantities appearing in (9.1) have the following meaning:-

f', f = absorption oscillator strengths of the lines

g', g = statistical weights of lower states of the lines

λ', λ = Wavelength of the lines

E', E = ionization potential of HeII and HeI respectively

E', E = Energy of upper states of the lines

N^+, N^{++} = The number density of singly and doubly charged ion respectively

kT_e = The electron temperature

The ratio N^{++}/N^+ is then assumed to be determined by the coronal equation (see 8.7).

$$\frac{N^{++}}{N^+} = \frac{S}{\alpha} \qquad (9.2)$$

where S is the ionization coefficient of N^+ and α the recombination coefficient of N^{++}. The term 'coronal equation' as used by Griem is not strictly accurate because collisional excitation and de-excitation of the upper levels and three body recombinations were taken into account by Griem, in addition to the radiative processes, when calculating S and α. Consequently, the validity condition (8.12) for the coronal model does not apply here. Griem estimates that the calculated intensity ratios should be valid for $N_e \leq 10^{18} cm^{-3}$.

In the present work the HeI 4471 A^o line was used instead of the HeI 5876 A^o. This had three advantages. Firstly because the HeI 4471 A^o line lies closer to the HeII 4686 A^o line the correction for the wavelength response of the detector can be made more accurately. Secondly, since the 4471 A^o line is weaker and broader than the 5876 A^o line it is less likely

to be self absorbed. Finally, the HeI 4471 A° line is more likely to be Stark broadened than either the HeI 5876 A° line or HeII 4686 A° lines and consequently a measurement of the line profile would not only yield the total line intensity but also an estimate of the electron density from the measured half width.

The intensity ratio (I'/II") of the HeII 4686 A° and HeI 4471 A° lines was derived from the ratio (I'/I) of the HeII 4686 A° and HeI 5876 A° lines calculated by Griem simply by multiplying this ratio by the ratio (I'/I") of the HeI 5876 A° and HeI 4471 A° lines. To calculate the ratio (I/I") it was assumed that the population densities of the upper states of the HeI 5876 A° and 4471 A° lines were related by their Boltzmann factors (see (8.5)). This gives for the ratio of the intensities:

$$I/I'' = \left(\frac{\lambda''}{\lambda}\right)^3 \cdot \frac{fg}{f''g''} \cdot \exp\left(\frac{E'' - E}{kT_e}\right) \qquad (9.3)$$

where the quantities appearing in (9.3) have a similar meaning to those appearing in (9.1).

Using (9.3) and the ratio (I'/I) taken from Griem (1), the ratio (I'/I") was calculated as a function of the electron temperature. The results are shown in Fig. (9.2).

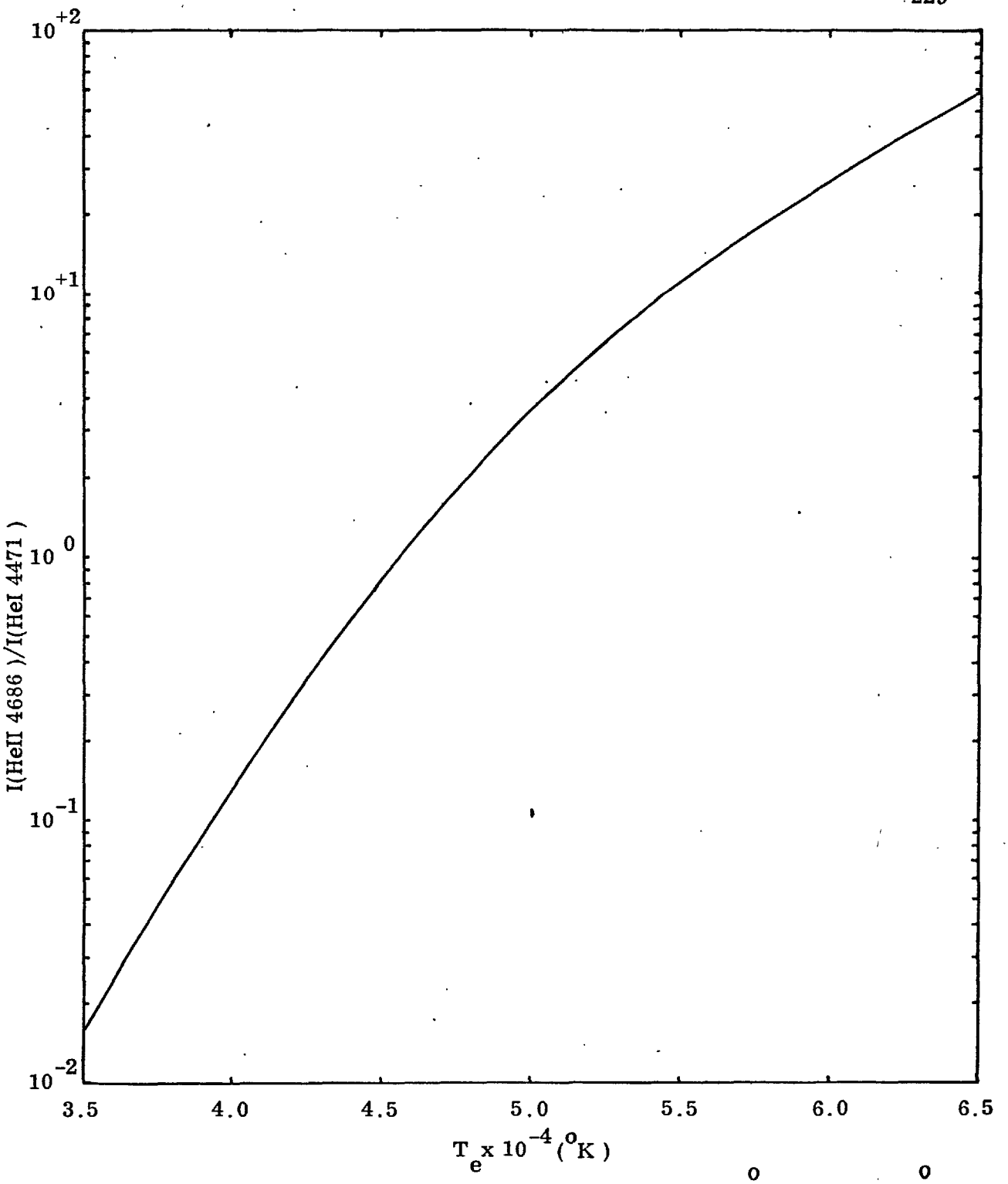

Fig.(9.2) Ratio of the Total Intensities of the HeII 4686 Å and HeI 4471 Å Lines as a Function of the Electron Temperature.

9.3.1. Measurement of the Ratio of the Intensities of the HeII 4686 A° and HeI 4471 A° lines

A detailed description of the method of scanning line profiles and the associated apparatus is given in Chapter X and only a brief description will be given here.

The line profiles were scanned on a shot to shot basis using a Hilger medium quartz spectrograph fitted with a photomultiplier scanning attachment. Observations were made in the axial direction and no attempt was made to spatially resolve the plasma emission. From these measurements the line profiles corresponding to the time of peak compression were constructed and the areas under the profile (excluding the continuum background) were measured to obtain the total line intensities. These results were then corrected for the wavelength response of the detector; this correction was determined with the aid of a tungsten ribbon lamp. Measurements were made for filling pressures ranging from 0.1 to 0.4 torr. For higher filling pressures the HeII 4686 A° line could not be observed.

9.3.2. Results

The spatially averaged electron temperature measured at peak compression for various filling pressures is shown in Fig. (9.3). It can be seen that a smooth increase in the electron temperature is observed as the filling pressure is lowered.

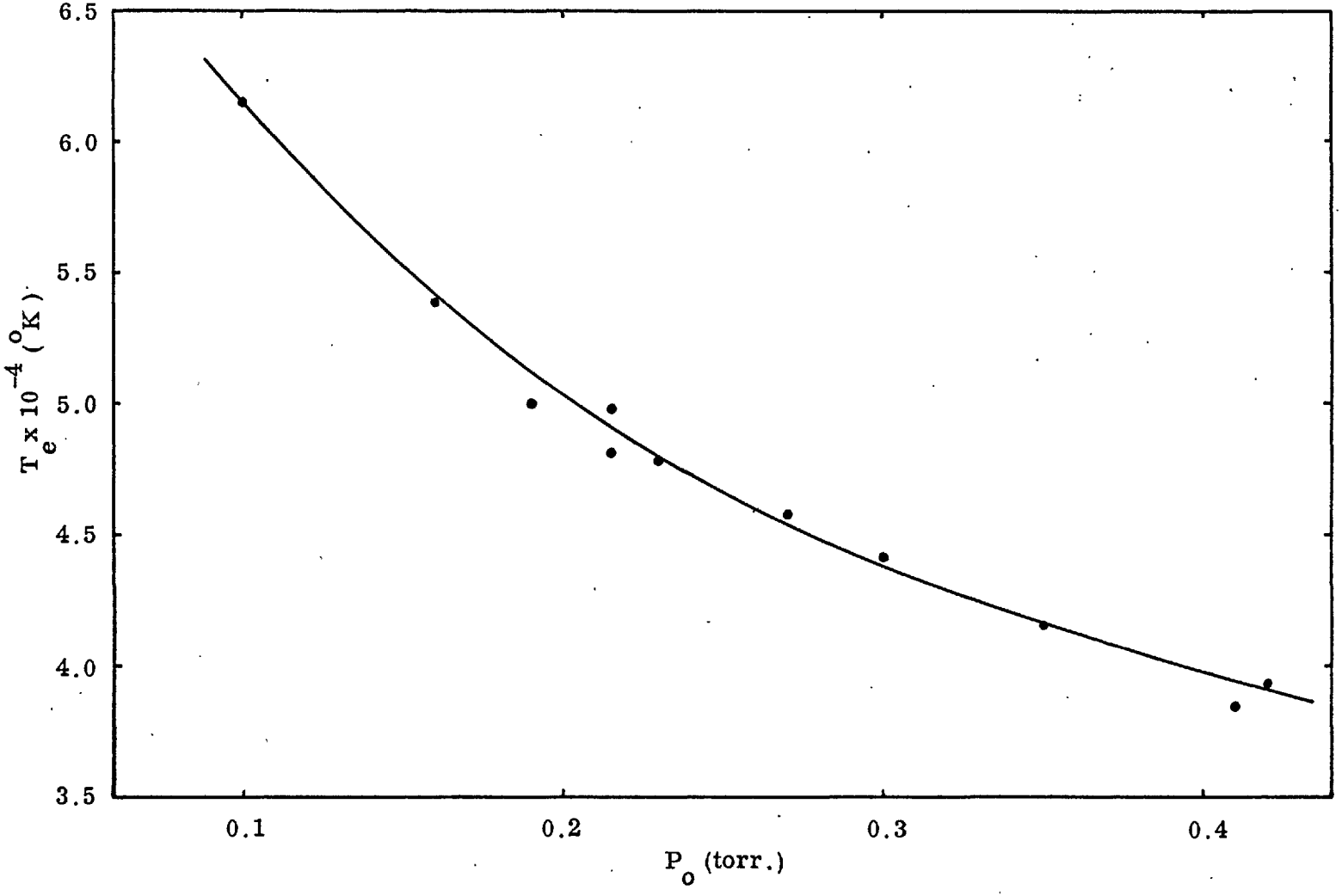

Fig.(9.3) Electron Temperature at Peak Compression Versus Filling Pressure.

Two factors contribute to the uncertainty in these measurements. Firstly, the ionization relaxation time for HeI and HeII (see 8.6) are such that the attainment of ionization equilibrium in the times of interest is at the best marginal. Consequently, the degree of ionization of the plasma will lag behind the instantaneous value of the electron temperature and because of this the electron temperatures given in Fig. (9.2) are probably systematically low. However, because the electron temperature is not strongly dependent on the intensity ratio (e.g. a change of a factor of 2 in the intensity ratio produces a change in electron temperature of only 10%, at 5×10^4 °K) the uncertainty should not be large.

Secondly, the spatially averaged electron temperature can be defined by:

$$\bar{T}_e \text{ (spatial)} = \frac{\int I'(V)\,dV}{\int I''(V)\,dV}$$

where the integration is over the plasma volume. The true average temperature of the plasma is defined by:

$$\bar{T}_e \text{ (true)} = \frac{\int T_e(V)\,dV}{\int dV}$$

Unless the plasma is homogeneous the average temperatures defined above can differ by arbitrarily large factors (see (53)).

In spite of the uncertainties mentioned above, the electron temperatures given in Fig. (9.2) are probably adequate for an investigation of the Stark broadening of spectral lines because the profile of a Stark broadened line is only weakly dependent on the electron temperature (see 11.1).

9.4. Electron Density Measurements

From the measured half widths $\Delta\lambda$ of the HeI 4471 A^{o} line and the value of its Stark broadening coefficient $C(N_e,T_e)$ calculated by Griem (1), an estimate of the electron density was obtained using the relationship (see 3.7.2)

$$N_e = C(N_e,T_e)\,\Delta\lambda^{3/2}$$

The results indicated that the electron density in the discharge satisfied $10^{15} < N_e \lesssim 10^{16}\,cm^{-3}$. A more precise estimate was not possible because the above equation is only valid if N_e is large enough to ensure that complete overlapping of the allowed and the forbidden component, which is present for $N_e \gtrsim 10^{14}\,cm^{-3}$. According to Griem this is ensured if $N_e \geqslant 10^{17}\,cm^{-3}$, i.e. at least an order of magnitude greater than the estimated electron density.

A precise measurement of the electron density of the plasma can be obtained by measuring its refractive index.

9.4.1. Theory of the Measurement of Electron Density from a Determination of the Refractivity of a Plasma

For light of frequency ω , the free electron contribution, n_e to the refractivity n of a plasma is given by:

$$n_e^2 = 1 - \left(\frac{\omega_p}{\omega}\right)^2 \qquad (9.4)$$

where ω_p is the electron plasma frequency. In terms of the wavelength of the incident radiation λ and the electron density N_e (9.4) becomes:

$$n_e^2 = 1 - \frac{r_o \lambda^2 N_e}{\pi} \qquad (9.5)$$

where r_o is the classical radius of the electron. Since n_e is close to unity for wavelengths in the visible (see (1)), the approximation $n_e^2 - 1 \approx 2(n_e - 1)$ can be made and (9.5) reduces to:

$$n_e = 1 - \frac{r_o \lambda^2 N_e}{2\pi} \qquad (9.6)$$

Hence, if the dominant contribution to the refractive index of

the plasma n is from free electrons the electron density can be determined by measuring n.

The preceding argument is the basis of the method used to measure N_e in the discharge. It should be noted that, in essence, the method requires no knowledge of the electron temperature of the plasma, is independent of the assumptions of Stark broadening theory and, if a laser is used to measure the refractive index of the plasma, good spatial resolution can be obtained.

9.4.2. Theory of the Measurement of the Refractivity of the Plasma

A Fabry-Perot interferometer system illuminated by the 6328 A^{o} radiation from an He-Ne laser was used to measure the refractivity of the plasma. This system is shown schematically in Fig. (9.4) and its use will be discussed in some detail in (9.4.3). But for the purpose of the present discussion it is sufficient to consider a system in which the discharge tube is placed within, and coaxial with, the cavity of a Fabry-Perot interferometer. This cavity is then illuminated with monochromatic radiation of wavelength λ and the transmission of the radiation through the cavity measured.

When plasma is generated within the discharge tube

the optical length of the interferometer cavity is altered by an amount S, and if it is assumed that the refractivity of the plasma is given by that of the free electrons, then S is given by:

$$S = \int_0^L n_e(\ell)\,d\ell \tag{9.7}$$

where $n_e(\ell)$ is the instantaneous value of the refractivity of the free electrons at a position ℓ on the axis of the plasma, and L is the length of the plasma. Substituting (9.6) in Eqn (9.7) S becomes:

$$S = \int_0^L \left(1 - \frac{r_o \lambda^2}{2} N_e(\ell)\right) d\ell \tag{9.8}$$

where $N_e(\ell)$ is the instantaneous value of the electron density at a position ℓ on the axis of the plasma. In terms of the electron density $\bar{N}_e$ averaged over the length of the tube, the above integral becomes:

$$S = L - \frac{r_o \lambda^2}{2\pi} \bar{N}_e L \tag{9.9}$$

From the theory of the Fabry-Perot interferometer (see Dangor (54)) a change ΔS in the optical length of the cavity alters the

intensity of the radiation transmitted through the cavity. There is a change from one transmission maximum to the next, a so called 'fringe', when $\Delta S = \lambda/2$. The corresponding change in electron density is found by differentiating (9.9) i.e.

$$\Delta \bar{N}_e = \frac{\pi}{r_o L \lambda} \qquad \text{(for one fringe)} \qquad (9.10)$$

Using L = 75 cm (the inter-electrode distance of the Z-pinch apparatus) and $\lambda = 6328\ A^o$

$$\Delta \bar{N}_e = 2.36 \times 10^{15} cm^{-3} \text{ (for one fringe)} \qquad (9.11)$$

Assuming that the electron density increases monatonically with time, and that the initial electron density is zero, then the electron density in the plasma, at any instant, will be proportional to the number of fringes recorded from the onset of the discharge. A minor complication arises because the interferometer does not discriminate between increasing and decreasing electron density. Usually, however, the instant of peak electron density (peak compression) can be determined either by a careful examination of the fringe sequence, or, by monitoring the continuum intensity of the plasma. This is proportional to the square of the electron density (see Chapter XII) and will therefore reach a maximum at the same instant as the electron density.

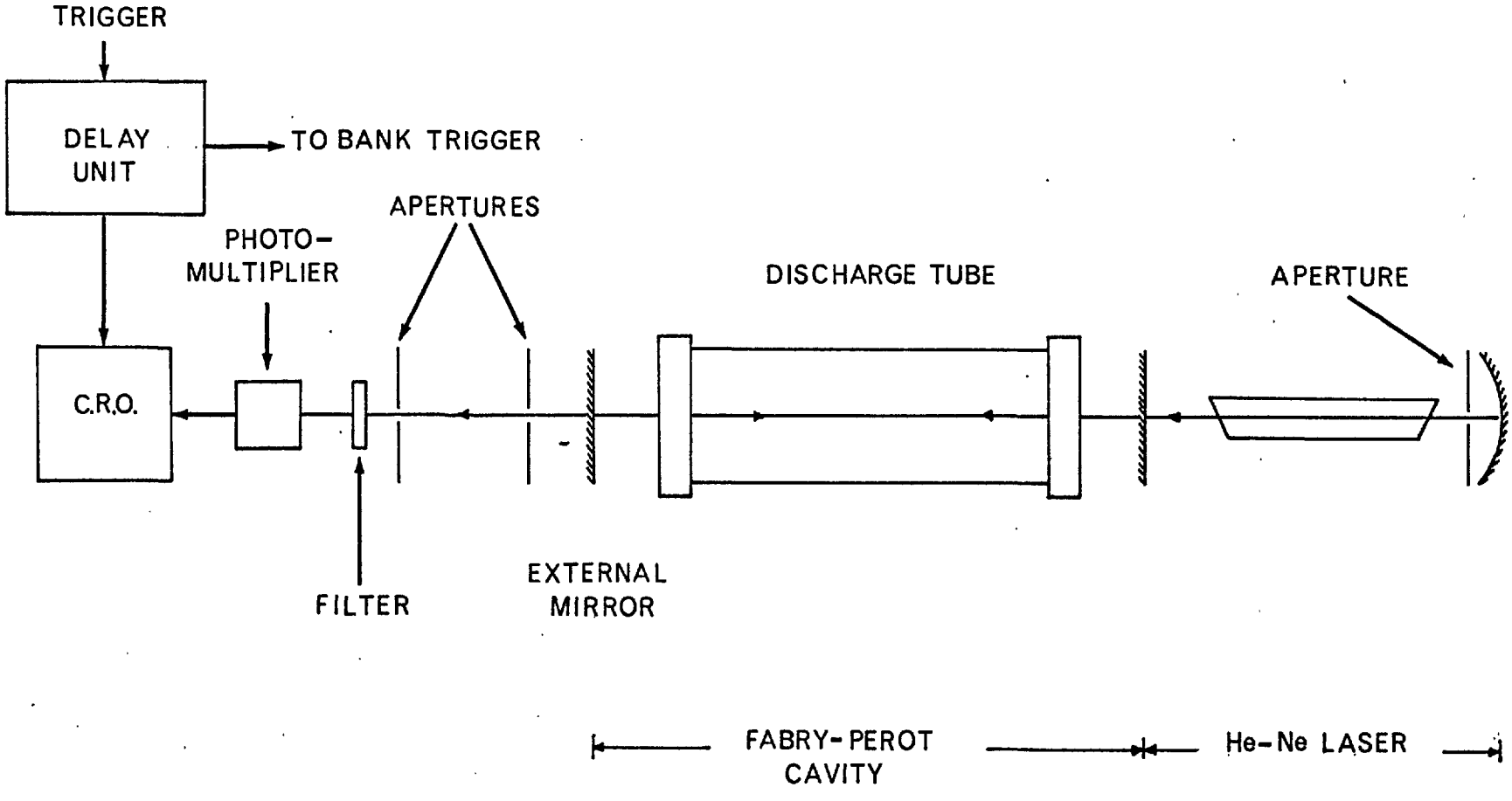

Fig.(9.4) Interferometer System.

The number of fringes recorded from the onset of the discharge to the time of peak compression is then proportional to the electron density at peak compression.

9.4.3. Measurement of the Refractivity of the Plasma

Fig. (9.4) shows the Fabry-Perot interferometer system used in the present investigation. It consisted essentially of an He-Ne laser which operated at 6328 A^{o} and was fitted with one plane mirror, one curved mirror (5 m focal length) and a small aperture stop to ensure that only the axial (TEM_{00q}) modes propagated. One mirror of the Fabry-Perot cavity (see Fig. (9.4)) was formed by the plane mirror of the laser and the other by a plane dielectric mirror with $\sim$ 45% reflectivity at 6328 A^{o}. This reflectivity was such that strong coupling between the two cavities (the laser cavity and the Fabry-Perot cavity) was prevented. The laser can therefore be considered as a source of constant illumination for the Fabry Perot cavity.

An R.C.A. 7265 photomultiplier connected to an L-type amplifier of a Tektronix 551 oscilloscope, was used to monitor the transmission of the laser beams through the Fabry-Perot cavity. The response time of this system was $\sim$ 0.02μs. In order to reduce optical pick up from the plasma the laser beam after transmission through the cavity was passed through two one millimeter apertures spaced one metre apart, and finally

through an interference filter with a 5 A^{o} bandwidth centred at the laser wavelength.

The following procedure was used to set up the interferometer. Apertures, consisting of a circular metal disc with a one millimeter hole at its centre, were placed at each end of the electrode assemblies and made concentric with them. These apertures served to define the axis of the discharge. Adjustments to the position of the laser were then made so that the beam passed through the apertures. The mirrors of the Fabry - Perot cavity were made parallel by adjusting the external mirror so that the laser beam was reflected back on itself. The output of the photomultiplier was then viewed on the oscilloscope using a slow time base ($\lesssim$ 2 ms/cm) and low amplitude fringes were usually observed owing to changes in the optical length of the cavity produced by mechanical vibrations. Fine adjustments to the external mirror were then made until fringes with a modulation of $\sim$ 80% were obtained.

The measurement procedure consisted simply of setting the required filling pressure in the discharge tube, firing the discharge and photographing the oscilloscope record of the fringe sequence together with a record of either the discharge current or the continuum intensity. These measurements were made for filling pressures ranging from 0.05 to 0.60 torr.

9.4.4. Results

Plate(9.2) shows an oscilloscope record of a fringe sequence obtained from the plasma together with discharge current. This was recorded at a filling pressure of 0.4 torr. From (9.11) one fringe corresponds to a change in electron density of $2.36 \times 10^{15} cm^{-3}$. It will be noted that as the time of peak compression is approached the modulation of the fringes decrease. This is caused by radial electron density gradients in the plasma which refract part of the laser beam of the axis of the discharge. The effect of this refraction is to reduce the finesse of the Fabry-Perot cavity and hence the fringe modulation.

In Fig. (9.5) the electron density at peak compression, derived from the laser measurements, is plotted as a function of the helium filling pressure. The electron density is seen to pass through a well defined maximum of $2.1 \times 10^{16} cm^{-3}$ at a filling pressure of $\sim$ 0.28 torr. On the low pressure side of the maximum the increase in the electron density with filling pressure is seen to be linear as is the decrease on the high pressure side of the maximum up to $\sim$ 0.5 torr after which a much slower fall off is observed.

A similar behaviour in the electron density at peak compression versus filling pressure curve was also observed when the discharge was operated in argon and hydrogen (see Burgess,

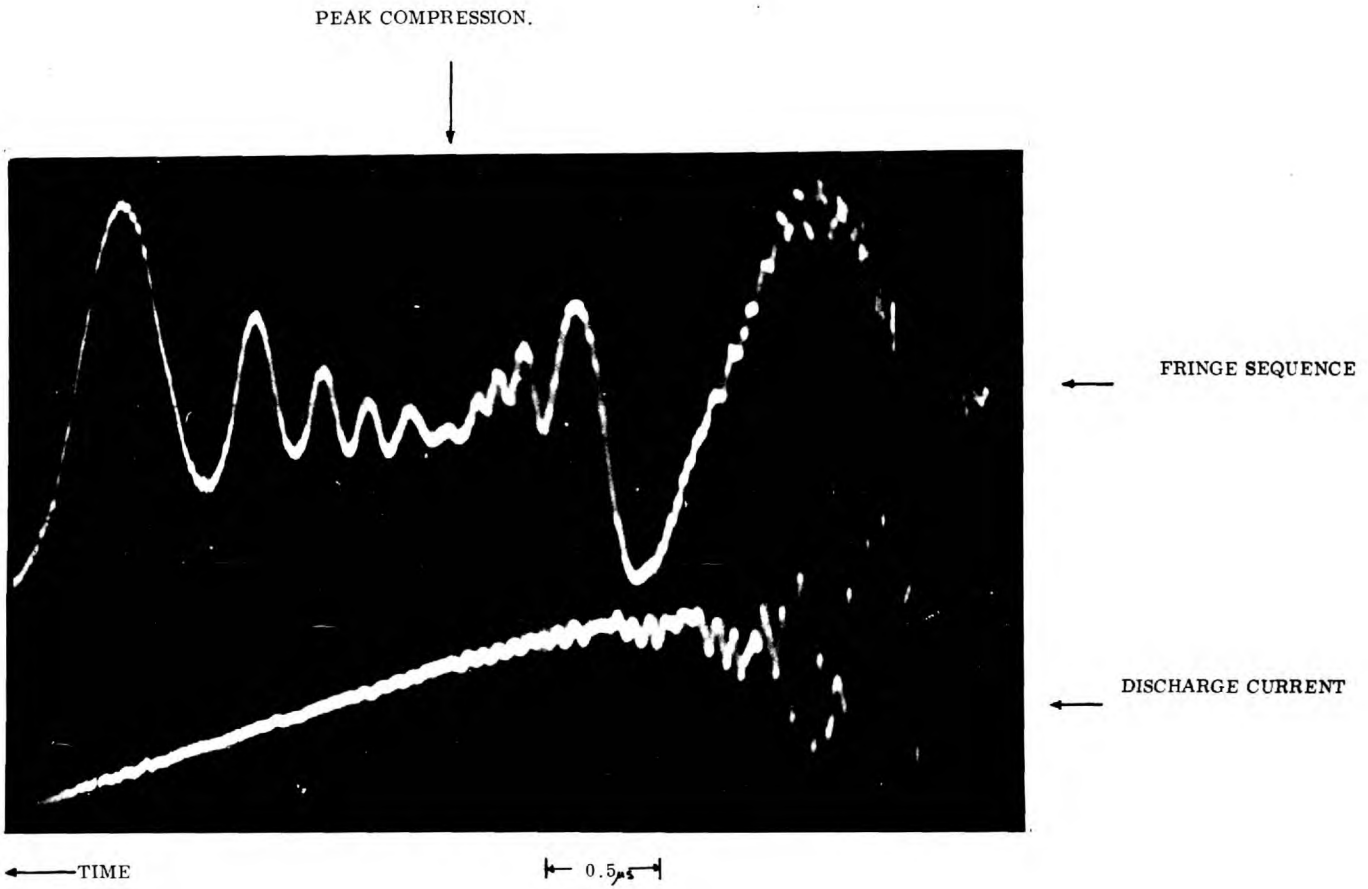

Plate (9.2) Fabry-Perot Fringe Sequence

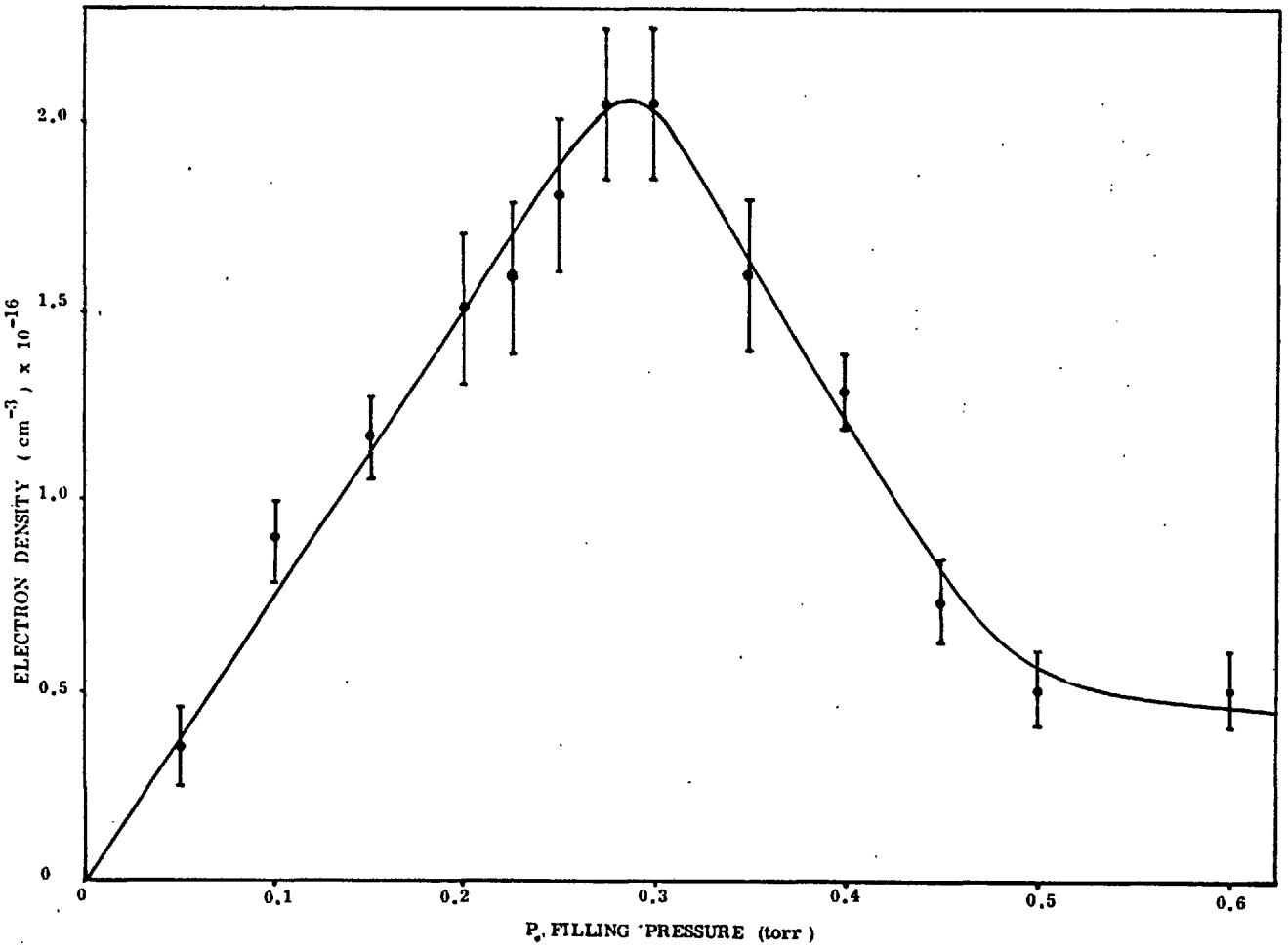

Fig.(9.5) Electron Density at Peak Compression Versus Filling Pressure.

Dangor and Jenkins (55) for further discussion). This phenomenon in the behaviour of a Z-pinch discharge was first reported by Burgess (3) and has also been observed by Zwicker and Schumacher(56) and Roberts (22) using Z-pinch discharges of markedly different parameters.

9.4.5. Estimates of the Contributions to the Refractivity of the Plasma from Sources other than Free Electrons

At this stage the results given in Fig. (9.5) must be treated with some caution because the assumption that the refractivity of the plasma is dominated by that of the free electrons has still to be verified.

When considering the various contributions to the refractivity of the plasma it is important to realize that since the method of measuring the electron density is based on the measurement of the refractivity of the plasma as a function of time the method, in principle, requires that free electron refractivity should dominate all other contributions to the plasma refractivity over this period of time. Obviously this is not possible because for early times in the history of the discharge it might be expected that the electron density on the axis is zero. It is, therefore, necessary to verify also that the contribution to the total fringe shift during these times is negligible.

The following sources may contribute to the refractive index of the plasma n:-

a) Atoms and Ions in Various Energy States

The contributions under this heading can be classified according to whether the wavelength of the incident radiation λ_L is less then, equal to, or greater than the wave length of the transitions λ_i between the various energy states.

$\lambda_L >> \lambda_i$:- Despite their remoteness from wave length of the incident radiation, resonance transitions can give a significant contribution to the refractive index. This is because of the very large population density of the ground state . Their contribution to n is given by (1).

$$n_a - 1 = \sum_m \frac{r_o}{2\pi} f_{m1} \lambda_{m1}^2 \left[1 + \left(\frac{\lambda_{m1}}{\lambda_L}\right)^2\right] N_1 \qquad (9.12)$$

where λ_{m1} is the wavelength of the resonance transition originating from state m, f_{m1} the corresponding oscillator strength and N_1 the ground state density of the species. Note that the sign of this contribution is opposite to that of the electrons. To be strictly accurate the summation in (9.12) should be extended over all excited states taking into account both upward and downward transitions, and also transitions from discrete states to the continuum. However, because excited state populations are usually negligible compared with that of the ground state

(9.12) is sufficiently accurate for the purpose of the present estimate.

The ratio of the above contribution to that of the free electrons is given by:

$$\frac{n_a-1}{n_e-1} = -\sum_m f_{m1}\left(\frac{\lambda_{m1}}{\lambda_L}\right)^2\left[1+\left(\frac{\lambda_{m1}}{\lambda_L}\right)^2\right]\frac{N_1}{N_e} \qquad (9.13)$$

The following approximations were made in order to evaluate the summation occurring in (9.13).

$$\text{a)} \quad \left(\frac{\lambda_{m1}}{\lambda}\right)^2 \ll 1$$

$$\text{b)} \quad \frac{\lambda_{m1}}{\lambda_L} = \frac{\lambda_{21}}{\lambda_L} \quad \text{for } m>2 \qquad (9.14)$$

The latter approximation ensures that, if anything, the summation is over-estimated. Finally, the summation over the absorption oscillator strengths was carried out using the sum rule (Allen (57))

$$\sum_m f_{m1} = \tfrac{1}{3}\,\frac{(\ell+1)(2\ell+3)}{2\ell+1} \qquad (9.15)$$

$$= 1 \text{ (for s - np transitions)}$$

Inserting (9.14) and (9.15) into (9.13) and evaluating the ratio

for $\lambda_L = 6328\ A^o$ the following results are obtained:

$$\frac{n_a - 1}{n_e - 1} \approx - 9 \times 10^{-3} \frac{N_1}{N_e} \quad \text{(for HeI)} \tag{9.16}$$

$$\frac{n_a^+ - 1}{n_e - 1} \approx - 2 \times 10^{-3} \frac{N_1^+}{N_e} \quad \text{for HeII)} \tag{9.17}$$

Clearly, the contribution from the HeII ions will be negligible at all times in the history of the discharge since at the worst, $N_1^+ = N_e$ (charge neutrality). Also the contribution from neutral helium atoms will be less than 1% if the degree of ionization is greater than 0.5. This degree of ionization is expected in helium for electron temperatures $\sim 3 \times 10^4\ ^oK$ (see Fig. (8.1) . For filling pressures less than 0.4 torr (the highest filling pressure at which electron temperature was measured) the electron temperature, measured at peak compression is found to be greater than $3 \times 10^4\ ^oK$ (see Fig. (9.3)) and, therefore, the contribution of neutral helium to the refractivity of the plasma will be negligible at the time of peak compression. However, at times prior to the time of peak compression the plasma temperature is probably much less than $3 \times 10^4\ ^oK$, and the contribution of neutral helium to the refractivity of the plasma may be important at these times; especially at high filling pressures. Further discussion on this point will be postponed

until after the other contributions to the refractivity of the plasma have been considered.

$\lambda_L \sim \lambda_i$:- If an atom or ion in the plasma has a transition which is close to the laser wavelength then significant contributions to refractivity of the plasma can arise through the phenomenon of anomalous dispersion. For a transition from state m to n the refractivity is given by (1):

$$n_a - 1 = \frac{r_o}{4\pi} \cdot f_{mn} \frac{\lambda_{mn}^3}{\Delta\lambda} \left[1 - \frac{g_n}{g_m} \frac{N_m}{N_n} \right] N_n \qquad (9.18)$$

where $\Delta\lambda = \lambda_L - \lambda_{mn}$, λ_L is the laser wavelength, λ_{mn} and f_{nm} are the wavelength and absorption oscillator strength of the transition respectively, and N_m, g_m and N_n, g_n are the population densities and statistical weights of the upper and lower states respectively. Eqn (9.18) is valid provided:

$$w << \Delta\lambda << \lambda_L ,$$

where w is the half-half width of the line. It should be noted that the sign of the contribution given by (9.18) depends on the sign of $\Delta\lambda$.

The ratio of the above contribution to that of the free electrons is given by:

$$\frac{n_a-1}{n_e-1} = -\tfrac{1}{2}\cdot\frac{f_{mn}}{\Delta\lambda}\cdot\frac{\lambda_{mn}^3}{\lambda_L^2}\cdot\left[1-\frac{g_n N_m}{g_m N_n}\right]\cdot\frac{N_n}{N_e} \qquad (9.19)$$

An examination of the published wavelengths of HeI and HeII transitions (see (35) and (38) respectively) shows that the lines listed in Table (9.1) lie closest to the laser wavelength.

TABLE (9.1)

TRANSITION	λ_{mn} (A°)	$\Delta\lambda$ (A°)	f_{mn}
HeI $2^1P - 3^1D$	6678	-350	.71
HeI $2^3P - 3^3D$	5876	452	.71
HeII 4 - 6	6530	-232	.18

The ratio (9.19) was evaluated for each line assuming that the population densities of the upper and lower states of a line were related by their Boltzmann factors (see 8.5) and that the population density of the lower state of the line was in partial L.T.E. with the ground state of the next higher ionization stage and the free electrons. It was found that at the time of peak compression the contribution to the refractivity of the plasma from anomalous dispersion was negligible in comparison with that from the free electrons and at all other times it was negligible in comparison with the contributions from neutral atoms in their ground state.

$\lambda_L \lesssim \lambda_i$:- Here λ_i is the wavelength of a transition between the reduced ionization potential and a bound state. The contributions which fall into this category are not contributions to the refractivity of the type discussed above but are instead additional contributions to the electron density. This additional contribution to the electron density arises because electrons in bound states which satisfy $\lambda_L \lesssim \lambda_i$ are so weakly bound that they behave as though they were free electrons. Hence the electron density found from interferometric measurements will be greater than the true free electron density. Griem (1) has estimated the magnitude of this contribution and concludes that it is only likely to be important in L.T.E. plasmas, and even here the correction is typically less than 1%. For a helium plasma to be in L.T.E. electron densities of at least $\sim 10^{18} cm^{-3}$ are required (see Chapter IIX). The electron densities encountered in this experiment are two orders of magnitude too low for the establishment of L.T.E. and consequently the correction to the interferometrically measured electron density will be negligible.

b) Fully Stripped Ions

The ratio of the refractivity of fully stripped ions to that of free electrons is given by (see Griem (1)).

$$\frac{n_i - 1}{n_e - 1} = \frac{Z m_e}{m_i} \qquad (9.20)$$

where Z and m_i are the nuclear charge and mass of the ion respectively. For a helium plasma this contribution is negligible because the maximum value of Z is 2 and m_i is $\sim 7 \times 10^3 m_e$.

Conclusion

Of the various sources which may contribute to the refractivity of the plasma only that resulting from neutral atoms in their ground state is likely to be significant.

9.4.6. Fringe Shifts due to Changes in Neutral Helium Density

The change ΔN in the neutral helium density required to produce a single fringe shift can be calculated in a similar manner to that used for the free electrons (see 9.4.2). Using the refractivity of neutral helium given in Allen (57) ΔN is given by:

$$\Delta N \approx 3.2 \times 10^{17} \text{cm}^{-3} \quad \text{(for one fringe)} \qquad (9.21)$$

From this result the change in the size of the plasma required to produce a single fringe shift can be calculated. Assuming that

the filling pressure is 0.4 torr and that no ionization takes place, the volume compression ratio required to produce one fringe shift is ~ 30 or, alternatively, the radius of the column of neutral helium must be reduced from 22.5 mm to ~ 4 mm (if ionization occurs the final radius would be even smaller). Now for the filling pressure of 0.4 torr the first fringe occurs ~1 μs after the discharge current commences (see Plate (9.2)) and if this fringe results from an increase in the neutral helium density then the maximum radius the plasma can have at this time is 4 mm. However, end on framing camera observations of the discharge showed that the plasma at this time filled the discharge tube and did not begin to collapse until ~ 0.5 μs later. Hence the initial fringe shifts can not be due to changes in the neutral helium density and must therefore arise from changes in the free electron density. Furthermore, if the initial fringe shifts had been caused by changes in the neutral helium density then because the free electron and neutral refractivities have opposite signs it might be expected that a point in time would be reached when the composition of the plasma was such that total refractivity is unity. The effect of this would be to introduce a turning point in the fringe sequence. Such behaviour was not observed, even at the highest filling pressure for which measurements were made.

It should be noted that by using two wavelength

interferometry the problem of the neutral helium refractivity can be eliminated entirely. This method relies on the fact that with the exception of the neighbourhood of spectral lines, the refractivity of neutral atoms is constant, whilst that of free electrons varies as λ^2.

9.4.7. Effects which Influence Directly the Free Electron Refractivity

So far the discussion has been concerned with effects which interfere with the measurement of the free electron refractivity. The following effects have a direct influence on it:

a) Particle Collisions

Essentially, the effect of collisions is to introduce into the equation of motion of the free electrons a damping term (the motion referred to here is that which takes place under the influence of the electric field of the incident radiation). If ω_c is the electron-electron collision frequency then the free electron contribution to the refractive index of the plasma, including collisional effects, is given by (44).

$$n_e^2 = 1 - \left(\frac{\omega_p}{\omega_L}\right) \frac{1}{1 + \left(\frac{\omega_c}{\omega_L}\right)^2} \qquad (9.21)$$

For $N_e \sim 10^{16} cm^{-3}$ and $T_e \sim 4 \times 10^4 {}^oK$ the value of ω , calculated from the Spitzer formula (48), is $\sim 10^{12} sec^{-1}$. This frequency is small in comparison with the frequency of the incident radiation of $\sim 5 \times 10^{14}$ cycles.sec^{-1}. Hence the term (ω_c/ω_L is negligible in comparison with unity and the influence of electron-electron collisions on n_e can be neglected. Since the collision frequencies associated with electron-ion and electron neutral encounters will be even smaller than the electron-electron collision frequency it follows that all collisional effects will be negligible.

b) Magnetic Fields

Because the presence of a magnetic field can modify the motion of an electron which is moving under the influence of an electric field, it can also effect the refractivity of the free electrons. The manner in which n_e is affected depends not only on the strength of the magnetic field but also on the relative orientations of the magnetic field and the electric field of the incident radiation (44). For example, there is no affect on n_e when the two fields are parallel, since the magnetic field has no affect on the motion of the free electrons. In general the effect of a magnetic field will be negligible if the electron cyclotron frequency ω_B satisfies:

$$\omega_B / \omega_L << 1 \qquad (9.22)$$

ω_B is given by:

$$\omega_B = \frac{eB}{mc} = 2.8 \times 10^6 \text{ B cycles/sec} \qquad (9.23)$$

where B is in gauss

The condition (9.22) will be easily satisfied for measurements of the axial electron density because the magnetic field on the axis of a Z-pinch discharge is effectively zero. For off axis measurements the magnetic field will be considerably larger with the maximum value occurring roughly at the edge of the plasma. The value of this field can be calculated from:

$$B = \frac{I}{5r} \quad \text{gauss}$$

where the plasma current I is in amps and the plasma radius r is in cm. Assuming that at the time of maximum current (5×10^3 amps) the discharge has a radius of ~ 5 mm the maximum magnetic field will be $\sim 2 \times 10^3$ gauss, which from (9.23) corresponds to a cyclotron frequency of 6×10^9 c/s. This frequency is much less than that of the incident radiation so that condition (9.22) is well satisfied even for off axial measurements and consequently the electron density measurements will not be influenced by the presence of a magnetic field.

Hence both particle collisions and magnetic fields have a negligible effect on the free electron refractivity.

9.4.8. Further Assumptions

In order to interpret the observed fringe shifts it is necessary to replace the electron density N_e occurring in (9.8) by $\overline{N}_e$ the electron density averaged over the length L of the plasma, i.e.

$$\overline{N}_e = \int_0^L \frac{N_e(\ell)d\ell}{L}$$

This procedure assumes that the length of the plasma is known. Also if this device is to be used as a spectroscopic light source it would be advantageous if the electron density is constant along the axis, since side on measurements of, say, line profiles can be directly compares with end on measurements.

The axial variation of electron density in a Z-pinch discharge has been investigated by Burgess (3). The discharge studied had an interelectrode distance and internal diameter of 50 cm and 15 cm respectively and was operated in argon at a filling pressure of 0.25 torr. Electron densities were measured at the time of peak compression at various distances along the axis of discharge, by observation of the Stark broadening of the Ar II 4806 A° line.

Burgess found that over a length of ~ 20 cm, at the centre of the discharge, the electron density was independent of the axial position. At distances of ~ 10 cm from each electrode sharp minima occurred. These had a half width of 5 cm and the electron density at the centre of the dip was ~ 25% below that found midway between the electrodes. Near the electrodes the electron density was found to drop sharply from a value close to that found at the centre of the discharge.

If $\bar{N}_e$ is calulated for the distribution of electron density measured by Burgess the resulting electron density is found to be ~ 10% lower than that measured at the centre of the discharge.

Since the interelectrode distance of the present discharge is greater than that of Burgess's (75 cm compared with 50 cm) axial variations of electron density and the uncertainty in the length of the plasma would be expected to be less significant. Line profiles measured in the axial and radial directions support this conclusion (see Chapter XI).

9.5. Summary of the Discussions Concerning the Electron Density Measurements

The measurements of electron densities in the discharge have been discussed in some detail because the accuracy and ease

with which this parameter can be measured is important in determining whether or not a discharge is suitable as a spectroscopic light source. These results are also important for the interpretation of measurements to be described in Chapter X.

It has been shown that the plasma refractivity is dominated at all times by the free electrons and effects which directly influence the free electron refractivity are negligible. Hence it was correct to interpret the observed fringe shifts (see 9.4.4.) asbeing due to changes in the free electron density. Assumptions concerning the length of the plasma and the axial variation of electron density have also been described.

CHAPTER X

MEASUREMENTS OF THE PROFILES OF SOME HELIUM LINES

10.1 Introduction

The following experiments concerning the Stark broadening of helium lines in a plasma were proposed in (4.3.2).

a) The measurement of the Stark broadening of HeII lines at electron densities of $\lesssim 10^{16} cm^{-3}$.

b) The investigation of the variation with electron density of the profile of a line which contains a forbidden component.

It was also proposed that the Z-pinch discharge described in the preceding chapters should be used as the source of helium plasma.

This chapter is concerned with the choice of suitable lines for the investigations mentioned above and the methods used to measure their profiles.

10.2 Choice of Lines

Two factors limited the choice of suitable lines for the investigations mentioned above. These were the resolution of the instrument to be used for the line profile measurements,

and the availability of theoretical profiles.

A Hilger medium quartz spectrograph fitted with a photomultiplier scanning attachment was available for the line profile measurements. The dispersion of this instrument falls off rapidly towards longer wavelengths so that in order to reduce the effects of instrumental broadening it was necessary to select lines with as short a wavelength as possible.

Theoretical profiles are available for two HeII lines (see (1)), the HeII 4686 and 3203 A^{o} lines. Of these, only the latter line could be measured since an examination of the theoretical profiles showed that the half width of the HeII 4686 A^{o} line was a factor of ~ 3 less than the instrumental width, even at the highest electron density obtainable in the discharge. In contrast, at electron densities as low as $\sim 5 \times 10^{15} cm^{-3}$, the calculated width of the 3203 A^{o} line was still a factor of 2 larger than the instrumental width.

At the time these investigations were started theoretical profiles of lines with forbidden components were not available. However, it was communicated to the writer that calculations were in progress of the profiles of the HeI 4471 A^{o} and 4921 A^{o} lines including forbidden components. As the previous measurements of the profile of the HeI 4471 A^{o} (see (9.4)) had shown that it was wide enough to be measured, this line was chosen.

Although the original proposals for the investigations were concerned with the measurement of the profiles of the HeII 3203 A^{o} and HeI 4471 A^{o} line, it was decided to measure also the profiles of two isolated HeI lines. These additional measurements were undertaken because the work presented in the first part of this thesis shows that good agreement can be expected between the calculated and experimental width of isolated lines, and, consequently, these measurements should provide a check on the measurement procedures. The two lines chosen for the measurements were the HeI 2945 A^{o} and 3965 A^{o} lines.

The lines chosen for study are summarised in Table (10.1).

TABLE (10.1)

SPECTRUM	TRANSITION	WAVELENGTH (A^{o})
HeII	3 - 5	3203
HeI	$2p\,^3P - 4d\,^3D$	4471
HeI	$2s\,^3S - 5p\,^3P$	2945
HeI	$2s\,^1S - 4p\,^1P$	3965

10.3 Competing Broadening Mechanisms

In Chapter II a number of mechanisms, in addition to Stark broadening, were discussed whereby the spectral lines emitted by an atom or ion immersed in a plasma may be broadened.

Consequently, in an investigation of Stark broadening of spectral lines, these competing mechanisms must be considered and, if found to be important, corrections must be made. The various possible competing mechanisms are considered below.

10.3.1. Natural Broadening

As discussed in (2.2), this broadening mechanism produces a line width of $\sim 10^{-4} A^{o}$. Compared with Stark, or even Doppler broadening (see below), this width is negligible.

10.3.2. Van der Waals Broadening

Since the electron temperatures, measured at peak compression are high enough to ensure degrees of ionization $\gtrsim 50\%$. Van der Waals broadening will be negligible in comparison with Stark broadening.

10.3.3. Resonance Broadening

Since none of the lines studied has a state in common with the upper state of the resonance line, resonance broadening need not be considered.

10.3.4. Zeeman Broadening

In (9.4.7.) it was estimated that the largest magnetic field occurring in the plasma is $\sim 2 \times 10^{3}$ gauss. Using the expression for Zeeman broadening given in (2.4.) and taking

λ = 4000 A^{o} as the average wavelength of the lines, the Zeeman broadening produced by this field is found to be $\sim$ 0.03 A^{o}, which is negligible in comparison with the Doppler broadening (see below).

10.3.5. Doppler Broadening

The amount of Doppler broadening can be estimated using (2.4). Taking = 4000 A^{o} as the average wavelength of the lines and $T_e = 6 \times 10^4$ ^{o}K (the highest temperature measured in the plasma) the Doppler width is found to be $\sim$ 0.4 A^{o}. Since this width is a factor of 4 smaller than the smallest half width expected from Stark broadening, the additional broadening produced will be $\sim$ 1% or less. However, if necessary, Doppler broadening can be taken into account using the procedure discussed in (2.8.).

10.3.6. Radiative Transfer

Although it is possible to estimate, using (2.8.) the amount of self absorption of a line, it was thought to be preferable to demonstrate experimentally the absence, or presence, of self absorption by comparing the profiles emitted in the axial and radial directions.

10.4. Profile Measurements

In the following sections the apparatus and procedures used for the profile measurements will be described.

10.4.1. Spectrometer

A Hilger medium quartz spectrograph was used to measure the line profiles. This instrument was fitted with a Hilger E720 photomultiplier scanning attachment which had been modified so that the drive screw, controlling the position of the exit slit could be operated manually. This modification had been made by a previous user so that the instrument could be used for shot to shot scanning. A scale calibrated in degrees was attached to the drive screw and served to determine the position of the exit slit. One revolution of the scale moved the exit slit through one millimetre, and the total number of revolutions was indicated by a revolution counter attached to the drive screw.

10.4.2. Detector and Recording Apparatus

The detector used with the above instrument was an R.C.A. 1P28 photomultipler. Stabilization of the dynode chain of the photomultipler, under pulsed signal conditions, was ensured by the presence of 0.1 μF capacitors across the last 4 dynodes and 0.01 μF capacitors across the remaining dynodes.

For D.C. recording the photomultiplier anode current was measured using a Keithley type 601 electrometer.

For pulsed operation, the voltage developed across an anode resistor of 680 Ω was fed via a co-axial cable of length 2 ft and characteristic impedance 50 Ω to an L-type amplifier of a Tektronix 551 dual beam oscilloscope. The use of an unmatched cable resulted in negligible ringing, and allowed measurements to be made further out on the wings of the profiles than would have been possible using a matched cable. A pick up loop placed close to the discharge tube was used to trigger the oscilloscope. The RC-time constant of the photomultipler-oscilloscope circuit was 0.06 μ s. Finally, to reduce electrical interference all cables were doubly screened and care was taken to eliminate ground loops.

10.4.3. The Linearity of the Photomultiplier and the Associated Circuits

The linear range of the photomultiplier and associated circuits, under pulsed conditions, was found by varying the intensity of the light entering the spectrometer in a known way (see below) and measuring the output current. From a graph of light intensity versus output current the linear range of the system was determined.

The pulsed light source used was the discharge itself and attenuation of the light was accomplished by placing various

calibrated neutral density filters in front of the entrance slit. The output was found to be linear to better than $\pm$ 5% for anode currents up to $\sim$ 20 mA. During the measurements the anode current rarely exceeded 2 mA.

10.4.4. Method of Focusing the Spectrometer

The spectrometer was focused photoelectrically using the following method. A wavelength calibration of the instrument was made using the spectrum emitted by a low pressure helium discharge lamp, the output of the photomultiplier being measured with the electrometer. Entrance and exit slits were then set at $\sim 5\mu$ and with the aid of the above calibration the exit slit was moved to the position of HeI line under investigation. By adjusting the position of the entrance slit relative to the collimating lens and then scanning through the peak of the line on each adjustment, a position was found where the peak intensity was a maximum. This position was taken as the focus. This procedure was repeated prior to the investigation of each of the line profiles.

10.4.5. Measurement of the Reciprocal Dispersion of the Spectrometer

Because of the relatively large separation of the lines in HeI spectrum and the rapid variation of the reciprocal dispersion of the spectrometer towards longer wavelengths the

calibration made using the helium discharge lamp could not be used to obtain accurate values of the reciprocal dispersion at the wavelength position of each of the lines studied. Instead the required values were determined by photoelectrically scanning through a region of the spectrum emitted by a suitable discharge lamp (usually either mercury, cadmium or neon) chosen such that identifiable lines lay close to, and on either side of, the line under investigation. From the known wavelengths and measured separation of the lines the reciprocal dispersion of the instrument at the wavelength of the line was obtained.

10.4.6. Measurement Procedure

For side-on measurements, the spectrometer was aligned, perpendicular to and in the plane of, the discharge tube axis by placing two small apertures on either side of the central slot in the theta pinch coil so that the axis defined by them intersected the axis of the discharge tube. A lamp laced behind the apertures then defined a reference beam for the alignment of the optical axis of the spectrograph. A similar procedure was used for end-on alignment. A quartz lens was used to image the plasma onto the spectrometer slit.

Ideally, for a pulsed device of this nature where the line profiles are obtained on a shot to shot basis, it is desirable to measure (or at least to monitor) the electron density on each shot in order to minimize any effects of shot to

shot fluctuations. Fortunately, the laser measurements (see 9.4) showed that the axial electron density, measured at peak compression was better than 5% on both a short and long term basis when the discharge was operated at pressures above 0.05 torr. This feature of the discharge enabled the electron density, at peak compression, to be set by simply fixing the filling pressure. The corresponding electron density was then obtained from the previously determined curve of electron density at peak compression against filling pressure Fig. (9.5).

Previous measurements (Chapter IX) had shown that the time to peak compression obtained from the laser measurements agreed well with that obtained from the peak in the continuum emission. Hence the latter was used to establish the time of maximum compression.

Prior to the start of a run the discharge tube was evacuated to a base pressure of $\sim 10^{-5}$ torr. The helium pressure was then set by means of the hot wire leak valve and allowed to stabilize. During this period a number of shots ($\sim$30) were fired to condition the discharge tube.

At the start of a run a film record was made of the continuum emission at 5400 A^{o} on one beam of the oscilloscope and the discharge current on the other. This measurement served to establish the time to maximum compression relative to the discharge current trace. Entrance and exit slits were then set

at~5 μ and the line profile scanned shot by shot, each point on the line profile being recorded three times by overlaying the traces, to allow for any small fluctuations in the light intensity. Each film record contained the light emission at one wavelength in the line profile, a base line for the light emission and the discharge current trace. The background emission to the line was found by making measurements at points far from the line centre. Finally, to check that no drifts had occurred during the run the continuum was re-recorded.

10.4.7. Reduction of Data

In order to analyse the films they were first enlarged by a factor of 10 using a photographic enlarger and the images traced onto graph paper. The continuum signal and the accompanying discharge current signal were then traced onto tracing paper. This was then placed over the traces on the graph paper and by matching the two current traces the time to peak compression could be established. The line profile was then obtained by plotting the amplitude of the traces, measured at the above time, for each of the wavelength positions recorded.

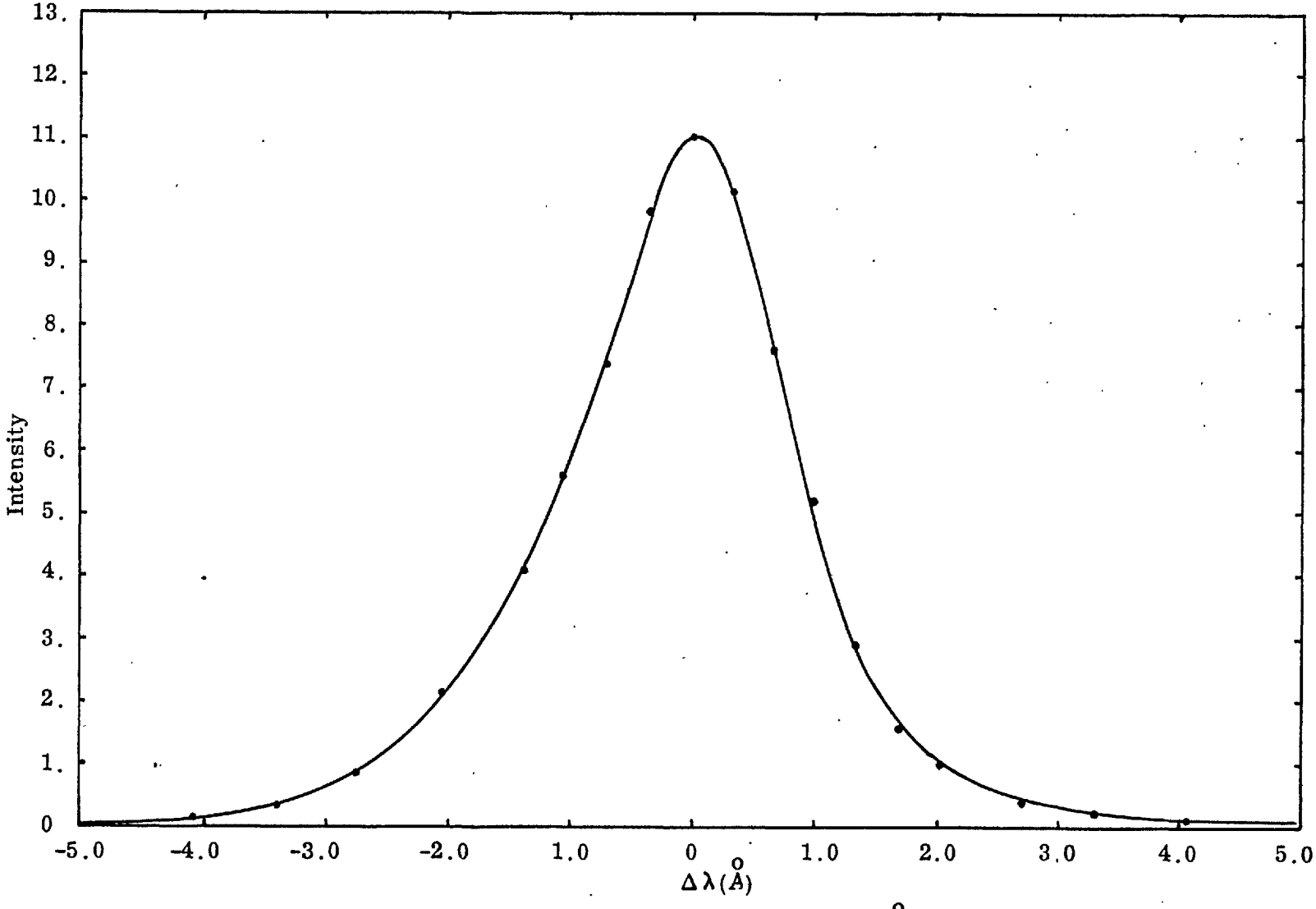

Fig.(10.1) Instrumental Profile for $\lambda = 4471$ Å

10.5 Determination of the Instrumental Profile

Before a comparison can be made between the observed and theoretical profiles the effects of instrumental broadening (see 2.7) must be taken into account. In order to do this the instrumental profile had to be determined.

Preliminary measurements of the instrumental profile, using a low pressure mercury lamp placed directly in front of the spectrometer slit, showed that the instrumental half width expressed in degrees of rotation of the exit slit drive shaft, was independent of the wavelength of the line used; indicating that a geometrical image of the entrance slit is formed. Hence, the instrumental profile in wavelength units can be obtained from a single measurement of the instrumental profile in degrees of rotation of the drive shaft and a knowledge of the reciprocal dispersion of the instrument at the wavelength of interest.

The instrumental profile was determined using the 3350 A^{o} line emitted by a low pressure mercury discharge lamp, and in order that the solid angle illuminated would be the same as that used in the line profile measurements, the lamp was placed within the discharge tube so as to occupy the same position as the plasma. Fig. (10.1) shows the instrument profile corresponding to the wavelength of the HeI 4471 A^{o} line.

CHAPTER XI

COMPARISON OF MEASURED PROFILES WITH THEORY

11.1. Procedures Used to Obtain the Theoretical Profiles

The following procedures were used to obtain the theoretical profiles of the HeII 3203 A^{o}, HeI 4471 A^{o}, HeI 2945 A^{o} and HeI 3965 A^{o} lines.

11.1.1. HeII 3203 A^{o} Line

The reduced Stark profiles $S(\alpha)$ (see 3.7.2.) of the HeII 3203 A^{o} line were obtained from (1) for $N_e = 10^{16} cm^{-3}$ and $T_e = 4 \times 10^4$ and 8×10^4 ^{o}K. Theoretical profiles, corresponding to the electron density N_e' at which a given profile was measured, were obtained from the reduced Stark profiles by means of the following transformations (see 3.7.2.).

$$I(\Delta\lambda) = S(\alpha)/F_o$$

where

$$\Delta\lambda = \lambda - \lambda_o = \alpha F_o$$

and

$$F_o = e\left(\frac{4 N_e'}{3}\right)^{\frac{2}{3}}$$

where the quantities appearing in the above equations are defined in (3.7.2.). Thus for each value of N_e' two profiles were

obtained, i.e. one for each of the values of T_e given above. An examination of the two profiles showed that they were only weakly dependent on T_e, and to avoid interpolation with respect to T_e, the profile derived for the value of T_e which lay closest to the experimentally determined electron temperature was used.

It was noted in (3.7.2.) that the value of F_o given above is only valid if the plasma is singly ionized. This should be a good approximation for the electron temperatures found in the discharge see (9.3).

11.1.2. HeI 4471 A^o Line

Recently, the profile of the HeI 4471 A^o ($2^3P - 4^3D$) line inclusive of the forbidden component ($2^3P - 4^3F$) at 4470 A^o has been investigated theoretically by Griem (12) and Barnard, Cooper and Shamey (11). A comparison of the profiles predicted by these two calculations showed them to be closely similar. It was decided to use the results of Barnard et al for the comparison with the measured profiles because they are tabulated in a slightly more convenient form than the results given in Griem's paper.

The theoretical profiles, calculated by Barnard et al, are tabulated for electron densities ranging from 10^{14} to

$3 \times 10^{17} cm^{-3}$ and electron temperatures ranging from 5×10^{3} to 4×10^{4} °K. Although graphical interpolation (see below) can be used to obtain theoretical profiles which correspond to the measured electron densities it was not possible to obtain agreement with the measured electron temperatures because for most of the conditions studied they were higher than those for which the theoretical profiles were calculated (see Fig. 9.3). It was necessary, therefore, to use the theoretical profiles corresponding to 4×10^{4} °K for all the conditions studied. An indication of the errors caused by neglecting the variation of the theoretical profiles with electron temperature can be obtained from Fig. (11.1) and Fig. (11.2) where the percentage variation in intensity, arising from a change in the electron temperature, has been plotted for various points on the profile. The intensity variations are measured relative to that at $T = 4 \times 10^{4}$ °K and are calculated for $T = 10^{4}$ °K and 2×10^{4} °K, and electron densities of 10^{16} and $3 \times 10^{16} cm^{-3}$.

From Figs (11.1) and (11.2) it can be seen that the features of the profile which are most strongly temperature dependent are the dip between the allowed and forbidden components where a factor of 4 decrease in the electron temperature produces a change in intensity of $\sim$ 50% (for $N_e = 10^{16} cm^{-3}$) and the red wing at wavelength separations from the line centre greater than 18 A°, where a similar change in electron temperature produces

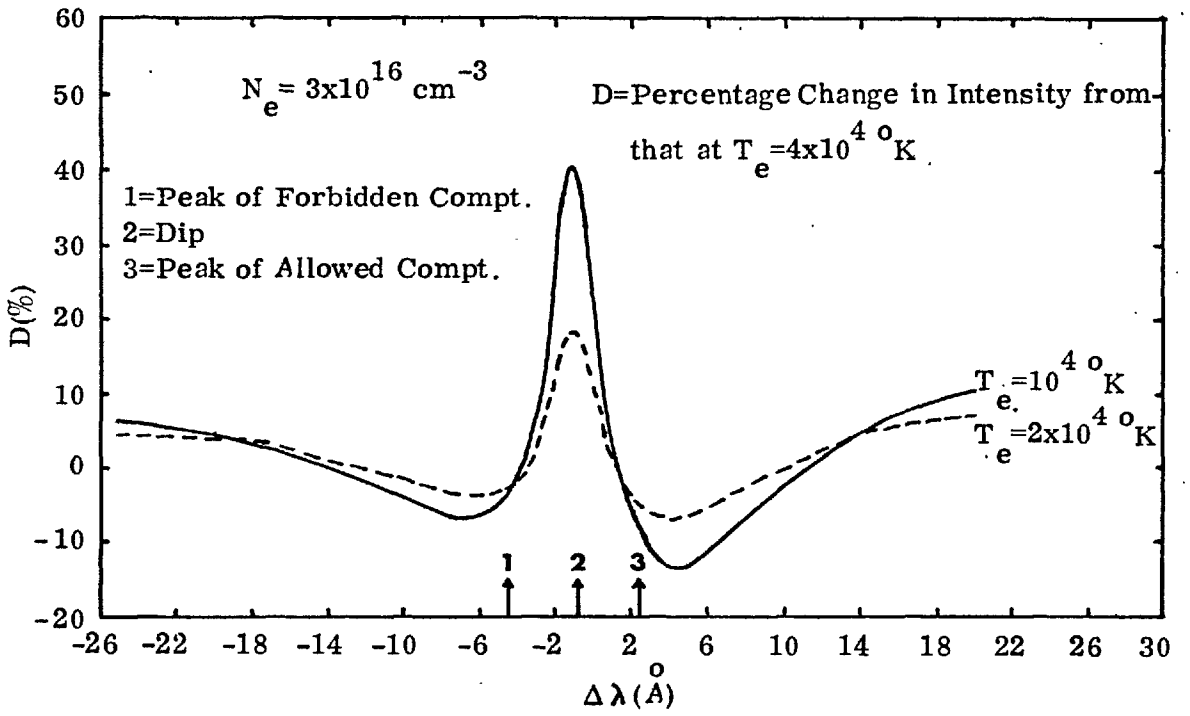

Fig.(11.1)

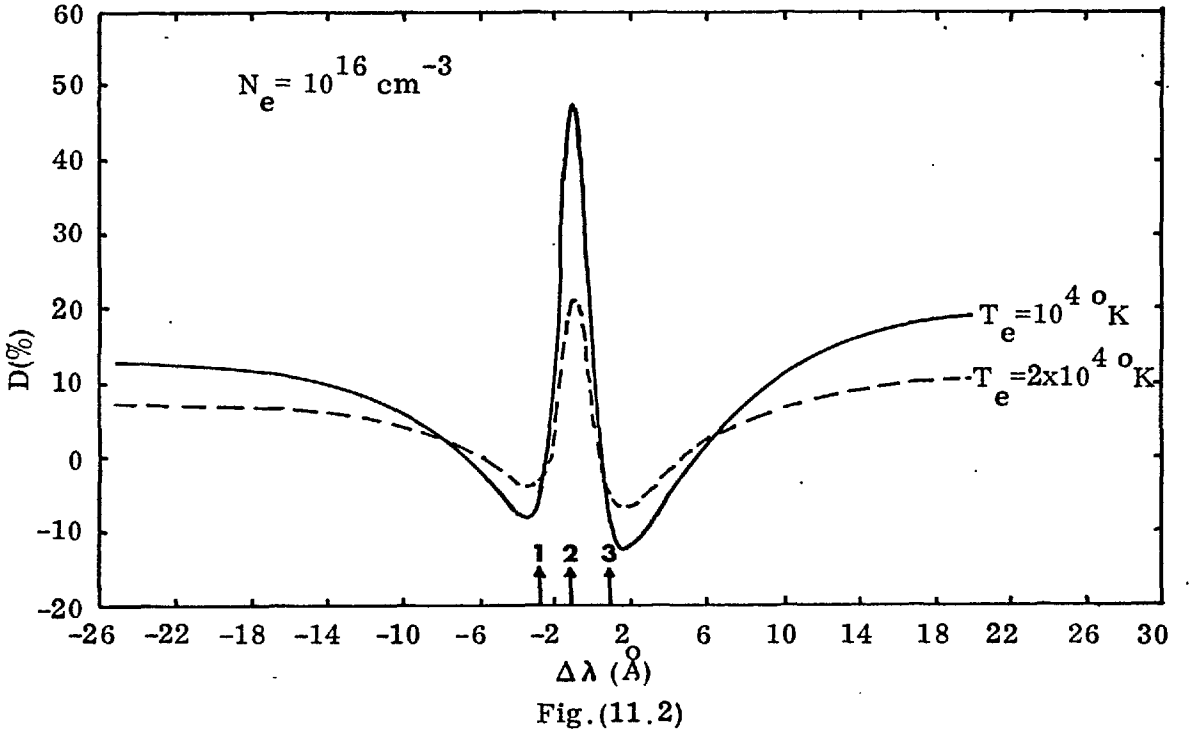

Fig.(11.2)

Figs.(11.1) and (11.2) Temperature Dependence of the Profile of the HeI 4471 Å Line.

a change of ~ 20% in intensity. However, for the major part of the profile the change in intensity is less than 15% for a factor of 4 change in electron temperature. Since the line profiles were measured for plasma conditions for which the electron temperatures were, at the most, a factor of ~ 1.5 greater than 4×10^4 °K the errors produced by neglecting the variation of the profile with electron temperature should be negligible; except possibly in the region of the dip between the allowed and forbidden components.

In order to obtain the theoretical profiles corresponding to the measured electron densities the theoretical profiles of Barnard et al were plotted for electron densities of 10^{15}, 3×10^{15}, 10^{16}, 3×10^{16} and 10^{17} cm^{-3}; using in each case the theoretical profile for $T_e = 4 \times 10^4$ °K. Using these graphs, logarithmic plots of the intensity at a fixed wavelength position on the line profile versus electron density were made for 30 positions across the line profile. The points on the theoretical profiles, corresponding to the measured electron densities, were then obtained fromthese curves and the theoretical profiles constructed.

11.1.3. HeI 2945 A° and 3965 A° Lines

Theoretical profiles for the isolated HeI 2945 A° and

3965 A^{o} lines were obtained from the reduced Stark profiles $j_R(x, \alpha)$ (see 3.7.1) by means of the transformations,

$$I(\Delta\lambda) = \frac{1}{w} j_R(x, \alpha)$$

$$\Delta\lambda = xw$$

where the quantities appearing in the equations above are defined in (3.7.1). The Stark broadening parameters w, α and R were calculated using the programme described in (Chapter VI) and the reduced Stark profile corresponding to these parameters were obtained from the tables in (1), by means of linear interpolation. For points on wings of the profiles, where x is large and $j_R(x, \alpha)$ is not tabulated, the asymptotic wing formulae (5.26) and (5.27) were used.

11.2. Methods of Accounting for the Influence of Instrumental Broadening

There are two methods of accounting for the influence of instrumental broadening on the measured profiles:-

a) A deconvolution procedure could be applied to the measured profile in order to remove the intrumental broadening. The resulting profile could then be directly compared with the theoretical profile.

b) The theoretical profile could be convolved with the instrumental profile and the result compared with the measured profile.

Because a direct comparison could be made between the observed profile (corrected for instrumental broadening) and the theoretical profile, method a) would appear to be the most useful. However, de Jager and Neven (59) have applied various deconvolution procedures to the profiles of indentical lines obtained with two intruments, one with very good, and the other with only moderate, resolving power. The authors concluded that only those profiles for which the ratio between the measured half width and the half width of the instrumental profile exceeds a factor of two can be corrected in such a way that the resulting profile is still meaningful'. More recently, Griffin (60) has presented an even more pessimistic view. Griffin points out that it is fundamentally impossible to recover the true profile from the observed and instrument profile because the optical system acts as a filter since it transmits only those spatial frequencies below a certain limit. It is thus impossible for any mathematical procedure to restore these frequencies. Griffin goes on to say that even if these high frequencies were in fact negligible deconvolution procedures can only be meaningfully applied to profiles obtained with high resolution and very low noise, i.e. to profiles which require only a small correction anyway. As the requirements of halfwidth, high resolution and low noise were unlikely to be attained in these measurements no attempt was made to use method a).

Method b) suffers from none of these difficulties since the theoretical and instrumental profiles are accurately known and the convolution integral (2.11) can be evaluated numerically to any degree of accuracy.

11.3. Convolution of the Instrumental and Theoretical Profiles

A computer programme written at Harvard College observatory, was used to evaluate the convolution integral (2.11). The input to the programme consisted of the instrumental and theoretical profiles in equal wavelength intervals, and the value of the required normalization for the convolved profile.

11.4. Normalization of the Measured and Theoretical Profiles

In all cases the theoretical profiles after convolution with the instrumental profile were normalized to the peak height of the corresponding observed profile. As absolute wavelength measurements were not made the observed and theoretical profiles were positioned so as to have their peaks approximately coincident; consequently, apparent shifts of the observed profile relative to the theoretical profile have no significance.

11.5. Comparison of Measured Profiles with Theory

In the following sections for line profiles measured by

the techniques described in Chapter X are compared with the theoretical profiles. The discussion on these results is postponed until (11.6.) and only the main features of the results are given here.

11.5.1. HeII 3203 A^{o} Line

Figures (11.3), (11.4) and (11.5) show the observed profiles of the HeII 3203 A^{o} line recorded at discharge filling pressures of 0.3, 0.2, and 0.1 torr together with the theoretical profiles. The electron densities corresponding to these filling pressures are $2.1 \pm 0.2 \times 10^{16}$, $1.5 \pm 0.2 \times 10^{16}$ and $7.5 \pm 0.15 \times 10^{15} cm^{-3}$ respectively. Observations were made from both axial and radial directions except for 0.3 torr where the line was too faint to be measured in the radial direction. The profiles obtained for the two directions were in good agreement; for convenience only the axial measurements are given in the figures. The vertical error bars on the measured profiles account for shot to shot fluctuations, photomultiplier noise, and the uncertainty in the determination of the background continuum. The horizontal bar indicates the instrumental width.

Measured and theoretical half widths of the HeII 3203 A^{o} line are given in Table (11.1) together with the ratio R of the measured and calculated half widths; note that the half widths

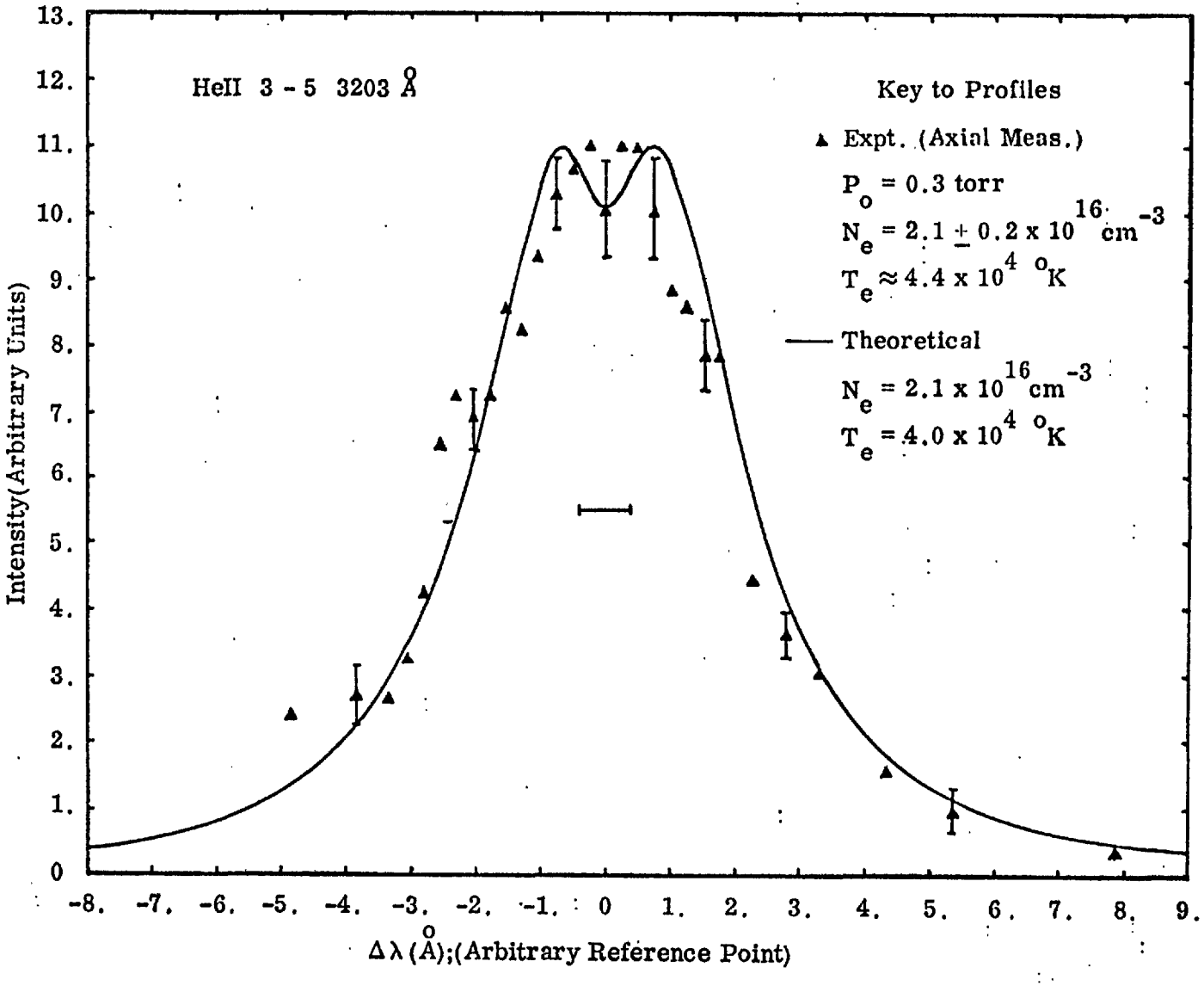

Fig.(11.3) Comparison of the Experimental and Theoretical Profiles.

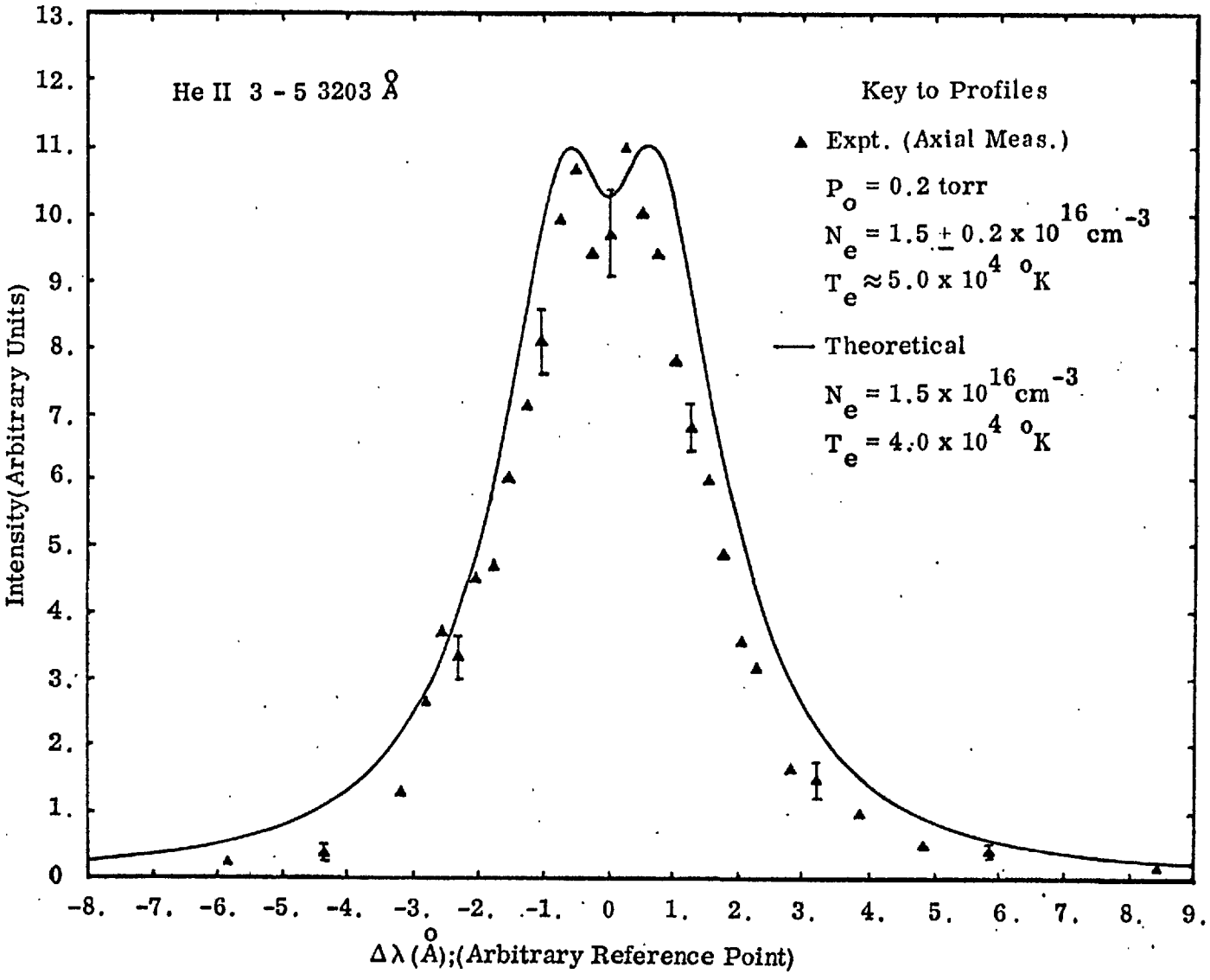

Fig.(11.4) Comparison of the Experimental and Theoretical Profiles.

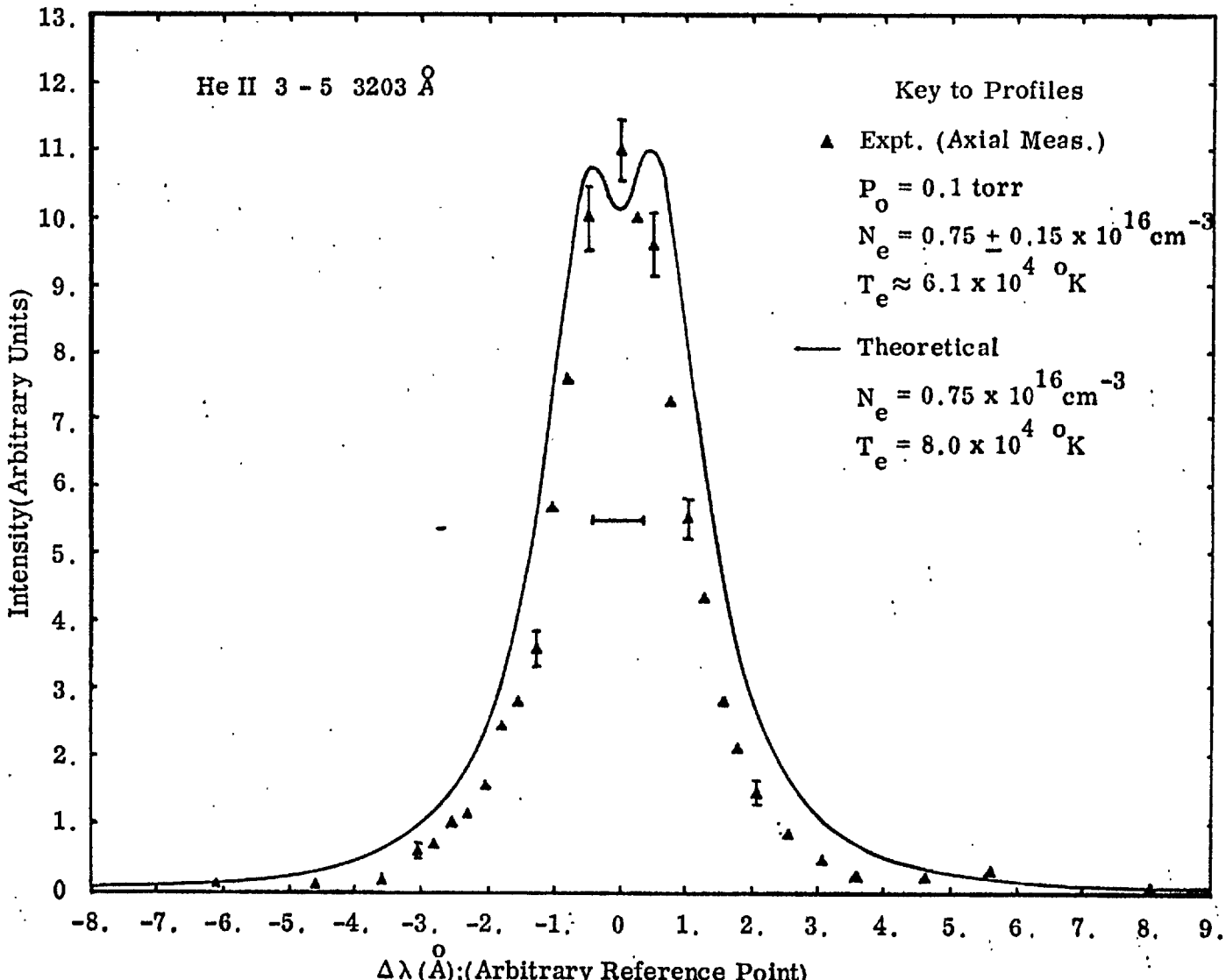

Fig.(11.5) Comparison of the Experimental and Theoretical Profiles.

given in Table (11.1) contain the instrumental broadening. The errors quoted for the observed half widths arise from uncertainties in the profile measurements (see above) whereas those for the theoretical half widths were calculated assuming that the errors arise entirely from the uncertainty in the electron density measurements (the uncertainty of $\sim$ 10% in the true theoretical profile has not been included).

TABLE (11.1)

Comparison of Measured and Calculated Halfwidths

P_0(torr)	$N_e(10^{16}cm^{-3})$	MEASURED HALF WIDTH (Including intrumental broadening)	THEORETICAL HALF WIDTH	R
0.3	2.1 $\pm$ 0.2	4.5 $\pm$ 0.2	4.65 $\pm$ 0.2	0.97
0.2	1.5 $\pm$ 0.2	3.4 $\pm$ 0.2	3.9 $\pm$ 0.3	0.87
0.1	0.75 $\pm$ 0.15	2.2 $\pm$ 0.2	2.7 $\pm$ 0.3	0.81

The errors in the theoretical half widths given in Table (11.1) resulting from the uncertainty in the electron density measurements, were estimated by an empirical method based on the use of Voigt profiles (5.7). It was assumed that the HeII 3203 A^o line profile and the instrumental profile could be represented respectively by a Lorentzian profile with a $\frac{1}{2}$-$\frac{1}{2}$ width equal to the theoretical $\frac{1}{2}$-$\frac{1}{2}$ width, and a Gaussian

profile with a $\frac{1}{2}$ width G equal to measured $\frac{1}{2}$ width. The convolution of these profiles results in a Voigt profile whose $\frac{1}{2}$ width B is given by:

$$B \doteq (D^2 + G^2)^{\frac{1}{2}} + D \qquad (11.1)$$

The values of D corresponding to the upper and lower limits on the measured electron densities were found using the relationship (see 3.7.2).

$$2D = [N_e/C(N_e,T_e)]^{\frac{2}{3}} \text{ A}^\circ \qquad (11.2)$$

Equation (11.1) is only approximate because a Lorentzian profile is not a good approximation for the profile of the HeII 3203 A° line. In order to improve the accuracy of (11.1), (11.1) and (11.2) were used to calculate the half widths of the profiles which had been obtained previously using the numerical convolution procedure (see (11.3)). By comparing the half-widths obtained by the two methods corrections to (11.1) were obtained. In all cases (11.1) predicted a smaller half width and the resulting correction factors ranged from 5 to 11%.

Main Features of the Results for the HeII 3203 A° Line

An examination of Figs (11.3), (11.4) and (11.5) and Table (11.1) shows the following features:

In the case of the 0.3 torr observations the agreement

between theory and experiment is excellent for practically the entire profile (the discrepancy on the blue wing at $\sim$ 2.2 A^{o} from the line centre is probably due to the presence of an underlying impurity line). But the agreement between theory and experiment becomes increasingly poorer as the discharge filling pressure is lowered. For 0.2 and 0.1 torr observations the experimental widths are $\sim$ 13% and $\sim$ 20% below the theoretical widths. Also the expected dip in the profile, measured at 0.1 torr, is absent.

11.5.2. HeI 4471 A^{o} Line

The profile of the HeI 4471 A^{o} line measured at filling pressures of 0.4, 0.35 and 0.3 torr is shown in Figs (11.6), (11.7) and (11.8). These filling pressures correspond to electron densities of $1.2\pm0.1 \times 10^{16}$, $1.6\pm0.2 \times 10^{16}$ and $2.1\pm0.2 \times 10^{16} cm^{-3}$. For the highest and lowest filling pressures observations were made in the axial and radial directions and both sets of observations are shown. The vertical error bars on the measured profiles account for shot to shot fluctuations, photomultiplier noise, and the uncertainty in the determination of the background continuum. The horizontal bar indicates the instrumental width.

No attempt was made to determine the uncertainty

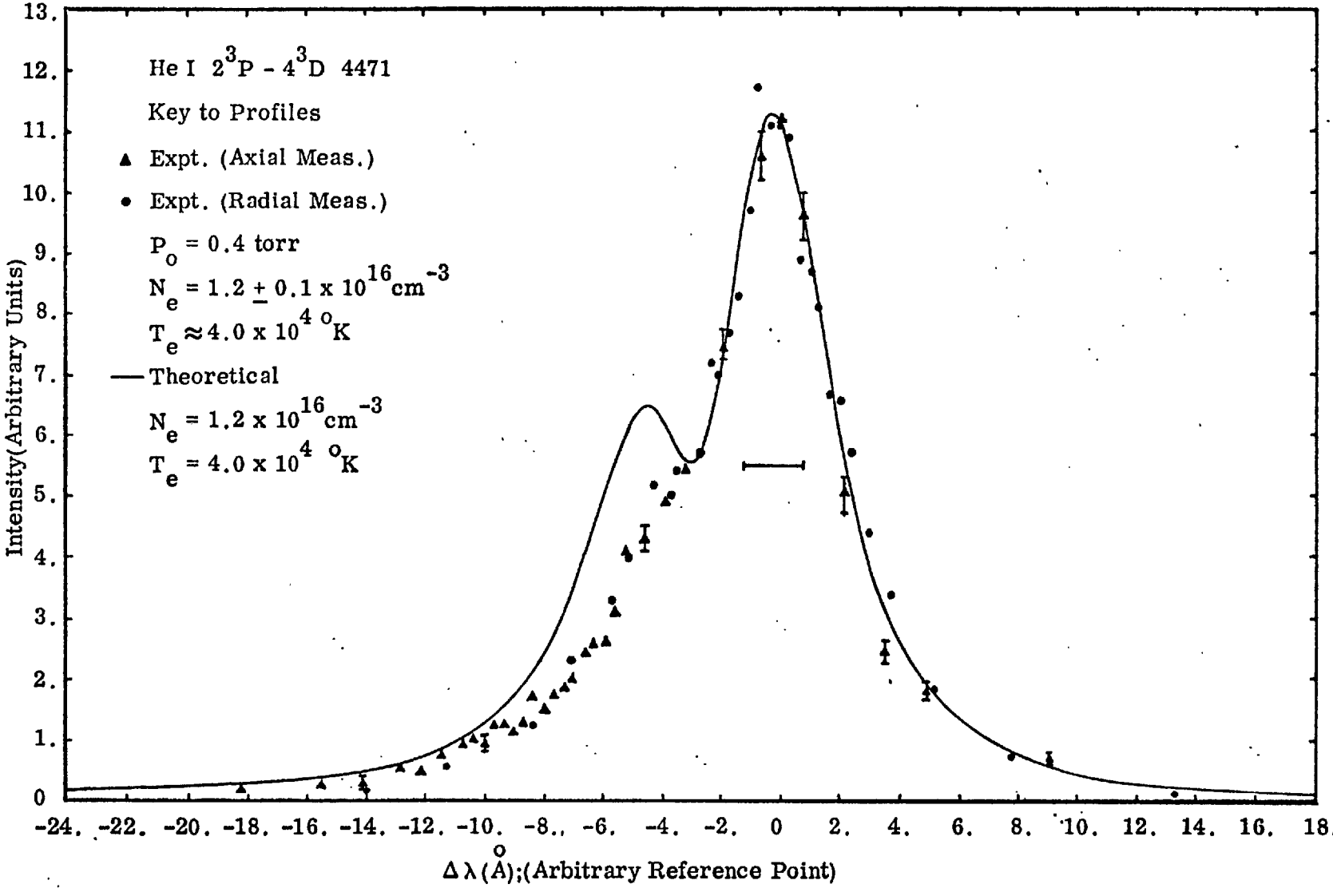

Fig. (11.6) Comparison of the Experimental and Theoretical Profiles.

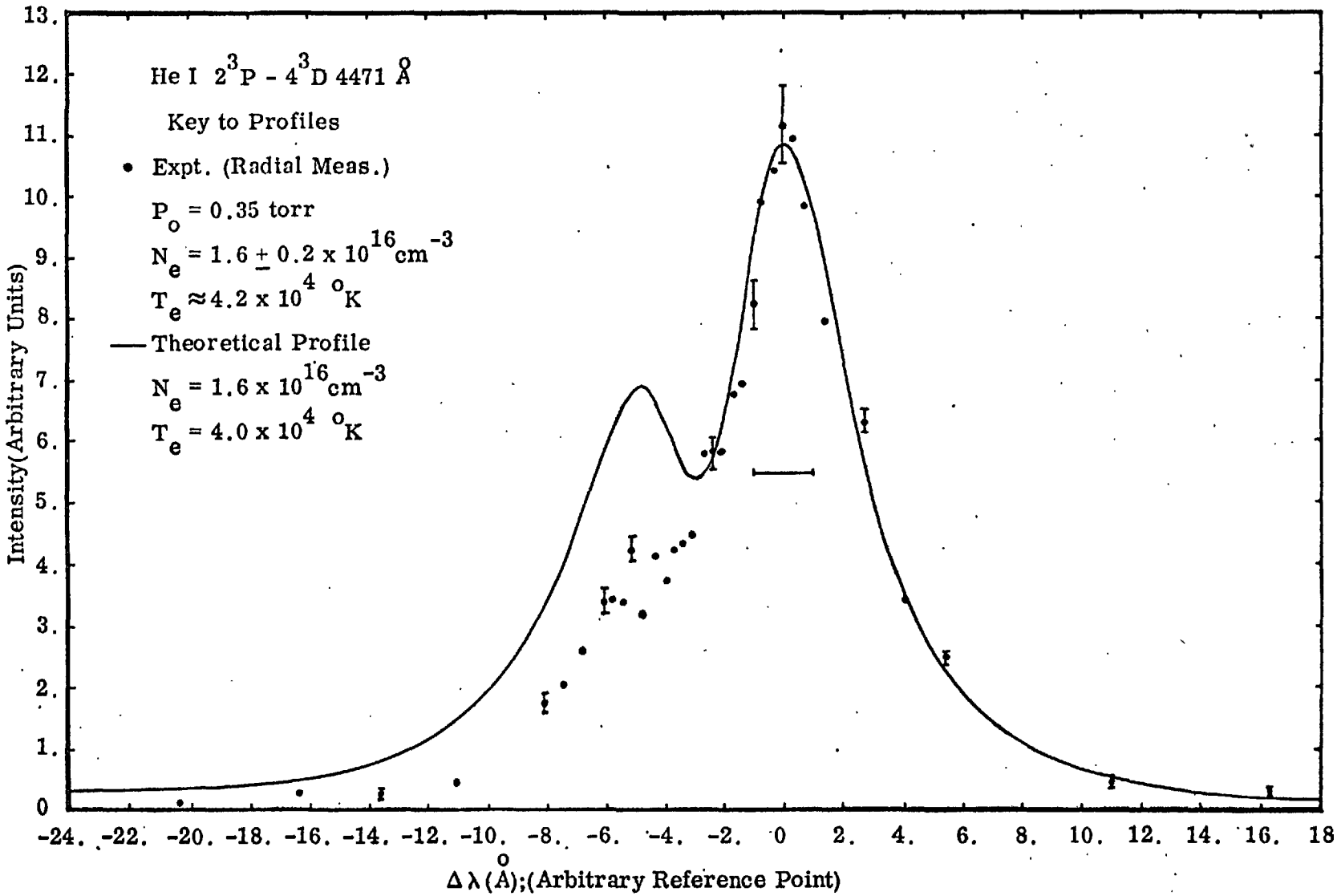

Fig. (11.7) Comparison of the Experimental and Theoretical Profiles.

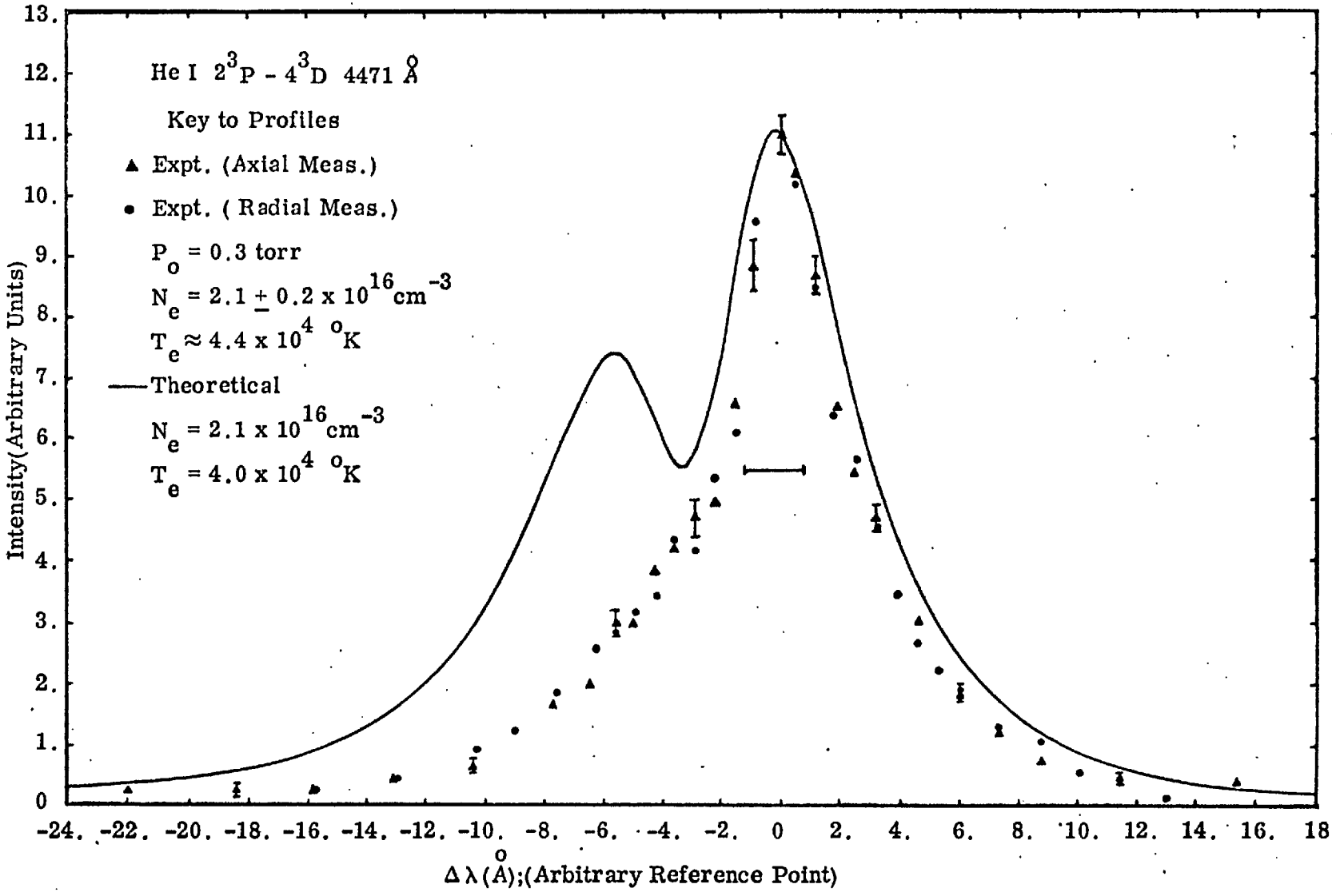

Fig. (11.8) Comparison of the Experimental and Theoretical Profiles.

in the theoretical profile arising from errors in the electron density measurements because it is apparent from an examination of the theoretical profiles (see Figs (11.4), (11.5) and (11.6)) that these errors could not account for the observed discrepancies.

Main Features of the Results for the HeI 4471 A° Line

It can be seen (see Figs (11.6) and (11.8) that in those cases where observations were made in the axial and radial directions the profiles are in excellent agreement. Since the axial and radial observations were made many weeks apart these results illustrate the long term reproducibility of the discharge. The 0.4 and 0.35 torr observations (see Figs (11.6) and (11.7) respectively) show extremely good agreement with theory over the entire red wing of the profiles. But for the 0.3 torr observations this wing is systematically low. The blue wing of the observed profile is systematically low for all the conditions studied and there is also no indication of the peak of the forbidden component; although some asymmetry is observed in this wing. However, for the 0.4 torr observations the agreement on the blue wing improved for wavelength separations greater than 9 A° from the peak of the allowed line. Measurements made at pressures below 0.3 torr (not shown) show that the discrepancies on both wings occurred and that these increased rapidly as the filling pressure was lowered. For filling

pressures $\lesssim 0.1$ torr the observed profile was found to be identical with the instrumental profile indicating that the Stark broadening was negligible, whereas the theoretical half width was a factor of $\sim$ 2 greater than the instrumental width. Also observations were made at filling pressures, on each side of the maximum of the electron density at peak compression versus filling pressure curve (see Fig. (9.5)), such that the axial electron density was the same. The results showed that the discrepancies in the line recorded on the low pressure side of the maximum in the above mentioned curve were much greater than those on the high pressure side. These discrepancies are too large to be attributed to the difference in the electron temperature which occurs on each side of the maximum of the above mentioned curve.

11.5.3. HeI 2945 A^{o} and 3965 A^{o} Lines

The observed and theoretical profiles of the HeI 2945 A^{o} and 3965 A^{o} lines, for measurements made at discharge filling pressures of 0.4 and 0.3 torr are shown in Figs (11.9), (11.10), (11.11) and (11.12) respectively. The electron densities corresponding to these filling pressures are $1.2 \pm 0.1 \times 10^{16} cm^{-3}$ and $2.1 \pm 0.2 \times 10^{16} cm^{-3}$ respectively.

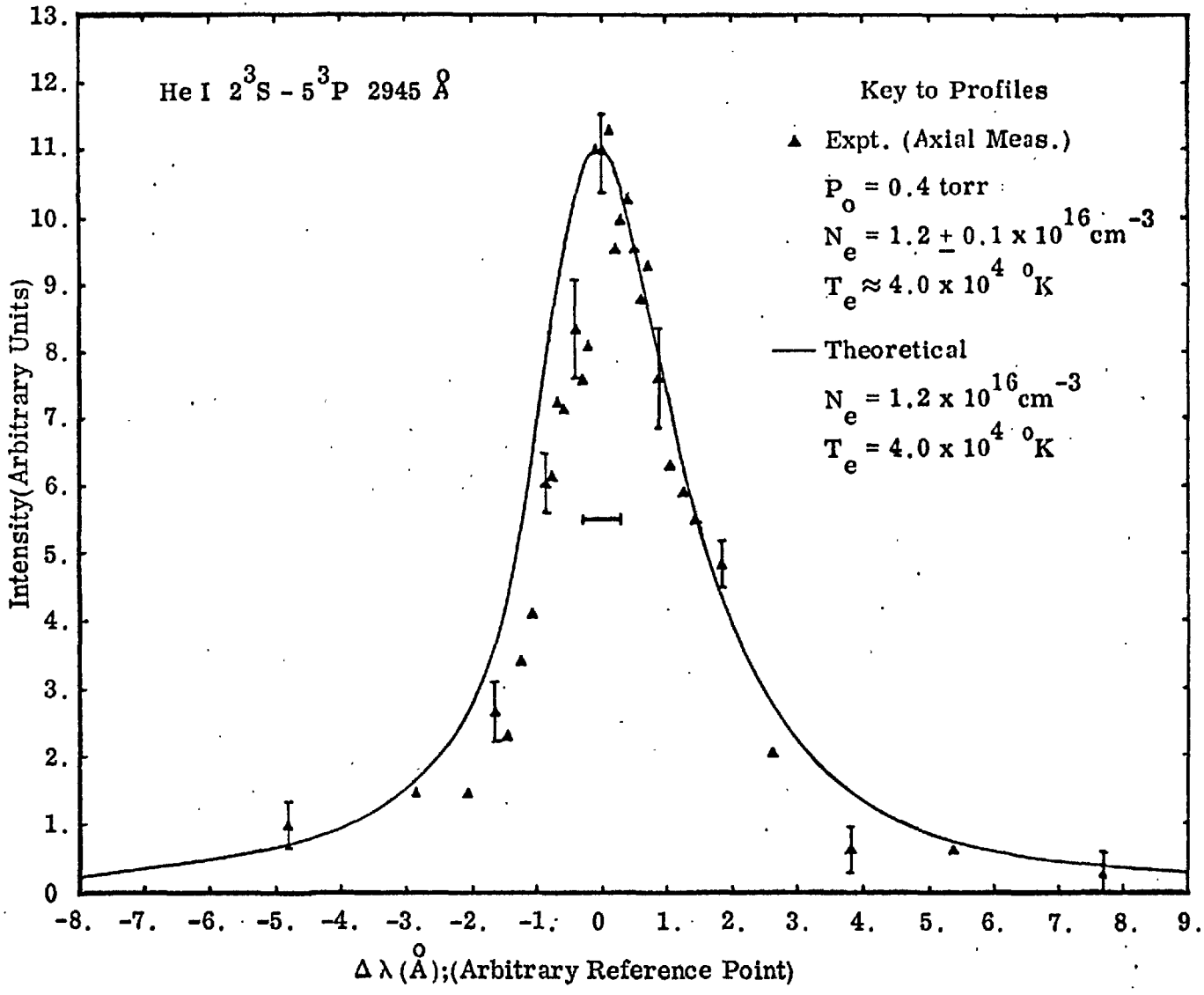

Fig. (11.9) Comparison of the Experimental and Theoretical Profiles.

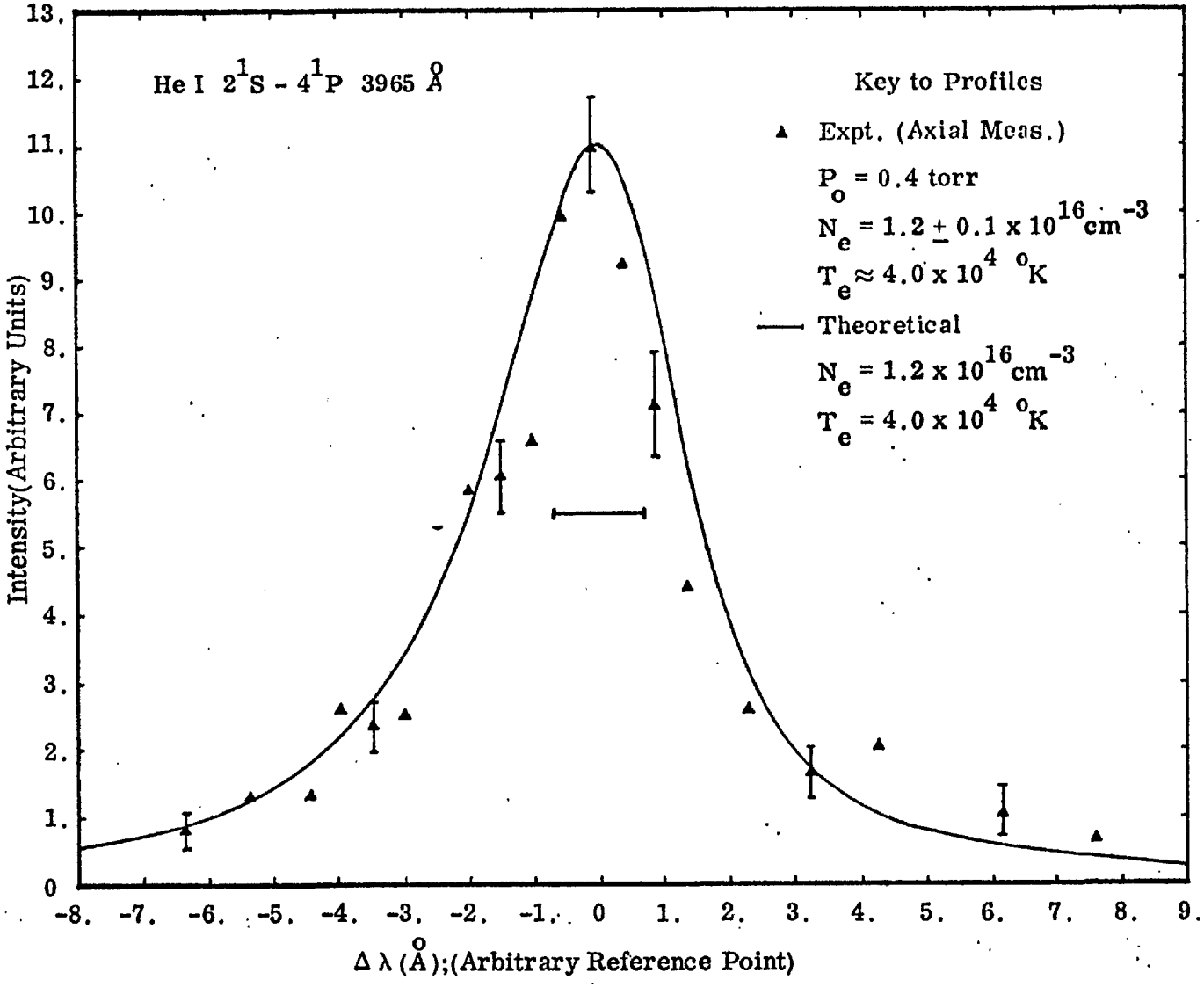

Fig.(11.10) Comparison of the Experimental and Theoretical Profiles.

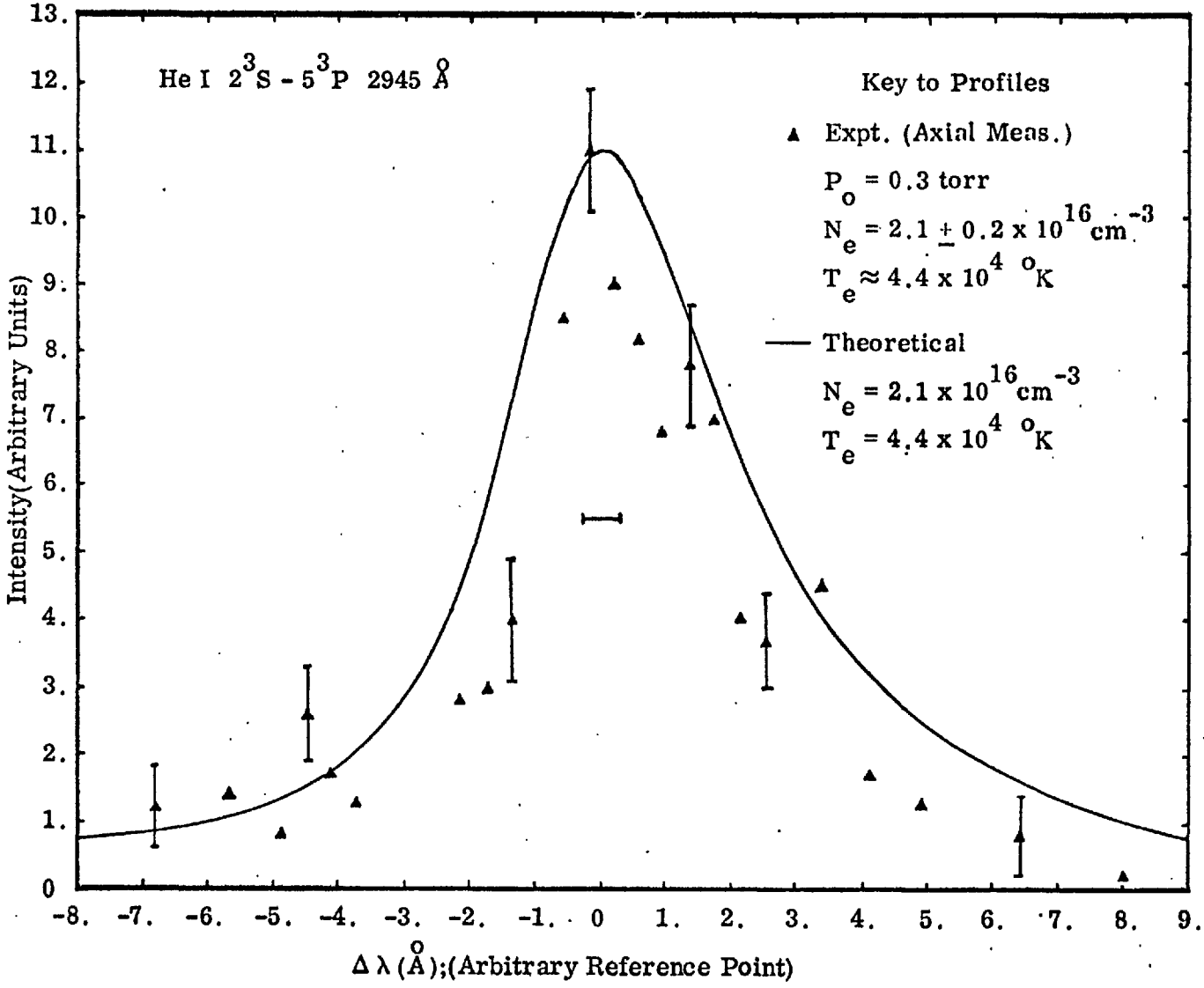

Fig.(11.11) Comparison of the Experimental and Theoretical Profiles.

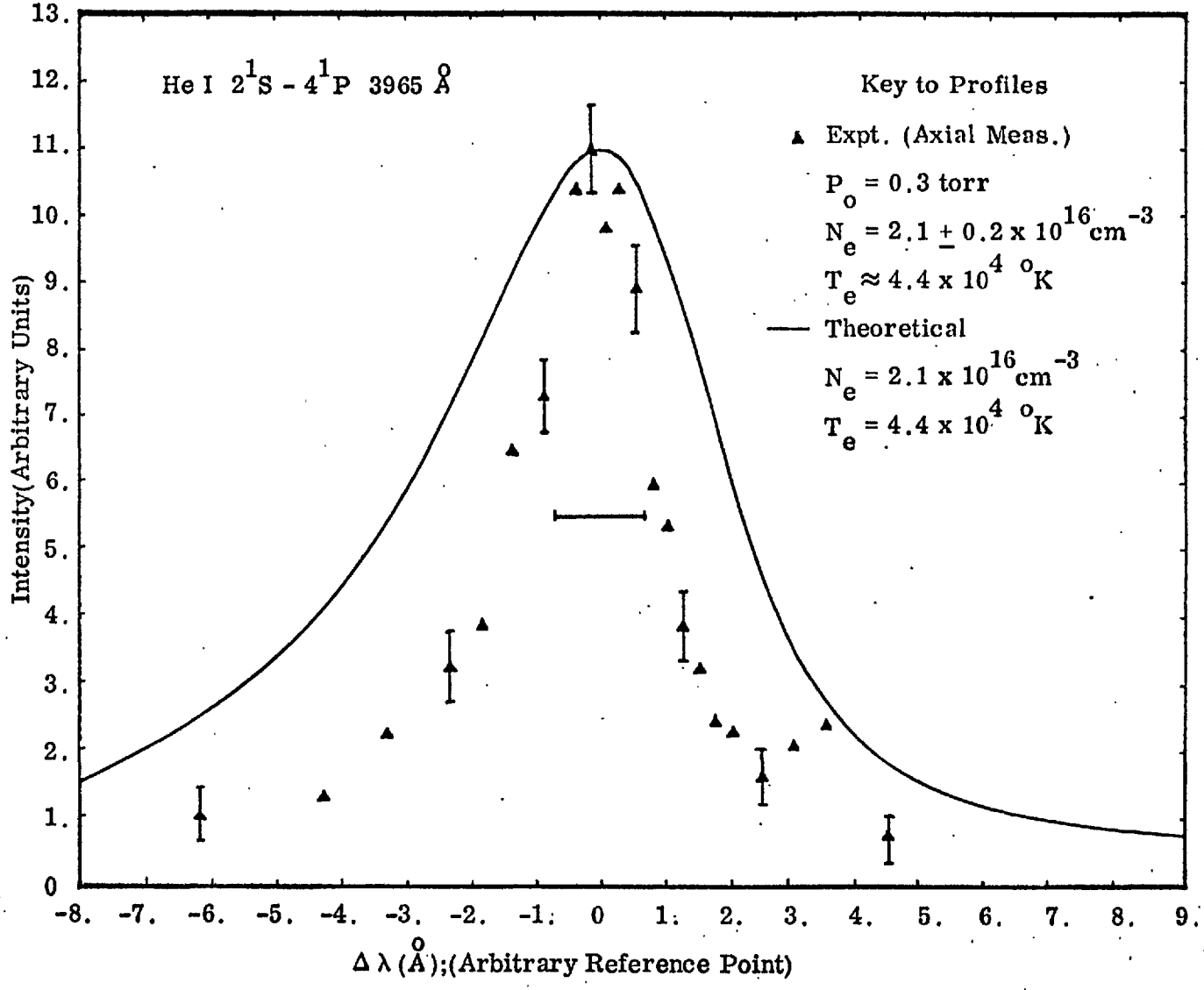

Fig.(11.12) Comparison of the Experimental and Theoretical Profiles.

TABLE (11.2)

Comparison of Measured and Calculated Halfwidths

P_o = 0.4 torr $N_e = 1.2 \pm 0.1 \times 10^{16} cm^{-3}$

LINE	MEAS. HALF WIDTH (Including Instrumental Broadening)	THEOR. HALF WIDTH	R
3965	2.9 ± 0.3	3.6 ± 0.2	0.83
2945	2.3 ± 0.3	2.7 ± 0.2	0.85

TABLE (11.3)

Comparison of Measured and Calculated Halfwidths

$P_o = 0.3$ torr $N_e = 2.1 \pm 0.2 \times 10^{16} cm^{-3}$

LINE	MEAS. HALF WIDTH (Including Instrumental Braodening)	THEOR. HALF WIDTH	R
3965	2.5 ± 0.4	5.4 ± 0.4	0.46
2945	2.6 ± 0.3	4.4 ± 0.4	0.59

Measured and theoretical half widths of the two lines are given in Table (11.2) for the observations made at 0.4 torr and Table (11.3) for the observations made at 0.3 torr. Again, it should be noted that the half widths given in Tables (11.2) and (11.3) include the instrumental broadening. Estimates of the uncertainty in the theoretical profile arising from errors in the electron density measurements were obtained in the same way as for the HeII 3203 A^{o} profile (see 11.5.1.), except that here D is given by:

$$D = [1 + 1.75\,\alpha(1 - 0.75\,R)]w \qquad (11.3)$$

where the quantities appearing in (11.3) are defined in (3.7.1).

Main Features of the Results for the HeI 2945 A^{o} and 3965 A^{o} Lines

Tables (11.2) and (11.3) show that the agreement between the experimental and theoretical half widths is poor, and, as with the other lines discussed so far, the discrepancies increase as the filling pressure is lowered, and are such that the observed profiles are systematically narrower than the theoretical ones. For the results obtained at 0.4 torr the discrepancies for the 2945 A^{o} and 3965 A^{o} lines are $\sim$ 15% but they increase to $\sim$ 40% and 50% respectively for measurements made at 0.3 torr. Observations made at lower discharge filling pressures (not shown) give results similar to those obtained for the HeI 4471 A^{o} line

(see 11.5.2.) i.e. at filling pressures $\lesssim 0.1$ torr the measured profiles were identical to the instrumental profile.

An examination of the profile of the HeI 2945 A° line, recorded at 0.4 torr (see Fig. (11.9)) shows that there is good agreement with theory for the red wing observed profile but the blue wing is systematically low. The results obtained for this line (see Fig. (11.11)) at 0.3 torr show that both wings of the observed profile are systematically low; although there is good agreement between experiment and theory for points on the blue wing at wavelength separations from the line centre greater than ~ 4 A°.

The profile of 3965 A° line recorded at 0.4 torr (see Fig. (11.10)) shows that the intensity of the blue wing of the observed profile is systematically low, as is also that of the red wing up to ~ 3 A° from the line centre. Beyond this point the observed intensity on the red wing is greater than the theoretical value. This latter effect, which is also observed for the 0.3 torr observations (see Fig. (11.12), is attributed to the presence of the forbidden component arising from the transition $2^1S - 4^1D$. This forbidden component has also been observed by Wulff(15). The profile of 3965 A° line, recorded at 0.3 torr (see Fig. (11.12)) shows that both wings of the observed profile are systematically low, and the feature attributed to the forbidden component is observed on the red wing.

The appearance of the forbidden component in the profile of the 3965 A^{o} line is important because it indicates the breakdown of the isolated line approximation (see (3.7.3)). Thus part of the discrepancies observed for 3965 A^{o} line may be attributable to the breakdown of the isolated line approximation.

11.6 Discussion of Results

Two distinct trends are evident in the results presented in the preceding section. They are:-

a) In all cases the discrepancies between the observed and theoretical profiles increase as the filling pressure is lowered.

b) The discrepancies are always such that the observed half widths are less than the theoretical values.

The good agreement between the profiles measured in the axial and radial directions (see(11.5.1.) and (11.5.2.)) suggests that self absorption is not responsible for the discrepancies noted above. In fact all the broadening mechanisms which, in addition to Stark broadening, take place within the plasma (see (Ch.II)) would lead to increased broadening and can, therefore, be dismissed as a cause of the discrepancies (see b) above).

The results obtained at 0.3 torr suggest that the most likely explanation of these discrepancies is that they are caused.

by radial gradients in the plasma. It will be recalled that at this filling the observed profile of the HeII 3203 A° line was in excellent agreement with theory whereas the HeI lines showed large discrepancies. There are two reasons for expecting the agreements between theory and experiment to be better for the HeII 3203 A° line than for the He I lines. Firstly, because of charge neutrality, the radial distribution of the HeII ions must be identical to that of the free electrons, that is, provided the electron temperature is low enough to ensure that the plasma is only singly ionized (which is the case at 0.3 torr). Consequently, the axially measured electron density would be expected to characterise the density of free electrons responsible for the broadening of the HeII 3203 A° line. There is no constraint, such as charge neutrality, for the neutral particles in the plasma and therefore the radial distribution of neutral helium atoms may differ from that of the free electrons. In the case of HeI lines then, the axially measured electron density need not characterize the density of the broadening electrons in the regions from which the bulk of the HeI emission takes place. Secondly, in the region of the plasma, presumably on the axis of the discharge, where the electron temperature is sufficient to excite the HeII spectrum, the density of neutral helium atoms will be diminished through

ionization. The HeI emission will, therefore, tend to be emitted from regions of the plasma away from the axis of the discharge, with the consequences that have already been mentioned above. Furthermore, since the electron density might be expected to decrease away from the axis of the discharge the emitted profile will be narrower than that expected on the basis of the axially measured electron density. With increasing electron temperature an increasing proportion of the HeI emission might be expected to come from off axial regions of the plasma; this proposition is confirmed in Chapter XII. If the electron temperature is high enough for the ionization of HeII ions then similar effects to those mentioned above for the HeI emission might also be expected to occur for the HeII emission.

If it is assumed that the effects of radial gradients are responsible for the observed discrepancies then it is of interest to consider qualitatively whether the observed discrepancies are consistent with this explanation.

11.7 The Effects of Radial Gradients on the Observed Profiles

For the purpose of this discussion it is sufficient to assume that the plasma, at the time of peak compression consists of an homogeneous cylindrical core surrounded by a region in which the electron density is somewhat less that that of the core. Most of the line radiation is assumed to originate from the core of the plasma.

For convenience the line profile which is emitted by the core of the plasma will be called the true profile and it will be assumed that this profile is identical to the theoretical profile corresponding to the plasma conditions of the core. The observed profile is assumed to result from the radiation emitted by the core of the plasma plus that from the low density region.

The line profile emitted by atoms in the low density region will be narrower than the true profile, and if shifts are ignored for the moment, this radiation will tend to contribute mainly to the central part of the true profile; the wings being less affected. Thus the peak intensity of the observed profile will be enhanced with respect to the true profile. If the theoretical profile is then normalized to the observed profile using the procedure given in (11.4) the latter will appear systematically narrower than the theoretical profile. This result is consistent with the observed discrepancies (see 11.6).

To procede further attention must be paid to the type of line studied.

11.7.2. HeII 3203 A^{o} Line

Since the HeII 3203 A^{o} line is hydrogenic it has a negligible shift and the conclusions reached above will apply. Hence, because of radial gradients the observed profile would be

expected to appear systematically, but symmetrically narrower that the theoretical profile. An examination of Figs (11.4) and (11.5) shows that this conclusion is in agreement with observation.

11.7.2. HeI 4471 A^{o} Line

Compared with hydrogenic and isolated lines, the profile of a line containing a forbidden component is expected to be more sensitive to the effects of radial gradients. This greater sensitivity arises because the line profile emitted by the low density region will not only be narrower than the true profile, but also the intensity of the allowed component will be increased relative to forbidden component (see 3.20). The radiation from the low density region will therefore result in an observed profile whose allowed and forbidden components have peak intensities greater than those of the true profile. Because the increase in the peak intensity of the allowed component will be greater than that of the forbidden component the procedure used to normalize the theoretical profile to the observed profile (see 11.4) will besides making the observed profile appear systematically narrower than the theoretical profile, also make the observed intensity of the forbidden component appear too low.

It can be seen from Figs (11.6), (11.7) and (11.8) that

the preceding arguments would partially explain the discrepancies in the region of the forbidden component but they would not explain why, at the same time, the red wing of the profile obtained at 0.4 and 0.35 torr can be in such good agreement with theory.

11.7.3. HeI 2945 and 3965 A° Lines

In the case of the HeI 2945 A° and 3965 A° lines, the line profile emitted by the low density region will not only be narrower than the true profile but also shifted towards the unperturbed position of the line. The peak intensity of the observed profile will, therefore, not only appear enhanced when compared with that of the true profile, but also the peak of the observed profile will tend to be shifted towards the unperturbed position of the line. Thus when the theoretical profile is normalized to the observed profile using the procedure given in (11.4) the observed profile would still be expected to appear narrower than the theoretical profile, but because the theoretical profile is effectively shifted towards the unperturbed position of the line the discrepancies on the wing closest to the unperturbed position of the line (the blue wing for the 2945 A° line and the red wing for the 3965 A° line) would be expected to be larger.

The results obtained at 0.4 torr for the HeI 2945 and 3965 A° lines (see Figs (11.9) and (11.10)) are in accordance

with the above conclusions; especially the 2945 A^{o} line. But the results obtained at 0.3 torr show only that the observed profile is narrower than the theoretical profile.

To summarise, the above discussion has shown that in general the observed discrepanceis are consistent with those which would be expected to occur if radial gradients are present in the plasma.

11.8. An Alternative Normalization Procedure

In the preceding discussion it is seen that when radial gradients are present in a plasma the most seriously affected part of the profile is the region near the peak. The wings tend to be affected less. Furthermore, if it is assumed that the electron density is a maximum on the axis (this assumption is verified in the next chapter) then because the wings of a line profile are caused by large electric fields, the wings of the observed line will tend to be characterized by the axially measured electron density. This suggests that an alternative normalization procedure would be to normalize the theoretical profile to a point or points on the wings of the observed profile.

It is important to realize that the alternative normalization procedure suggested above is only unique in certain circumstances. This point can be illustrated by considering a

Lorentzian profile, the equation of which is:

$$I(\Delta\lambda) = \frac{I_o}{1 + \left(\frac{\Delta\lambda}{w}\right)^2}$$

where I_o is the peak intensity of the line, w is the $\frac{1}{2}$-$\frac{1}{2}$ width and $\Delta\lambda$ the separation from the line centre. On the line wing ($\Delta\lambda >> w$) the equation above reduces to:

$$I(\Delta\lambda) = I_o w^2/\Delta\lambda^2$$

from which it can be seen that normalizing to the line wing corresponds to fixing the product $I_o w^2$ and from knowledge of w I_o can be found. However, if both these quantities are unknown no unique solution exists.

Although the profile of the lines studied do not have analytic forms, the above procedure can still be used because the necessary constraint on the halfwidth will be present. There are difficulties associated with this normalization procedure, notably the choice of the points on the wings. If they are chosen too near the peak they may be affected by radiation from the low density regions. Alternatively, if they are chosen too far out on the wing the intensities are likely to be inaccurate because of the poor signal to noise ratio and the difficulty in determining the continuum background.

11.9. Results

The alternative normalization procedure was applied to profiles which appeared to be affected least by radial gradients. The results are given below:

11.9.1. HeII 3203 A° Line

The normalization procedure described above was applied to the observations made at 0.2 torr and 0.1 torr, of the HeII 3203 A° line. Curves were drawn through the observed points on both wings of the profile and the average intensity was found at points equidistant from the line centre. This value was used to normalize the theoretical profiles. For the 0.2 and 0.1 torr observations the points were chosen 3.0 and 2.0 A° from the line centre respectively. The results are shown in Figs. (11.13) and (11.14). The 0.1 torr profile shows good agreement on both wings for points at distances greater than 1.5 Å from the line centre. Similar results were obtained from the 0.2 torr observations although agreement on the blue wing is not as good as that on the red owing to scatter in the measurements made at about 2 Å from the line centre. The scatter is also observed at the same position for the 0.3 torr observations (see Fig. (11.3)) and is thus attributed to the presence of an underlying impurity line.

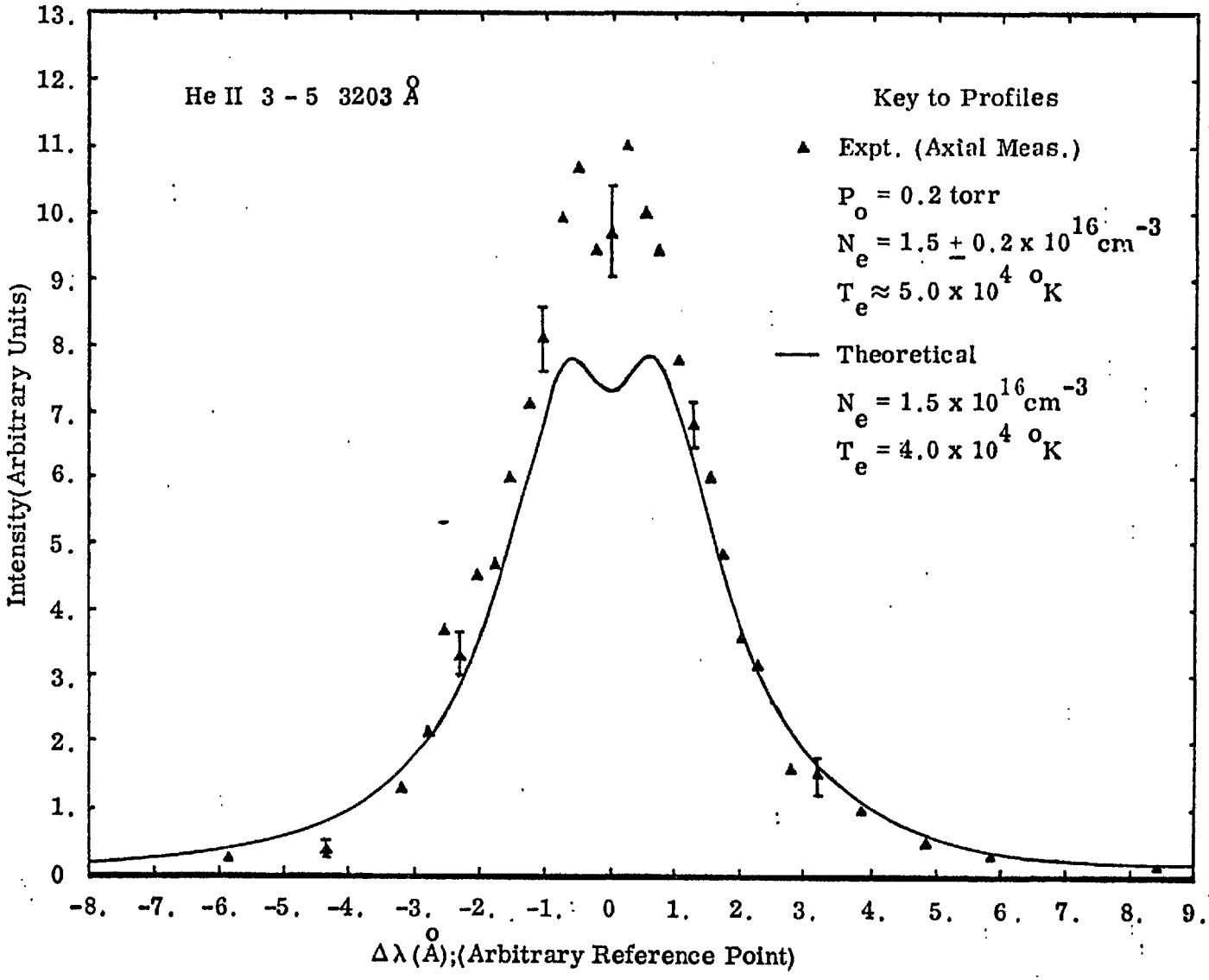

Fig. (11.13) Comparison of the Experimental and Theoretical Profiles.

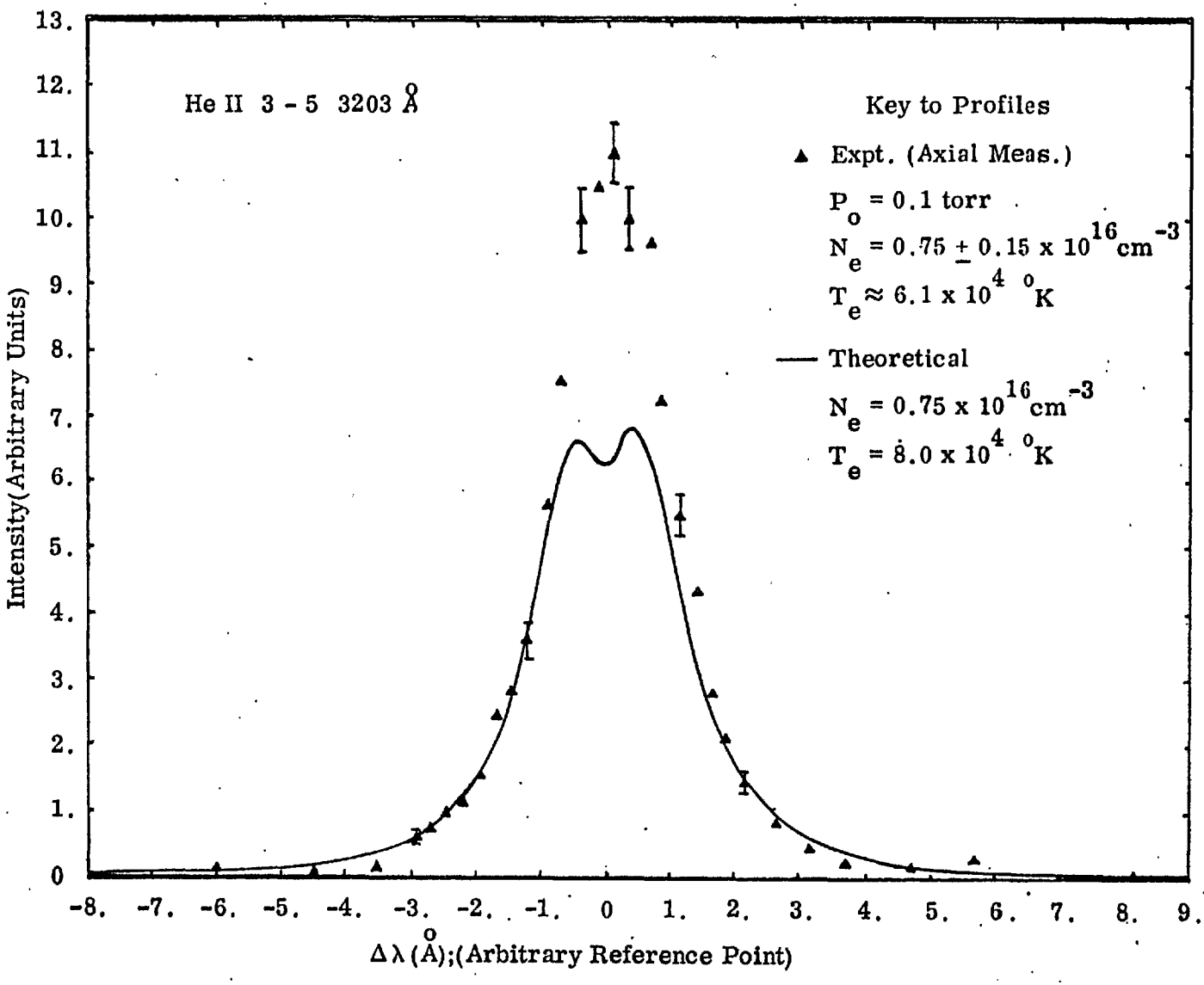

Fig. (11.14) Comparison of the Experimental and Theoretical Profiles.

The possibility of using the above data to verify the asymptotic wing formula for the line,(see(1)), was investigated. However, it became evident that this was not feasible because of insufficient data at large wavelength separations from the line centre.

Estimates of the amount of radiation contributing to the observed profile from low electron density regions of the plasma were obtained from the above results by subtracting the total intensity of the theoretical profile from that of the observed profile. The additional contributions amounted to ~8 and ~26% for the 0.2 and 0.1 torr observations respectively.

11.9.2. HeI 4471 A^{o} Line

It is apparent from the observation of the HeI 4471 A^{o} line made at P_{o} = 0.4 torr (see Fig. (11.6)) that the alternative normalization procedure would not lead to any improvement because the far wings of the observed profile are in excellent agreement with theory. The alternative normalization procedure was not, therefore, applied to the results for the HeI 4471 A^{o} line.

11.9.3. HeI 2945 and 3965 A^{o} Lines

For the HeI 2945 and 3965 A^{o} lines the normalization procedure is complicated by the fact that the peak of the observed

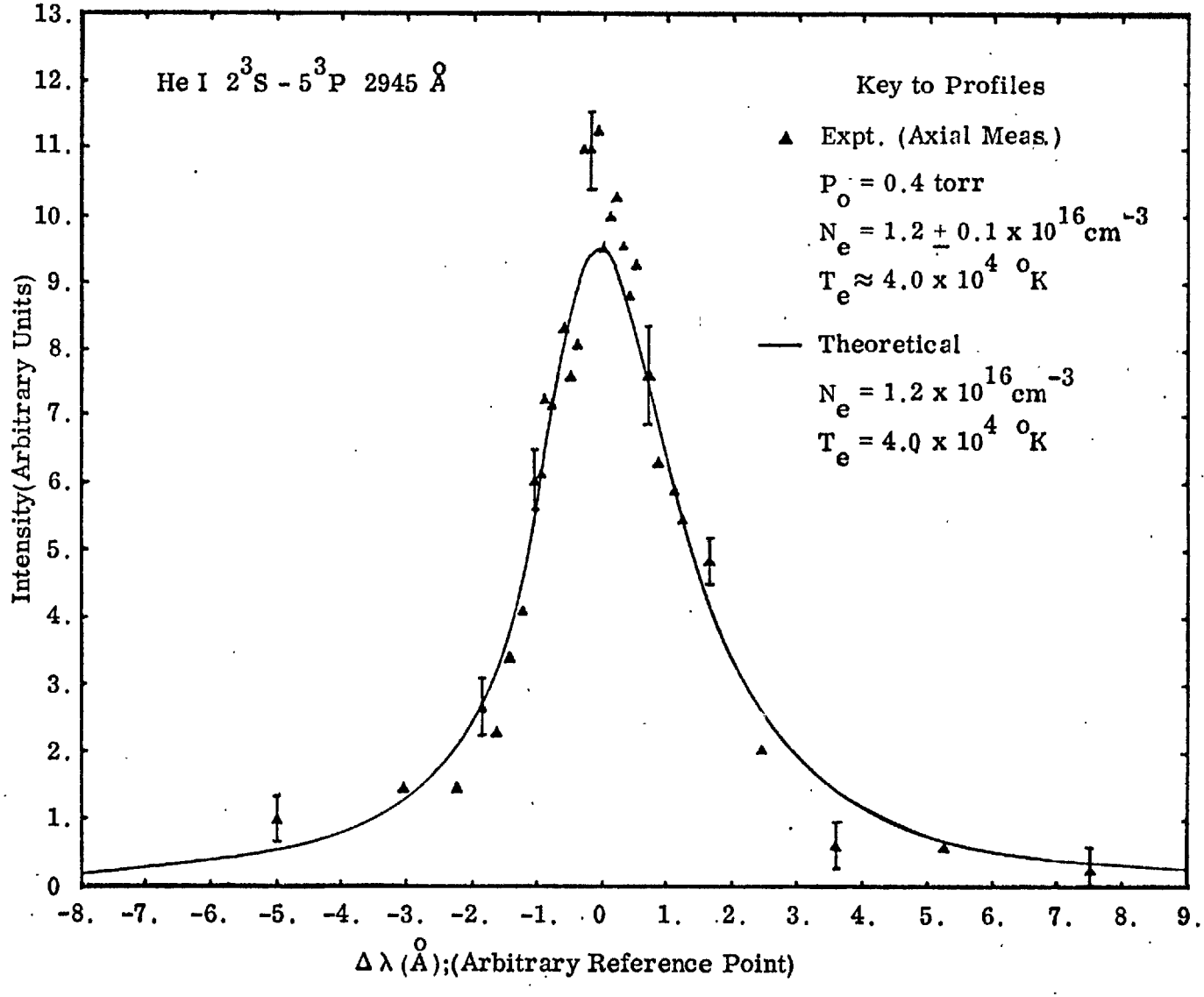

Fig.(11.15) Comparison of the Experimental and Theoretical Profiles.

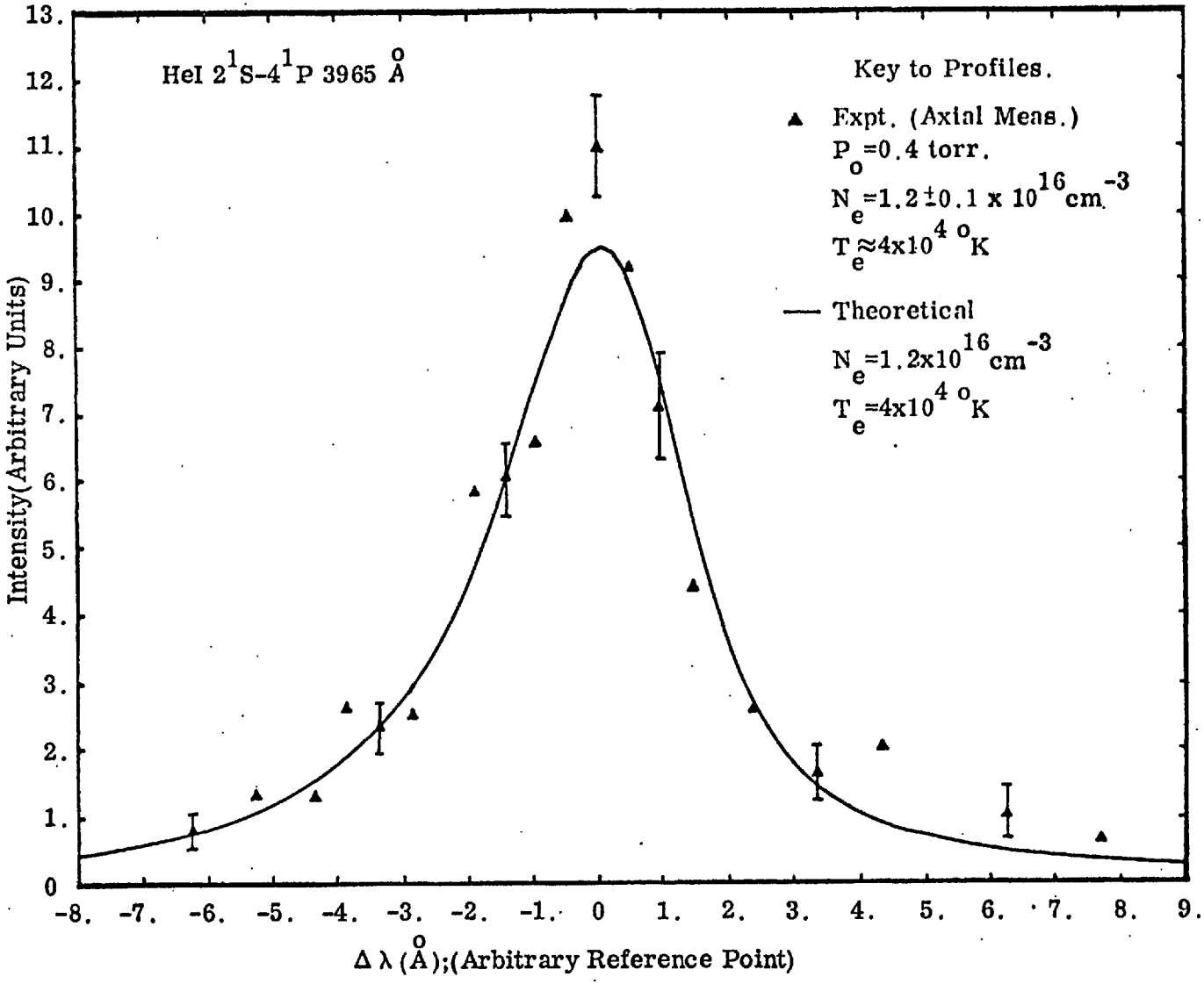

Fig.(11.16) Comparison of the Experimental and Theoretical Profiles.

profile is expected to be shifted with respect to the wings of the profile (see 11.7.3.). Because of this there will not be a one to one correspondence between the wavelengths on the observed profile and those on the theoretical profile, for the results given in Figs (11.9) and (11.10). Consequently, the procedure used to normalize the HeII 3203 A° theoretical profile (see 11.9.1) can not be used here. The method used to overcome this difficulty was as follows. A tracing was made of theoretical profile and this was placed over the observed profile and shifted so that the wings of the theoretical profile lay symmetrically over those of the observed profile. The theoretical profile was then normalized to a point on the wing of the observed profile.

The results are shown in Figs (11.15) and (11.16), for the measurements made at 0.4 torr. For both lines the agreement is extremely good for practically the entire profile. A comparison of the observed and calculated halfwidths (including intrumental broadening is given in Table (11.4).

From Table (11.4) it can be seen that the measured and theoretical half widths, for 3965 and 2945 A° lines are in agreement to within 6% and 4% respectively. Estimates of the intensity contribututions, for the low density regions of the plasma, to the observed profile were obtained in an identical manner to that used in (11.9.1). The contributions were found to be ~3 % and ~7 % for the 2945 and 3965 A° lines respectively. Since these

contributions are small when compared with the total intensity of the lines, the results suggest that the radial gradients are small.

TABLE (11.4)

Comparision of Measured and Calculated Halfwidths

$P_o = 0.4$ torr, $N_e = 1.2 \pm 0.1 \times 10^{16} cm^{-3}$

Line	MEAS. HALFWIDTH (Including Instrumental Broadening)	THEOR. HALFWIDTH	R
3965	3.3 ± 0.3	3.6 ± 0.2	0.92
2945	2.6 ± 0.3	2.7 ± 0.2	0.96

Conclusions

It has been shown that the discrepancies which have been observed between the measured and theoretical profiles are consistent with the effects which would be expected to occur if radial gradients existed in the plasma. However, the discussion which led to this conclusion has been of a qualitative nature only. In the next chapter the discussion of the effects of radial gradients will be put on a quantitative basis.

CHAPTER XII

MEASUREMENTS OF THE RADIAL GRADIENTS EXISTING IN THE PLASMA AND THE CALCULATION OF THEIR EFFECTS ON THE OBSERVED PROFILE OF THE HEI 4471 A^{o} LINE

12.1. Introduction

In order to put the discussion of radial gradients on a quantitative basis the work in this chapter is directed towards;

a) The measurement of the radial distributions of the electron density and the total intensity of the HeI 4471 A^{o} line at discharge filling pressures of 0.4 and 0.1 torr.

b) The calculations using a model of the plasma based on the above measurements, of the effects of radial gradients on the profile of the HeI 4471 A^{o} line

The main purpose of the measurements in section a) was to investigate the suggestion, put forward in (11.6) that the discrepancies observed for HeI lines (see (11.5.2.) and (11.5.3.)) arise because as the filling pressure is lowered an increasing proportion of the HeI line emission comes from regions of the plasma where the electron density is less than that measured on the axis of the discharge.

Although the profiles of a number of lines were measured,

the HeI 4471 A^{o} line was chosen for the investigation in section b) because firstly, it was expected to be the line most seriously affected by radial gradients and secondly, the results obtained for this line were found to be the most difficult to explain (see 11.5.2)

12.2. Measurement of the Radial Distribution of the Electron Density

12.2.1. Theoretical Basis of the Method

The continuum intensity I_c emitted by a helium plasma in a unit wavelength interval centred at a wavelength λ is given by:

$$I_c \approx (S^{+}N^{+} + S^{++}N^{++}) \frac{N_e}{\lambda^2} \cdot (\frac{1}{kT_e})^{3/2} \cdot \exp(\frac{-hc}{\lambda kT_e}) \quad (12.1)$$

where S^{+} and S^{++} are weakly temperature dependent factors which contain the free-bound and free-free Gaunt factors for HeI and HeII respectively, and N^{+} and N^{++} are the number densities of singly and doubly charged ions respectively. Eqn (12.1) is based on an expression, given by Griem (1) for the continuous emission coefficient of a plasma (see also Chapter XIV).

The ion densities appearing in (12.1) are related to each other and to the electron density N_e by the condition for charge neutrality:

$$N_e = N^+ + 2N^{++} \qquad (12.2)$$

The temperature dependence of I_c for $\lambda = 5400\ A^o$, was investigated and it was found that provided the electron temperature satisfies $T_e \geq 3 \times 10^4\ ^oK$, I_c is insensitive to changes of electron temperature. Therefore, provided the above condition on T_e is satisfied (12.1) may be written as:

$$I_c \approx (K^+N^+ + K^{++}N^{++})N_e \qquad (12.3$$

where K^+ and K^{++} may be considered to be constant.

A further approximation can be made if T_e is high enough to satisfy the above condition but at the same time is low enough to ensure that $N^+ >> N^{++}$. Then from (12.2) and (12.3) the following result is obtained:

$$I_c \propto N_e^2 \qquad (12.4)$$

Here the factor K^+ has been omitted.

Alternatively, if T_e is sufficiently high that $N^{++} >> N^+$ then again from (12.2) and (12.3) the following result is obtained:

$$I_c \propto N_e^2$$

Here the factor $K^{++}/2$ has been omitted.

Hence, providing the conditions on T_e are fulfilled the radial distribution of the electron density can be derived from measurements of the radial distribution of the continuum intensity by using the relationship:

$$N_e(r) \approx I_c^{\frac{1}{2}}(r) \qquad (12.5)$$

The spatially averaged electron temperature measured at $P_o = 0.4$ torr was found to be $\sim 4 \times 10^4$ °K. At this temperature the plasma is expected to be only singly ionized (see Fig. (8.1)) and therefore the above can be used. For $P_o = 0.1$ torr the spatially averaged electron temperature is $\sim 6 \times 10^4$ °K and at this temperature Fig. (8.1) shows that double ionization is just beginning to take place. In view of the uncertainty in the temperature measurements (see 9.3.2) and the fact that Fig. (8.1) is unlikely to describe accurately the degree of ionization in the plasma, it is possible that the plasma will be substantially ionized. If this were the case then the method can still be used (see above). Even if the number of singly and doubly charged ions in the plasma were equal, the measured continuum distribution could still give an indication of the position of the charged particles in the plasma.

12.2.2. Measurement of the Radial Distribution of the Continuum Intensity

To avoid the procedure of Abel inversion, the measurement of the radial distribution of the continuum intensity were made by observing the plasma in the axial direction. A system of circular apertures placed in front of the entrance slit the spectrometer, and attached to it by means of an optical bench, was used to isolate a narrow cone of plasma radiation. This system was placed on a kinematic mounting which allowed it to be moved, by a known amount, in a direction perpendicular to the axis of the plasma. By this means the acceptance cone of the system was scanned across the plasma. The resolution of the system was determined by the diameter and separation of the apertures and was $\sim$ 2 mm at the centre of the tube. A He-Ne laser was used to align the optical axis of the spectrometer-aperture system parallel with the optical axis of the discharge tube.

The measurement procedure consisted of setting the exit slit of the spectrometer on a band of continuum centred at $\lambda \sim 5400$ A^{o} and recording the intensity as a function of time at various positions across the discharge tube. Analysis of the C.R.O. traces at the pinch time gave the radial distribution of the continuum at that time.

12.3. Measurement of the Radial Distribution of the Total Intensity of the HeI 4471 A° Line

With the exception that the exit slit of the spectrometer was set to view the total intensity I_L of the HeI 4471 A° line, the radial distribution of I_L was measured in an identical manner to that used above. For the measurements made at P_o = 0.1 torr it was necessary to subtract the continuum intensity underlying the line because of the low intensity of the line.

12.4. Factors Affecting the Accuracy of the Measured Distributions

Apart from errors arising from shot to shot fluctuations, the measurement of the traces, etc. the accuracy of the continuum intensity distribution, and hence the electron density distribution, depends on two factors. They are:

a) The distortion of the continuum distribution produced by the instrumental broadening.

b) The effects produced by the temperature dependence of the continuum intensity becoming important near the edges of the plasma.

In order to investigate the accuracy of the measured radial electron density distribution measurements of this distribution, for P_o = 0.4 torr, were made using the method of laser interferometry (see 9.4.)

12.5. Measurement of the Radial Distribution of the Electron Density using Laser Interferometry

The electron density distribution was measured in a similar manner to that described in (9.4.) except that here the laser was aligned parallel to, but atvarying distances from the axis of the discharge. Measurements were made at distances of 2.5, 7.5 and 12.5 mm from the axis.

The analysis of these results is more complicated than for those measured on axis. In an off axis position the electron density will first increase through the ionization of the neutral helium. If the distance of the point of observation from the axis of the discharge is greater than the final pinch radius the electron density will ultimately decrease as the magnetic forces drive the plasma past the observation point. As the electron density increases fringe shifts will occur until a turning point, corresponding to a maximum in the electron density, is reached. Further fringes will then occur as the electron density decreases. The electron density at the off axis position at the time of maximum compression can be obtained from this fringe sequence by first counting the number of fringes from time zero to the turning point and then subtracting the number of fringes that occur between here and the time of maximum compression The net number of fringes then gives the required electron density.

It can be seen from the discussion above that in order

to measure the electron density in an off-axial position the times of maximum compression and the occurence of the turning point must be accurately established. The time to peak compression was found by recording the oscilloscope traces corresponding to the discharge current and the fringe sequence, measured in an off axis position, on the same film and then overlaying this film with a similar record containing an axial fringe sequence. With the present interferometer system the turning point can only be found by a careful examination of the fringe sequence. For measurements made near to the axis this was not difficult, but at points remote from the axis, where the number of fringe shifts recorded were small, it was impossible and the results obtained were only useful in establishing an upper limit to the density.

12.6. Discussion of the Results of the Radial Distribution Measurements

Figs (12.1) and (12.2) show, for measurements made at filling pressures of 0.4 and 0.1 torr respectively, the observed radial distributions of the continuum intensity at $\lambda \sim 5400$ A°, the electron density derived from this distribution using (12.4), and the total intensity of the HeI 4471 A° line. Also shown in Fig. (12.1) is the electron density distribution obtained from the laser. In all cases the distributions have been normalized to unit peak height.

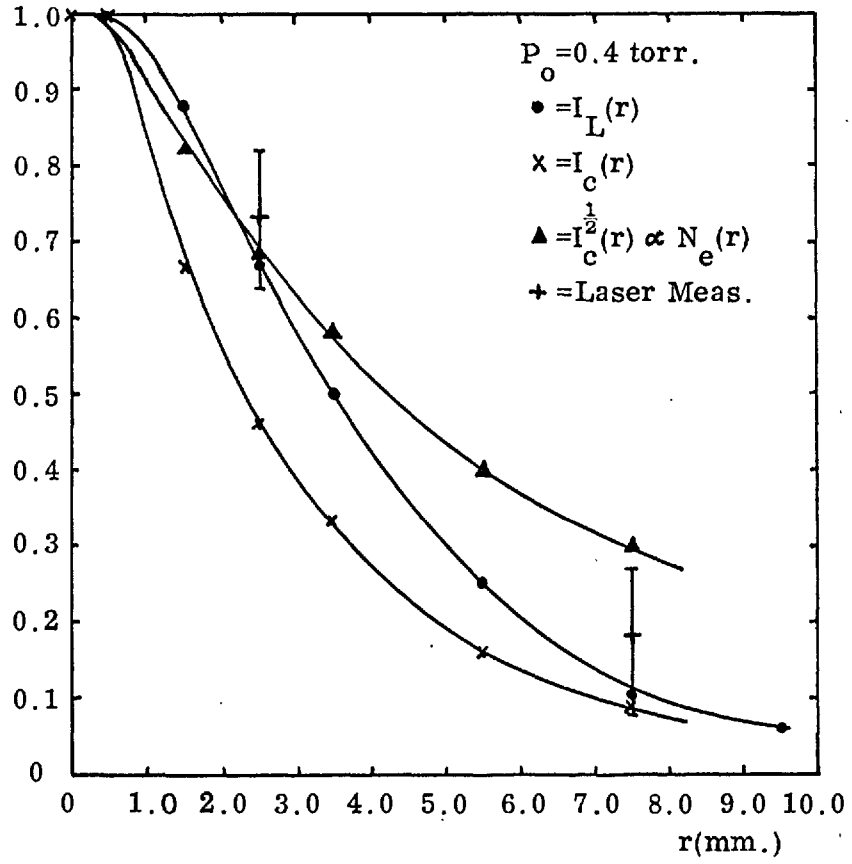

Fig.(12.1)

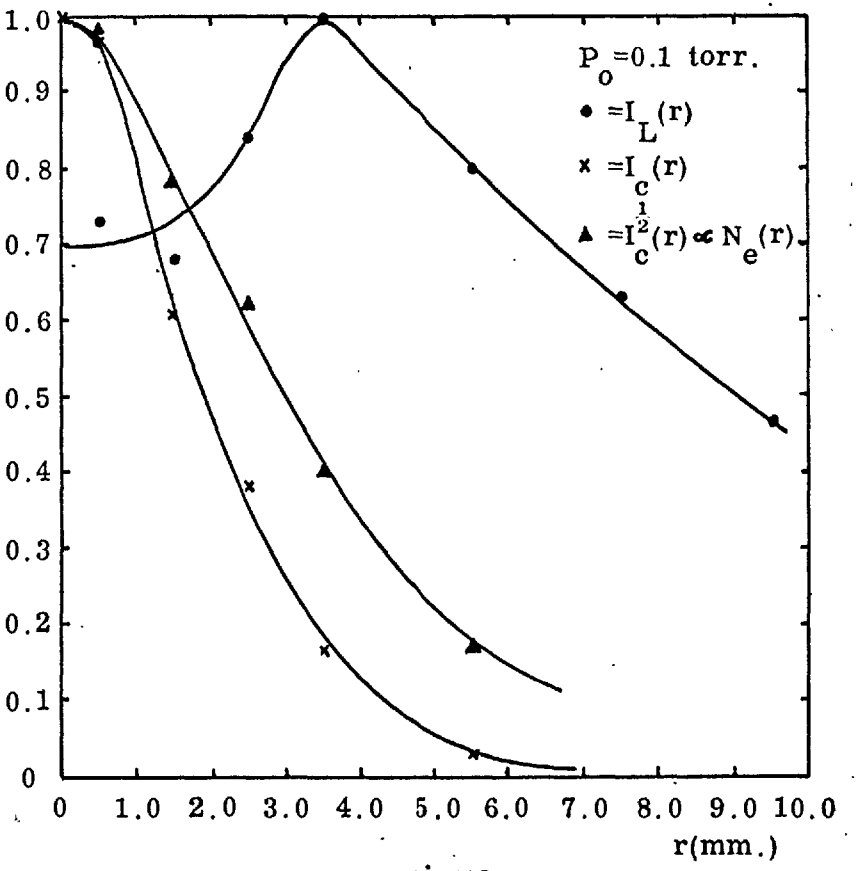

Fig.(12.2)

Figs.(12.1) and (12.2) Measured Radial Distributions.

Table (12.1) gives the measured half widths of the continuum intensity distribution $I_c(\frac{1}{2})$, the electron density distribution $N_e(\frac{1}{2})$, and the line intensity distribution $I_L(\frac{1}{2})$

TABLE (12.1)

Comparison of the Half widths of the Measured Distributions

P_o(torr)	$I_c(\frac{1}{2})$(mm)	$N_e(\frac{1}{2})$(mm)	$I_L(\frac{1}{2})$(mm)
0.4	5.0	8.6	7.0
0.1	4.0	6.0	18.0

The half widths given in Table (12.1) are upper limits for two reasons. Firstly, no correction has been made for instrumental broadening. Secondly, the measured distributions indicated that the optical axis of the scanning system and the axis of the discharge were mis-aligned by ~ 6 seconds of arc. This mis-alignment will cause some additional broadening of the true distributions.

A comparison of the electron density distribution obtained from the continuum measurement with that obtained from the laser measurements (see Fig. (12.1)) shows that at a distance of 2.5 mm from the axis the two methods are in agreement. But at a distance of 7.5 mm from the axis the electron density

derived from the continuum measurements is ~ 50% greater than that from the laser. This discrepancy is probably caused by the neglect of the temperature dependence of the continuum intensity, but in part it may also result from the instrumental broadening and the mis-alignment of the optical axis the scanning system and the axis of the discharge mentioned above.

Considering the measurements made at P_o = 0.1 torr first the results show (see Fig. (12.2)) that most of the HeI emission originates from off-axial regions of the plasma and the radial distribution of the total line intensity is such that the maximum of the distribution occurs at a radius where the electron density is at least a factor of 2.5 below that measured on the axis. However, because of the circular symmetry of the plasma, the amount of light received by the spectrometer from a given radial position in the plasma, will depend on the product of the radius and the intensity of the line at that radius. When the circular symmetry of the plasma is taken into account it is found that most of the light entering the spectrograph originates from plasma at a radius of 8 mm. At this radius the electron density is at least a factor 20 below that measured on the axis. Since the measured axial electron density is $7.5 \times 10^{15} cm^{-3}$ the electron density at a radius of ~8 mm will be $\sim 4 \times 10^{14} cm^{-3}$. For this electron density the half width of the HeI 4471 A^o line is ~ 0.1 A^o which is negligible

in comparison with the instrumental width of 2.2 A°. This result explains why the profile of the HeI 4471 A° line, measured at P_o = 0.1 torr was found to be in agreement with the instrumental profile.

Although Fig. (12.1) showsthat the distributions, measured at P_o = 0.4 torr of electron density and total line intensity are somewhat similar,it is found that on the basis of the preceding arguments,most of the line intensity reaching the spectrometer arises from plasma at a radius of ~ 3 mm. At this radius the electron density is ~40% below that measured on axis. This result appears to be in conflict with the conclusions drawn from the measurement of the profiles of the HeI 2945 A° and 3965 A° lines (see 11.9.3.) that the radial gradients are small at this filling pressure. However, a reduction in the width of the total line intensity distribution, and hence the radius from which most of the line emission originates, would be expected if the distorting influences on the distribution were taken into account.

The measurements at P_o = 0.4 torr show that the distributions $N_e(r)$ and $I_L(r)$ are somewhat similar, whereas those made at P_o = 0.1 torr show that the distribution $I_L(r)$ has a much greater extent than that of $N_e(r)$. It is reasonable, therefore, to expect that if measurements of the two distributions

had been made at filling pressures intermediate to those considered above, they would have shown a steady increase in the extent of the $I_L(r)$ distribution with respect to $N_e(r)$, as the filling was lowered. Thus the results tend to confirm the suggestion (see 11.6) that as the filling is lowered an increasing proportion of the HeI emission originates from off-axial regions of the plasma. A possible explanation of this behaviour is (see (44)) that at low filling pressures the rate of ionization will be relatively small, because the frequency of collisions between neutral and charged particles will be reduced and consequently when the charged particles are swept inwards by the rapidly rising magnetic field the neutral particles may be left behind.

12.7. Calculation of the Effects of Radial Gradients on The Profile of the HeI 4471 A° Line

12.7.1. Theoretical Model of the Plasma at the time of Peak Compression

The model of the plasma used to calculate the emitted profile of the HeI 4471 A° line for the plasma conditions corresponding to P_o = 0.4 torr, is based on the following assumptions:

a) The plasma at the time of maximum compression is a radially symmetrical cylinder.

b) The radial distributions of the electron density and the total intensity of the HeI 4471 A^{o} line vary smoothly over the radius and are a maximum on the axis.

c) Gradients in the axial direction are negligible.

d) The cross section of the plasma lies entirely within the acceptance cone of the spectrometer for both side and end on measurements.

e) Re-absorption of the line by the plasma is negligible.

The validity of assumption a) was inferred from forming camera observations and is a well established result for most cylindrical Z-pinches. Assumption b) is in agreement with the radial distribution measurements made at $P_o = 0.4$ torr (see 12.6). Axial gradients are discussed in (9.4.8) and it is shown that assumption c) is valid. Finally, calculation of the optical depth of the plasma for the line using (2.10) and the observation that profiles measured side on and end on are in good agreement shows that e) is valid.

12.7.2. Calculation of the Emitted Profile

For convenience only the side on profile measurements will be considered since the solid anglesinvolved are more easily defined. Let the plasma have a length d and a radius R.

The emission coefficient $\epsilon(r, \lambda)$ of the plasma at a wavelength and distance r from the axis of the plasma is given by:

$$\epsilon(r,\lambda) = \frac{hc}{4\pi\lambda} L(N_e,T_e,\lambda)N(N_e,T_e)A \qquad (12.6)$$

where $L(N_e,T_e,\lambda)$ is the line profile normalized so that $\int L(\lambda)d\lambda = 1$, A is the spontaneous transition probability for the line. N is the population density in the upper state of the line and $N_e=N_e(r)$ and $T_e=T_e(r)$. Since the line profile is only weakly dependent on T_e the following approximation is made:

$$L(N_e,T_e,\lambda) \approx L(N_e,\lambda) \qquad (12.7)$$

The intensity $I(r, \lambda)$ emitted at a wavelength λ by an annulus of plasma of radius r, width dr and length $d\ell$ ($d\ell$ = 3mm is defined by the width of the slot in the theta pinch coil (see Plate (9.1))) into the solid angle Ω subtended by spectrograph slit, is given by:

$$I(r,\lambda) = \epsilon(r,\lambda)\ \Omega\ 2\pi r\ dr\ d\ell$$

using (12.6) and (12.7) the expression above reduces to:

$$I(r,\lambda) = \frac{C}{\lambda} L(N_e,\lambda)N(N_e,T_e)r\ dr$$

where C is a constant. In the expression above it has been assumed that Ω is constant for all positions on the annulus. This is justified for the side on measurements because R is much less than the distance from the axis of the plasma to the spectrometer and only a small length of the plasma is viewed. The total intensity emitted at a wavelength λ is given by.

$$I(\lambda) = \int_0^R I(r,\lambda)dr$$

$$= \frac{C}{\lambda} \int_0^R L(N_e,\lambda)N(N_e,T_e)r\ dr \qquad (12.8)$$

To proceeed further the functions $N_e(r)$ and $T_e(r)$ must be specified. The distribution $N_e(r)$ can be based on the results given in (12.6), but $T_e(r)$ has not been measured and indeed would be very difficult to measure with any degree of reliability. However, the radial distribution of the total line intensity $I_L(r)$ has been measured and this can be related to $N(N_e,T_e)$ as follows.

The total line intensity emitted by a volume of plasma dv (defined by the acceptance cone of the scanning system(see(12.2.2)),at a radius r, into a solid angle Ω' subtended by the entrance aperture of

the scanning system is given:

$$I_L(r) = \Omega' \, dv \int \epsilon(r, \lambda) d\lambda$$

Using (12.6) and evaluating the integral the expression above reduces to:

$$I_L(r) = \frac{C'}{\lambda} N(N_e, T_e) \tag{12.9}$$

where C' is a constant. Here it has been assumed that to a good approximation that the extent of the line is small compared with λ and that the solid angle Ω' which will vary from one end of the plasma to the other, has been replaced by some suitably defined average value.

From (12.8) and (12.9) the total intensity emitted by the plasma at a wavelength λ is:

$$I(\lambda) \approx \int_0^R L(N_e, \lambda) I_L(r) dr \tag{12.10}$$

where numerical factors and the wavelength λ have been omitted. Since the factors in the integrand of (12.10) are not analytic the integral above must be replaced by a summation of the form

$$I(\lambda) \approx \sum_{i=1}^{i=n} r_i L(N_e, \lambda) I_L(r_i) \Delta r_i \qquad (12.11)$$

where $N_e = N_e(r_i)$.

12.7.3. Evaluation of the Summation

The first step in evaluating the summation is the division of the plasma into annular zones and for good accuracy the number of zones should be as large as possible. In practice the number used is limited because the theoretical profiles have only been tabulated for rather large density steps. Consequently profiles for intermediate densities had to be obtained by interpolation, using the methods described in (11.1.2)

Initially six zones were chosen; although this number could have been increased if necessary. For convenience the measured electron density distribution was approximated by the distribution shown in Fig. (12.3). The figure also shows the manner in which the plasma was divided into zones and the densities ascribed to them. For simplicity and to a good approximation the radial distribution of the total intensity of the HeI 4471 A^o line was assumed to be Gaussian and in order to obtain an indication of the sensitivity of the limited profile to the form of the intensity distribution, two distributions were taken. These are also shown in Fig. (12.3).

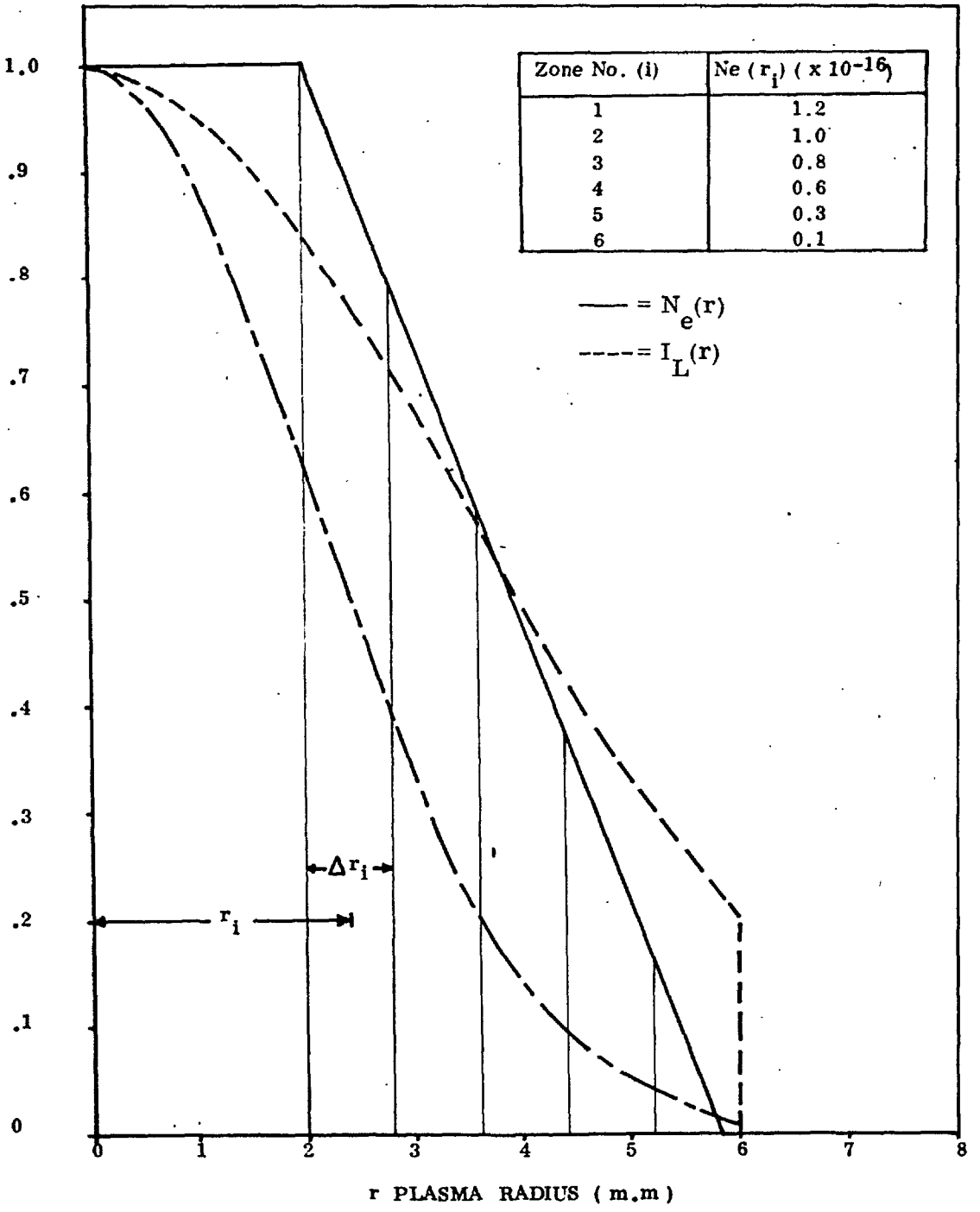

Fig.(12.3) Assumed Distributions of N_e and I_L

A computer programme was written to evaluate the summation The input data consisted of the intensity of the theoretical profile, at a given wavelength, corresponding to the densities of the six zones (~ 40 wavelength positions were taken) and the position and width of the zones. The output consisted of the line intensity at a given wavelength and (for comparison purposes) the profile corresponding to axial density. These profiles were then convolved with the instrument profile and normalized to the peak height of the experimentally measured profile.

12.7.4. Results

The results are shown in Fig. (12.4). Curve (1) shows the profile that would be emitted by a homogenous plasma whose density corresponds to that measured on the axis of the plasma. Curves (2) and (3) are the line profiles corresponding for the two line intensity distributions. Circles and triangles indicate the measured points.

The calculated profile which best describes the measured profile is obtained for the intensity distribution which is ~30% narrower than that measured. Although this result is possibly fortuitous it does tend to add support to suggestion put forward in (11.9.3) that the measured total line intensity

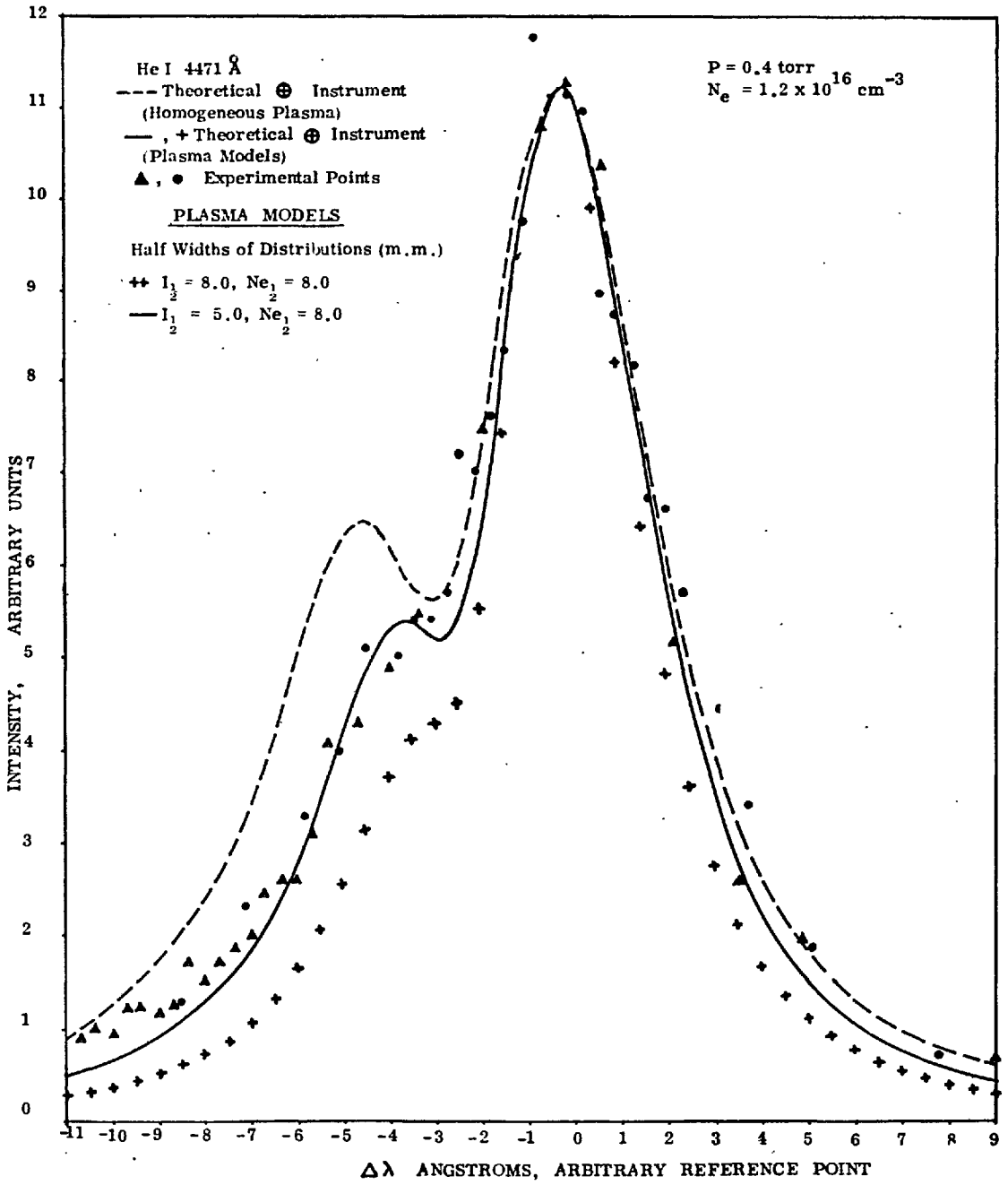

Fig.(12.4) Results of Model Calculations and Comparison with Experiment.

distribution is too wide. Of greater interest is the overall behaviour of the calculated profiles. Firstly, the model correctly predicts the observed shift of the forbidden component towards the allowed line. Secondly, the red wing of the profile is much less sensitive than blue wing to the assumed intensity distribution which would explain why the experimental profile shows such good agreement for the red wing whilst at the same time large discrepancies are observed on the blue wing (see Fig. (11.6). Reasons for the sensitivity of the profile to the effects of radial gradients have been given in (11.7.2).

12.7.5. Conclusions

From the preceding investigation it can be concluded that the discrepancies that are observed (see 11.5) between the measured and theoretical profile of the HeI 4471 A^{o} line are caused by the presence of radial gradients in the plasma and not by gross errors in the theoretical profiles. Unfortunately, because of the approximations made in calculating the emitted profile it is not possible to obtain information about the accuracy of the theoretical profiles.

The results also show that in order to investigate lines with forbidden components either for comparison with theory or diagnostic purposes, extremely homogeneous plasmas

are required, or alternatively, steps must be taken to observe only the homogeneous parts of the plasma. If line profiles are measured for diagnostic purposes then it is advisable to chose hydrogenic or isolated lines rather than lines with forbidden components which do not completely overlap with the allowed component.

Finally, an extremely important result can be inferred from the measured profiles of the HeI 4471 A^{o} line (see 11.5.2), that is, the agreement between profiles measured by observing the plasma in the axial and radial directions does not necessarily ensure that the profile is unaffected by radial gradients in the plasma.

CHAPTER XIII

SUMMARY AND CONCLUSIONS FOR WORK IN PART II

The investigation which is described in Part II of this thesis was undertaken to examine the suitability of a Z-pinch discharge for use as a source of helium plasma for Stark broadening measurements.

It has been found that the discharge possesses many of the requirements for such a light source, i.e. good short and long term reproducibility, the operating conditions can be varied by simply adjusting the filling pressure and the electron density can be measured accurately by means of a method which is independent of the assumptions of Stark broadening theories.

The electron temperature was found to be difficult to measure accurately because firstly, the operating conditions were such that more than one ionization stage was usually present in the plasma, and secondly the ionization relaxation times are of the same order as the heating and containment times of the plasma; in the final chapter a method of temperature measurement will be described whereby these difficulties can be overcome.

The major difficulty which has been encountered when the Z-pinch discharge was the problem of radial density gradients. When the work was commenced it was thought that such effects might present problems, but on the basis of two previous

investigations which have used a Z-pinch discharge for Stark broadening studies, it appeared that these effects might be small. In general, this has been found not to be the case for the discharge studied here since for some operating conditions severe distortion of the profiles produced by radial density gradients was observed.

There are three possible reasons as to why the radial density gradients are more noticeable for the discharges studied here than for those which have been used previously. Firstly, when making the line profile measurements, described in this work, the discharge has been operated over a comparatively wider range of filling pressures than was used in the previous works, and for each condition studied the entire measured profile has been compared with theory rather than just the half widths. Such measurement procedures might be expected to be a more sensitive indication of the presence of radial density gradients. Secondly, because the diameter of the discharge tube used here is a factor of ~ 2 smaller than that used in the previous investigations it might be expected that for a given filling pressure, the diameter of the plasma at peak compression would be larger than that found here and consequently, the radial gradients would be less severe. This is especially true in the case of the discharge used by Roberts (22) since this device was stabilised by means of axial magnetic field and this tends

to increase the diameter of the plasma at peak compression. Thirdly, whereas the previous investigators studied the broadening and shift of isolated lines emitted by singly charged ions only, here lines emitted by neutral atoms have been studied and it was found that because of the manner in which the plasma is generated and confined the lines emitted by neutral atoms are more likely to be affected by radial density gradients than those emitted by ions. Finally, a line containing a forbidden component has been studied and it is found that the profile of such a line is more senstive to the effects of radial density gradient than are isolated lines.

Although most of the profiles studied in this investigation have been affected by radial gradients it must be emphasised that these measurements have been made without attempting to spatially resolve the light emitted by the plasma. If in the future experiments of this nature a system of apertures is used to limit the region of plasma, which the spectrometer views, to that close to the axis of the discharge, the difficulties encountered here could be reduced and perhaps even eliminated. Some improvement might also be expected if the diameter of the discharge tube is increased. For low density Stark broadening studies observations can be made in the afterglow of the discharge and since the afterglow tends to fill the entire discharge tube the effects of radial gradients should be less

severe. Such observations have recently been made using a Z-pinch discharge identical to that described here (see Cairns (62)).

In spite of the presence of radial gradients in the plasma a number of conclusions can be drawn from the results of the line profile measurements. The results obtained for the HeII 3203 A^{o} line at $N_e \doteq 2.1 \pm 0.2 \times 10^{16} cm^{-3}$ ($P_o = 0.3$ torr) show that, with the exception of that part of the profile near the central dip, the shape of the observed profile (uncorrected for instrumental broadening) and that of the theoretical profile (with the instrumental broadening included) are in good agreement; the half widths of these profiles are in agreement to within $\sim 3\%$. Radial density gradients appear to be responsible for the discrepancies near the central dip in the profile. The discrepancy between the half width of the true observed profile (the observed profile corrected for instrumental effects) and that of the theoretical profile was estimated to be $\sim 5\%$. The measurements of the HeII 3203 A^{o} line profile made at lower filling pressures were more seriously affected by radial density gradients than the measurements discussed above. However, by normalizing the observed and theoretical profiles to points on the wings of the theoretical profiles where the distorting effects of radial gradients are less serious, the agreement between theory and experiment on the wings of the profile was found to be good.

The profiles of the HeI 2945 and 3965 A^{o} lines were measured at $N_e = 1.2 \pm 0.1 \times 10^{16} cm^{-3}$ ($P_o = 0.4$ torr) and $2.1 \pm 0.2 \times 10^{16} cm^{-3}$ ($P_o = 0.3$ torr). A preliminary analysis

of the results obtained at P_o = 0.3 torr showed that the profiles were seriously distorted by the effects of radial density gradients and no further attempt was made to analyse the results. The results obtained at P_o = 0.4 torr for the HeI 2945 A^o line showed that providing the distorting effects of radial gradients were taken into account by normalizing the observed profile and the theoretical profile (corrected for instrumental effects), there was good agreement between theory and experiment for the majority of the profile. The half width of these profiles were in agreement to ~ 4% and the agreement between the true observed profile (see above) and the theoretical profile was 5%. The results obtained for the HeI 3965 A^o at P_o = 0.4 torr were treated in an identical manner to those for HeI 2945 A^o line, but here the agreement with theory was not so good, e.g. the discrepancy between the true observed profile and theoretical profile was ~ 14%. This result was to be expected because the measured profile showed that a forbidden component was present and the appearance of the forbidden component indicates the breakdown of the isolated line approximation which had been used to derive the theoretical profile.

The main conclusion that can be drawn from the results of the measurements of the HeI 4471 A^o line, including the forbidden component was that lines with forbidden components are especially sensitive to radial gradients.

CHAPTER XIV

AN EXTENSION OF THE 'LINE TO CONTINUUM RATIO' METHOD OF MEASURING ELECTRON TEMPERATURES TO L.T.E. AND NON-L.T.E. HELIUM PLASMAS WITH MORE THEN ONE IONIZATION STAGE PRESENT

14.1. Introduction

In hydrogen and helium plasmas, where accurate continuum intensities can be calculated, the electron temperature can be determined by measuring the ratio of the intensity of a line to its underlying continuum (see Griem (1)). The basis of this method is that in a plasma in which one ionization stage is dominant the intensity of a suitably chosen line and its underlying continuum can both be expressed in terms of the product of the ground state population density of the next higher ionization stage and the free electron density. Hence the line to continuum ratio is independent of these quantities and depends only on the electron temperature.

For a helium plasma the method can be used for $T_e \lesssim 3 \times 10^4$ °K if a HeI line is used and for $T_e \gtrsim 7.5 \times 10^4$ °K if a HeII line is used. At intermediate values of T_e more than one ionization stage is present and the method can be used only if the plasma composition can be calculated accurately. Such a calculation is possible only if the plasma is in L.T.E. and since this requires

electron densities of $\sim 10^{19} cm^{-3}$ (see Chapter IIX), the method would have a limited application only. In this chapter a method of extending the line to continuum ratio method of measuring electron temperatures in L.T.E. and non-L.T.E. helium plasmas with more than one ionization stage present will be described.

14.2. Continuum Intensity for a Helium Plasma with more than one Ionization Stage present

Griem (1) has given a method of calculating the continuous emission coefficient of a plasma. This method will be used as the basis for calculating the continuum intensity for a helium plasma with more than one ionization stage present. As only three results of Griem's calculations will be presented the reader is referred to (1) for further discussion.

The intensity I_c of a band of continuum of width $\Delta\lambda$ centred at a wavelength λ, arising from recombination and bremsstrahlung radiation on singly and doubly charged helium ions is given by::

$$I_c = \frac{64(\alpha a_o)^3}{3^{3/2}} \pi^{\frac{1}{2}} c E_H \left(\frac{E_H}{kT_e}\right)^{3/2} S N_e \frac{1}{\lambda^2}$$

$$\exp\left(\frac{-hc}{\lambda k T_e}\right) \Delta\lambda \qquad (14.1)$$

where α is the fine structure constant, a_o is the Bohr radius, c is the velicity of light, and E_H is the ionization potential of hydrogen. The term S contains the free-free and free-bound Gaunt factors, and is given by:

$$S = \left[\frac{N_1^+}{N^+} S_1^+ + S_2^+ + S_3^+\right]N^+ + \left[S_2^{++} + S_3^{++}\right]N^{++} \qquad (14.2)$$

The terms in the brackets account for the continuum radiation pro-duced by singly N^+ and doubly N^{++} charged ions respectively. Taking these terms separately S_1^+ arises from recombination into the low-lying non-hydrogenic levels, (defined by $n \leq 3$) of HeI and, is given by:

$$S_1^+ = \sum_{n,\ell}^{n=3} \frac{1}{n^3} g_n^{(1)}(\lambda) \exp\left(\frac{E_\infty^o - E_{n,\ell}^o}{kT_e}\right) \qquad (14.3)$$

where $g_n^{(1)}(\lambda)$ is the relative continuum absorption cross-section for HeI, n, ℓ and $E_{n,\ell}^o$ are respectively the principal and orbital quantum numbers and energy of the level into which recombination takes place and E^o is the ionization potential of HeI. Multiplication of this term by N_1^+/N^+, the ratio of singly charged ions in the ground state to the total number of such ions, accounts for the fact that recombination can only take place into low lying levels of the atom if the ion is originally in its ground state.

The term S_2^+ arises from recombination into hydrogenic levels (defined by $n \geqslant 4$) of HeI and is given by:

$$S_2^+ = \sum_{n=4}^{n=n_1-1} \frac{g_n^{(1)}(\lambda)}{n^3} \cdot \exp\left(\frac{E_H}{n^2 kT_e}\right) \qquad (14.4)$$

where $g_n^{(1)}(\lambda)$ is the free bound Gaunt factor for hydrogen averaged over the sub-levels of the level n.

S_3^+ arises from free-free transitions and from recombination into merged levels, this is given by:

$$S_3^+ = g_{ff}^{(1)}(\lambda) \cdot \frac{kT_e}{E_H} \cdot \exp\left(\frac{E_H}{n_1^2 kT_e}\right) \qquad (14.5)$$

where $g_{ff}^{(1)}(\lambda, T_e)$ is the free-free Gaunt factor averaged over a Maxwellian velocity distribution, n_1 is the principal quantum number of the last discrete level and is given by:

$$n_1 = \left(\frac{z^2 E_H}{E^{z-1}}\right)^{\frac{1}{2}} \qquad (14.6)$$

where z=1 for HeI etc. and ΔE^{z-1} is the so-called 'advance of the series limit' and is given by:

$$\Delta E^{z-1} = 4z^{4/5}\left[a_o^3 N_e\right]^{4/15} E_H \qquad (14.7)$$

From (14.6) and (14.7) n_1 is given by:

$$n_1 = \tfrac{1}{2} z^{3/5} \left[a_o^3 N_e\right]^{-2/15} \qquad (14.8)$$

With n_1 fixed by (14.8) the summation in S_2^+ is terminated at the value of n given by $n=n_1-1$.

The principal and orbital quantum numbers at which the first summation S_1^+ is commenced, is determined by the wavelength of interest, the condition being that the summation is started at the first level satisfying:

$$E^o_{n,\ell} \geqslant E^o_\infty - \Delta E^o - \frac{hc}{\lambda} \qquad (14.9)$$

If λ is such that none of the non-hydrogenic terms satisfy this condition then the summation starts with S_2^+, the first term is again chosen so that (14.9) is satisfied.

The terms in the second bracket account for continuum radiation produced by doubly charged ions. Since the recombined atom is hydrogenic there is no term corresponding to S_1^+.

The first term S_2^{++} in the second bracket is analogous to S_2^+ for a system with z=2 and is given by:

$$S_2^{++} = 16 \sum_{n}^{n=n_1-1} \frac{g_n^{(2)}(\lambda)}{n^3} \exp\left(\frac{4E_H}{n^2 kT_e}\right) \qquad (14.10)$$

where $g_n^{(2)}(\lambda)$ is the free bound Gaunt factor for hydrogenic ions with nuclear charge z=2, the other quantities have their usual meaning. The factor 16 arises because of the z^4 dependence of the recombination continuum.

The second term S_3^{++} is again analogous to S_3^+ and is given by:

$$S_3^{++} = 4g_{ff}^{(2)}(\lambda, T_e) \cdot \frac{kT_e}{2E_H} \cdot \exp\left(\frac{4E_H}{kT_e}\right) \qquad (14.11)$$

$g_{ff}^{(2)}(\lambda, T_e)$ being the average free-free Gaunt factor for hydrogenic ions with z=2. The factor 4 arises from the z^2 dependence of the free-free continuum radiation.

Similarly, n is calculated from (14.8) with z=2 and the first term contributing to the summation S_2^{++} is given by:

$$E_n^1 \geqslant E_\infty^1 - E^1 - \frac{hc}{\lambda} \qquad (14.12)$$

E_∞^1 is the ionization potential of HeII and ΔE^1 is obtained from (14.7) with z=2

14.3. Line to Continuum Ratio

The intensity I^{z-1} of a line of wavelength λ arising from a transition from an upper level in to lower level n is

given by:

$$I^{z-1} = 32\,\pi^{7/2}\,a_o^5\,\alpha\,cE_H\left(\frac{E_H}{kT_e}\right)^{3/2}\cdot\frac{g_n^{z-1}}{g_1^z}\;f^{z-1}$$

$$N_e N_1^z \frac{1}{\lambda^3}\exp\left(\frac{E^{z-1} - E_m^{z-1}}{kT_e}\right) \qquad (14.13)$$

where $z-1 = 0$ for HeI lines, etc. g_n^{z-1} and g_1^z are respectively the statistical weights of the lower level of the line and the ground state of the next higher ionization stage, N_1^z is the population density of the ground state of the next higher ionization stage, and f^{z-1} is the absorption oscillator strength of the line. The other quantities appearing in (14.13) have been defined previously. To avoid misunderstandings, it should be realized that $N_1^1 \equiv N_1^+$ and $N_1^2 \equiv N_1^{++}$.

From (14.13) and (14.1) the line to continuum ratio is

$$\frac{I^{z-1}}{I_c} = \frac{3^{3/2}\pi^3}{2}\cdot\left(\frac{a_o}{\alpha}\right)^2\cdot\frac{g_n^{z-1}f^{z-1}}{g_1^z}\cdot\frac{N_1^z}{S}\cdot\frac{1}{\lambda\Delta\lambda}\cdot$$

$$\exp\left(\frac{E_\infty^{z-1} - E_m^{z-1}}{kT_e}\right)\cdot\exp\left(\frac{hc}{\lambda kT_e}\right) \qquad (14.14)$$

Using $hc/\lambda = E_m^{z-1} - E_n^{z-1}$, and expressing λ in angstrom units with $\Delta\lambda = 100$ A$^\circ$ centred at the line (14.14).

$$\frac{I^{z-1}}{I_c} = 4.24 \times 10^3 \frac{g_n^{z-1} f^{z-1}}{g_1^z} \cdot \frac{N_1^z}{S} \cdot \frac{1}{\lambda} \exp\left(\frac{E_\infty^{z-1} - E_n^{z-1}}{kT_e}\right) \qquad (14.15)$$

If the depressions of the two ionization potentials (see (1)) which occur in (14.15), are neglected the electron density enters (14.15) only through choice of n_1 and from (14.8) this is seen to be only a weak function of N_e. In fact the choice of n_1 is not critical since any change corresponds merely to shifting a term in the free bound contribution to the free-free contribution or vice versa.

Eqn (14.15) is valid provided that firstly N_e is sufficiently high to ensure that the upper state of the line and the states which contribute to the free-bound continuum are in L.T.E. with the ground state of the next highest ionization stage and the free electrons. Eqn (8.7) can be used to ascertain whether this is true or not. Secondly, N_e is sufficiently low that the depression of the ionization potentials can be neglected. The depression of the ionization potential $\Delta E_\infty{}^{z-1}$ is given by:

$$\Delta E_\infty^{z-1} = \frac{ze^2}{\rho_D}$$

where ρ_D is the Debye radius and z=1 for HeI etc.

14.4. Theory of the Method of Measuring Electron Temperatures

From (14.2) and (14.5) the general expression for the line to continuum ratio, in the case of a helium plasma, can be expressed in the form,

$$\frac{I^{z-1}}{I_c} = \frac{F_1[\lambda, T_e, (E_\infty^{z-1} - E_m^{z-1})] N_1^z}{F_2(T_e, \lambda) N^+ + F_3(T_e, \lambda) N^{++}} \qquad (14.16)$$

where the forms of the functions F_1, F_2 and F_3 need not concern us.

Suppose that R_1 and R_2, the line to continuum ratios for a neutral and ionized helium respectively, have been measured. From (14.16) these ratios are given by:

$$R_1 = \frac{F_1[\lambda_1, T_e, (E_\infty^o - E_n^o)] N^+}{F_2(T_e, \lambda_1) N^+ + F_3(T_e, \lambda_1) N^{++}} \qquad (14.17)$$

$$R_2 = \frac{F_1[\lambda_2, T_e, (E_\infty^1 - E_n^1,)] N^{++}}{F_2(T_e, \lambda_2) N^+ + F_3(T_e, \lambda_2) N^{++}} \qquad (14.18)$$

Here the approximations $N_1^+ \approx N^+$ and $N_1^{++} \approx N^{++}$ have been made. These are usually very good approximations; especially in non-L.T.E. plasmas, if (14.17) and (14.18) are divided throughout by N^{++} and a parameter β is introduced which is defined by:

$$\beta = N^{+}/N^{++} \tag{14.19}$$

then R_1 and R_2 are of the form:

$$R_1 = G_1(T_e, \beta) \tag{14.20}$$

$$R_2 = G_2(T_e, \beta) \tag{14.21}$$

Since R_1 and R_2 have been measured, two equations with two unknown T_e and β, are obtained. By solving these equations not only can T_e be found but also β, and if the electron density is also known N^{+} and N^{++} can be found from β and the condition of charge neutrality.

To solve Eqns (14.20) and (14.21) a graphical procedure can be used. This involves first plotting R_1 versus R_2, calculated from (14.20) and (14.21) for various values of β with T_e held constant and secondly plotting on the same graph R_1 versus R_2 for various values of T_e with β held constant. A series of intersecting curves is obtained (see Fig. (14.2)) from which the value of T_e and β, corresponding to the measured values of R_1 and R_2 can be read.

14.5. Calculation of the Line Continuum Ratios and Results

In order to illustrate the procedure for measuring T_e

and β which has been outlined above, the line to continuum ratios R_1 and R_2 of the HeI 4471 and HeII 4686 A^o lines respectively were calculated for $N_e = 10^{16} cm^{-3}$ and for various values of T_e and β . Relative continuum absorption cross-sections $g_n^{(1)}(\lambda)$ (see Eqn (14.3)) for HeI were taken from (1) and hydrogenic free-free and free-bound Gaunt factors from (61). Energy levels were taken from (35) and (58) for HeI and HeII respectively.

Verification of the accuracy of the calculations was obtained by calculating R_1 and R_2 for the case where one ionization stage only is present and comparing the results with the similar calculations of Griem (1) . The results are shown in Fig. (14.1) where the points taken from Griem's calculations are seen to be in good agreement. For general interest R_1 and R_2 calculated for various values of β are also shown in Fig. (14.1); note that for HeI 4471 A^o line the results are presented for various values of $1/\beta$.

Fig. (14.2) shows the graph of R_1 versus R_2 plotted for values of β ranging from 10^{-2} to 2×10^3 and values of T_e ranging from 3 to 15 eV. These curves should be valid for $N_e \sim 10^{16} cm^{-3}$ but for N_e considerably greater than $10^{16} cm^{-3}$ errors will arise because the depression of the ionization potential has been neglected; note, if one ionization only is present the depression of ionization potential cancels out in the line to continuum ratio.

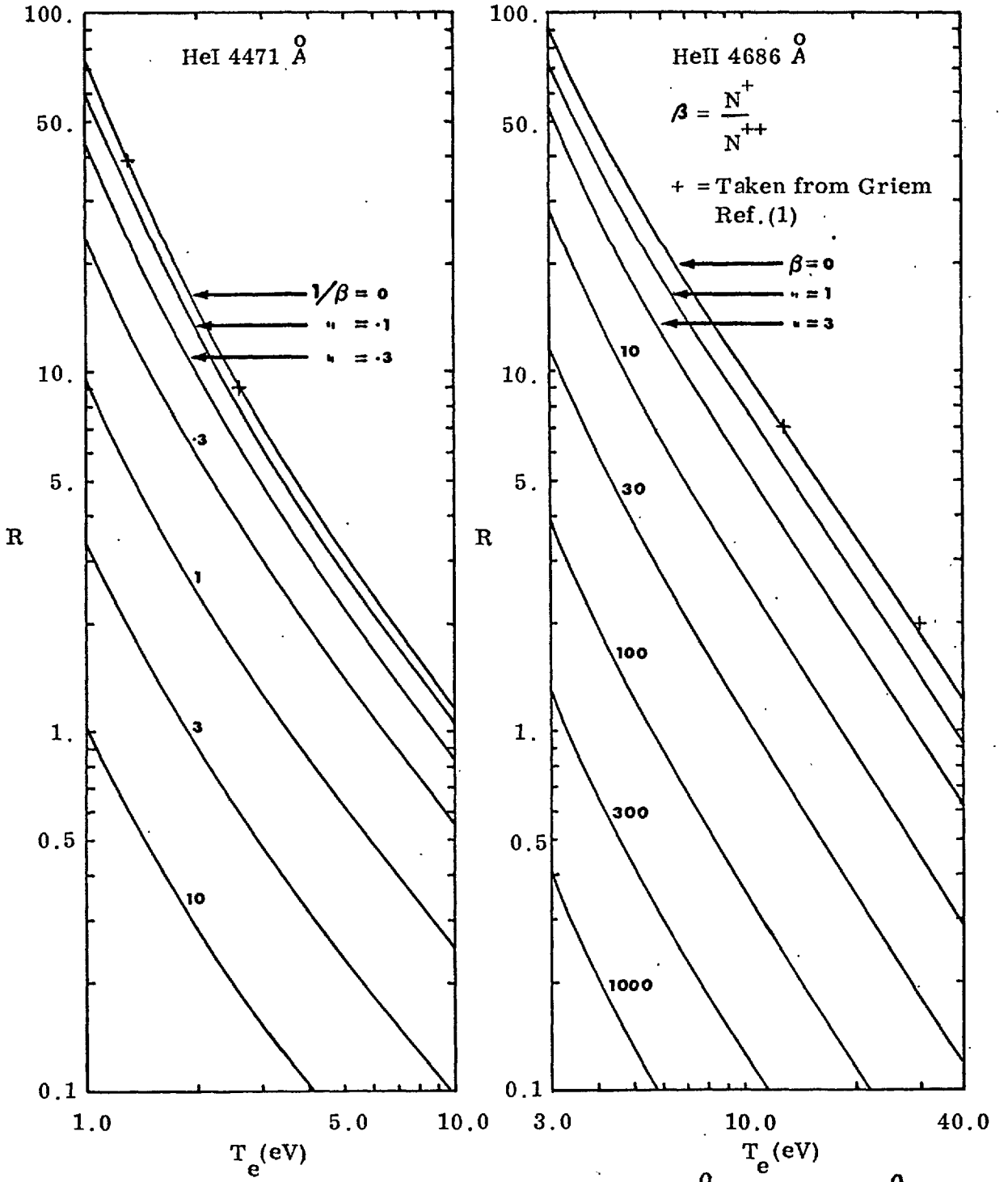

Fig. (14.1) Line-to-Contiuum Ratio of the HeI 4471 Å and HeII 4686 Å Lines for Various of $\beta = N^{+}/N^{++}$

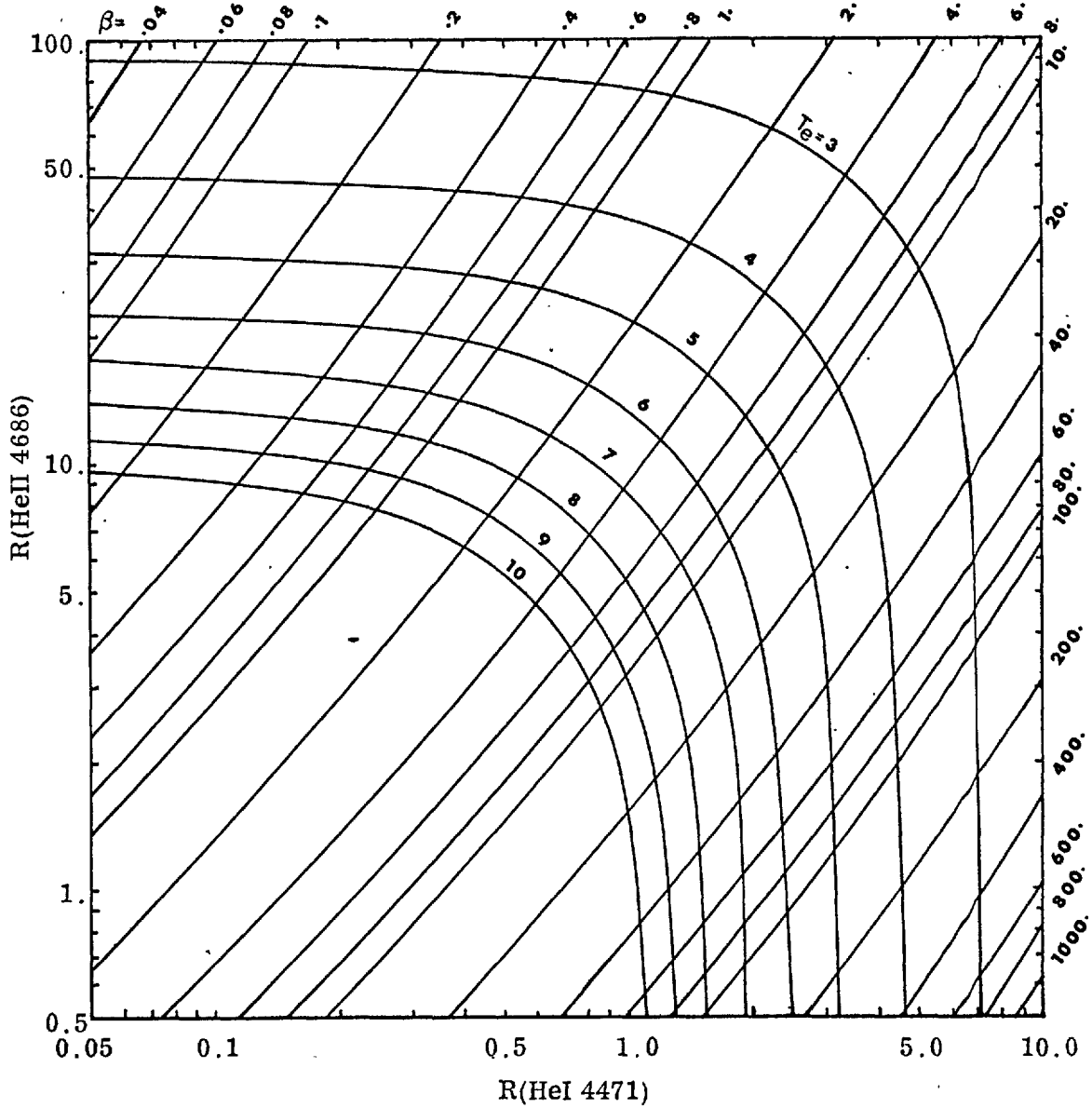

Fig.(14.2) Line-to-Continuum Ratio of the HeII 4686 Å Line Versus that of the HeI 4471 Å Line for Values of β and T_e.

REFERENCES

1. GRIEM, H. R., "Plasma Spectroscopy", McGraw-Hill Book Co., Inc, New York, 1964.

2. WIESE, W. L., "Plasma Diagnostic Techniques", edited by R. H. Huddlestone and S. L. Loenard, Academic Press, New York, Ch. 6, 1965.

3. BURGESS, D. D., Ph. D. Thesis, University of London, 1965.

4. BARANGER, M., "Atomic and Molecular Processes", edited by D. R. Bates, Academic Press, New York, Ch. 13, 1962.

5. BURGESS, D. D., Imperial College Internal Report, 1967.

6. FOSTER, J. S., Proc. Roy. Soc. London, A 117, 137, 1928.

7. BREENE, R. G., "The Shift and Shape of Spectral Lines", MacMillan,

8. BARANGER, M., Phys. Rev., 111, 494 and 112, 514, 1958,

9. KOLB, A. C. and GRIEM, H. R., Phys. Rev., 111, 514, 1958.

10. GRIEM, H. R., BARANGER, M., KOLB, A. C., and OERTEL, G. K., Phys. Rev., 125, 177, 1962.

11. BARNARD, A. J., COOPER, J. and SHAMEY, L. J., Astron. and Astrophysics, 1, 28, 1969.

12. GRIEM, H. R., Astrophys. J., 154, 1111, 1968.

13. GRIEM, H. R. and SHEN, K. Y., Phys. Rev., 122, 1490, 1961.

14. GRIEM, H. R., KOLB, A. C., and SHEN, K. Y., Astrophys. J., 135, 272, 1962.

15. WULFF, H., Z. Physik, 15, 614, 1958.

16. BERG, H. F., ALI, A. W., LINCKE, R. and GRIEM, H. R., Phys. Rev., 125, 199, 1962.

17. BURGESS, D. D. and COOPER, J., Proc. Phys. Soc., 86, 1333, 1965.

18. BERG, H. F., KFA-Bericht, Julich, 182-PP, 1965.

19. BOTTICHER, W., RODER, O. and WOBIG, K. H., Z. Physik., 175, 480, 1963.

20. RODER, O. and STAMPA, A., Z. Physik, 178, 348, 1964.

21. LINCKE, R., Ph. D. Thesis, University of Maryland,

22. ROBERTS, D. E., Ph. D. Thesis, University of London,

23. OERTEL, G. K., Paper presented at the Annual Meeting of the Am. Phys. Soc., Div. of Plasma Physics, Boston, 1966.

24. OERTEL, G. K., Proc. 8th Int. Conf. on Ioniz. Phen. in Gases, 279, Vienna, 1967.

25. SADJIAN, H., WIMMEL, H. K. and MARGENAN, H., J.Q.S.R.T., 1, 46, 1961.

26. HERMEL, A. and SELIGER, K., Monatsbkerichte der Deutschen Akademie der Wissenschaften zu Berlin, Band 8, Heft 4, 1966.

27. GRIEM, H. R., Phys. Rev., 128, 515, 1962.

28. BARANGER, M. and MOZER, B., Phys. Rev., 118, 626, 1960.

29. COOPER, J. and OERTEL, G. K., Phys. Rev., 180, 286, 1969.

30. SAHAL-BRECHOT, S., Astron. and Astrophys., 1, 91, 1969.

31. ALDER, K. et al, Rev. Mod. Phys., 28, 432, 1956.

32. SEATON, M. J., Proc. Phys. Soc. London, 79, 1105, 1962.

33. CHAPPEL, W. R., COOPER, J. and SMITH, E. W., J.Q.S.R.T., 9, 149, 1969.

34. BURGESS, D. D., Phys. Rev., 176, 150, 1968.

35. MARTIN, W. C., J. Res. Natl. Bur. Std., A 64, 19, 1960.

36. UNSOLD, A., Z. Astrophys., 44, 75, 1944.

37. MULLER, K. G., J.Q.S.R.T., 5, 403, 1965.

38. WIESE, W. L. and MURPHY, P. W., Phys. Rev., 131, 2108, 1963.

39. GREIG, J. R. et al., Phys. Rev., 172, 148, 1968.

40. BARANGER, M. and MOZER, B., Phys. Rev., 123, 25, 1961.

41. KOLB, A. C. and GRIEM, H. R., "Atomic and Molecular Processes", edited by D. R. Bates, Academic Press, New York, Ch. 5, 1962.

42. SEAY, G. L., Los Alamos Sci. Lab. Rept. LAMS-2125, 1957.

43. BERG, H. F. et al., Proc. 8th Int. Conf. on Ioniz. Phen. in Gases, 439, Vienna, 1967.

44. GLASSTONE, S. and LOVEBERG, R. H., "Controlled Thermonuclear Reactions", D. Van Nostrand Co. Inc., Princeton, New Jersey, 1960.

45. JALUFKA, N. W., OERTEL, G. K. and OFELT, G. S., Phys. Rev., 16, 1073, 1966.

46. McWHIRTER, R. W. P., "Plasma Diagnostic Techniques", edited by R. H. Huddlestone and S. L. Leonard, Academic Press, New York, Ch. 5, 1965.

47. WILSON, R., J.Q.S.R.T., 2, 477, 1963.

48. SPITZER, L., "Physics of Fully Ionized Gases", Interscience Publ., John Wiley & Sons, New York, 1965.

49. DRAWIN, H. W., Z. Naturforschg, 19a, 1451, 1964.

50. DEUTSCH, C., Physics Letters, 28a, 525, 1969.

51. DRAWIN, H. W., EUR-CEA-FC-453, Fontenay-aux-Roses, 1967.

52. DRAWIN, H. W., EUR-CEA-FC-302, Fontenay-aux-Roses, 1965.

53. OERTEL, G. K., N. A. S. A. Technical Note, NASATN D-3737,

54. DANGOR, A. E., Ph. D. Thesis, University of London, 1970

55. BURGESS, D. D., DANGOR, A.E. and JENKINS, J. E., Brit. J. Appl. Phys., 16, 319, 1967.

56. ZWICKER, H. and SCHUMACHER, V., Z. fur Physik, 183, 453, 1965.

57. ALLEN, C. W., "Astrophysical Quantities", 2nd edition, Athlone Press, University of London, 1963.

58. GARCIA, J. D. and MACK, J. E., J. O. S. A., 55, 654, 1965.

59. DE JAGER, C. and NEVEN, L., Bull. Astr. Inst. Netherlands, 18, 306, 1966.

60. GRIFFIN, R. F., Mon. Not. R. Astr. Soc., 143, 319, 1969.

61. KARZAS, W. J. and LATTER, R., Astrophys. J., Suppl. VI, 1961.

62. "Handbook of Mathematical Functions", National Bureau of Standards Applied Mathematics Series 55, 1964.

63. CAIRNS, C., Ph.D. Thesis, University of London, to be published.

PUBLICATIONS

"Pressure Dependent Behaviour of the Z-Pinch Discharge"

Brit. J. Appl. Phys., 16, 319, 1967.

(co-authored with D. D. Burgess and A. E. Dangor)